MODELLING NEURAL INTERACTION, DYSFUNCTION AND DEGENERATION IN PARKINSON'S DISEASE

Laura Rebeca Lestón Pinilla

NOTTINGHAM TRENT UNIVERSITY

A thesis submitted in partial fulfilment of the requirements of Nottingham Trent University for the degree of Doctor of Philosophy (PhD).

September 2023

The work presented (including data generated and data analysis) was carried out by the author. Part of the content within Chapter 1 has previously been published by the author as an open access review article:

Lestón Pinilla, L., Ugun-Klusek, A., Rutella, S., & De Girolamo, L. A. **(2021)**. Hypoxia signaling in Parkinson's disease: there is use in asking "What HIF?". Biology, 10(8), 723.

.

To my dad,

and to everyone who left too soon,

before scientific research could offer hope.

We'll get there someday

INDEX

ACKNOWLEDGEMENTS

Firstly, I would like to thank my brilliant supervisory team, Dr. Luigi De Girolamo, Dr. Aslihan Ugun-Klusek and Dr. Alan Hargreaves. Gino, thanks for all your support and guidance during this PhD. I would also like to thank our collaborators. Thanks to Dr. Graham Hickman for his help with microscopy, Dr Amanda Courts for the stable SH-SY5Y cell lines and letting me use her flow cytometer and Dr Jay Vadakekolathu for his help with the Nanostring. I would also like to thank the people who make research possible, so thanks to everyone working in the technician team, cleaning services, stores, purchasing and states. I would like to thank the DTA and NTU for funding this PhD.

Thanks to all my lab colleagues in IBRC, and also over ISTEC and JvG. Thanks to the past and current members of IBRC: Awais, Max, Chris, Anhua, Sri Nithiya and Ozde. Also, a very special mention to the Italian team, who have hosted me these lasts months of PhD writing: Elisa, Maria Pia, Melanie and Amalia, it has been just fantastic to be a part of your group. And specially thank you to Nacho and Bishr, who have been the best friends one could ask for. It´s been great to share this PhD, and many meals, chats and outings, with all of you.

Thanks to all my family: Mum, Dad, my sis Raquel, my cousins Julia and Andrea, my aunts Nuria and Feli and my grandma Elvira. They have always supported me and inspired my academic journey, and I would be where I am without their encouragement. I just wish my dad was here to see me submit this thesis, but I know he'd be proud.

And lastly, thanks to the best partner ever, Eric. This PhD would not have been possible without him. Thanks for teaching me how to use Illustrator, which I have utilised to make almost every figure on this thesis. Thanks for moving with me to the UK and for being my number one cheerleader during this PhD, bringing a constant supply of emotional support, coffee and chocolate whenever needed. I can't wait to start the post-PhD chapter of my life with you.

ABSTRACT

Parkinson's disease (PD), the second most prevalent neurodegenerative disorder, is characterized by the loss of dopaminergic neurons in the substantia nigra pars compacta (SNpc) of the midbrain, which results in movement impairments. The underlying cause of neuronal degeneration in PD remains poorly understood, but genetic and environmental factors are thought to be contributory factors. The genetic mutations and environmental toxins associated with PD development primarily affect three key pathways: mitochondrial homeostasis, oxidative stress, and protein degradation. These pathways diminish with age, the leading risk factor for PD. Furthermore, ageing can give rise to reduced blood flow to the brain, leading to low oxygen levels (hypoxia). As hypoxia can damage dopaminergic neurons, it is possible that it plays a role in the neurodegenerative process that leads to PD. The cellular response to hypoxia is mainly orchestrated by the Hypoxia-inducible factor 1α (HIF-1α), a transcription factor that coordinates the expression of genes that help cells adapt and survive in hypoxia. Despite the observation that HIF-1α signalling is disrupted in PD patients, the specific pathways involved in this process remain to be determined. In addition, HIF-1α stabilizers have been shown to have neuroprotective effects in animal and cellular models of PD.

This project investigates the interplay between hypoxia/HIF-1α and the genes and pathways involved in PD pathogenesis. We also assessed the protective effect of novel chemical HIF-1α inducers and identified HIF-1α targets in neurodegeneration. This investigation was performed in immortalized cellular models, including neuronal SH-SY5Y and LUHMES cells and astrocytic U-87MG cells.

This research found that HIF-1α stabilisation reduced the protein levels of PD-related PINK1 in neuronal cells. Subsequently, compounds that deregulated mitochondrial function, reactive oxygen species production, and protein degradation impaired HIF-1α stabilization. The protective effect of a range of HIF-1α stabilizing drugs was evaluated with ML228 identified as a compound able to alleviate the consequence of complex 1 impairment in SH-SY5Y. ML228 improved a range of parameters, including cell viability, mitochondrial density, mitochondrial membrane potential, ROS production, autophagy markers, cell cycle distribution, and Ca^{2+} levels. Finally, we uncovered a set of previously unknown potential HIF-1α targets involved in pathways that are important for neuronal homeostasis and linked to PD.

This constitutes the first comprehensive investigation into the interplay between the response to hypoxia via HIF-1α and PD. Our findings suggest a mechanism by which pathways disrupted in PD can decrease HIF-1α stabilization, possibly leading to an impaired hypoxia response, which has been reported in PD patients. Additionally, our study demonstrates the potential of HIF-1α stabilizing drugs as a therapeutic strategy for PD. Overall, our findings suggest that further research into the role of HIF-1α in PD could lead to new insights into PD pathogenesis and treatment.

ABBREVIATIONS

AAPH	2,2'-Azobis(2-amidinopropane) dihydrochloride
2-DG	2-Deoxyglucose
3-MA	3-methyladenosine
2',7'-DCFDA	5-(and-6)-carboxy-2′,7′-dichlorodihydrofluorescein diacetate
AQ	Adaptaquin
ABZ	Albendazole
RA	all-trans-retinoic acid
AD	Alzheimer's Disease
AD-PD	Autosomic Dominant Parkinson's Disease
ALS	Amyotrophic Lateral Sclerosis
AIF	apoptosis inducing factor mitochondrial 1
Apaf-1	Apoptotic Peptidase Activating Factor 1
AR-PD	Autosomic Recessive Parkinson's Disease
ASC	Ascorbic Acid
BAF	Bafilomycin A1
bHLH	basic helix-loop-helix
BLAST	Basic Local Alignment Search Tool
BNIP3	Bcl-2 interacting protein 3
BAK	Bcl-2-antagonist/killer 1
BAX	Bcl-2-associated X
BCA	Bicinchoninic Acid
BSA	Bovine serum albumin
BDNF	Brain derived neurotrophic factor
BSO	buthionine sulfoximine
CHOP	C/EBP homologous protein
CA9	Carbonic anhydrase 9
CCCP	Carbonyl cyanide m-chlorophenylhydrazone
CNS	Central nervous system
CBF	cerebral blood flow

CMA	chaperone-mediated autophagy
CQ	Chloroquine
ChIP	Chromatin immunoprecipitation
CIH	chronic intermittent hypoxia
JNKs	c-Jun N-terminal kinases
CQL	Clioquinol
CHIP	C-terminus of Hsc70-interacting protein
Cdk2	Cyclin dependent kinase 2
DFO	Deferoxamine
DEG	Differentially expressed gene
dLUHMES	differentiated LUHMES
DMSO	dimethyl sulfoxide
DMOG	dimethyloxalylglycine
DA	Dopamine
DAT	dopamine transporter
DAergic	dopaminergic
PBS	Dulbecco's phosphate buffered saline
ETC	electron transport chain
EPO	erythropoietin
EPD	Eukaryotic promoter database
ERKs	Extracellular signal-regulated kinases
FIH	Factor Inhibiting HIF-1
FBS	Foetal Bovine Serum
GABA	Gamma-Aminobutyric Acid
GO	Gene ontology
GDNF	Glial derived neurotrophic factor
GSK3	Glycogen synthase kinase 3
HK	hexokinase
HAS	HIF ancillary sequence
PHDs	Prolyl hydroxylases

HIF-1α	Hypoxia inducible factor 1α
HRE	hypoxia response elements
HAF	hypoxia-associated factor
Higd-1a	Hypoxia-induced gene domain protein-1a
HUMMR	Hypoxia-upregulated mitochondrial movement regulator
H/I	hypoxic/ischemic
PI3KIII	III PI3-kinases
IPSC	Induced Pluripotent Stem Cells
IAP	inhibitor of apoptosis
IPAS	Inhibitory PAS domain protein
KEGG	Kyoto Encyclopedia of Genes and Genomes
LACT	Lactacystin
LDHA	lactate dehydrogenase
Lf	Lactoferrin
lncRNAs	long non-coding RNAs
Tm	Melting Temperature
miRNA	micro RNAs
mtROS	mitochondrial ROS
MFN1	Mitofusin-1
MFN2	Mitofusin-2
MAPK	mitogen-activated protein kinase
MAO-B	monoamine oxidase B
MEF	Murine embryonic fibroblast
cAMP	N6,2′-O-Dibutyryladenosine 3′,5′-cyclic monophosphate
NAC	N-Acetylcysteine
NS	Nervous system
NEAAS	Non-essential aminoacids
NA	noradrenaline
NLS	nuclear localization signal
OSA	Obstructive sleep apnea
OXPHOS	Oxidative phosphorylarion

ODDD	oxygen-dependent degradation domain
PD	Parkinson's Disease
PLK3	Polo-like kinase 3
PCR	polymerase chain reaction
PI	propidium iodide
PDH	pyruvate dehydrogenase
PDK1	pyruvate dehydrogenase kinase
ROS	reactive oxygen species
RACK1	receptor of activated protein kinase (PK)C
qRT-PCR	Reverse transcription quantitative real-time polymerase chain reaction
Smac	second mitochondrial activator of caspases
SNpc	substantia nigra pars compacta
SI	Supplementary information
Sph-1	Synphilin-1
TRAIL	TNF-related apoptosis-inducing ligand
TAD	transactivation domains
TF	Transcription factor
TfR	transferrin receptor
TBI	Traumatic brain injury
TCA	tricarboxylic acid
TNF	tumor necrosis factor
TH	tyrosine hydroxylase
UPS	ubiquitin-proteasome system
VEGFA	vascular endothelial growth factor A
pVHL	Von Hippel Lindau factor
α-Syn	α-Synuclein
β-Syn	β-Synuclein

CHAPTER I

INTRODUCTION

1.1. SYSTEMIC AND CELLULAR RESPONSE TO HYPOXIA

Molecular oxygen (O_2) is a key factor in the evolution of life on Earth. The rise of the atmospheric O_2 concentration prompted the development of aerobic organisms, capable of producing energy very efficiently through oxidative phosphorylation (OXPHOS), which gave these organisms an evolutionary advantage while making them reliant on oxidative metabolism (Semenza, 2007). Consequently, in response to low O_2 availability (hypoxia), organisms and cells undergo a series of systemic and molecular changes to adapt and survive.

The importance of O_2 to humans is highlighted by the existence of extremely sensitive O_2 detection systems that allow for a rapid dynamic cardiorespiratory response to hypoxia. Type I glomus cells in the carotid and aortic bodies detect the partial pressure of O_2 within the bloodstream (Lopez-Barneo et al., 2016), whilst pulmonary neuroepithelial body cells sense O_2 fluctuations in inspired air (Cutz et al., 2013). These hypoxia detection neuroendocrine centres signal through chemoafferent fibres that transmit stimuli into the central nervous system (CNS), which triggers a cardiovascular and respiratory adjustment within seconds. This response consists of increased pulmonary ventilation rate and vasoconstriction, tachycardia and general vasodilation in order to maximize gas exchange in the lungs and enhance O_2 delivery to tissues (Kane et al., 2020).

The multisystem adaptation to hypoxia suggested the existence of a widely distributed and evolutionary conserved cellular O_2 sensing system. Indeed, the Hypoxia inducible factor (HIF) family of proteins controls the molecular response to hypoxia by influencing gene expression as transcription factors (TF). This family encompasses three HIFs, which consist of a dimer formed by a O_2-sensitive α subunit and a stable nuclear β subunit (Wang et al., 1995). The α subunits that have been discovered in vertebrates are HIF-1α, HIF-2α and HIF-3α, encoded by the genes *HIF1A*, *EPAS1* and *HIF3A* respectively, and the three β subunits identified are HIF-1β, HIF-2β and HIF-3β, corresponding to the genes *ARNT, ARNT2* and *ARNTL*, although HIF-α paralogs bind preferentially to HIF-1β (Weidemann and Johnson, 2008). HIF-α and HIF-1β subunits dimerize and are able to bind DNA thanks to the basic Helix-Loop-Helix–Per-ARNT-Sim (bHLH-PAS) domain (Jiang, 1995). The responsiveness of the HIF-1 system to O_2 levels relies on a distinct oxygen-dependent degradation domain (ODDD) in the α subunit, which controls its stability (Huang et al., 1998). Towards the C-terminal, HIF-1α and HIF-2α have two transactivation domains (N-TAD and C-TAD), while HIF-3α contains only the NTAD

(Fig.1.1). While the bHLH-PAS domains present high sequence homology between the α subunits, the presence of distinct N-TAD and C-TAD domains recognised by different cofactors, allows for unique regulation of each α subunit (Dengler et al., 2014). The remarkably specific structure of the HIF-α subunits is key to controlling their stability and transcriptional activity to respond to O_2 levels.

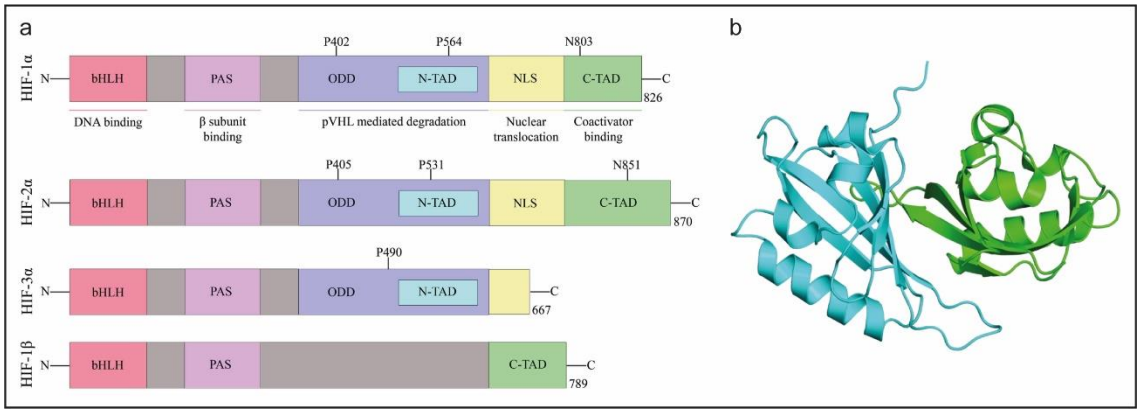

Figure 1.1. a. Domain structure of human HIF. Image showing the different domains and associated functions present in the HIF-α isoforms and HIF-1β (Davis et al., 2019). **b. HIF-1α/ARNT heterodimer.** Illustration of the interaction between the PAS domains of HIF-1α and HIF-1β (PDB ID 4H6J).

To ensure rapid availability upon descending O_2 levels, the α subunits of HIF are constantly being synthesised and then regulated post-translationally. In normoxia, HIF-α proteins are hydroxylated on proline residues (P402 and P564 in human HIF1-α) present on the ODD domain by HIF-Prolyl hydroxylases (PHDs) (Epstein, 2001). There are three isoforms of HIF-PDHs in humans, PHD1, PHD2, PHD3 and PHD4 encoded by the genes *EGLN2*, *EGLN1*, *EGLN3* and *EGLN4* respectively. PHD2 is the most abundant isoform and most sensitive O_2 sensor, specifically maintaining the proline hydroxylation of HIF-1α in normoxia (Berra et al., 2003). In order to catalyse the hydroxylation reaction, HIF-PDHs utilise 2-oxoglutarate (2-OG) and O_2, as well as the iron present in their active site and ascorbate as cofactor, producing succinate and CO_2 (Fig.1.2). All HIF-PDHs hydroxylate human HIF-1α at P564 while only PHD1 and PHD2 hydroxylate P402. These hydroxylation signals are recognised by the E3 ubiquitin ligase complex containing the von Hippel–Lindau tumour suppressor protein (pVHL), elongins B and C, cullin 2, and Ring box protein 1, which targets HIF-α for proteasomal degradation (Maxwell et al., 1998). As the presence of O_2 is rate limiting for PHD enzymes, being active at physiological O_2 concentrations in tissues, their hydroxylation activity is hampered by hypoxia, allowing HIF-α stabilization and accumulation. Consequently, HIF-α enters the nucleus where it binds to HIF-1β. The HIFs αβ dimers recognise specific hypoxia-responsive elements (HREs) in the genome with the consensus sequence 5′–RCGTG-3′,

which is facilitated by the transcriptional coactivators CREB-binding protein (CBP) and p300, triggering the expression of several genes (Partch and Gardner, 2011). In recent years, additional positive and negative transcriptional regulators of HIF-α have been discovered (Dengler, et al., 2014). The process of HIF-1 mediated gene transcription is also regulated. In fact, the asparaginyl hydroxylase factor inhibiting HIF-1 (FIH-1), catalysing the same reaction as PHDs, hydroxylates an asparagine residue in the C-TAD of HIF-1 and HIF-2 (N803 in human HIF-1α), inhibiting the recruitment of the coactivators, thereby limiting gene expression induction by HIFs in normoxia (Lando et al., 2002). HIF-PHDs and FIH-1 are both members of the 2-OG- and iron (II)-dependent dioxygenases enzyme family but display some differences, with FIH-1 presenting a higher affinity for molecular O_2 and PHDs being more substrate specific (Janke et al., 2013). This disparity seems to be important to connect different hypoxia levels and substrate availability to the regulation of HIF target genes. Indeed, HIF-1α, HIF-2α and HIF-3α activate convergent but distinct transcriptional programmes (Tolonen et al., 2020). While hydroxylation is the main posttranscriptional modification controlling the abundance and activity of the HIF proteins, other modifications including phosphorylation and acetylation can also influence factors such as HIF nuclear localisation, transcriptional coactivator recruitment and stability (Albanese et al., 2021). This research will focus on HIF-1α, the most studied factor with over 1000 potential gene targets identified (Kunej et al.,2021).

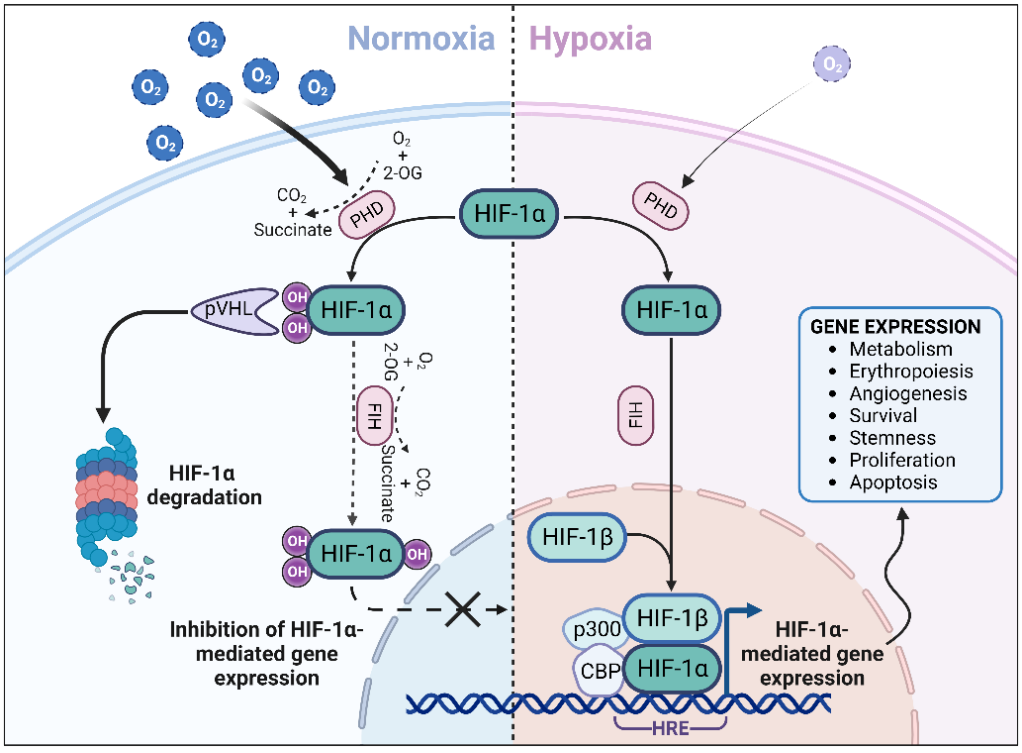

Figure 1.2. Regulation of HIF-1α stability. HIF-1α is degraded in normoxia due to its hydroxylation by PHDs, which is recognised by pVHL as a ubiquitination signal. HIF-1α is also hydroxylated by FIH, blocking its interaction with transcriptional cofactors, thereby inhibiting the expression of HIF-1α gene targets. In hypoxia, PHDs and FIH activity is inhibited due to low O2 availability, which results in HIF-1α accumulation, binding to HIF-1β and transcription cofactors and induction of the HIF-1α mediated transcriptional response. This illustration has been adapted from a template with Biorender.com.

1.1.1. HIF-1α target genes

The role of HIF-1α is to induce the expression of numerous target genes that promote cellular homeostasis under hypoxic environments. Although the number of genes regulated by HIF-1α varies due to different conditions, such as cell type, hypoxia severity and duration, chromatin status and transcriptional coactivator availability, a specific set of genes constitute the core HIF-1α transcriptional response. These genes are involved in O_2 redistribution and utilization via angiogenesis and metabolic rewiring respectively. Indeed, O_2 delivery is improved by increased expression of Erythropoietin (EPO) (Wang et al., 1996), which stimulates red blood cell synthesis, and angiogenic factors such as Vascular Endothelial Growth Factor (VEGFA) (Forsythe et al., 1996), Angiopoietin-2 and 4 (Yamakawa et al., 2003), Transferrin (Rolfs, 1997) and its receptors, which enhances vascularization.

In order to minimize O_2 consumption, HIF-1α drives O_2-independent mitochondrial energy production. Mitochondria are organelles formed by two membranes that constitute the powerhouses of the cell, producing energy via OXPHOS in the form of Adenosine triphosphate (ATP), utilised to carry out crucial cellular functions. Briefly, several carbon fuels, mainly glucose, are transformed into pyruvate, which is subsequently transported into the space within the inner membrane, the mitochondrial matrix, and converted to Acetyl-CoA. This intermediate enters the Tricarboxylic acid (TCA) cycle, where its oxidation produces the reduced cofactors NADH and $FADH_2$, which act as electron donors for the Electron transport chain (ETC), a series of protein complexes situated on the inner mitochondrial membrane that are capable of transporting electrons via successive redox chemical reactions. The electrons from NADH and $FADH_2$ are transferred through the ETC to O_2 and protons (H^+). Although this is an efficient system, some electrons can leak and reduce O_2, forming reactive oxygen species (ROS), which can damage biomolecules and modify signalling pathways. The series of reactions catalysed by the ETC produce the release of energy, which is utilised to pump H^+ into the intermembrane space, creating an electrochemical gradient. This potential energy is utilised by the membrane-bound enzyme complex ATP synthase to power the synthesis

of ATP from ADP and inorganic phosphate by shifting H^+ back to the mitochondrial matrix (Alberts et al., 2002). This process is clearly dependent on O_2 availability. Thus, when O_2 tension is minimal, pyruvate is diverted away from OXPHOS and into anaerobic energy synthesis, which produces a lower yield of ATP. HIF-1α controls most of the enzymes participating in mitochondrial energy production, increasing glucose uptake via Glucose transporters 1 and 3 (GLUT1, GLUT3) and its transformation into pyruvate by upregulating several genes involved in this pathway, such as Hexokinase (HK) and phosphoglycerate kinase-1 (PGK1) (Ebert et al., 1996). Pyruvate conversion to Acetyl-CoA and subsequent entry into the TCA cycle is inhibited by HIF-1α, which downregulates Pyruvate dehydrogenase (PDH) activity by promoting the expression of its inhibitor Pyruvate dehydrogenase kinase 1 (PDK1). In turn, HIF-1α facilitates the conversion of pyruvate into lactate by increasing the levels of Lactate dehydrogenase A (LDHA) (Semenza et al., 1994). These modifications allow cells to produce ATP under hypoxic conditions via lactate fermentation. Although this process is faster than oxidative ATP synthesis, it produces only 2 ATP molecules per glucose unit compared to the approximate 36 ATP molecules synthesised via oxidative cellular respiration, so anaerobic energy production is only tolerated for short periods of time in most human cells (Alberts et al., 2002). Interestingly, HIF-1 stabilisation is coupled to mitochondrial function, as PHDs and FIHs use 2-OG, a TCA cycle metabolite, as a substrate for their activity (Papandreou et al., 2006). Therefore, high levels of 2-OG or its synthetic analogues, such as dimethyloxalylglycine (DMOG), can inhibit PHDs and FIHs, leading to normoxic HIF-1α stabilization (Mole et al., 2003). Hypoxia can intensify H^+ leakage from the ETC, triggering an increase in mitochondrial ROS (mtROS), which can regulate hypoxic signalling and HIF-1 stabilisation (Guzy et al.,2005). To reduce the flow of electrons passing through the ETC and therefore the amount of mtROS being produced, HIF-1α downregulates mitochondrial complexes I and III (Fukuda et al.,2005; Tello et al., 2011).

Besides influencing O_2 availability, HIF-1α manages the resultant low energy levels by controlling cell survival, proliferation and apoptosis. In fact, HIF-1α regulates the gene expression of several growth factors, such as Insulin-like growth factors 1 and 2 (Feldser et al.,1999) and proteins implicated in apoptosis like Bcl-2 interacting protein 3 (BNIP3). BNIP3 participates in autophagy, vital process consisting of degradation of damaged or redundant cellular elements, which is also linked to cell death and controlled by HIF-1α (Greijer and van der Wall, 2004). Furthermore, HIF-1α controls cell proliferation by

regulating various factors involved in cell cycle progression (Koshiji, 2004). Interestingly, HIF-1α targets include several genes involved in pathways such as stemness, differentiation, matrix remodelling, transcriptional regulation and immune signalling (Benita et al.,2009).

In summary, the main function of HIF-1α is to control gene expression to foster cellular adaptation to hypoxic insults and maximise survival probability. However, HIF-1α also regulates genes outside of the canonical pathways affected by environmental hypoxia, suggesting a role for HIF-1α in additional physiological processes and pathologies.

1.1.2. Role of HIF-1α in the nervous system

The nervous system (NS), composed of nervous tissue, relies on specialized neurons that facilitate rapid and precise signal transmission via electrical impulses that propagate along axonal projections, either directly transmitted via electrical synapses or triggering the release of neurotransmitters at chemical synapses. Recent research highlights a critical role for HIF-1α in NS physiology, particularly during embryonic development which naturally occurs in a hypoxic environment. Conditional inactivation of neural *HIF1A* gene in mice impairs the correct development of the brain and sympathetic NS (Tomita et al., 2003; Bohuslavova et al., 2019; Sakai et al., 2022), which can be linked to the defective neural crest cell migration observed in HIF-1α KO mice embryos (Cornpemolle et al., 2003). HIF-1α supports the survival and proliferation of several types of embryonic neural precursor cells (Milosevic et al., 2009; Roitback et al., 2010; Eyrich et al., 2019) and adult hippocampal progenitors (Carrica et al., 2019). In addition, cultivating induced pluripotent stem cells (iPSCs) in a hypoxic environment promotes their differentiation into mature neurons (Yamazaki et al., 2016). Strikingly, energy-consuming neuronal activity in adult mice leads to an endogenous 'functional hypoxia' state, characterized by widespread neuronal HIF-1α stabilization and activation of the expression of its associated genes (Butt et al., 2021). This evidence suggests that HIF-1α is heavily involved in both embryonic and adult neurogenesis as well as neuronal proliferation, survival, differentiation and activity. Thus, HIF-1α is not only necessary for embryonic NS development but may also play a role in neuronal functions also present in adults like memory formation and neuroplasticity (Carrica et al., 2019; Butt et al.,2021). In addition to neurons, the NS contains glial cells, which support neuronal communication, metabolism and structure and can be categorized into three main types: astrocytes, oligodendrocytes and microglia. Emerging evidence suggests the HIF-1α-mediated

hypoxia response pathway influences glial cell function, particularly in astrocytes. Astrocytes participate in a wide variety of functions, such as metabolite trafficking, synapse homeostasis, regulation of blood blow and inflammatory damage response (Sofroniew et al.,2010). During hypoxia, HIF-1α in astrocytes not only promotes their survival but also boosts lactate production, which can then be shuttled to neurons as an alternative fuel source (Badawi et al., 2012; Brix et al., 2012). Interestingly, astrocytes can directly respond to declining oxygen levels within brain circulation by inducing dilation of cerebral blood vessels, thereby enhancing blood flow to counteract hypoxia (Christie et al., 2023).

Beyond its importance in NS function, HIF-1α is also involved in disease states. The NS is a highly energy-demanding organ, requiring a constant supply of O_2 and nutrients to maintain its proper function. OXPHOS is the primary metabolic pathway by which the NS generates energy from O_2 and glucose. In mammals, the brain consumes approximately 20% of the body's total O_2 pool (Erecińska et al., 2001). This high energy demand is due to the complex and dynamic nature of neuronal signalling, which requires the continuous synthesis and degradation of neurotransmitters, as well as the maintenance of ionic gradients across cell membranes (Bélanger et al., 2011). This O_2 availability is dependent on constant delivery through the circulatory system, as the O_2 stored in the brain is very limited (Hall et al., 2012). As a result, the brain is highly susceptible to O_2 deprivation, which can occur due to low O_2 levels in the blood (hypoxia) or blocked blood flow (ischemia), which can be fatal within minutes. When neurons are deprived of O_2, they produce more free radicals and have reduced antioxidant capacity. This leads to rapid depletion of ATP and increased levels of intracellular calcium, which cause reduced synaptic activity, loss of dendrites, and membrane depolarization. This can induce hyperexcitability and eventually death of neuronal populations (Nieber et al., 1999). The detection of similar pathological changes within the hypoxic brain and those associated with neurodegeneration and aging suggests that O_2 deficiency may be a contributing factor in the pathogenesis of these conditions. In fact, many pathologies affecting the NS are characterized by hypoxia, which is present in diseases like ischemic stroke, CNS tumours, neuroinflammatory disorders, seizures, traumatic brain injury (TBI) and neurodegenerative conditions, such as Alzheimer’s Disease (AD), Amyotrophic Lateral Sclerosis (ALS) and Parkinson´s Disease (PD) (Burtscher et al., 2021). HIF-1α can have a dual role in these disorders. Indeed, research supports both a protective and harmful effect of HIF-1α in pathologies such as such as ischemic stroke (Mitroshina et al., 2021),

neonatal hypoxia (Chen et al., 2009) and TBI (Sen and Sen, 2016; Fang et al., 2020). In neuroblastoma, HIF-1α is correlated with tumour aggressiveness (Chen et al., 2015) while in neurodegenerative disorders it has been shown to be neuroprotective (Mitroshina et al, 2021). For instance, animal studies show that exposure to hypoxia increases toxic protein buildup and neuronal death in AD and triggers motor neuron loss in ALS (Kim et al., 2013; Zhang and Le, 2010). Mouse models of these conditions additionally revealed dysregulation of the HIF-1α pathway, which can contribute to the detrimental effect of hypoxia (Nagara et al., 2013; De Gasperi et al., 2010). Interestingly, research suggests that targeted induction of moderate HIF-1α levels exerts neuroprotective effects in experimental models of these neurodegenerative diseases (Zhang et al., 2011).

The specific genes and pathways controlled by HIF-1α in neuronal homeostasis and pathology have not been fully investigated and further knowledge on the role of HIF-1α in this context would be valuable for the development of novel therapeutic approaches. Indeed, while hypoxic events are linked to the development of neurodegenerative diseases, neurons can adapt to hypoxia and improve their survival through activation of the HIF-1α signal transduction pathway (Ostrowski and Zhang, 2020). Similarly, several aspects of PD pathophysiology have been linked to hypoxia. This has led to the development of experimental HIF-1α-based therapies, which will be discussed in detail, alongside the connection between PD and hypoxia, in the following sections.

1.2. PARKINSON'S DISEASE

Parkinson's Disease (PD) is a progressive neurodegenerative movement disorder defined by the loss of dopaminergic (DAergic) neurons in the substantia nigra pars compacta (SNpc) in the midbrain and linked to the occurrence of Lewy bodies, intraneuronal insoluble aggregates of the protein α-synuclein (α-Syn) (Armstrong et al., 2020). Dopamine (DA) is a neurotransmitter that regulates muscle contraction and tone, so its deficiency triggers the characteristic PD motor impairments, including tremor, rigidity, bradykinesia and postural instability (Korchounov et al., 2010). PD patients can report some non-motor symptoms, such as cognitive decline and depression, due to the role of DA in controlling other behavioural features such as reward and motivation, and the presence of damage to other neural groups and neurotransmitter pathways (Schapira, et al.,2017).

The fundamental mechanisms behind SNpc DAergic neuronal degeneration remain to be elucidated. A complex interplay of subtle gene expression and protein function

differences, as well as high energy demand and particular electrophysiological properties, appear to be instrumental in the vulnerability of these neurons (Brichta et al., 2014). PD is primarily a neurodegenerative disorder affecting SNpc Daergic neurons, but recent research suggests that other cell types, such as astrocytes, might play a role. Several proteins encoded by PD-related genes control astrocytic functions, including inflammation, mitochondrial fitness, lysosome trafficking and lipid metabolism, hinting a likely impact of PD-related mutations on astrocyte biology (Booth et al.,2017). In fact, PD patients' iPSCs-derived astrocytes show dysfunctional inflammatory function, increased α-Syn expression and accumulation, deregulated Ca^{2+} signalling and reduced mitochondrial respiration (Booth et al.,2019; Domenico et al.,2019; Sonninen et al.,2020). Therefore, a comprehensive understanding of PD requires investigation into both the root causes of neuronal dysfunction and the potential involvement of astrocytes.

Recent research into PD pathophysiology has shed significant light on the disease process, although key questions remain unanswered. In fact, PD is now regarded as a multifactorial disorder in most patients, resulting from the cumulative effects of genetic predisposition, environmental influences and lifestyle factors, although in a small percentage of patients PD onset can be traced back to precise gene polymorphisms, such as certain mutations in the gene coding for α-Syn (*SCNA*) (Karimi-Moghadam et al., 2018). However, the origin of the majority of PD cases remains unknown, mainly due to the difficulty of assessing the specific impact of non-genetic factors. These idiopathic cases have been linked to dysfunction of specific molecular pathways like protein clearance, ROS production and mitochondrial homeostasis and specific risk factors including age, exposure to toxic chemicals and head injury (Simon et al., 2018). The incredibly complex aetiology of PD, typically related to highly heterogeneous manifestations and variable severity of the disease between individuals, can complicate diagnosis. PD is diagnosed by analysing patient medical history and neurological symptoms, such as motor and coordination impairments, in conjunction with brain imaging techniques, specifically magnetic resonance to assess the appearance of the SN, and genetic testing in some cases (Bloem et al., 2021). Thus, the development of more reliable biomarkers at asymptomatic stages of the disease, and the use of genetic profiling of patients will surely permit a more effective treatment of PD.

The unclear aetiology of Parkinson's disease hampers the development of curative and preventive strategies. While existing treatments can temporarily alleviate symptoms, they cannot halt the progression of the disease (Emamzadeh and Surguchov, 2018). PD is the

second most common neurodegenerative disorder in the world, after AD, with an incidence of 149 people affected in the UK and around 120 people affected globally per 100,000 person-years (Ou et al., 2019; Okunoye et al., 2022). The number of people with PD is increasing worldwide, and this trend is expected to continue as the population ages (Feigin et al., 2017). As a result, PD has become a major cause of disability and a significant economic and healthcare burden. Thus, it is of outmost importance to investigate the specific causes of genetic and idiopathic PD development, as well as novel disease-modifying therapies. Interestingly, several genes, pathways and risk factors associated with PD are linked to hypoxia and the HIF-1α response, and a variety of drugs stabilising HIF-1α have shown neuroprotective effects in animal and cellular PD models, which will be discussed in the following sections.

1.3. CROSSTALK BETWEEN HYPOXIA, HIF-1α AND PD-RELATED GENES

To date, over 20 PD-linked genetic mutations have been identified, accounting for about 5-10% of PD cases (Blauwendraat et al., 2020). Although quite rare, these PD-specific mutations have been extensively studied to unravel the signalling pathways responsible for monogenic PD development and assess the frequency of disruption of related molecular cascades in sporadic PD. Intriguingly, a connection exists between several of these genes and the hypoxic response.

α-synuclein (PARK1; SNCA) is widely expressed in the neuronal cells, specifically in presynaptic terminals, where it controls membrane curvature, thereby contributing to synaptic trafficking, vesicle budding and neurotransmitter release (Benskey et al., 2016). Impaired α-synuclein function due to mutations or multiplication of the SNCA gene cause autosomal dominant (AD-PD) PD (Polymeropoulos et al., 1997). Indeed, the characteristic Lewy bodies that can appear in the brain of PD patients contain aggregated α-synuclein and are thought to arise from a transition to fibril formation driven by posttranslational modifications and structural rearrangement (Benskey et al., 2016). This oligomerization and fibril formation process of α-synuclein can be induced by hypoxia, contributing to neuronal dysfunction and death (Chen et al., 2019). Interestingly, exogenous α-synuclein oligomers facilitate HIF-1α accumulation in normoxic primary microglia, promoting their migration (Qiao et al., 2017).

Leucine-rich-repeat kinase 2 (PARK8; LRRK2) is involved in diverse cellular processes including autophagy, mitochondrial function and cytoskeletal dynamics, consistent with

its multiple enzymatic and protein- interacting domains (Wallings et al., 2015). Mutations in LRRK2 that link to AD-PD cluster within two catalytic domains, and often result in increased LRRK2 kinase activity (West et al., 2005). HIF-1α has emerged as a LRRK2 phosphorylation target in normoxia in human breast cancer cells. This phosphorylated HIF-1α isoform presents greater affinity for its transcriptional cofactor p300, which facilitates the expression of HIF-1α target genes (Lin et al., 2016). Conversely, upon traumatic brain injury, HIF-1α can directly bind the LRKK2 promoter and induce LRKK2 expression in the brain, which exacerbates neuronal injury (Bae et al., 2018).

ATP13A2 (PARK9) is a P-type ATPase that localises to intracellular vesicles and regulates cation homeostasis. This, in turn, impacts on endosomal-lysosomal homeostasis and ensures correct autophagy processing, mitochondrial maintenance and heavy metal detoxification (van Veen et al., 2014). Loss of function mutations that disrupt ATP13A2 function result in development of autosomal recessive (AR-PD) PD (Al-Din et al., 2006). ATP13A2 gene promoter contains HREs, so HIF-1α stabilization by either hypoxia, PHD2 pharmacological inhibition with IOX2 or PHD2 knockdown, induces ATP13A2 expression in DAergic neurons (Rajagopalan et al., 2016; Xu, Q. et al., 2012)

DJ-1 (PARK7) protects cells against oxidative stress through a variety of signaling pathways (Biosa et al., 2017). Mutations causing defective DJ-1 activity lead to an increased vulnerability to ROS and can trigger early onset AR PD development (Bonifati et al., 2003). Reduced DJ-1 expression correlates with impaired HIF-1α stabilisation in hypoxia in several cancer cell lines, mouse embryonic fibroblasts (MEFs), primary neurons and even lymphoblasts from PD patients with DJ-1 mutations (Parsanejad et al., 2014; Sheng et al., 2013; Vasseur et al., 2009; Zheng, H. et al., 2018). However, DJ-1 knockout has been related to normoxic HIF-1α stabilisation in SH-SY5Y cells and MEFs (Foti et al., 2010a; Requejo-Aguilar et al., 2015).

PTEN-induced kinase (PARK6; PINK1) is a serine/threonine kinase mainly involved in maintaining mitochondrial quality and fitness via control of ROS production, oxidative respiration, mitochondrial dynamics and mitobiogenesis. In addition, PINK1 plays a pivotal role in the regulation of mitophagy. During severe mitochondrial stress, mitochondrial depolarization facilitates PINK1 accumulation, which triggers a cascade of events, including Parkin recruitment, leading to mitophagy (Deas et al., 2009). Characteristically, PINK1 mutations result in loss-of-function and are linked to juvenile AR PD (Valente et al., 2004). Hypoxia can significantly alter mitochondrial homeostasis and OXPHOS. As a consequence, PINK1 knockouts in MEFS and primary murine

cortical neurons result in elevated ROS and HIF-1α stabilisation (Requejo-Aguilar et al., 2014) and remain unable to accumulate HIF-1α under hypoxic conditions (Lin, William et al., 2014). Low oxygen environments can alter PINK1 expression, reducing mitobiogenesis in tumour cell lines (Kung-Chun Chiu et al., 2019) indicating PINK1 expression can be altered as an adaption to change of oxygen levels.

Parkin (PARK2; PRKN) is a E3 ubiquitin ligase whose interplay with PINK1 controls mitochondrial homeostasis through regulating mitophagy as well as mitochondrial dynamics and biogenesis (Seirafi et al., 2015). Genetic mutations resulting in the loss of Parkin function lead to a failure of mitochondrial quality control and trigger the accumulation of defective mitochondria, which can manifest as early onset AR PD (Kitada et al., 1998). Cell line specific studies show that Parkin can target HIF-1α for degradation in HeLa and breast cancer cell lines, MEFs and human keloids (Lei et al., 2019; Liu, et al., 2017; Sarraf et al., 2013). In contrast, the Parkin/PINK1 pathway promotes HIF-1α expression in SH-SY5Y and HeLa cells by promoting the degradation of Inhibitory PAS domain protein (IPAS), an effective suppressor of HIF-1α transcription (Kasai et al., 2015). In glioblastoma-derived cell lines, Parkin knockout facilitates HIF-1α accumulation in normoxia while blocking hypoxic HIF-1α stabilization (Maugeri et al., 2016).

Intriguingly, DJ-1, PINK1 and Parkin knockouts show impaired HIF-1α stabilization in hypoxia, indicating that the HIF-1α-mediated response to hypoxic episodes may be defective if loss-of-function mutations in these genes are present. As HIF-1α can directly influence the expression of two PD-related genes, LRRK2 and ATP13A2, through the HREs present in their promoters, and hypoxia can trigger α-synuclein accumulation, it would be of interest to explore the impact of hypoxia and HIF-1α in the expression of other PD-related genes to elucidate possible common mechanisms. Since the aforementioned studies have been performed in a variety of cell lines and animal models, it is of paramount importance to investigate the impact of hypoxic stress and HIF-1α stabilization on PD- related genes in SNpc DAergic neurons and PD animal models in order to adequately establish the role of these pathways in PD.

1.4. HYPOXIA AND HIF-1α SIGNALLING IN PATHWAYS ASSOCIATED WITH PD

Genetic mutations in PD can be broadly classified within three distinct pathways: protein clearance, ROS control and mitochondrial function (Malkus et al., 2009). Dysregulation of these pathways, also found in sporadic PD patients, is believed to be the underlying cause of DAergic neuronal death in the SNpc. Hypoxia significantly affects these specific pathways and HIF-1-mediated transcription can precisely modulate them. Below we evaluate how hypoxia and HIF-1 signalling can interact with PD-related genes and potentially regulate these key pathways.

1.4.1. Protein degradation

Protein degradation is carried out by the autophagic pathway and the ubiquitin-proteasome system (UPS). Autophagy, divided in macroautophagy, chaperone-mediated autophagy (CMA) and microautophagy, promotes the proteolytic degradation of cellular substrates and organelles through lysosome involvement (Glick et al., 2010) while the UPS targets proteins by adding ubiquitin residues, which directs damaged and redundant proteins for degradation via the proteasome (Nandi et al., 2006).

Macroautophagy (referred to as 'autophagy') is a homeostatic process comprising the degradation of intracellular components through their engulfment by double membrane vesicles, the autophagosomes, which ultimately fuse with lysosomes, facilitating substrate degradation. The autophagic pathway begins with ULK1 activation to initiate autophagosome formation, driven by LC3-II, Beclin-1, numerous ATG proteins and p62 acting as an anchor for proteins targeted for degradation (Glick et al., 2010) . In CMA, selected proteins bind to chaperones forming a complex that is recognised by the lysosomal receptor LAMP2A (Glick et al., 2010). Deficiencies in both types of autophagy types have been detected in PD patients' peripheral blood mononuclear cells (Papagiannakis et al., 2015) as well as lysosomal vacuole accumulation was detected in DAergic SN neurons (Anglade et al., 1997). Several of the known PD-related gene mutations can directly and indirectly influence the autophagic process. For example, autophagy impairment facilitates α-synuclein accumulation in the brain (Friedman et al., 2012) and, in turn, α-synuclein aggregation can further hinder autophagy (Winslow et al., 2010).A loss of function of PINK1 or DJ-1 results in blockade of autophagy and CMA respectively (Krebiehl et al., 2010; Michiorri et al., 2010) while overactivation of LRKK2 reduces both autophagy and CMA (Albanese et al., 2019; Orenstein et al., 2013) . Furthermore, inhibition of ATP13A2 function also causes lysosomal dysfunction,

accompanied by decreased autophagosome clearance (Bento et al., 2016; Dehay et al., 2012; Wang, Ruoxi et al., 2019). Therefore, autophagy induction, as well as modulation of autophagic proteins, have been considered as possible therapeutic strategies for PD, with a primary purpose of promoting α-synuclein clearance (Fowler and Moussa, 2018).

It is well established that hypoxia can trigger autophagy through several mechanisms (Fig.1.4). HIF-1α upregulates BNIP3/NIX activity, promoting Beclin-1 release from Bcl-2 or Bcl-xL initiating a signalling cascade (Bellot et al., 2009). In addition, HIF-1α can facilitate LC3-I conversion to LC3-II leading to the formation of autophagosomes (Gui et al., 2016). Both HIF-1α stabilization and hypoxia-mediated ATP depletion activate the master energy sensor of the cell, AMPK, capable of inhibiting mTORC1 and phosphorylating ULK1, triggering autophagy (Bohensky et al., 2010; Papandreou, I. et al., 2008). Recent studies point to the involvement of hypoxia-induced ROS in autophagy activation (Zhang, J. et al., 2019). In addition, hypoxia increases LAMP2A expression, promoting CMA (Dohi et al., 2012). Basal autophagy is essential for neuronal homeostasis with several studies showing that an autophagy blockade can induce neurodegeneration (Hara et al., 2006; Koike et al., 2006). Despite autophagy playing a key role in maintaining cell viability through substrate clearance, hypoxia-mediated autophagy is considered a double-edged sword, as it is also involved in provoking apoptotic cell death (Mazure and Pouysségur, 2009). In the event of a hypoxic episode affecting the brain, hypoxia-induced autophagy can govern cell fate. Upon hypoxic/ischemic (H/I) brain injury, autophagy is activated, promoting either cell survival (Carloni et al., 2008; Dohi et al., 2012; Li, P. et al., 2018) or cell death (Chu, 2008; Koike et al., 2008), dependent on the extent of the hypoxia-mediated damage.

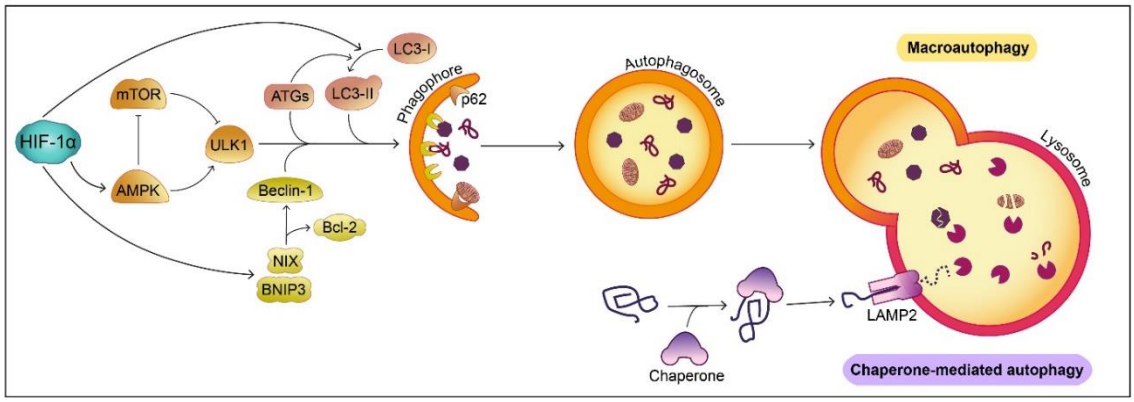

Figure 1.4. Impact of HIF-1α on autophagy in mammalian cells. a. Macroutophagy is controlled by the energy sensor AMPK, induced by HIF-1α. AMPK promotes ULK1 activity while blocking mTOR, inhibitor of ULK1. ULK1 triggers the start of the macroautophagic pathway, facilitating the recruitment of several ATG proteins, Beclin-1 and LC3-II, necessary for the formation of the double membrane, termed phagophore, where the cytoplasmic components targeted for degradation are attached through anchor proteins such as p62. HIF-1α promotes this process by increasing LC3-I lipidation to form LC3/II and inducing the expression of BNIP3 and NIX, which separate Beclin-1 from its inhibitor Bcl-2. Macroautophagy progresses as the autophagic cargo is enclosed in a double membrane organelle called autophagosome, which fuses with the lysosome, forming the autophagolysosome. The lysosomal enzymes are responsible for degrading the substrates. HIF-1α has not been linked to Chaperone-mediated autophagy, which starts with the unfolding of damaged proteins by chaperones. The unfolded substrate is detected by the lysosomal LAMP2 receptor, which translocates this substrate to the lysosome for its degradation. (Lestón Pinilla et al., 2021)

Evidence suggests that the UPS is impaired in PD patients, compromising α-synuclein degradation (McNaught et al., 2001) which accumulates, further hindering proteasome activity (McKinnon et al., 2020). Indeed, treatment with proteasomal inducers promotes α-synuclein clearance in PD models (Li, T. et al., 2018; Zhou et al., 2019). Besides targeting proteins for proteasomal degradation, Parkin can also directly enhance proteasome activity (Um et al., 2010). Contrarily, hypoxic stress reduces proteasome activity (Abu-El-Rub et al., 2019) . Since HIF-1α is predominantly degraded by the proteasome, inhibition of proteasomal activity leads to its accumulation.

HIF-1α-mediated induction of BNIP3 and the autophagic machinery can compensate for impairments in protein degradation and constitutes a potential therapeutic strategy to resolve the protein aggregation caused by aberrant proteostasis in PD patients.

1.4.2. Mitochondrial function

Mounting evidence suggests defective mitochondrial function, including biogenesis, dynamics, energy production and mitophagy, in the SN and other selected peripheral tissues of PD patients (Park et al., 2018).

Mitochondrial biogenesis is primarily induced upon energy shortage or increased metabolic demand by PGC-1α, a co-transcriptional regulation factor that promotes Nrf1 and Nrf2 transcription, facilitating TFAM expression (Ploumi et al., 2017). The PINK1/Parkin pathway regulates the phosphorylation and ubiquitination of PARIS, a known repressor of PGC-1α and Nrf1, facilitating protective biogenesis in SN DAergic neurons (Lee, Y. et al., 2017; Pirooznia et al., 2020). Interestingly, hypoxia induces a stimulatory response to mitigate mitochondrial defects and promotes mitobiogenesis via induction of PGC-1α, Nrf1 or TFAM through pathways involving AMPK, HMGB1 or

NOS dependent on cell type (Gutsaeva et al., 2008; Tohme et al., 2017; Zhu et al., 2010). Hypoxia-induced PGC-1α directly upregulates VEGF and EPO expression (Arany et al., 2008) and the increased oxygen consumption due to PGC-1α -mediated biogenesis can promote HIF-1α stabilization (O'Hagan et al., 2009). Consequently, HIF-1α exerts a compensative response, reducing mitochondrial biogenesis in order to save energy by inhibiting both the expression of PGC-1α either directly or via its repressor DEC1 and c-myc, positive regulator of PGC-1α expression, via upregulation of c-myc inhibitor MXI1 (LaGory et al., 2015; Zhang et al., 2007) (Fig.1.5a).

Excessive mitochondrial injury triggers mitochondrial membrane depolarization resulting in mitochondrial degradation. Dissipation of membrane potential activates PINK1, which phosphorylates both Parkin and ubiquitin to stimulate their interaction and initiate the Parkin-dependent ubiquitination of mitochondrial substrates. This ultimately triggers mitochondrial clearance through mitophagy (Eiyama and Okamoto, 2015). As expected, PD related mutations in Parkin or PINK1 affect mitochondrial degradation and clearance via mitophagy resulting in the accumulation of dysfunctional mitochondria (Geisler et al., 2010). Despite being able to induce PINK1/Parkin mediated mitophagy in certain conditions (Jiang, Y. et al., 2020; Li, S. et al., 2019), hypoxia promotes mitophagy via alternative pathways. Low oxygen induces the activation of two mitochondrial membrane proteins, FUNDC1 and E2F3d, capable of interacting with LC3-II and triggering mitophagy (Araki et al., 2019; Liu, L. et al., 2012). Although the involvement of HIF-1α in these pathways has not been studied, HIF-1α can induce mitophagy through the canonical BNIP3/NIX-dependent pathway (Koentjoro et al., 2017; Zhang, H. et al., 2008), which in turn promotes PINK1/Parkin-mediated mitophagy (Zhang, T. et al., 2016) (Fig.1.5b).

Mitochondria undergo continuous morphological modifications, including fission, driven by Drp1, and fusion, controlled via mitofusins (Mfn1 and Mfn2) and OPA1 (Scott and Youle, 2010). These processes protect against excessive ROS production and prevent accumulation of defective mitochondria within the cell. LRRK2 directly interacts with Drp1, promoting its recruitment to mitochondria and therefore stimulating fission (Wang, Xinglong et al., 2012). Likewise, overexpression of α-synuclein promotes fission independently of Drp-1 (Nakamura et al., 2011). In contrast, the PINK1/Parkin pathway promotes mitochondrial fusion with PINK1/Parkin knockouts exacerbating Drp1-mediated mitochondrial fragmentation (Dagda et al., 2009; Lutz et al., 2009). Interestingly, upon mitochondrial depolarization, PINK1/Parkin can promote fission prior

to mitophagy via regulation of Mfns and Drp1 (Chen, Yun and Dorn, 2013; Pryde et al., 2016). Hypoxia can promote mitochondrial fission through Drp1 induction via HIF-1α -dependent and independent pathways (Kim, Hyungsoo et al., 2011; Wan et al., 2014). BNIP3, a HIF-1α target gene, can inhibit OPA1-mediated fusion, causing mitochondrial fragmentation (Landes et al., 2010). Conversely, hypoxia facilitates the expression of Hypoxia-induced gene domain protein-1a (Higd-1a), which binds to OPA1 promoting fusion (An et al., 2013) to generate enlarged mitochondria as a compensatory mechanism in a process driven by HIF-1α-mediated expression of BNIP3 and NIX, which promote Mfn1 function (Chiche et al., 2010) (Fig.1.5c). In addition, hypoxia can induce Parkin-mediated degradation of both Mfns and Drp, potentially suppressing mitochondrial dynamics (Song et al., 2016).

Mitochondrial transport is essential in neurons as it responds to regional modifications in ROS and ATP levels by shuttling mitochondria to sites with high energy demand or increased degradation. Therefore, mitochondrial trafficking has been extensively studied in neuronal axons, where retrograde and anterograde transport are regulated by dynein or kinesin respectively (Zheng, Y. et al., 2019). These motor proteins bind mitochondria by means of the adaptor proteins Miro and Milton, which can form a complex with PINK1 (Weihofen et al., 2009). It has been shown that PINK1 can phosphorylate Miro, promoting its degradation via Parkin, thereby inhibiting mitochondrial movement and thereby segregating damaged mitochondria before mitophagy (Wang, Xinnan et al., 2011). PD-associated LRRK2 and α-synuclein mutations interfere with mitochondrial transport along the axon (Hsieh et al., 2016; Prots et al., 2018). Hypoxia has a very specific effect on mitochondrial trafficking, as it induces the accumulation of mitochondria in the perinuclear region. This precisely targeted concentration of mitochondria induces high local ROS production with increased oxygen consumption, which contributes to HIF-1α stabilization and stimulates oxidation of the HRE in the VEGF gene to allow its activation (Al-Mehdi et al., 2012). HIF-1α stabilisation through hypoxia facilitates the expression of CHCHD4, further promoting a perinuclear mitochondrial shift (Thomas et al., 2017) while inducing Hypoxia-upregulated mitochondrial movement regulator (HUMMR), which can interact with Miro, fostering anterograde transport (Li, Y. et al., 2009) (Fig.1.5d).

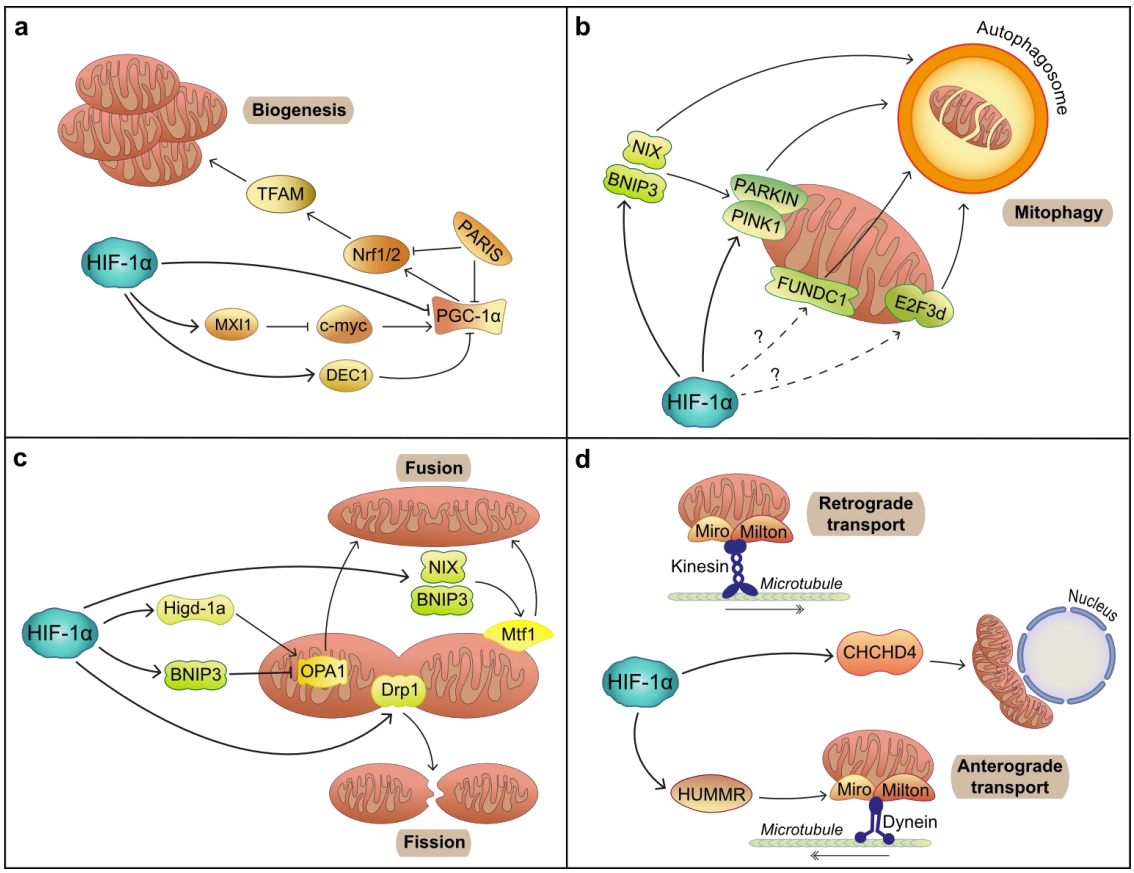

Figure 1.5. Effect of HIF-1α on mitochondrial number, morphology and distribution in mammalian cells. 1.5a. Mitochondrial biogenesis. HIF-1α represses mitochondrial biogenesis by preventing activation of the main effector of this process, PGC-1α, either directly or via induction of DEC1, a direct inhibitor of PGC-1α or MXI1, or indirectly through repression of c-myc, which activates PGC-1α. **1.5b**. Mitophagy. HIF-1α induces mitophagy mainly through BNIP3 and NIX. HIF-1α can also promote mitophagy via PINK1/PARKIN directly or through BNIP3. FUNDC1 and E2F3d mitophagic pathways are induced by hypoxia, although the involvement of HIF-1α has not been demonstrated. **1.5c**. Mitochondrial dynamics. HIF-1α is capable of inducing fission by promoting Drp1 activity. Fission can be both induced and inhibited by HIF-1α. Fission is promoted by HIF-1α by BNIP3/NIX activation, which promotes Mtf1 function, as well as via HIF-1α-induced Higd-1a, which triggers OPA1 activation. Conversely, BNIP3 can prevent OPA1 activity, hindering mitochondrial fission. **1.5d**. Mitochondrial transport. HIF-1α induces perinuclear mitochondria accumulation by activating CHCHD4 expression. Additionally, HUMMR, whose levels are controlled by HIF-1α, interacts with Miro to promote anterograde transport of mitochondria. (Lestón Pinilla et al., 2021)

Mitochondrial oxidative respiration and subsequent ATP production have been found to be reduced in PD. PINK1 loss has been linked to impaired activity of several ETC complexes as well as low ATP synthesis, and it has been hypothesized that this respiratory dysfunction causes the collapse of mitochondrial membrane potential (Gegg et al., 2009; Morais et al., 2014). As discussed, hypoxia has a heavy impact on mitochondrial energy production, as reduced oxygen availability impairs the ATP synthesis powered by the ETC. Thus, HIF-1α switches off oxidative energy production, favoring glycolytic metabolism. HIF-1α facilitates the expression of hexokinase (HK) and enolase 1 (ENO1), thereby accelerating the production of pyruvate, which is converted to lactate by HIF-1α-

induced lactate dehydrogenase (LDHA) (Semenza et al., 1996) instead of being transformed to Acetyl-CoA. This is facilitated by HIF-1α-mediated inhibition of pyruvate dehydrogenase (PDH) activity by promoting the expression of pyruvate dehydrogenase kinase (PDK1) (Kim et al., 2006) (Fig.1.6). By lowering Acetyl-CoA levels and decreasing the flux of substrates into the TCA cycle, substrate availability for ETC-mediated ATP synthesis is reduced. Thus, HIF-1α indirectly regulates the deceleration of the ETC. Indeed, HIF-1α induces the expression of NDUFA4L2, which downregulates complex I activity (Tello et al., 2011) and facilitates the expression of LON, a mitochondrial protease that degrades cytochrome c oxidase COX4-1 subunit. The action of LON facilitates the exchange of COX4-1 for the more efficient COX4-2, whose expression is also controlled by HIF-1α (Fukuda et al., 2007) (Fig.1.6). In addition, HIF-1α can directly translocate to mitochondria upon oxidative damage to downregulate the transcription of mitochondrial genes, further suppressing ETC activity (Li et al., 2019) (Fig.1.6).

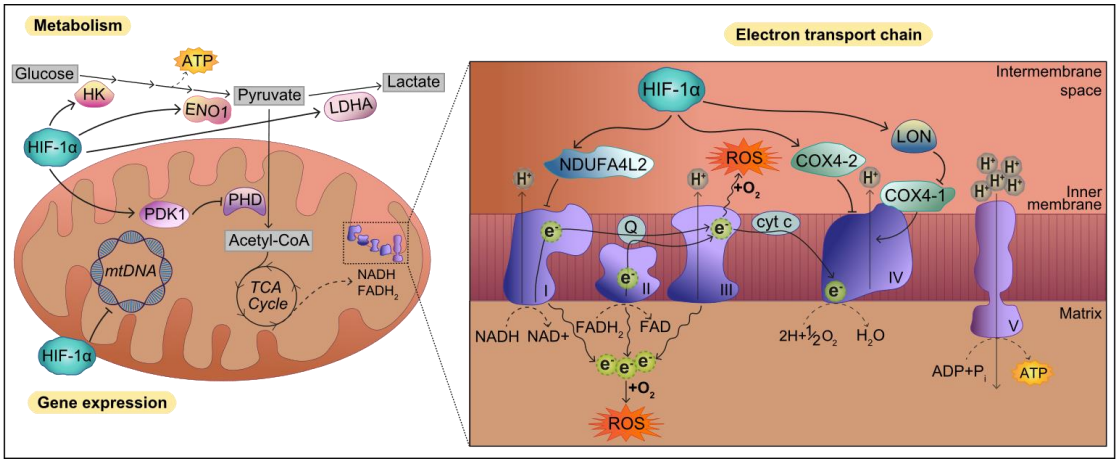

Figure 1.6. Influence of HIF-1α on mitochondrial energy and ROS production. Due to the limited oxygen availability under hypoxia, HIF-1α promotes alternative ATP synthesis via glycolysis by upregulating the expression of HK and ENO1, which facilitate the conversion of glucose in pyruvate. HIF-1α boosts lactate production from pyruvate by inducing LDH expression while blocking PHD-mediated lactate transformation in Acetyl-CoA through enhancing PDK1 expression. Consequently, the TCA cycle is slowed down and production of ETC substrates NADH and FADH2 is dampened. In order to attenuate ETC activity and reduce ROS, HIF-1α downregulates the activity of complex I by facilitating NDUFA4L2 expression. Additionally, HIF-1α promotes the expression of LON, a protease that degrades cytochrome c oxidase COX4-1 subunit, which is then substituted for COX4-2, whose expression is controlled by HIF-1α. To further diminish ETC activity, HIF-1α blocks mtDNA expression when recruited to mitochondria following oxidative stress damage. (Lestón Pinilla et al., 2021)

With mitochondria being the main cellular oxygen consumers, it is not surprising that HIF-1α controls every aspect of mitochondrial function in order to provide protection against hypoxia. In fact, HIF-1α ensures the preservation of energy production via a metabolic switch and maintains correct disposal of damaged mitochondria trough

induction of mitophagy, control of the fusion/ fission ratio and support of mitochondrial trafficking. Thus, HIF-1α upholds mitochondrial homeostasis, potentially allowing to bypass PD-related mitochondrial dysfunction. Nevertheless, more in-depth research into the mitochondrial role of HIF-1α in a PD context is needed.

1.4.3. Oxidative stress

Oxidative stress is caused by elevated levels of reactive oxygen species (ROS). ROS is an umbrella term describing a class of highly reactive molecules formed from O_2. They can be classified into non-radical, such as hydrogen peroxide (H_2O_2), and free radical species, such as superoxide anion radical ($O_2^{\cdot-}$), hydroxyl radical (·OH) and peroxyl radical (ROO·) (de Almeida et al., 2022). Intracellular ROS are mainly produced by the mitochondrial respiratory chain complexes, the cytochrome P-450 in the endoplasmic reticulum and several enzymes, in particular, NADPH oxidase and nitric oxide synthase (Finkel et al., 2012). ROS can be harmful at high levels due to their capacity to damage biomolecules and promote certain pathological processes (Fig.1.7). However, at lower concentrations, ROS have been found to be essential components of homeostatic signalling cascades by acting as second messengers (Sies et al., 2020). Redox homeostasis is also determined by the organism's antioxidant defence system comprising of antioxidant enzymes, transcription factors and non-enzymatic compounds that reduce ROS formation and counteract ROS-mediated damage (Pisoschi et al., 2015).

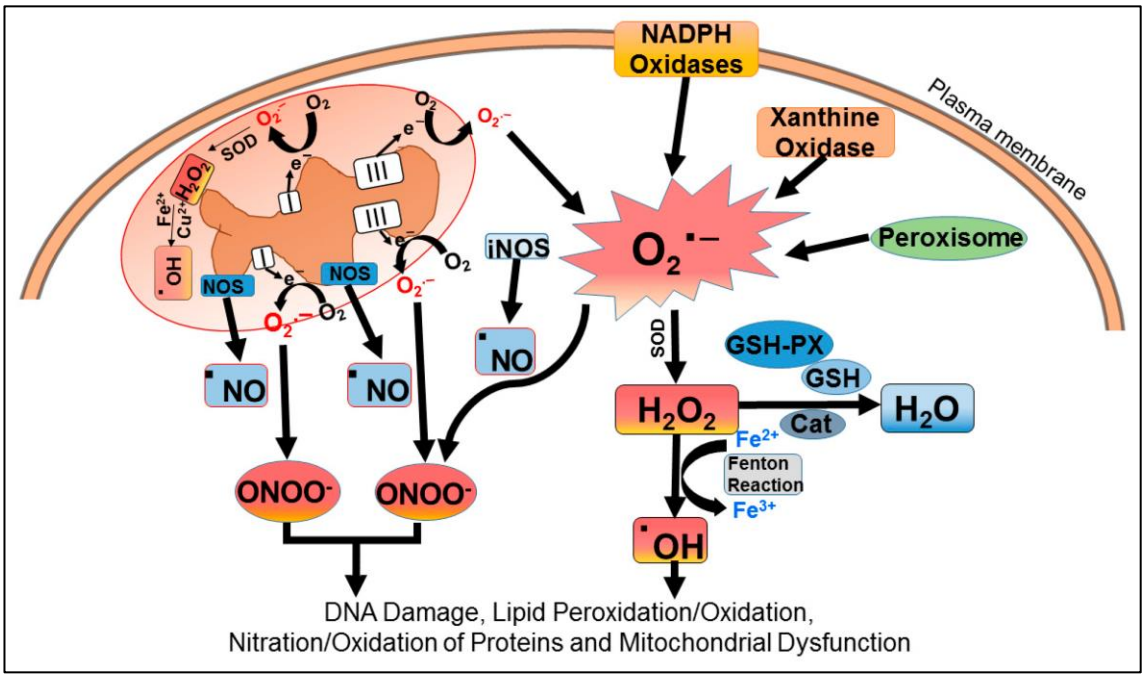

Figure 1.7. ROS production in the cell. ROS are generated in cells by both enzymatic and non-enzymatic redox reactions during normal and disease states. The first ROS generated is typically the superoxide anion ($O_2^{\bullet-}$), which is produced in mitochondria, the plasma membrane, peroxisomes, and the cytosol. Superoxide dismutase (SOD) transforms $O2^{\bullet-}$ to hydrogen peroxide (H_2O_2). H_2O_2 can then react with reduced transition metal ions, such as iron and copper, in a Fenton reaction to produce highly reactive hydroxyl radicals (OH•). In addition to ROS, cells also generate reactive nitrogen species (RNS), such as nitric oxide (•NO), peroxynitrite ($ONOO^-$), and nitrogen dioxide (•NO2). ROS and RNS can cause oxidative damage to DNA, lipids, proteins, and mitochondria. (Kaushal, 2019).

Accumulation of ROS is associated with increased SNpc DAergic neuron death in PD (Weng et al., 2018). Indeed, PD patients exhibit a widespread reduction of antioxidant defenses in the SNpc (Trist et al., 2019) and lower antioxidant protein levels in peripheral blood (Wei et al., 2018). DJ-1 is a major regulator of the antioxidant response, able to induce the expression of several antioxidant genes trough Nrf2 dependent and independent functions (Dolgacheva et al., 2019). Subsequently, PD-related DJ-1 mutants present reduced antioxidant activity and impaired interaction with the Nrf2/Keap1 pathway (Takahashi-Niki et al., 2004).

The specific role that ROS and antioxidants play in the regulation of HIF-1α remains unresolved with studies reporting divergent effects of redox mechanisms and molecules on HIF-1α homeostasis. Inhibition of mitochondrial activity was found to block HIF-1α stabilization during hypoxia, which led to the proposal of two models to explain this phenomenon. The ROS model establishes that a functional complex III of the mitochondrial ETC is required for hypoxia-dependent HIF-1α stabilization via ROS-mediated PHD inhibition or secondary signalling cascades (Guzy et al., 2005; Brunelle et al., 2005; Mansfield et al., 2005; Goyalet et al., 2004; Bell et al., 2007), while the O_2 availability theory proposes that mitochondrial O_2 consumption rate modulates HIF-1α protein levels by reducing the quantity of O_2 available for PHD enzymes to utilize (Hagen et al., 2003; Gong et al., 2005; Chua et al., 2010; Kumar et al., 2021).

In normoxia, ROS seem to be able to increase HIF-1α levels (Patten et al., 2010; Moonet al., 2010; Lee et al., 2016). Indeed, the HIF-1α promoter contains active binding sites for the ROS-responsive transcription factors NF-κB and Nrf2 (Bonello et al., 2007; Lacher et al., 2018). Interestingly, increased ROS due to DJ-1 loss create a pseudohypoxic environment that stabilizes HIF-1α (Foti et al., 2010b). ROS-mediated activation of certain signalling pathways, modulation of intracellular PHD cofactor concentrations, and oxidation of PHD bound Fe^{2+} can all lead to PHD inactivation, which will stabilize HIF-1α (Hayashi et al., 2019). However, ROS can inhibit HIF-1α accumulation when it's

stabilized by hypoxia or other factors (Huang et al., 1996; Callapina et al., 2005; Cattaneo et al., 2011; Jin et al., 2011; Badawi et al., 2012).

The results disparity across studies might be explained by the use of different cell lines, timepoints, intracellular O_2 gradients, oxidant compounds and ROS detection techniques. Nonetheless, it seems clear that the redox regulation of HIF-1α levels is determined by a variety of elements, including HIF-1α stabilization status by hypoxia or alternative factors and cell type.

HIF-1α counteracts ROS production through reorganization of oxygen consumption by the mitochondrial respiratory chain complexes, as well as by downregulating the expression of mtDNA-encoded mRNAs, as previously discussed. Therefore, HIF-1α-mediated control of ROS could prove to be beneficial for neuroprotection against aberrant oxidative stress present in PD.

1.5. PD RISK FACTORS AND HYPOXIC STRESS

Age is the predominant predisposing risk factor for PD (Collier et al., 2017). Whilst aging alone is not responsible for the significant increase in SNpc DAergic neuronal death, it causes reduced DA availability and α-Syn accumulation that contribute to the dysfunction of several pathways regulating protein degradation, oxidative stress and inflammation (Collier et al., 2017). Deregulation of these signalling cascades can be exacerbated by hypoxia via crosstalk with molecular aging mechanisms involving ULK1, AMPK or mTORC1 (Yeo, 2019). Indeed, advancing age is associated with cerebral hypoperfusion which reduces cerebral blood flow (CBF) potentially creating a permanent mild hypoxic state in the brain. Interestingly, the ability of cells to respond to hypoxia declines during aging. Impaired HIF-1α expression and stabilisation with a consequent decrease in HIF-1α target genes, accompanied by increased PHD levels was demonstrated by several independent studies in both human and murine aging tissues (Anderson et al., 2009; Frenkel-Denkberg et al., 1999; Hoenig et al., 2008; Kim, Hyungsoo et al., 2003; Ndubuizu et al., 2009). Of note, HIF-1α has been shown to have an anti-aging role in *C.elegans* (Mehta et al., 2009) and can induce the expression of human telomerase, which protects against cellular senescence (Nishi et al., 2004).

Exposure to pesticides, like rotenone or paraquat, or toxins such as MPTP is an extensively studied risk factor for PD (Hatcher et al., 2008). This has been attributed to their capacity to damage mitochondria by blocking the ETC and producing exacerbated

ROS along with their ability to suppress proteasome activity (Chen, Tingting et al., 2017). Indeed, both ROS production and UPS state can modulate HIF-1α state, as discussed previously. Furthermore, complex I inhibitors, including rotenone, are reported to impair HIF-1α stabilisation (Heinz et al., 2017). This could be attributed to the reduction in O_2 consumption within mitochondria due to ETC dysfunction, which elevates cytosolic O_2 levels. Together these mechanisms provide a potential link between hypoxia and PD pathogenesis.

Several other PD risks factors exist but exhibit weaker predictors of PD development. For example, obstructive sleep apnea (OSA) has been identified as predisposing factor for PD development, particularly in the elderly (Sun, A. et al., 2020). These patients exhibit increased levels of α-synuclein in their plasma (Sun, H. et al., 2019). Interestingly, OSA is characterized by repeated episodes of breathing impairment during sleep, which causes chronic intermittent hypoxia (CIH), a known inducer of oxidative stress in the SN (Snyder et al., 2017).

Traumatic brain injury (TBI), which causes regional brain H/I injury with concomitant neuronal death, is also associated with an increased risk of PD development (Gardner et al., 2018). The resultant hypoxia can accelerate the accumulation of protein aggregates, contributing to the chronic process of neurodegeneration. This evidence is supported by the identification of elevated α-Syn levels in cerebrospinal fluid and neuronal axons of TBI patients (Mondello et al., 2013; Uryu et al., 2007).

These physiological and molecular phenomena are of potential importance and further evaluation would help to understand whether CIH and H/I can contribute to the pathogenesis of PD.

1.6. EVIDENCE OF HYPOXIC INJURY IN THE PD BRAIN

Further indications that hypoxia may play a role in PD pathogenesis come from analysis of hypoxia related events in the PD brain. Chemodetection of systemic hypoxia and resultant initiation of a ventilatory adjustment (Onodera et al., 2000) alongside brain perfusion deficits exist in PD patients, resulting in a reduced oxygen supply to the brain (Lin et al., 2017). This could encourage a hypoxic brain environment that can be further depleted of oxygen due to the ventilatory dysfunction arising from reduced DAergic innervation of respiratory muscles in PD patients (Baille et al., 2018). Furthermore, SNpc

DAergic neurons have long arborized axons, are abundant in synapses and retain spontaneous activity to trigger DA release, features that require continuous energy input, making DAergic neurons especially susceptible to hypoxia which can compromise energy production (Surmeier et al., 2017). Although further research is needed, it appears that H/I events can trigger severe neuronal injury in the SN (Burke et al., 1992; Oo et al., 1995). Intriguingly, HIF-1α is involved in the development and survival of SNpc DAergic neurons via VEGF signaling (Milosevic et al., 2007) and can induce the expression of tyrosine hydroxylase (TH), the rate-limiting enzyme for DA synthesis, and the dopamine transporter (DAT), key proteins for DAergic neuronal function (Lim et al., 2015).

If hypoxia can influence PD pathogenesis, modulating HIF-1α activity could be essential as a neuroprotective strategy for DAergic survival. However, HIF-1α signaling appears attenuated in PD patients, as gene expression profiling analyses show reduced levels of HIF-1α and its target genes, including VEGF and HK, and upregulation of PHD2 in the SNpc of PD patients when compared to age-matched controls (Elstner et al., 2011; Grünblatt et al., 2004; Miller et al., 2006). Several factors could explain this impairment of HIF-1α activation and signaling. For example, the SNpc of PD patients exhibits elevated Fe^{2+} concentrations that contribute to DAergic neuron degeneration (Jiang, H. et al., 2017). Excess Fe^{2+} promotes PHDs activity, resulting in sustained HIF-1α degradation, which subsequently blocks HIF-1α-mediated expression of iron homeostasis genes such as transferrin, HO-1 and ferroportin (Peyssonnaux et al., 2008). Moreover, the protein levels of HIF-1α transcriptional inhibitor IPAS were increased in the SNpc DAergic neurons of sporadic PD patients (Kasai et al., 2015). As noted previously, several genetic mutations and disrupted signaling pathways characteristic of PD can block HIF-1α expression and its stabilization. This has wide ranging effects on HIF-1α mediated signaling in SNpc DAergic neurons and would, not least, functionally impact on parameters of iron homeostasis, antioxidant capacity, mitochondrial fitness, proteostasis and metabolic function.

Thus, insufficient oxygen supply in conjunction with an impaired capacity to trigger the systemic and cellular response to hypoxia may contribute to PD development.

1.7. HIF-1α-BASED THERAPEUTIC STRATEGIES FOR PD

Existing PD medications target DA deficiency in the SN by administering dopamine precursors, such as levodopa or L-DOPA, dopamine agonists or monoamine oxidase B (MAO-B) inhibitors, which block DA breakdown (Emamzadeh and Surguchov, 2018). Replacement of the lost DA can transiently mitigate PD motor symptoms although progression of the disease continues. Thus, the search for a definitive and effective PD cure is still ongoing. HIF-1α has gained recent attention as potential candidate due to its ability to influence DA production, iron metabolism, mitochondrial function, ROS generation and autophagy. Indeed, a growing number of studies are exploring direct and indirect PHD inhibitors, as well as other molecules that induce HIF-1α stabilization, as novel therapies to modulate aberrant pathways to treat PD.

1.7.1. Indirect PHD inhibitors

PHDs are indirectly blocked through iron deprivation. The widely used DFO can trigger iron depletion with consequent HIF-1α accumulation and has been shown to be protective against PD features in DAergic cells and PD murine models. In DAergic SH-SY5Y neuroblastoma cells, DFO treatment reduces apoptosis, oxidative stress and ATP loss triggered by 6-OHDA, a compound that selectively destroys DAergic neurons, whilst promoting autophagy through increased autophagolysosome formation and lysosomal enzyme expression (Bergström et al., 2012; Rakshit et al., 2020). DFO treatment also increases the autophagic flow via HIF-1α/Beclin-1, protecting SH-SY5Y cells from rotenone and MPP+, a toxic MPTP metabolite (Wu et al., 2010). In the 6-OHDA rat model, intranasal, local or systemic DFO administration has a widespread neuroprotective effect, promoting SN DAergic neuron survival, reducing DA loss in the striatum, controlling ROS production and improving motor behaviour (Dexter et al., 2011; Fine et al., 2014). Besides attenuating movement deficits, intranasally delivered DFO reduces α-synuclein aggregation in a α-synuclein rAAV rat model (Febbraro et al., 2013). Although the involvement of HIF-1α was not examined in these *in vivo* studies, DFO-mediated HIF-1α induction drives neuroprotection and motor improvement in a MPTP murine model, and thus HIF-1α is likely to play a role in other in vivo DFO treatment paradigms (Guo et al., 2016). Non-invasive intranasal DFO administration represents a promising approach to attenuate the loss of DAergic neurons as DFO readily crosses the blood brain barrier and arrives swiftly to the brain, reducing off-target effects.

Oral administration of M30, an iron chelator, also offers positive results, as it attenuated MPTP-mediated loss of striatal DA and its metabolites, increased TH expression and activity and diminished DAergic neuron death in mice (Gal et al., 2010). The neuroprotective role of M30 has been linked to its ability to promote HIF-1α-mediated expression of prosurvival genes (Kupershmidt et al., 2011). Similarly, the iron chelator Clioquinol (CQL) can also stabilize HIF-1α, providing protection against SN DAergic neuron loss caused by MPTP (Lee, D. W. et al., 2009). CQL reduces the formation of α-synuclein inclusions and protects against α-synuclein mediated cell death in the SN in transgenic mice expressing the α-synuclein hA53T mutation (Finkelstein et al., 2015). Additionally, CQL mitigates motor deficiencies in a MPTP-induced monkey model of PD. In this model, CQL decreases iron uptake via TfR and efflux through ferroportin while reducing ROS levels (Shi et al., 2020).

Lactoferrin (Lf), an iron-binding glycoprotein, mitigates MPTP-mediated DAergic neuronal damage and subsequent dyskinesia in mice through reductions in iron uptake and ROS production (Xu, S. et al., 2019). Lf elicits its neuroprotective function by upregulating HIF-1α, VEGF, and brain derived growth factor levels and modulating several signalling cascades. Furthermore, experiments performed in SH-SY5Y and MN9D cells showed that stabilization of HIF-1α via Lf was responsible for the induction of TH and several neuroprotective factors leading to increased neuronal viability against MPP+ toxicity. The non-competitive PHD inhibitor FG-0041 can induce HIF-1α stabilization in DAergic cells through iron chelation. FG-0041 induces DA synthesis and metabolism through induction of TH expression in PC12 cells and rat mesencephalic neurons as well as in vivo in the rat striatum (Bergström et al., 2012; Johansen et al., 2010; Witten et al., 2009). Furthermore, FG-0041 attenuates 6-OHDA-mediated dissipation of mitochondrial membrane potential and ATP depletion while preserving cell viability in PC12 cells (Johansen et al., 2010). Together, this data implicates PHD block via iron chelation and subsequently HIF-1α regulation as targets to enhance neuronal function and viability.

1.7.2. Competitive PHD inhibitors

Competitive PHD inhibition is achieved by directly blocking the interaction of PHDs with its cofactor 2-OG through 2-OG mimicking drugs. One of the first compounds identified was DMOG, which can ameliorate motor impairments and DAergic neuron death associate with parkinsonism caused by manganese toxicity in mice (Yang et al., 2016). Increased MPTP-mediated apoptosis of murine cortical neurons, in both WT and DJ-1

KO, can also be rescued by DMOG pretreatment via its ability to stabilise HIF-1α (Parsanejad et al., 2014). The anaemia drug FG-4592 inhibits PHDs and can able to protect against MPP+-induced apoptosis in SH-SY5Y cells through the restoration of mitochondrial membrane potential, oxygen consumption, ATP production and mitochondrial biogenesis. Similarly, MPP+-mediated autophagy blockade is alleviated by FG-4592 treatment, through a mechanism that enhances LC3-II levels. Furthermore, FG-4592 induces the expression of a range of antioxidant genes including Nrf2, HO-1 and superoxide dismutase, reducing MPP+-mediated ROS production. In MPTP-treated mice, FG-4592 administration restores striatal TH and DA content and preserves DAergic neurons in the SN, alleviating locomotor impairment (Li, X. et al., 2018). In addition, the 2-OG competitive drug JNJ-42041935 can induce HIF-1α stabilization and restore ATP loss provoked by 6-OHDA in SH-SY5Y cells (Bergström et al., 2012) (Bergström,2013). Similarly, IOX2, which can displace 2-OG from PHDs, supresses MPTP-induced iron accumulation and apoptosis and restores mitochondrial membrane potential in human iPSC-derived DAergic neurons. These processes depend on HIF-1α activity and ATP13A2 levels (Rajagopalan et al., 2016). This evidence further highlights how PHD inhibition has the potential to improve neuronal outcomes.

1.7.3. Atypical HIF-1α inducers

Several compounds have been shown to induce HIF-1α through different pathways other than PHD inhibition. In fact, the antiparasitic medication Albendazole (ABZ) promotes HIF-1α and VEGF mRNA expression and diminishes PHD transcription in the presence of rotenone in the rat SN. ABZ counteracts rotenone toxicity by reducing α-synuclein levels, inhibiting the expression of proinflammatory cytokines and enhancing DA synthesis. This ultimately results in reduced rotenone-mediated neuronal injury and motor dysfunction (Kandil et al., 2019) . Protection against rotenone-induced apoptosis is also provided via agmatine, a biogenic amine with neuromodulation properties, which has been shown to promote HIF-1α activation in differentiated SH-SY5Y cells. Additionally, Agmatine restores the loss of mitochondrial membrane potential provoked by rotenone, thereby reducing ROS levels (Ferlazzo et al., 2020). The hypertension drug hydralazine increases antioxidant capacity and SOD activity and minimizes 6-OHDA induced oxidative stress in SH-SY5Y cells while preserving TH and DAT expression and maintaining cell viability. Interestingly, through an undefined mechanism, Hydralazine can upregulate HIF-1α and VEGF protein levels (Mehrabani et al., 2020). Similarly, Orexin-A, a neuropeptide released by hypothalamic neurons, promotes HIF-1α

accumulation resulting in induction of downstream target genes VEGF and EPO. These are essential for Orexin-A mediated mitigation of apoptosis of SH-SY5Y cells triggered by MPP+ (Feng et al., 2014). The flavonoid Baicalein significantly improves motor performance of MPTP-treated mice. Of interest is that gene expression profiling studies show that Baicalein rescues the MPTP-mediated reduction of HIF-1α expression, triggering a neuroprotective effect in these mice (Gao et al., 2015).

Intriguingly, it appears that PHDs can be inhibited via alternative mechanisms. Upon MPP+ exposure, the hsp90-p23 chaperone complex interacts with PHD2, blocking its degradation. Thus, the p23 inhibitor gedunin reduces PHD2 stabilization, which protects N27 cells and human iPSC-derived DAergic neurons from MPP+-mediated cell death (Rane et al., 2018) . In addition, Adaptaquin (AQ), a selective inhibitor of HIF-PHDs through an unknown mechanism, maintains cell viability by inhibiting the Trip3 prodeath pathway triggered by either MPTP or 6-OHDA in PC12 cells and mice. Interestingly, AQ prevents 6-OHDA-mediated depletion of Parkin levels in PC12 cells. In a mouse model, AQ protected TH+ neurons and their projections to the striatum against 6-OHDA toxicity, thereby maintaining motor performance (Aimé et al., 2020). Therefore, a growing body of evidence exists that identifies modulation of PHD and HIF-1α can positively improve DAergic neuronal function and survival.

1.8. RESEARCH AIM

As discussed in the introduction, there are numerous links between PD and the hypoxia response. Thus, this project aims to elucidate the exact mechanisms underlying this association utilising neuronal SH-SY5Y and LUHMES cells and astrocytic U-87MG cells. Differences between cell types will be evaluated throughout the study to pinpoint neuronal-specific mechanisms and cell-dependent variations in the HIF-1α pathway. This investigation focuses on several key areas:

- To investigate further links between PD-related genes and HIF-1α/hypoxia, the gene expression and protein levels of genes associated with PD will be investigated using low O_2 and chemically induced HIF-1α stabilisation. This preliminary study will assess the potential link between HIF-1α/hypoxia and genetic PD, paving the way for further investigation.
- With the objective of clarifying the impact of PD-related pathway dysregulation on HIF-1α stabilisation, a variety of toxins and chemicals will be utilised to mimic mitochondrial dysfunction, impaired protein degradation and increased oxidative stress, hallmarks of the disease. The protein and mRNA levels of HIF-1α will be assessed under these circumstances to evaluate changes in its expression, stabilisation and degradation. This will serve as an initial investigation to determine whether disruption of cellular processes associated with PD can lead to deregulation of the HIF-1α pathway, which can lead to increased cellular susceptibility to low O_2.
- As HIF-1α inducers have been shown to prevent cytotoxicity in PD models, we will assay novel HIF-1α stabilising compounds to evaluate their neuroprotective effect in an *in vitro* neuronal PD model by evaluating parameters such as mitochondrial function and ROS levels using various techniques. This investigation will evaluate the therapeutic effect of HIF-1α stabilization, which holds promise for addressing the multifaceted nature of PD by targeting multiple pathways.
- We aim to characterise the role of HIF-1α in the NS and uncover potential novel targets in neurodegeneration by performing RNA profiling of neuronal cells exposed to HIF-1α stabilising drugs. By investigating the transcriptome, we intend to elucidate the specific pathways regulated by HIF-1α in the NS and explore their potential connection to PD pathogenesis..

CHAPTER II

MATERIALS AND METHODS

2.1.INTRODUCTION

The methods utilised in this investigation are described below, accompanied by relevant information on the materials used, including the company from which they were purchased and the product code. The tables detailing compounds, Western Blot gel composition, antibodies and primers utilised in this project can be found in the Supplementary information (SI).

2.2.CELL CULTURE

2.2.1. Maintenance of SH-SY5Y and U-87MG cell lines

SH-SY5Y neuroblastoma cells (94030304, ECACC) and U87-MG glioblastoma cells (89081402, ECACC) were cultured in DMEM/F-12 1:1 with 15 mM HEPES and 2 mM L-Glutamine media (LZBE12-719F, Lonza) supplemented with 5 % (v/v) Foetal Bovine Serum (FBS; 10500064, Thermo Fisher), 100 units/ml penicillin, 10 µg/ml streptomycin (17-603E, Lonza) and 1 % (v/v) Non-Essential Amino acids (NEAAS; 11140035, Thermo Fisher). SH-SY5Y expressing GFP-LC3 and mCherry-mitochondria were kindly gifted by Dr. Amanda Coutts and cultured in the previously described media. Cells were maintained at 37°C in an incubator with a humidified atmosphere of 95 % air and 5 % CO_2. Cells were passaged by trypsinisation once the cells reached 70-80% confluence. Briefly, the medium in the flask was discarded and cells were carefully washed with Dulbecco's phosphate buffered saline without Ca^{2+} and Mg^{2+} (PBS; 14190144, Fisher). Cells were then incubated with 250 µg/ml trypsin (11609970; Fisher) diluted in PBS for 5 minutes at 37ºC. The trypsin was inactivated by adding supplemented media and cells were harvested by centrifugation at 300g for 5 minutes. The pellet was resuspended in fresh complete media and transferred to a new flask.

2.2.2. Differentiation of SH-SY5Y cells

SH-SY5Y were plated at a density of 6900 cells/cm^2 and incubated overnight in complete medium. Then, media was aspirated and replaced with differentiation media containing 0.5% (v/v) FBS, 1% (v/v) NEAAS, 100 units/ml penicillin, 10 µg/ml streptomycin and 10 µM all trans-retinoic acid (RA; R2625, Merck) in DMEM/F-12 media, which was replaced every 2 days. Cells were cultured for 5 days in differentiation media with RA or grown with RA for 5 days followed by 50 ng/ml Brain derived growth factor (BDNF; 450-02, Peprotech) for 3 days. Cells were exposed to treatments after the described differentiation periods.

2.2.3. Maintenance of LUHMES cell line

LUHMES cells (CRL-2927, ATCC) were cultured in Advanced DMEM/F12 media (12634010, Fisher) with 2 mM L-glutamine (35050087, Thermo Fisher), 1 % (v/v) N-2 supplement (11520536, Thermo Fisher Scientific) and freshly added 40 ng/ml basic recombinant human Fibroblast Growth Factor (233-FB-025, Bio-Techne). Culture flasks were pre-coated with 50 µg/mL poly-L-ornithine (P3655, Merck) and 1 µg/mL human fibronectin (F0895, Merck) for 3h at 37°C before plating. LUHMES cells were maintained at 37°C in an incubator with a humidified atmosphere of 95 % air and 5 % CO_2. For passaging, the medium was removed and the cell monolayer was washed with PBS after the addition of pre-warmed Trypsin-EDTA 0.05% (25300054, Thermo Fisher Scientific) diluted 1:1 in PBS. The cells were incubated for 3 minutes at 37ºC and once the cells were detached, supplemented LUHMES media was added and cells were collected for centrifugation at 200g for 5 minutes. The pellet was resuspended in fresh complete LUHMES media and transferred to a new pre-coated flask.

2.2.4. Differentiation of LUHMES cells

For standard differentiation as previously described (Scholz, 2011), LUHMES were seeded into standard LUHMES media for 24h in poly-L-ornithine/fibronectin pre-coated flasks and then changed to differentiation media, consisting of Advanced Dulbecco's modified Eagle's medium/F-12, 2mM L-glutamine, 1 % (v/v) N-2 supplement, 1 mM N6,2′-O-Dibutyryladenosine 3′,5′-cyclic monophosphate sodium salt (cAMP; D0627, Merck), 1 µg/mL tetracycline (T7660, Merck) and 2 ng/mL recombinant human Glial Cell Derived Neurotrophic Factor (GDNF; 450-10, Peprotech). After 2 days, cells were trypsinized and seeded into poly-L-ornithine/fibronectin pre-coated multi-well plates with fresh differentiation media and cultivated for 3 days. Cells were treated at day 5 of differentiation.

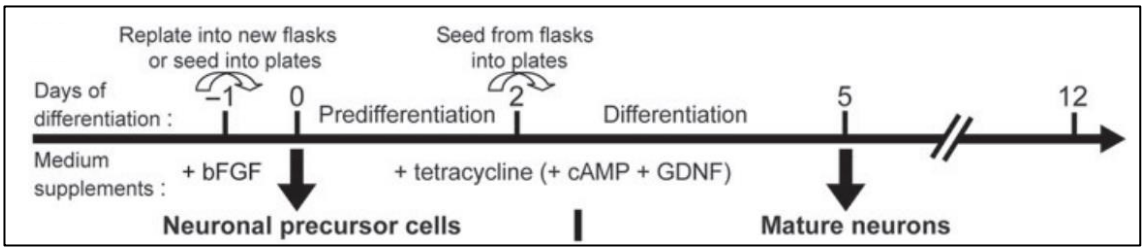

Figure 2.1. Differentiation protocol for LUHMES cells. Scheme representing the 2-step differentiation protocol of LUHMES to post-mitotic mature neurons (Scholz et al., 2011).

2.2.5. Cell counting

In order to estimate the number of cells present on a suspension, cells are diluted 1:10 and counted using a haemocytometer (BR717805-1EA, Sigma-Aldrich). Cell density was calculated as $Cells/ml = Average\ cell\ count\ (1\ mm^2) \times 10^4 \times dilution\ factor$.

2.2.6. Cryopreservation and thawing

For long term cell storage, cells were frozen in liquid nitrogen. The subculturing process for the specific cell lines was performed until centrifugation as described in sections 2.1.1.1 and 2.1.1.3. The pellets for SH-SY5Y and U-87MG cell lines were resuspended in 1 ml of ice-cold freezing media containing complete DMEM/F-12 media supplemented with 10% (v/v) dimethyl sulfoxide (DMSO; D2650, Merck). LUHMES pellets were resuspended in complete LUHMES growth medium supplemented with 20% FBS and 10% (v/v) DMSO. Cell suspensions were transferred to cryogenic vials, which were pre-cooled at -80ºC for 48 hours and subsequently stored in liquid nitrogen tanks.

For the recovery of cells after freezing, cryovials containing preserved cells were removed from liquid nitrogen storage and thawed in a 37°C water bath before being transferred dropwise to a sterile tube containing the growth media specific for each cell line. Then, cell suspensions were centrifuged and transferred to flasks containing fresh supplemented media as described in sections 2.1.1.1 and 2.1.1.3.

2.2.7. Mycoplasma testing

Testing for mycoplasma was carried out every 3 months and immediately after thawing a new cell vial using the Mycostrip Detection Assay (rep-mys-20, Invivogen), which is based on an isothermal polymerase chain reaction (PCR), according to manufacturer's instructions. Briefly, 1 ml of cell culture supernatant was added to a sterile tube and centrifuged at 16000g for 5 minutes. The supernatant was carefully discarded and the pellet was resuspended in PBS. To set up the reaction, 5 µl of prepared sample were mixed with 5 µl of reaction buffer and 15 µl of reaction mix. The tubes were incubated at 65ºC for 40 minutes with a heat block before the addition of 200 µl of migration buffer. The processed samples are pipetted into the cassette containing the detection strip. Results were compared to the positive control included in the experiment.

2.2.8. Treatments

Hypoxic treatment was performed in an incubator maintained with 1 % O_2, 5 % CO_2 and 94% N_2 (MCO-170M, PHCbi). Chemicals utilised for cell treatment are detailed in SI Table 8.1.

2.3 CELLULAR VIABILITY AND METABOLISM ASSESSMENT

2.3.1. Cell confluence analysis

The Incucyte S3 live-cell analysis system (Sartorius) was used to measure cell confluence, interpreted as an indicator of cytotoxicity, in the presence of several compounds. SH-SY5Y and U-87MG cells were cultured in 96-well plates and treated as indicated for each experiment. After treatment, plates were introduced in the Incucyte S3 system. Phase contrast images were acquired automatically every 4 hours for up to 72 hours using the 10X objective and analysed using the Incucyte software package to measure cell confluence. Results were normalised to the first timepoint.

2.3.2. Caspase-3/7 activation assay

Activation of executioner caspases 3 and 7 is a hallmark of apoptotic cell death and thus indicates a reduction in cell viability. Caspase-dependent apoptosis was detected using the Incucyte Caspase-3/7 Red dye for Apoptosis (4704, Sartorius), which couples the activated caspase-3/7 recognition motif to a DNA intercalating dye to enable quantification of apoptosis over time, as cleavage of the dye by Caspase-3/7 stains nuclear DNA. In this assay, cells were seeded at a density of 5000 cells per well in a 96-well plate and grown for to obtain a ~50% confluency. Treatments were prepared in DMEM/F-12 complete media containing 0.5 µM Caspase-3/7 Red Dye and added to the plate. The plate was placed in the Incucyte S3 live-cell analysis system (Sartorius) to monitor cell growth and apoptosis using phase contrast and red fluorescent channels respectively. The Incucyte system was programmed to acquire images with the 10X objective every 2 hours for a total of 72 hours. Each sample was assayed in triplicate. Kinetic activation of caspase-3/7 was quantified using the Incucyte integrated software analysis tools and normalised to the first timepoint and phase cell confluence.

2.3.3. Neurite length analysis

Maintenance of neurite extension is closely linked to neuronal health. The Incucyte S3 live-cell analysis system (Sartorius) was used to obtain phase contrast images of 96-well

plates containing treated SH-SY5Y cells as described in section 2.1.2.1. These images were analysed with the Incucyte Neurotrack Analysis Software Module (Cat. No. 9600-0010), which masks the images to quantify neurite length measured as average μm.

2.3.4. MTT reduction assay

The rate of cellular metabolic activity was determined using a MTT colorimetric assay. In this assay, NAD(P)H-dependent oxidoreductases in metabolically active cells catalyse the formation of purple formazan crystals from the yellow tetrazolium salt (3-(4,5-dimethylthiazol-2-yl)-2,5-diphenyltetrazolium bromide (MTT). Cells were plated at 5.000 cells per well in 96 well plates and treated. After treatment exposure, the cell medium was replaced with a 0.5 mg/ml MTT (M2128, Merck) solution in supplemented DMEM/F12, except for a set of cells used as blanks. Plates were incubated at 37ºC in a humidified atmosphere of 95% air and 5% CO_2 for 90 minutes. The medium was removed from the wells, whereupon DMSO was added to each well to solubilise the formazan product. Plates were placed on a plate shaker for 5 minutes to dissolve the formazan product. Absorbance was read at 570 nm with a CLARIOSTAR plate reader (BMG Labtech).

2.4. QUANTIFICATION OF PROTEIN LEVELS

2.4.1. Immunofluorescence

HIF-1α accumulation and location in SH-SY5Y cells exposed to $CoCl_2$ was evaluated by immunofluorescence (IF). In this protocol, SH-SY5Y cells were plated onto glass coverslips in 6-well plates at a density of $1x10^5$ cells/well. After 24 hours, the cells are washed with PBS and fixed with ice-cold 90% (v/v) Methanol (320390, Merck) in TBS at -20ºC for 20 minutes. The cells were rinsed with PBS three times and permeabilised with a solution of 0.5% Triton X-100 (T8787, Merck) in PBS for 5 minutes at room temperature. The cells were then washed with 0.0025% PBS/Tween-20 (10485733, Fisher Scientific) and incubated overnight with the primary antibody to HIF-1α (ab255733, Abcam) prepared at a 1:100 dilution in 0.0025% PBS/Tween-20. The coverslips are washed with 0.0025% PBS/Tween-20 and incubated with the secondary antibody (Donkey anti-Rabbit IgG Secondary Antibody, Alexa Fluor 488; A-21206, Invitrogen) prepared at a 1:250 dilution in 0.0025% PBS/Tween-20 for 1 hour at room temperature. The coverslips are washed again and mounted on microscope slides with anti-fade mounting medium with DAPI (Abcam, ab104139). The coverslips were sealed with

transparent varnish and stored at 4ºC until imaging. Slides were imaged using a Leica THUNDER Imager Live Cell & 3D Assay inverted fluorescence microscope (Leica Microsystems) with 100X oil immersion lens.

2.4.2. Preparation of cell lysates for Western Blot

Cells were plated at a density of $0.5x10^6$ cells in 6-well plates and treated with the selected treatments. To avoid protein degradation, cells were washed with PBS and quickly lysed with a cell scraper in 50 µl of ice-cold radio immunoprecipitation assay (RIPA) buffer (R0278, Merck) supplemented with 1X protease (SKU: 42506, Expedeon) and phosphatase (78420, Thermo Fisher Scientific) inhibitors. Then, the samples were vortexed, incubated on ice for 15 mins and subsequently centrifugated at 16000g for 20 mins. The supernatant was collected and stored at -20°C until needed.

2.4.3. Subcellular fractionation for mitochondrial protein extraction

The Mitochondria Isolation Kit for Cultured Cells (89874, Thermo Fisher Scientific) was utilised according to the manufacturers protocol to obtain pure fractions of mitochondrial proteins. Briefly, $2.5x10^7$ cells were harvested by centrifugation at 850g for 2 minutes. The supernatant was discarded and 800 µl of Mitochondria Isolation Reagent A supplemented with proteasome inhibitors were added. The mixture was vortexed and incubated in ice for 2 minutes and 10 µl of Mitochondria Isolation Reagent B were after added to the suspension, which was quickly vortexed at maximum speed and incubated on ice for 5 minutes. Then, 800 µl of Mitochondria Isolation Reagent C with protease inhibitors was added to the sample, which was mixed by tube inversion and centrifuged at 700g for 10 minutes at 4°C. The supernatant was transferred to a new tube and centrifuged at 3000g for 15 minutes at 4°C. 500 µl of Mitochondria Isolation Reagent C with protease inhibitors were added to the tube containing the isolated mitochondria, which was centrifuged at 12000g for 5 minutes. The supernatant was removed, and the pellet was kept on ice until further processing following the protocol detailed in section 2.1.3.2.

2.4.4. Total protein quantification with Bicinchoninic Acid

Total protein quantification of samples was carried out utilising the colorimetric Bicinchoninic Acid (BCA) Kit for Protein Determination (BCA1, Merck) following manufacturer's instructions. Firstly, the BCA mix was prepared by making a 1:50 solution

of Cu (II) Sulfate pentahydrate and BCA reagent. The samples were diluted 1:10. Then, the BCA solution was mixed with the Bovine Serum Albumin (BSA) (A9418, Merck) protein standards (0-1 mg/ml) and samples on a 1:8 proportion. 20 µl of the processed samples and standards was added to a 96-well plate in duplicate and subsequently incubated at 37ºC for 30 minutes. Absorbance was read at 565 nm with a CLARIOSTAR plate reader (BMG Labtech). Protein concentration was estimated from a linear standard curve created with the BSA standards.

2.4.5. Western Blotting

Western blotting is a method for detecting proteins in a sample. It involves separating proteins by size on a gel, transferring them to a nitrocellulose membrane, and then probing the membrane with antibodies that bind to the protein of interest. Previously isolated cellular protein lysates (25 to 50 µg) were mixed in a 1:1 ratio with Laemmli 2× Buffer and boiled on a block heater for 5 minutes at 65 ºC to denaturalise the proteins. The samples were loaded in equal amounts alongside 2 µl of the protein ladder (1610374, Bio-Rad) and separated by size on sodium dodecyl sulphate polyacrylamide gels (SDS-PAGE) of varied percentages according to protein size (SI Table 8.2 and 8.3). Gels were run in a Mini-PROTEAN Tetra Vertical Electrophoresis Cell (1658005, Bio-Rad) and PowerPac Basic Power Supply system (1645050, Bio-Rad) using a Tris-glycine SDS-PAGE running buffer composed of 25mM Tris (B2005, Melford Laboratories Ltd.), 192mM glycine (A13816.36, Thermo Fisher Scientific) and 0.1 % (w/v) Sodium dodecyl sulfate (SDS; 436143, Merck) at 180V for 1 hour at room temperature. Following electrophoresis, the proteins were transferred to nitrocellulose membranes by semi-dry transfer using the Trans-Blot Turbo RTA Mini 0.2 µm Nitrocellulose Transfer Kit (1704270, Bio-Rad) and Trans-Blot Turbo Transfer System (1704150, Bio-Rad). Transfer success was evaluated by staining the membrane with Ponceau S (P7170, Merck), which was removed with 12mM NaOH. Membranes were blocked with a 3 % (w/v) skimmed milk powder solution prepared in 0.1% (v/v) TBS/Tween 20 at room temperature for 1 hour and then incubated with the primary antibody (SI Table 8.4) diluted in TBS/Tween overnight at 4°C. This was followed by three washes with TBS/Tween and an incubation with the secondary antibody (SI Table 8.5) for 2 h at room temperature. After washing the membranes three times with TBS/Tween, these were incubated for 1 minutes with an enhanced chemiluminescence (ECL) substrate solution (K1-0170, Geneflow) and chemiluminescence images were captured by an ImageQuant LAS 4000 (GE healthcare). Densitometric analysis was performed using the Image Studio Lite software version 5.2

(Licor). Using the rectangle tool, a region encompassing the first band of each image was selected. The remaining bands were then highlighted, using the same the shape and size of the predefined rectangle. The signal for every protein of interest was corrected for background defined as a clear portion of the membrane and normalised against a housekeeping protein within its lane (α-Tubulin or β-Actin).

2.4.6. Stripping and Reprobing Western Blotting Membranes

Previously immunoprobed blots kept at 4ºC were washed with TBS/Tween and incubated with Restore PLUS Western Blot Stripping Buffer (46430, Thermo Fisher Scientific) for 10 minutes at room temperature. The stripping buffer was removed, and the membrane was washed again with TBS/Tween. The membrane was then blocked and immunoprobed as described in section 2.1.3.5.

2.4.7. Protein quantification with Proteome arrays

The proteome profiler antibody arrays were utilised to quantify relative levels of more than 25 proteins on a singles experiment by utilising nitrocellulose membranes that contain capture and control antibodies spotted in duplicate. The arrays utilised were the Human Apoptosis Array Kit (ARY009, R&D Systems) and the Human Cell Stress Array Kit (ARY018, R&D Systems). To commence the assay, cell lysates were obtained by rinsing the cells with PBS and solubilising the cells at $1x10^7$ cells/ml by scraping with lysis buffer. The suspension is transferred to a tube that was kept on ice for 30 minutes. The samples were then centrifuged at 14000g for 5 minutes and the proteins present in the supernatant were quantified by BCA Assay as indicated in section 2.1.3.4. The array procedure starts by blocking the provided membranes with Array Buffer 1 for 1 hour. The samples are then prepared by adding a volume containing 300 µg of protein per sample to a final volume of 1.5ml of Array Buffer 1. Prepared samples are then added to the arrays and incubated overnight at 4°C on a rocking platform shaker. The arrays were washed with Wash Buffer three times and then incubated with reconstituted detection antibody cocktail for 1 hour while shaking. The arrays where then washed and incubated with streptavidin-HRP for 30 minutes. After rinsing, the membranes were submerged in the Chemo Reagent mix for 1 minute. The arrays were subsequently images with the ImageQuant LAS 4000 (GE healthcare). Densitometric analysis was carried out using the Image Studio Lite software version 5.2 (Licor). Pixel density was analysed for each duplicate pair of spots in the array representing a protein, averaged and corrected for

background with negative control spots. The signals of different arrays were compared to evaluate changes in protein levels between samples.

2.5.ANALYSIS OF GENE EXPRESSION

2.5.1. RNA isolation

Cells were lysed and RNA was extracted with the GenElute Mammalian Total RNA Miniprep Kit (RTN70, Sigma-Aldrich) according to manufacturer's instructions. Firstly, the lysis solution provided was added directly to the cells to avoid loss of HIF-1α. The solution was incubated for 2 minutes., collected, and filtered through a filtration column. An equal volume of 70% ethanol solution was added to the filtered lysate, and the mixture was mixed thoroughly. A binding column was assembled, and the lysate/ethanol mixture was pipetted onto the column. The column was centrifuged and subjected to three consecutive washing steps. If the sample was to be used for Nanostring analysis, an on-column DNAse I digestion (DNASE10, Sigma-Aldrich) was performed before the washes as per manufacturer's protocol. The column was then centrifuged to remove any residual wash solution. Finally, elution solution was pipetted into the binding column, and the column was centrifuged. The purified RNA was collected in the flow-through eluate and was immediately stored on ice for subsequent use or kept at -70ºC until needed. The concentration and quality of the RNA obtained was determined by spectrophotometry using the Nanodrop 8000 spectrophotometer (Thermo Fisher Scientific).

2.5.2. Real time quantitative real-time polymerase chain reaction

The real time quantitative real-time polymerase chain reaction (qRT-PCR) was used to quantify gene expression. This experiment was performed with the iTaq Universal SYBR Green One-Step Kit (1725150, Bio-Rad) using 0.5 µg RNA as input and 0.25 µM of forward and reverse primers, which are mixed with 5 µl of the reaction mix and 0.25 µl of iScript reverse transcriptase for a final volume of 10 µl. The RT-qPCR reaction was prepared in duplicates on PCR plates (E1403-7700; Starlab) sealed with an adhesive sheet (AB-0558, Thermo Fisher Scientific). The plate was placed in the QuantStudio™ 5 Real-Time PCR System (Applied Biosystems) and was set to run at nicotinamide adenine dinucleotide 50°C for 10 min for the reverse transcription reaction, then at 95°C for 5 min followed by 40 cycles of 95°C for 30 s, Tm °C for 30 s and 72°C for 1 min, with a final extension of 72°C for 10 min. Variations in RNA expression were monitored using the $2^{-\Delta\Delta Ct}$ method (Rao et al., 2013), and *BACT* was used as the internal control. Primer sequences were obtained from PrimerBank (https://pga.mgh.harvard.edu/primerbank/)

and evaluated with the PCR primer stats tool (http://www.bioinformatics.org/sms2/pcr_primer_stats.html). Primer sequences and their melting temperatures (Tm) can be found in SI Table 8.6.

2.5.3. Gene expression profiling using the Nanostring technology

The nCounter Analysis System with a specific human Neuropathology Panel (115000200, Nanostring Technologies) was utilised to evaluate the expression of over 700 gene targets involved in NS homeostasis. This is achieved by hybridization of target RNA to fluorescent gene-specific probes coupled with subsequent high-throughput analysis. The protocol was followed as suggested by the manufacturer. Briefly, 100 ng of RNA extracted as previously described in section 2.1.4.1 were added to a PCR tube containing 8 µl of a mix of hybridisation buffer and the Reporter CodeSet. 8 µl from the the Capture ProbeSet solution were added just before the tube was placed in a thermal cycle at 65ºC for 20 hours to induce probe hybridisation. The nCounter Prep station liquid-handling robot was used to carry out post-hybridization processing. Excess probes were removed, and stable probe/target complexes were aligned and immobilized in the nCounter cartridge. The cartridge was then placed in the nCounter Digital Analyzer for image acquisition and data processing. This process generates a reporter code count file (RCC) for each lane, which contains the target molecule counts acquired by imaging and can be loaded, alongside the reporter library files (RLF), which contain the information to link fluorescent barcodes to specific genes, into the NanoString nSolver v 4.0 software (Nanostring Technologies) for analysis. The software was used to assess quality control parameters, quantify the raw counts for each transcript, and normalize the data using predetermined software settings. Normalized counts were transformed to the logarithmic scale to facilitate the interpretation of results. The results obtained were validated by RT-qPCR and Western blot as described in sections 2.1.4.2. and 2.1.3.5 respectively.

To identify pathways enriched in the samples utilised, a list of genes of interest was loaded into the Enrich platform (https://maayanlab.cloud/Enrichr/), which provides an overview of databases that encompass enrichments in pathways, ontologies, diseases and cell types. Gene Ontology biological processes identified using Enrichr were ranked by adjusted p-value and the top 50 were selected. Due to high levels of redundancy between these Gene Ontology terms, this list was curated with the REVIGO platform (http://revigo.irb.hr/), which summarises lists of repetitive GO terms (Supek et al., 2011). This step grouped closely related pathways into main representative pathways, as shown

in SI Table 8.7. Additionally, the NanoString panel has its own system for clustering the genes into different pathways. Therefore, when presenting data, both pathway classifications were considered, as described in SI Table 8.8.

2.6.EVALUATION OF MITOCHONDRIAL HOMEOSTASIS

2.6.1. Bioluminescent detection of ATP

Bioluminescent detection of cellular ATP levels was performed using the Vialight Plus kit (LT07-221, Lonza) as per the manufacturer's instructions. To measure cellular ATP levels, cells were seeded in a 96-well plate and treated for 24 or 48 hours. Samples were assayed in triplicate. The cells were then washed with 100 µL of serum-free DMEM/F-12 media, followed by the addition of 50 µL of serum-free DMEM/F-12 media and 25 µL of lysis reagent. The mixture was incubated for 10 minutes, and 50 µL aliquots of the cell lysate were transferred to a white-walled luminescence 96-well plate. 50 µL of ATP monitoring reagent plus was added to each well to generate luminescence, which was read after a 2-minute incubation using a CLARIOSTAR plate reader. (BMG Labtech). Results were normalized to cell confluence, as calculated from images of the plate used for ATP detection taken with the Incucyte S3 system (Sartorious) before the assay.

2.6.2. JC-1 staining

To visualize and quantify changes in mitochondrial membrane potential, cells were treated for the indicated time and then incubated with 30 µM JC-1((5′,6,6′-tetrachloro-1,1′,3,3′-tetraethylbenzimidazolylcarbocyanine iodide; CAY15003-5, Cayman Chemical) in DMEM/F-12 phenol red free supplemented media (21041025, Thermo Fisher Scientific) for 30 minutes. Cells were then washed twice with PBS and imaged in both red and green fluorescent channels using the Incucyte S3 system (Sartorious). JC-1 is a fluorescent dye that accumulates in the mitochondria and changes colour depending on the mitochondrial membrane potential, forming red aggregates or green monomers at high and low mitochondrial potentials respectively. In this experiment, mitochondrial membrane potential is measured as ratio of red aggregates to red aggregates of the fluorescent probe JC-1 based on the images taken with the Incucyte S3 system.

2.6.3. Evaluation of mitochondrial morphology by fluorescent microscopy

SH-SY5Y stably expressing mitochondria tagged with mCherry were utilised to investigate mitochondrial morphology. The cells were prepared for imaging as outlined in section 2.1.3.1, but addition of antibodies was omitted. Images were acquired with the

Leica THUNDER Imager Live Cell & 3D Assay inverted fluorescence microscope (Leica Microsystems) using the 100X oil immersion objective. Analysis of mitochondrial morphology was carried out using the ImageJ/Fiji software version 1.53t as previously described (Chaudhry et al., 2020). Briefly, images were loaded to the software and split into fluorescent channels to obtain images containing only the mitochondria. As outlined in the cited protocol, a series of background subtractions and filters are applied to obtain a clear image of the mitochondrial network and minimise noise. After applying the relevant modifications, the values of mitochondrial area, perimeter, aspect ratio and circularity were obtained with the "Analyse particles" plugin. A total of 21 images were analysed from three independent experiments, with 7 randomly selected images quantified from each repeat.

2.7.OXIDATIVE STRESS MEASUREMENT

2.7.1. Quantification of ROS levels

Measurement of ROS production was achieved with the 2′,7′-Dichlorofluorescin diacetate (2′,7′-DCFDA) fluorescent probe (D6883, Merck). Cells were seeded at a density of 5000 cells per well in 96-well plates in triplicates and treated as indicated. After 24 h, the media was removed and replaced with DMEM/F-12 Phenol-Red free supplemented with FBS, P/S and NEAAS containing 25 µM 2′,7′-DCFDA. Cells were incubated at 37ºC in a humidified atmosphere of 95% air, 5% CO2 for 30 min. The solution was aspirated and replaced with DMEM/F-12 Phenol-Red free growth media. Fluorescence was measured with the Incucyte S3 system (Sartorius) and normalised to phase cell confluence.

2.7.2. Total reduced Glutathione (GSH) determination

Total cellular GSH levels were estimated using a commercially available glutathione fluorometric kit (CS1020, Merck). Following treatment cells were mechanically detached, centrifuged at 300g for 5 minutes and then washed with PBS. After the cells were pelleted, they were incubated with lysis buffer for 15 minutes on ice, then centrifuged at 16000g for 5 minutes and the supernatant collected. Standards (1.3-10 nM GSH) and samples were then pipetted into a 96-well plate with 82.5 µl of assay buffer. Glutathione S-transferase (5 µl) and substrate solution (2.5 µl) were added to start the reaction. The plate was then incubated at 37°C for 1 hour. Fluorescence was measured at an excitation wavelength of 390 nm and emission wavelength of 480 nm with a CLARIOSTAR plate reader (BMG Labtech). Experiments were performed in

quadruplicate and the results were expressed as GSH nmoles per µg of protein. The BCA assay was utilised to quantify the protein content of samples as described in section 2.1.3.4.

2.8. Evaluation of autophagy

SH-SY5Y stably expressing the autophagy-related LC3 protein tagged with GFP were utilised to investigate autophagy activation. To this effect, fluorescent green channel and phase contrast images were acquired automatically with the Incucyte S3 system (Sartorious) every 4 hours for up to 72 hours using the 20X objective. The images acquired were analysed using the Incucyte software package to quantify green fluorescence and cell confluence. Elevated autophagy was measured as increased green fluorescence produced by GFP-LC3 normalised to the initial timepoint and to phase confluence.

2.9. PROTEASOME ACTIVITY ASSESSMENT

2.9.1. Preparation of proteasome extracts

Lysates were prepared by mechanically detaching cells into growth media and centrifuging at 300g for 5 minutes to harvest them. The supernatant was discarded, and the pellet was resuspended in ice-cold PBS and centrifuged at 300g at 4°C for 5 minutes before resuspension in ice-cold homogenization buffer composed by 20 mM Tris/HCl, (pH 7.2), 0.1 mM EDTA (E6758, Merck), 1 mM 2-mercaptoethanol (M6250, Merck), 5 mM ATP (A3377, Merck), 20% (v/v) glycerol and 0.4% (v/v) Igepal CA-630 (I8896, Merck). Samples were vortexed thoroughly for 30 seconds followed by centrifugation at 14000g for 2 minutes at 4°C. The resultant supernatant was transferred to a fresh tube and assayed for protein concentration.

2.9.2. Protein quantification with the Bio-Rad assay

The Bio-Rad Protein Assay (5000001, Bio-Rad) was performed as per the manufacturer's instructions to estimate protein concentration in proteasome extracts. Samples were diluted 10-fold in H_2O and BSA standards were prepared at concentrations from 0 to 25 µg/ml. 200 µl of Bio-Rad solution were added to each standard and sample tube, and the tubes were vortexed. Triplicates of 100 µl from each tube were pipetted into a 96-well plate, and the absorbance was read at 595 nm with a CLARIOSTAR plate reader (BMG

Labtech). Protein concentration was inferred from a linear standard curve prepared with BSA standards.

2.9.3. Proteasome activity assay

To set up the proteasome activity assay, 10 µl of lysate aliquots were incubated at 37°C with 50 µM 20S proteasome fluorogenic substrate for chymotrypsin-like activity for the 20S proteasome named Suc-Leu-Leu-Val-Tyr-7-amido-4-methylcoumarin (BML-P802, Enzo Life Sciences) in assay buffer containing 50 mM HEPES (H3375, Merck), pH 8.0 and 5 mM EGTA (324626, Merck). Using the CLARIOSTAR plate reader (BMG Labtech), readings were taken every 5 minutes for 1 hour at excitation and emission wavelengths of 360 nm and 465 nm, respectively. The line of best fit by the least squares method was used to calculate the change in fluorescence. The experiment was performed in triplicates, and the results were reported as the change in fluorescence units per minute per µg of protein. The Bio-Rad protein assay was used to estimate protein concentration, as described in section 2.1.8.2.

2.10. Cell cycle analysis

This method uses the fluorescent nucleic acid dye propidium iodide (PI) to identify the proportion of cells in each stage of the cell cycle. Firstly, the cells were gently detached with a scraper into growth media, collected and spun at 300g for 5 minutes at 4°C. The cell pellet was washed with PBS and resuspended in 1 ml of ice-cold fixing solution containing 70% ethanol (v/v) for 1 hour at 4°C. The cells were then centrifugated at 300g for 5 minutes at 4°C. The supernatant was discarded, and the pellet was washed with cold PBS. Subsequently, the cells were spun at 300g for 5 minutes at 4°C. Fixed cells were washed once with PBS and stained with a 2% PI (P1304MP, Thermo Fisher Scientific) solution in PBS containing protease and DNAse free RNase A at 125 U/ml (EN0531, Thermo Fisher Scientific). Flow cytometry was performed using an Accuri C6 flow cytometer (BD Biosciences) to analyse the cell cycle distribution of cells, following the gating strategy described in Fig 2.2.

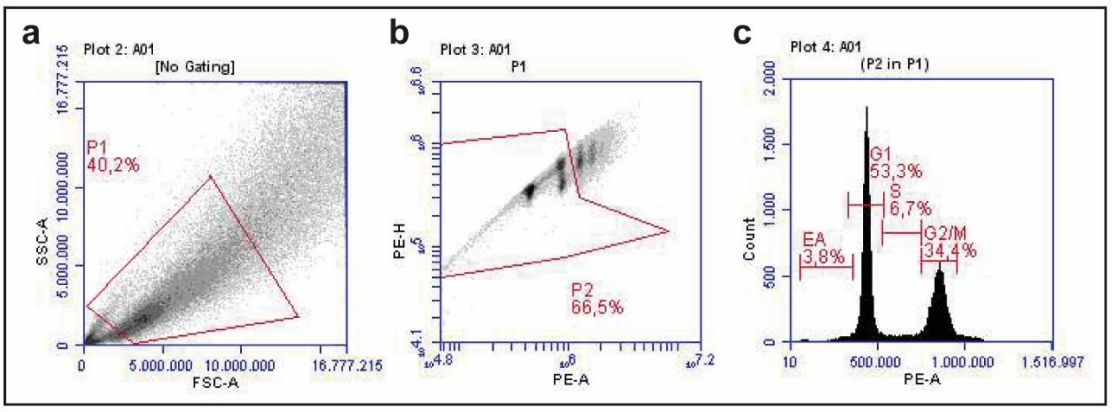

Figure 2.2. Cell cycle analysis in SH-SY5Y cells stained with PI. a. Single cells were defined by gating on forward vs scatter area (P1). **b.** PI-stained cells were gated in P2. **c.** Histogram of cell cycle distribution of P2-gated cells, with different phases of the cell cycle outlined as early apoptotic, G1, S, and G2/M.

2.11. Intracellular Ca^{2+} levels measurement

Intracellular Ca^{2+} levels were measured with the Fluo-4 NW Calcium Assay Kit (F36206, Thermo Fisher Scientific), which contains a dye that emits fluorescence upon binding to Ca^{2+}. This protocol was carried out as indicated by the manufacturer. Cells were cultured in 96-well plates and treated as indicated. A 250 mM stock solution of probenecid, which sequesters the dye inside the cells, was prepared by adding 1 ml of assay buffer to one vial of probenecid. The dye loading solution for the kit was prepared by adding 10 ml of assay buffer and 100 µl of the probenecid stock solution to one bottle of Component A. The growth medium was removed from the adherent cell cultures, and 100 µl of the dye loading solution was added to each well of a 96-well plate. The plate was incubated at 37°C for 30 minutes, then at room temperature for an additional 30 minutes. Fluorescence was measured using with a CLARIOSTAR plate reader (BMG Labtech) programmed to read for excitation at 494 nm and emission at 516 nm. Prior to the start of the assay, plates were introduced in the Incucyte S3 system (Sartorious) to acquire cell confluence data that was used to normalise the calculated from images of the plate used for ATP detection prior to the start of the protocol acquired with the Incucyte S3 system (Sartorious). To account for differences in cell density, results were normalized to cell confluence, which was calculated from images of the plate used for Ca^{2+} detection taken with the Incucyte S3 system (Sartorious) after the assay.

2.12. Statistical analysis

Results were reported as the mean ± SD of at least three separate experiments. Statistical significance was determined by unpaired two-tailed Student's t test for single comparisons and one-way ANOVA followed with Dunnett's post-hoc test to compare the means of three or more independent groups. A two-way ANOVA with Tukey's post-hoc test was utilised when comparing groups on two different categorical variables. Statistical analyses were conducted using GraphPad Prism 10 software version 10.0.2. (GraphPad). A value of $p < 0.05$ was considered significant and p values were recorded as * ($p< 0.05$), ** ($p<0.01$) and *** ($p<0.001$).

2.13. Figure preparation

Graph plotting was conducted with GraphPad Prism 10 software version 10.0.2, with the exception of Bubble Plots, Volcano Plots and Venn Diagrams, which were generated with SRplot (http://www.bioinformatics.com.cn/srplot), an online platform for data analysis and visualization. The figures were prepared with Adobe Illustrator 2020 (Adobe) and the illustrations were created with BioRender (https://www.biorender.com).

CHAPTER III

IDENTIFICATION OF PD-LINKED GENES REGULATED BY HIF

3.1.INTRODUCTION

PD can be caused by specific inherited gene mutations. While some of these genes have been investigated as HIF-1α transcriptional targets, as discussed in the introduction, no studies have evaluated the existence of HREs in an extended set of known familial PD-causing genes. As hypoxia has been implicated in neurodegeneration, the study of the regulation of PD-related genes by HIF-1α in neural cells could expand our knowledge of the link between hypoxia and PD. This study will employ both neuronal and astrocytic cell lines to elucidate cell type-specific differences in HIF-1α-mediated regulation of genes associated with familial PD.

3.1.1. Experimental models in the study of PD

The study of neurodegenerative diseases such as PD is challenging due to the difficulty of accessing the brain, the main organ affected by these diseases, to obtain samples. Postmortem brain samples can still be utilised and constitute a valuable resource for research on PD and other neurodegenerative diseases, but they can be difficult to obtain due to stringent ethical guidelines and their value can be limited by factors like the long-term use of drugs and end-stage disease, potentially altering disease hallmarks, including protein levels, thus limiting their applicability to early disease research (Hartmann et al., 2004). Nonetheless, postmortem brain samples can be used to corroborate the relevance of findings derived from experimental PD models to human disease. Experimental models of PD have been created by treating animals such as flies, rodents and non-human primates with neurotoxins, such as the mitochondrial ETC inhibitors MPTP and rotenone or pesticides paraquat and maneb, by introducing disease-causing mutations in genes like *SCNA*, *PARKN* or *PINK1* or by inducing α-Syn pathology with the use of synthetic α-Syn preformed fibrils (Dovonou et al., 2023). Animal models have been instrumental in the discovery of new treatments for PD, specially mice which present a strong correlation between motor deficits and DAergic neuron loss in the SNpc . However, no single animal model perfectly replicates all the pathological characteristics of PD, such as the progressive loss of DA-producing neurons in the SNpc, accumulation of α-Syn in the form of Lewy bodies and parkinsonian motor and neurological symptoms (Jiang et al., 2018). In addition, their use is being increasingly limited due to ethical reasons. Computational modelling has gained traction in recent years, as it avoids the ethical concerns associated with animal models and has proven useful for investigating the neuronal networks affected in PD (Muddapu et al., 2019). However, current

computational knowledge does not accurately recreate neurodegenerative diseases due to their complexity.

As the obtention of PD patient brain samples, use of animal models, and creation of precise computational models poses significant limitations, the implementation of iPSCs and immortalised cell lines as PD models has become commonplace in the investigation of neurodegenerative diseases. In the context of PD, patient-derived iPSCs presenting mutations in genes like *SNCA* or *PINK1*, or obtained from sporadic PD patients, are differentiated using specific protocols to create a uniform population of functional DAergic neurons. These neurons recapitulate cardinal hallmarks of PD pathology, including shortened neurites, compromised mitochondrial function, mtDNA damage, increased ROS production, endoplasmic reticulum stress, and elevated α-synuclein levels (Avazzadeh et al., 2021). *In vitro* experiments in a specific human-derived cell type in a controlled environment provide several advantages, including the ability to modify PD-related genes, conduct high-throughput assays, screen drugs rapidly, and investigate pathways and protein interactions involved in PD while maintaining costs low and avoiding the need for ethical approval (Falkenburger et al., 2016). Modelling PD with most cell lines is challenging due to their inherent lack of age-related features, limiting their ability to capture the full spectrum of disease pathology. Consequently, although these cell-based models of neurodegeneration do not allow the study of behavioural symptoms or systemic drug distribution and activity, they provide a platform for investigating cell-specific processes involved in PD.

3.1.1.1. SH-SY5Y neuroblastoma cell line

SH-SY5Y cells are a subclone of the of the SK-N-SH cell line which was isolated from a metastatic bone tumour of a 4-year-old female neuroblastoma patient in 1970. SH-SY5Y characterisation revealed a catecholaminergic phenotype, as these cells present detectable levels of TH and DA-β-hydroxylase, which converts DA to noradrenaline (NA), and therefore can synthesise both DA and NA (Xicoy et al., 2017). Although this cell line exhibits certain chromosomal abnormalities due its cancerous origin, the SH-SY5Y genome has a high degree of conservation of the genes that are involved in the main PD pathways (Krishna et al., 2014). These cells can also be easily differentiated via different strategies, such as the use of RA and BDNF, to a more neuronal phenotype promoting neurite outgrowth and the expression of neuronal-specific markers (Şahin et al., 2021). The differentiation of SH-SY5Y cells can be manipulated to produce specific neuron

subtypes, which makes them a powerful tool for studying a wide range of neurobiological diseases, including PD, AD, ALS and ischemia (Kovalevich et al., 2013).

While not purely DAergic, the neuroblastoma SH-SY5Y cell line is extensively used in PD research as it offers numerous advantages (Ioghen et al., 2023). Firstly, these cells present phenotypically homogenous neuronal characteristics that can be accentuated by relatively rapid differentiation and are able to produce and uptake DA. They are easily cultured and have a high proliferation rate, which makes them a good model for studying primary DAergic neurons, which are difficult to access and have a very limited growth rate. In addition, the pathological features of PD can be recapitulated in SH-SY5Y cells by triggering neuronal apoptosis, PD-related pathway dysfunction and α-Syn accumulation through the use of neurotoxins or genetic modifications, which allows the evaluation of neuroprotective compounds. In conclusion, the SH-SY5Y cell line is a well-established and reliable model, constituting a valuable starting point for PD research that can be complemented by experiments performed in more comprehensive *in vitro* and *in vivo* experimental systems.

3.1.1.2. LUHMES cell line

LUHMES is a neuronal-like cell obtained from a mesencephalic biopsy of a human female 8-week-old patient in 1998. This cell line is derived from MESC2.10, a human mesencephalic-derived cell line that was immortalized with a LINX v-myc retroviral vector and stably overexpresses v-myc under tetracycline control. LUHMES cells subjected to a 7-day treatment with db-cAMP, GDNF and tetracycline differentiate into mature neurons presenting DAergic biochemical, morphological, and functional characteristics (dLUHMES), making them a valuable model for PD research (Tüshaus et al., 2020). In fact, several neurotoxin-based models of PD are being developed using dLUHMES to screen potential therapies (Zhang et al., 2014; Beliakov et al., 2023) while some studies are utilising this cell line to investigate the pathways contributing to DAergic neuron loss in PD (Höllerhage et al., 2022). In conclusion, LUHMES cells are an easily accessible and useful cell line for PD research because they can be rapidly proliferated to generate large cell numbers and differentiated into post-mitotic DAergic-like neurons that are similar to primary murine midbrain neurons (Tüshaus et al., 2020).

Although both neuronal cell lines are derived from young patients and potentially lack the full spectrum of age-related PD features, these cell line-based models remain valuable

tools for dissecting disease mechanisms through investigations of specific gene/protein function and relevant cellular pathways, which is the main goal of this project.

3.1.1.3. U-87MG glioblastoma cell line

U-87MG (HTB-14) is a cell line obtained from malignant gliomas from an adult male patient, likely suffering from Glioblastoma, in 1968 (Allen et al., 2016). U-87MG cells have been used as model system for primary astrocytes, as they display astrocytic morphology and markers (Chemmarappally et al., 2020) and can produce and release neurotrophic factors (Zabłocka et al., 2015). The U-87MG cell line has previously been utilised in PD research to investigate several processes, such as α-Syn propagation (Bayati et al., 2022) and PD-related pathway dysfunction (Currim et al., 2021). Similarly to SH-SY5Y cells, this cell line allows to easily perform high-throughput experiments, avoiding expensive stem cells and the ethical approval needed for primary cells. In addition, this cell line also shows no abnormalities in genes known to cause familial PD (Clark et al., 2010) and the results obtained would require validation with additional experiments in other biological systems.

3.1.2. HIF-1α stabilization

3.1.2.1. Hypoxia

HIF-α stabilization in vivo is induced by hypoxia-mediated PHD inhibition. Studies in rodents have shown that both HIF-1α and HIF-2α levels increase in most major organs upon subjecting the animals to short-term mild hypoxia (Stroka, 2001; Wiesener,2003). In human lung and neuroblastoma cancer cell lines, as well as primary human umbilical vein endothelial cells, a HIF switch is observed in which HIF-1α is rapidly stabilized by low O_2 but is eventually surpassed by higher levels of HIF-2α in chronic hypoxia (Uchida et al., 2004; Holmquist-Mengelbier et al., 2006; Jaśkiewicz et al., 2022). The time course of HIF-1α predominance over HIF-2α in hypoxic environments varies across studies, with HIF-1α generally peaking at around 4 hours and then declining, although it is still detectable at 24 hours, while HIF-2α, on the other hand, increases later on but maintains its levels for a longer period of time. Time-dependent HIF-1α degradation may be due at least in part to the destabilization of *HIF1A* mRNA after prologued hypoxia and the reactivation of PHDs due to increased O_2 levels resulting from reduced mitochondrial metabolism (Jaśkiewicz et al., 2022). However, the response to long term hypoxia in

PC12 cells, but not SH-SY5Y cells, relied on HIF-1α rather than HIF-2α (Zhdanov et al.,2013) while HIF-1α/HIF-2α balance in primary murine astrocytes during chronic hypoxia is regulated both by O_2 content and glucose concentration (Guo et al., 2019). This information suggests that the impact of hypoxia on the balance between HIF-1α and HIF-2α protein levels is dependent on multiple factors such cell type, hypoxia duration, O_2 tension and metabolite availability. Importantly, the cellular response to hypoxia is not limited to the transcriptional program controlled by HIF-α, as low O_2 levels can induce the activity of additional TFs or directly modify chromatin to promote gene expression (Kenneth et al., 2008; Batie et al., 2019). Thus, when studying the HIF-α response using hypoxia, it is advisable to also investigate the effect of drugs that directly block PHDs in order to minimize off-target effects and validate the changes observed during hypoxia.

3.1.2.2. PHD inhibitors

PHD inactivation and consequent HIF-α stabilization can be achieved in normoxia through the use of PHD inhibitors. These drugs were originally developed to treat anaemia, but they are now being investigated for their potential to treat other disorders, such as cardiovascular and respiratory diseases, neuropathologies and delayed wound healing. An important fact to take into consideration when designing PHD inhibitors is that different PHD isoforms show diverging affinity for different HIFs. Indeed, PHD2 has a stronger preference for HIF-1α, while PHD3 has a more pronounced effect on HIF-2α. HIF-2α is also more resistant to hydroxylation by PHDs and FIH-1 than HIF-1α, which can result in the stabilization and activation of HIF-2α at lower concentrations of PHD inhibitor (Appelhoff et al., 2004). PHD inhibitors can work through a variety of mechanisms, such as displacing iron, chelating iron, disrupting 2-OG binding, and competing with HIF-α.

Several metals, such as cobalt, copper and nickel, can displace iron from the active site of PHDs, inactivating these enzymes. An example is the compound $CoCl_2$, which can block PHDs via replacement of Fe^{2+}, although it might also contribute to HIF-α stability by depleting ascorbate, blocking the HIF-α-pVHL interaction and increasing ROS (Muñoz-Sánchez et al., 2018). Studies in SH-SY5Y cells find that $CoCl_2$ increases cell proliferation at lower concentrations while causing ROS-mediated apoptosis at higher doses (Lee et al., 2020). This compound has been widely used due to its low cost and dose-dependent quick stabilization of HIF-1α, with consequent induction of its transcriptional targets. Expectedly, iron chelators can also stabilize PHDs by reducing

overall Fe^{2+} levels. This class of drugs includes commonly utilised compounds that have been found to be protective in PD, as commented in the introduction, like DFO or CQ (Lestón Pinilla et al., 2021). Evidently, an important disadvantage of compounds reducing general iron binding is that they do not confer specificity, as all PHD isoforms would be inactivated.

2-OG is necessary for PHD activity and its binding site at the enzyme is mapped and constitutes an objective for drug development. Indeed, multiple PHD inhibitory drugs are 2-OG analogues designed to specifically block the active site of PHDs and minimize their effect on other 2-OG-dependent enzymes. These include Daprodustat (GSK1278863), Roxadustat (FG-4592), Vadadustat (AKB-6548) and Molidustat (Bay 85-3934) which have been developed for the treatment of anaemia derived from chronic kidney disease (Locatelli et al., 2022). Other 2-OG mimics have been synthesised for basic laboratory research on HIF-α, such as DMOG, JNJ-42041935 and IOX2-4. The IOX drug family is comprised of three selective PHD2 inhibitors, IOX2, IOX3 (FG-2216) and IOX4. FG-2216 is shown to trigger the accumulation of HIF-1α with consequent increase of expression of its target genes without an effect on cell viability in PC12 cells (Singh et al., 2020). IOX4 is a very potent and highly selective PHD2 inhibitor, showing higher induction of HIF-1/2α proteins and the HIF transcriptional response than other PHD inhibitors and poor affinity for other 2-OG oxygenases (Yeh et al., 2017). Interestingly, systemic administration of IOX4, but not IOX2, to mice causes stabilization of transcriptionally active HIF-1/2α in the brain, which suggests that IOX4 can cross the blood-brain barrier efficiently and could be used to treat disorders affecting the brain, such as neurodegenerative diseases (Chan et al., 2015). As mentioned in the introduction, some of these drugs, including FG-4592, DMOG and IOX2, have been investigated as PD treatments (Lestón Pinilla et al., 2021), while the potential of other 2-OG mimetics as therapy for this disease has not been explored to date.

To avoid off-target effects by directly blocking HIF-α-PHD interaction, a group of drugs that reproduce the same three-dimensional structure as the HIF peptide at the PHD active site were developed (Poloznikov et al., 2021). Two members of this group, adaptaquin and neuradapt, have been identified and are at the stage of pre-clinical investigation, although adaptaquin showed a neuroprotective effect in a PD animal model, as noted in the introduction (Lestón Pinilla et al., 2021).

3.1.2.3. pVHL inhibitors

Two compounds, VH032 and VH298, which can selectively block pVHL interaction with HIF-α and consequent HIF-α degradation, have recently been characterised. VH298 is not cytotoxic and can induce HIF-1/2α accumulation and subsequent HIF-mediated transcriptional response *in vitro* and *in vivo* (Frost et al., 2016; Qiu et al., 2019). However, pVHL might not constitute an adequate target, as pVHL is a tumour suppressor protein and loss-of-function mutations in the *VHL* gene cause predisposition to a variety of cancers (Maher et al., 2011).

3.1.3. HIF-1α-mediated control of gene expression

Once stabilized, HIF-α subunits are directed to the nucleus. HIF-α subunits present a nuclear localization signal (NLS) in their C-terminal portion, which is recognised by specific nuclear transport proteins named importins that facilitate the entry of HIF-αs into the nucleus via the nuclear pore complex (Depping et al., 2008). Studies show that other proteins are involved in facilitating HIF-1α nuclear entry by increasing HIF-1α binding to importins (Golan et al., 2013; Lee et al., 2019). Physiological processes such as aging can reduce importin levels and thus impair HIF-1α access to its target genes (Ahluwalia et al., 2010). In addition, HIF-1α nuclear export is assisted by its interaction with the CRM1 protein, which can be disrupted by phosphorylation of HIF-1α by MAPK (Mylonis et al., 2006). Although HIF-α stabilization has been a matter of exhaustive study, the factors governing HIF-α interaction with nuclear importins and exportins, such as adaptor proteins and post translational modifications, have not been thoroughly investigated. Nevertheless, current evidence supports that the transfer rate of HIF-α from the cytoplasm to the nucleus is a key step in the regulation of its transcriptional activity.

In the nucleus, HIF-α subunits dimerize with HIF-β to bind HREs in promoters of specific genes in order to induce gene expression. These HREs are surrounded by a highly variable flanking sequence and are sometimes accompanied by a HIF ancillary sequence (HAS), an imperfect inverted repeat of the HRE consensus motif with the sequence 5'-CA(G|C)(A|G)(T|G|C)-3' present 5-20 nucleotides upstream or downstream from HREs (Rashid et al., 2019). Employing chromatin immunoprecipitation followed by sequencing (ChIP-seq), researchers have shown that HREs are frequently located close to the Transcription start site, although a significant percentage of HIF binding sites were located in distal promoters, and that they are to be preferentially situated at sites presenting open chromatin in normoxia, which may help trigger a rapid transcriptional

response by HIFs (Schodel et al., 2011). The HRE sequence is ubiquitously present through the genome, but only about 1% HREs are functional, suggesting that the presence of a consensus HIF-1 binding sequence accompanied by a HAS is not the only determinant involved in this process (Schodel et al., 2011). For example, several HREs in the promoter of a known HIF-1α target gene *EPO* can show varying levels of activity depending on different factors such as cell type (Orlando et al., 2020). This points to the existence of additional mechanisms involved in HRE activation, which include other TFs and chromatin modifications. Indeed, nucleotide alterations in the sequence of accessory TFs reduced the HIF-mediated transcriptional response, indicating that HRE functionality is also determined by cooperative DNA binding or recruitment of additional coactivators (Rocha et al., 2007). Binding of HIFs or other TFs to consensus sequences can be modified by chromatin accessibility, which can be influenced by histone demethylases that are direct HIF-1α targets (Xia et al., 2009). Thus, epigenetic modifications to these sequences can modify HIF-mediated gene transcription. Indeed hypoxia-mediated ROS can cause oxidative changes in the HREs present in *VEGFA*, which signal the recruitment of TFs that are essential for HIF binding (Pastukh et al., 2015). HIF binding to transcriptional coactivators can be regulated by factors other than FIH-mediated hydroxylation of the C-TAD transactivation domain. Indeed, HIF-α C-TAD – CBP/p300 interaction can also be disrupted by post-translational modifications of this domain, such as phosphorylation. As p300/CBP functions as coactivator for a wide variety of TFs, elevated levels of competing TFs like p53 could displace p300/CBP from binding HIF, repressing its transcriptional activity (Blagosklonny et al., 1998). These types of post-translational modifications and competitions between cofactor binding could also influence other TFs modulating HIF-α activity. Additionally, ChIP-Seq data reveals that while most HIF-binding sites harbour the known HRE sequence, a minority lack it, suggesting recognition through non-canonical mechanisms (Mole et al., 2009). In summary, although the presence of HREs is generally essential for HIF-mediated gene expression, it is not sufficient and the functionality of these sequences is tightly controlled by an array of factors, including chromatin remodelling, cooperation with accessory TFs, availability of transcriptional coactivators and post transcriptional modifications, which determine factors such as promoter accessibility by HIF and RNA polymerase recruitment. Interestingly, several studies show HIF-dependent downregulation of hundreds of genes upon hypoxic treatment but HIF interaction with these genes was not observed, which suggests that HIF-1 functions primarily, or even exclusively, as a

transcriptional activator, with repression achieved indirectly by HIF-mediated induction of transcriptional repressors and non-coding RNAs (Mole et al., 2009).

Investigating HIF-1α's specific targets presents a challenge. Current methods for inducing HIF-α stabilization, including hypoxia and the chemical treatments discussed, non-selectively activate both HIF-1α and HIF-2α isoforms. This limitation arises from their shared regulation by PHD/VHL enzymes, albeit with varying sensitivities. Physiologically, both isoforms are active under hypoxic or hypoxia-mimicking conditions and present some functional overlap in gene induction, which ensures a robust transcriptional response to hypoxia even if HIF-1α is impaired. The unique regulatory mechanisms controlling HIF-1α already prevent its basal activity, making traditional methods for identifying specific gene targets, such as silencing RNA, ineffective unless employed in conjunction with hypoxia or HIF-stabilizing agents.

3.1.4. Bioinformatic screening for potential HIF target genes

While the presence of HRE does not guarantee that a gene is a HIF target, it remains the first fact to be evaluated when screening for novel genes induced by HIF. The promoter sequences of the genes of interest can be obtained from the Eukaryotic promoter database (EPD) and analysed for the presence of HIF binding sequences with the JASPAR database search motif tool. The search motif tool scans promoter regions with curated and non-redundant transcription factor binding profiles in the form of position weight matrices to find putative binding sites, providing a JASPAR relative score that is the percentage of the maximal score that can be obtained from a specific position weight matrix (Castro-Mondragon et al., 2022). The Ensembl platform can be used to map the candidate gene promoters for HASs. As mentioned, HIFs can manipulate gene expression via alternative mechanisms so in addition to investigating the occurrence of HREs, the existence of links between HIFs and candidate targets is frequently investigated using interaction databases like STRING. The STRING database is a comprehensive resource for protein-protein interactions, including both physical interactions and functional associations, pooled from a variety of sources, including experimental data, computational predictions, and text mining (Szklarczyk et al., 2023).

3.1.5. Aims of the chapter

The goal of this investigation is to identify and assess the response of known familial PD-causing genes to hypoxia/HIF-1α stabilisation in neural cell populations. This investigation aims to elucidate whether the HIF-1α response to hypoxia represents a potential link between hypoxic risk factors, such as OSA or TBI, and PD onset. Furthermore, by examining how HIF-1α interacts with familial PD genes, we can determine its protective or detrimental role in the disease process. This aim will be achieved by:

1) Analysing the presence of HREs and HAS in known PD-related genes through bioinformatic analysis.
2) Evaluating the functional interactions between HIF-1α and known PD-related genes.
3) Following bioinformatic identification of PD-associated genes of interest, this study will investigate changes in their protein expression and mRNA levels upon exposure to hypoxia and HIF-α stabilizing treatments.

3.2. METHODOLOGY

Bioinformatic analysis of PD-related genes was performed to identify candidate HREs and HAS. The promoter sequences of the genes of interest were obtained from the Eukaryotic promoter database and entered into the JASPAR database search motif tool selecting the HIF1::ARNT binding motif matrix. The three results with the highest JASPAR relative scores were chosen as sample for further study. The potential link between HIF-1 and PD-related genes was evaluated using the protein-protein interaction network database STRING. The effect of HIF-α stabilization on the proteins encoded by these candidate genes was also investigated. A preliminary evaluation of the PHD inhibitor $CoCl_2$ was performed by analysing its impact on cell viability by Incucyte confluence analysis and MTT reduction and assessing the levels of HIF-1α by WB and IF. The levels of gene and protein expression under hypoxia or following HIF-α stabilising treatment were detected by qRT-PCR and WB, respectively. Chapter II can be referred to for full details on the methodology used.

3.3.RESULTS

3.3.1. PD genes show potential HREs and interactions with HIF-1α

A bioinformatic analysis of known PD-related genes was conducted to map the presence of HREs within these, which would help identify PD target genes that have the potential to be influenced by HIF. The results from the analysis are showed in Table 3.1. All PD-related genes, except *GBA*, exhibit HIF binding sites. *ATP13A2*, which presents the highest relative score, has already been proven to be regulated by HIF-1 (Xu et al., 2012). Interestingly, *DJ1* and *PINK1* also show a high relative score but regulation of these genes by HIF has not been demonstrated to date. Several other genes, such as *PRKN* or *VPS35*, also present high scores for their candidate HREs and well positioned HAS. This bioinformatic analysis can be validated *in vitro* to assess whether the proteins encoded by these PD-related genes are induced by HIF-α stabilization or hypoxia.

Gene	Gene strand	HRE position	HRE sequence	HAS position	HAS sequence	HRE/HAS strand	JASPAR relative score
ATP13A2	Reverse	-162	GG**ACGTG**C	-183	CACAG	Reverse	100.00
		-185	GT**GCGTG**C	-163 -215	CACGT CAGGC	Forward	94.69
		-897	AG**ACGTG**G	-879	CACGT	Forward	93.88
DJ1	Forward	-80	GG**ACGTG**A	N/A	N/A	Forward	95.88
		-6	GT**GCGTG**C	N/A	N/A	Forward	94.69
		-10	GC**GCGTG**C	N/A	N/A	Forward	94.42
DNAJC6	Forward	-1903	GT**ACGTG**A	N/A	N/A	Forward	95.51
FBXO7	Forward	-941	CC**ACGTG**A	-925	CAGAG	Reverse	92.99
		-226	GT**GCGTG**G	N/A	N/A	Reverse	90.97
GBA	Reverse	N/A	N/A	N/A	N/A	N/A	N/A
LRRK2	Forward	-234	AG**GCGTG**C	-215 -221	CACGG CACGG	Forward	92.66
		-8	GG**GCGTG**G	-16	CAGGC	Forward	91.34
		-230	GT**GCGTG**G	-215 -221	CACGG CACGG	Forward	90.97
PINK1	Forward	-1754	CC**ACGTG**C	-1182	CACGC	Forward	97.12
		-1754	GC**ACGTG**G	-1731	CAGGT	Reverse	95.64
		-140	CC**ACGTG**G	N/A	N/A	Forward	93.39
PLA2G6	Reverse	-10	CC**ACGTG**A	N/A	N/A	Forward	92.99
		-873	GG**GCGTG**G	-863	CACGC	Reverse	91.34
		-1396	AG**GCGTG**A	-1373	CACGG	Reverse	88.54
PRKN	Reverse	-38	GC**GCGTG**C	-63	CAGGC	Reverse	94.42
		-101	AG**GCGTG**A	N/A	N/A	Reverse	88.54
SNCA	Reverse	-1019	GT**GCGTG**T	N/A	N/A	Reverse	89.89
		-111	CA**GCGTG**C	N/A	N/A	Forward	88.21
		-872	CA**GCGTG**A	N/A	N/A	Forward	84.08

SYNJ1	Reverse	-199	GG**GCGTG**G	-208	CAGAG	Reverse	91.34
		-1494	GG**GCGTG**G	N/A	N/A	Reverse	91.34
		-1438	CG**GCGTG**A	N/A	N/A	Reverse	88.68
VPS13C	Reverse	-1732	GA**ACGTG**G	N/A	N/A	Reverse	91.68
		-85	GC**GCGTG**A	-65 -106	CAGGC CAGGC	Forward	90.30
VPS35	Reverse	-810	GG**ACGTG**T	-838	CACGG	Reverse	95.20
		-1873	GT**GCGTG**C	-1857	CACAC	Reverse	94.69
		-320	GA**ACGTG**G	-333	CAGAT	Reverse	91.68

Table 3.1. Several PD-related genes present potential HREs. The table shows a list of genes involved in PD accompanied by candidate HREs identified by the JASPAR database, which provides a relative score also included. Only the three higher HREs scores for each gene were included, provided that the score surpassed the cutoff of 85%. HAS motifs were mapped with Ensembl.

An assessment of potential links between HIF-1α and PD-related proteins was conducted by STRING. Proteins involved in PD are extensively linked, forming an interconnected cluster, while HIF-1α shows weak links with several of these proteins (Fig. 3.1). Closer inspection of the links established between HIF-1α and PINK1, α-Syn and DJ-1 (*PARK7*) shows that these are obtained from text mining and do not constitute proof of interaction. Parkin and LRRK2 are experimentally determined HIF-1α interacting partners since they influence HIF-1α degradation and phosphorylation, respectively (Liu et al., 2017; Lin et al., 2016). Interestingly, although the discovery of ATPase 13A2 and LRKK2 as HIF-1α transcriptional targets was performed experimentally (Xu et al., 2012; Bae et al., 2018), it is not detected by the STRING database, with the only evidence available coming from text mining.

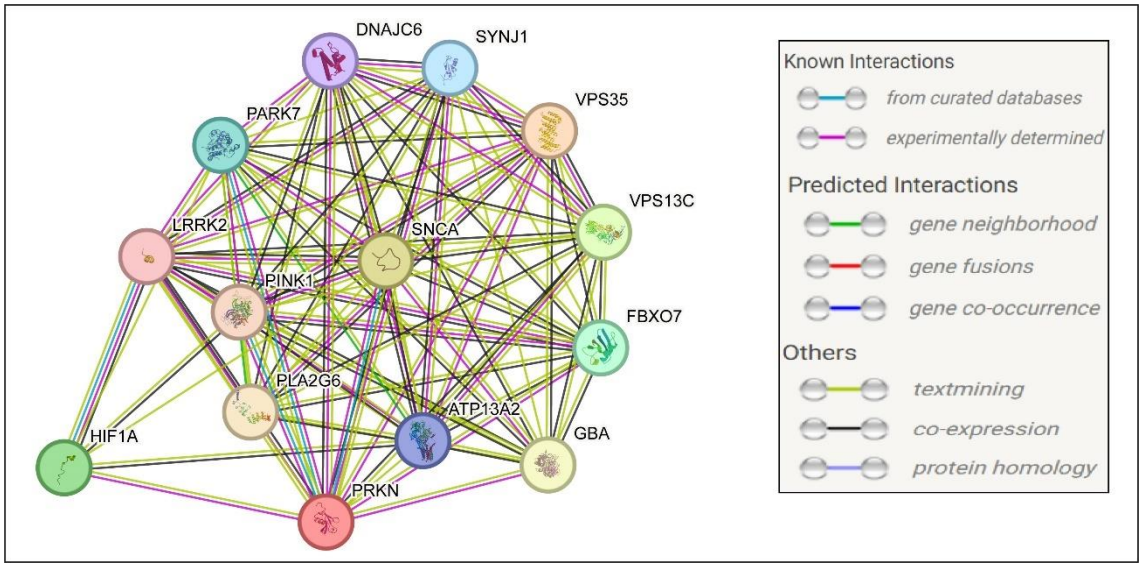

Figure 3.1. Several PD-related genes present links to HIF-1α. The image shows a selection of proteins involved in PD as well as HIF-1α linked by the interactions predicted by the STRING database with the low confidence setting. The legend contains the meaning of the interaction line colouring.

3.3.2. $CoCl_2$ stabilizes HIF-1α without affecting SH-SY5Y cell viability

To investigate the impact of stabilizing HIF-α on PD-related proteins on an *in vitro* cellular system, the effect of $CoCl_2$ in SH-SY5Y cells was investigated. Cell proliferation analysis during 24 hours treatment with $CoCl_2$ shows a small but not significant increase in proliferation up to 12 hours but resembles control cultures beyond 20 hours growth (Fig. 3.2a). The levels of HIF-1α were assessed at selected timepoints of $CoCl_2$ treatment by Western Blotting. The results demonstrate potent HIF-1α accumulation that steadily decreases over time but remains detectable and significant elevated against the control at 24h (Fig. 3.2b). MTT reduction analysis shows that 24h $CoCl_2$ treatment does not have a significant impact on cellular metabolic activity when compared to the control (Fig. 3.2c). HIF-1α stabilization at this timepoint was investigated by immunofluorescence staining of HIF-1α levels in the presence and absence of $CoCl_2$. The images show widespread HIF-1α accumulation through the cell body, nucleus and neurites following $CoCl_2$ treatment that is not detectable in the control (Fig. 3.2d). Thus, $CoCl_2$ can be utilised as a potent HIF-1α stabilizing compound that is not toxic to SH-SY5Y cells at the concentration and timepoints assayed, supported by previous approaches utilised by other researchers (Lee et al., 2020).

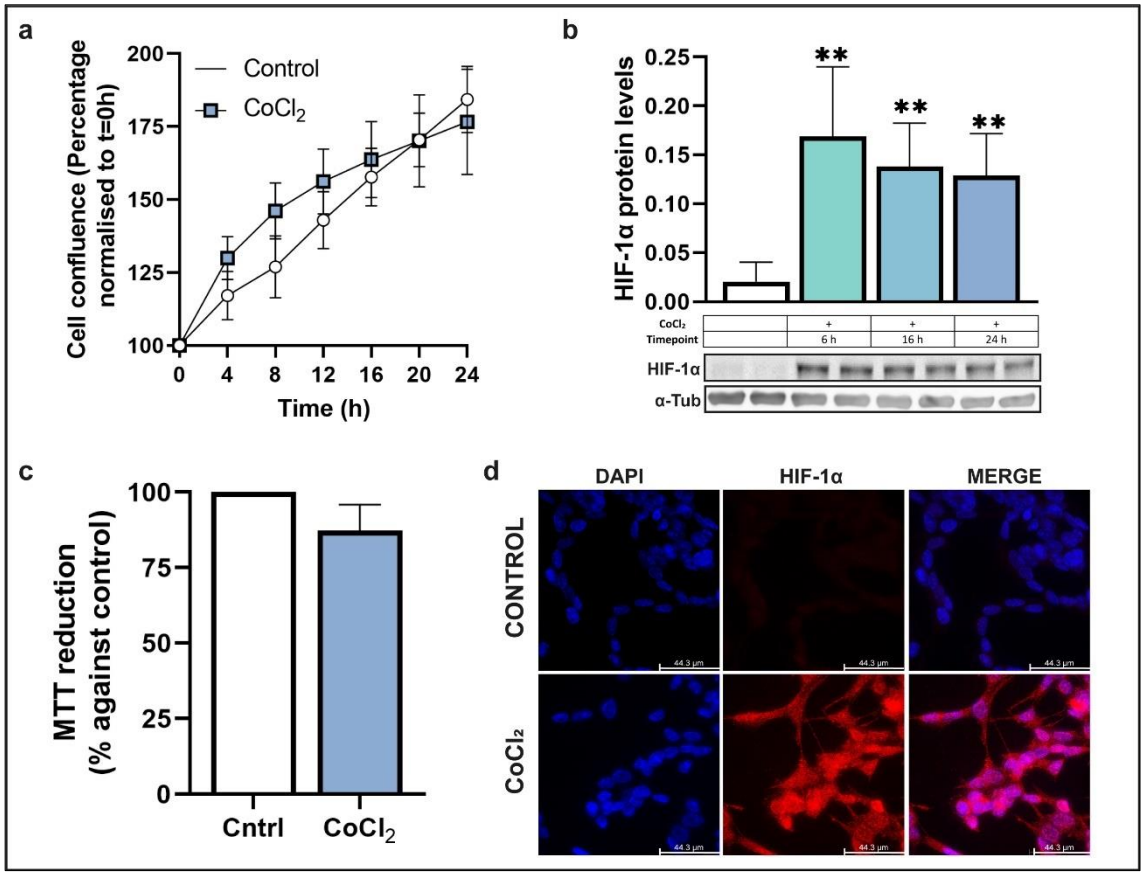

Figure 3.2. $CoCl_2$ treatment induces HIF-1α accumulation in SH-SY5Y cells without impacting cell viability. a. Confluence analysis of SH-SY5Y cells (n=4) during 24h of 100 μM $CoCl_2$ treatment performed with the Incucyte S3 live cell analysis system **b.** Representative Western Blot image showing HIF-1α (~120 kDa) and α- Tubulin (~55 kDa, loading control) proteins in lysates from SH-SY5Y cells treated with 100 μM $CoCl_2$ for 6, 16 and 24h accompanied by densitometric analysis (n=4). **c.** Graph showing MTT reduction in SH-SY5Y cells treated with 100 μM $CoCl_2$ for 24h (n=4). **d.** Immunofluorescence staining of control and 100 μM $CoCl_2$-treated SH-SY5Y cells for 24 hours. Cells were fixed, permeabilised and co-stained with HIF-1α Ab (red) and DAPI (blue). Coverslips were visualised using a Leica Thunder Cell Imager microscope with a 100X objective. Scale bar = 44.3 μm**.** Statistical significance was obtained with an unpaired two-tailed Student's t test where $p<0.05$ was recorded as "*" with respect to control.

3.3.3. PD-related protein levels are modified by PHD inhibitors

To investigate the findings of the bioinformatic analysis, the protein levels of PD-related proteins were analysed following $CoCl_2$ treatment. Interestingly, although several genes encoding these proteins show highly scored predicted HREs, none of these proteins are induced by 24h treatment with 100 μM $CoCl_2$ (Fig. 3.3a-f), which has previously shown to stabilize HIF-1α. Remarkably, significant slight reductions in protein levels after $CoCl_2$ exposure were observed in ATPase13A2 and PINK1 (Fig. 3.3a, c). In order to rule out an off-target effect of $CoCl_2$ on these proteins, selected targets were also investigated using other PHD inhibition strategies.

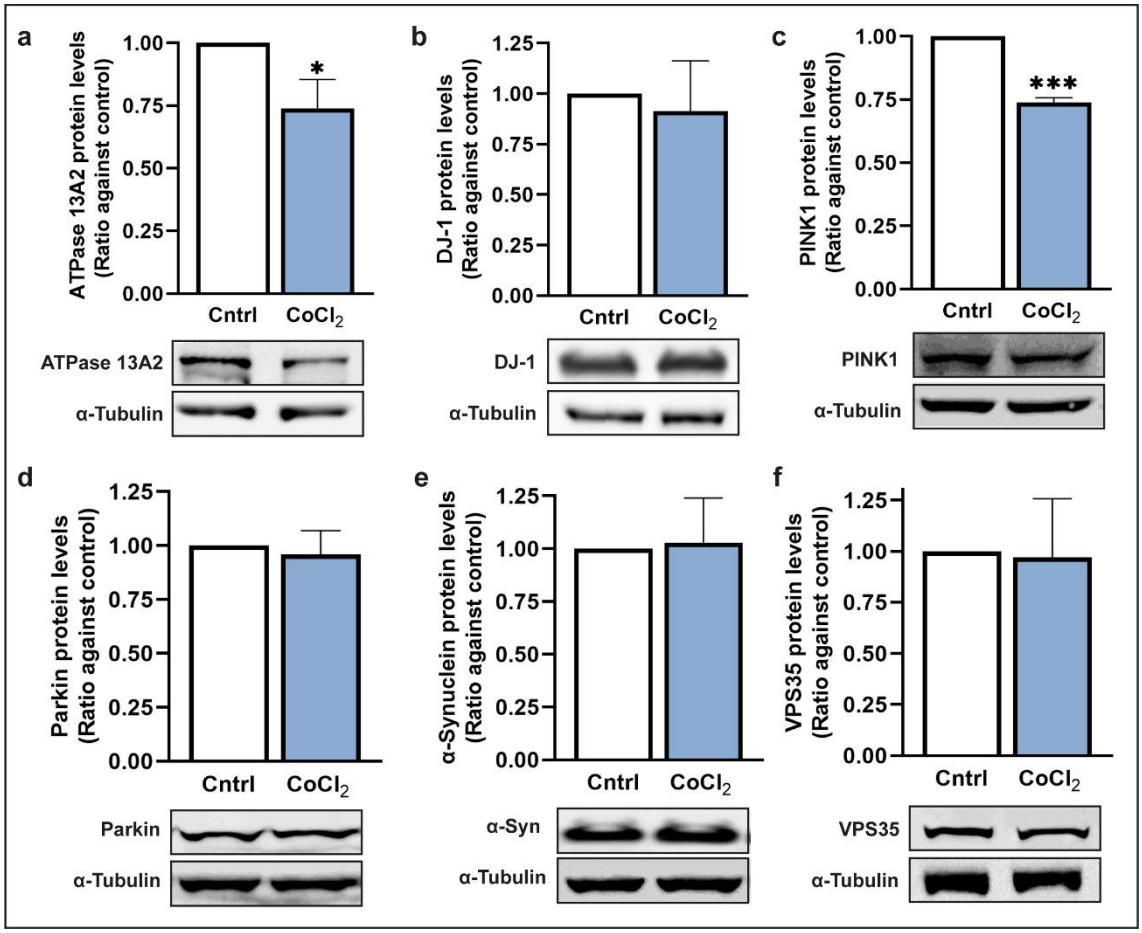

Figure 3.3. $CoCl_2$ treatment reduces the levels of ATPase 13A2 and PINK1 proteins in SH-SY5Y cells. a. Representative Western Blot image showing ATPase 13A2 (~125 kDa) and α- Tubulin (~55 kDa, loading control) proteins in lysates from SH-SY5Y cells treated with 100 μM for 24h accompanied by densitometric analysis (n=4). **b.** Representative Western Blot image showing DJ-1 (~25 kDa) and α-Tubulin (~55 kDa, loading control) proteins in lysates from SH-SY5Y cells treated with 100 μM $CoCl_2$ for 24h accompanied by densitometric analysis (n=4). **c.** Representative Western Blot image showing PINK1 (~65 kDa) and α- Tubulin (~55 kDa, loading control) proteins in lysates from SH-SY5Y cells treated with 100 μM $CoCl_2$ for 24h accompanied by densitometric analysis (n=4). **d.** Representative Western Blot image showing Parkin (~52 kDa) and α- Tubulin (~55 kDa, loading control) proteins in lysates from SH-SY5Y cells treated with 100 μM $CoCl_2$ for 24h accompanied by densitometric analysis (n=4). **e.** Representative Western Blot image showing α-Synuclein (~15 kDa) and α- Tubulin (~55 kDa, loading control) proteins in lysates from SH-SY5Y cells treated with 100 μM $CoCl_2$ for 24h accompanied by densitometric analysis (n=4). **f.** Representative Western Blot image showing VPS35 (~92 kDa) and α- Tubulin (~55 kDa, loading control) proteins in lysates from SH-SY5Y cells treated with 100 μM $CoCl_2$ for 24h accompanied by densitometric analysis (n=4). Statistical significance was obtained with an unpaired two-tailed Student's t test where $p<0.05$ was recorded as "*" with respect to control.

As ATPase 13A2 has been identified as a transcriptional HIF-1α target by researchers in neuronal cells, it was decided to investigate if the reduction of the protein levels of ATPase 13A2 upon $CoCl_2$ treatment observed in this experiment was also present when using other PHD inhibitors. To confirm that the effect reported was not due to other factors, such as the specific inhibition of HIF by iron substitution or off-target mechanisms triggered by this process, the PHD inhibitor IOX4, which acts by displacing 2-OG from the binding site of PHD2, was used. In addition, several timepoints were assayed in order to investigate the observed reduction of ATPase 13A2 levels over time. IOX4 is a potent inducer of HIF-1α accumulation, and this effect is sustained for at least 24 hours (Fig. 3.4a). Coinciding with the effect of $CoCl_2$, IOX4 treatment causes a reduction in ATPase 13A2 protein levels at all the timepoints assayed (Fig. 3.4b).

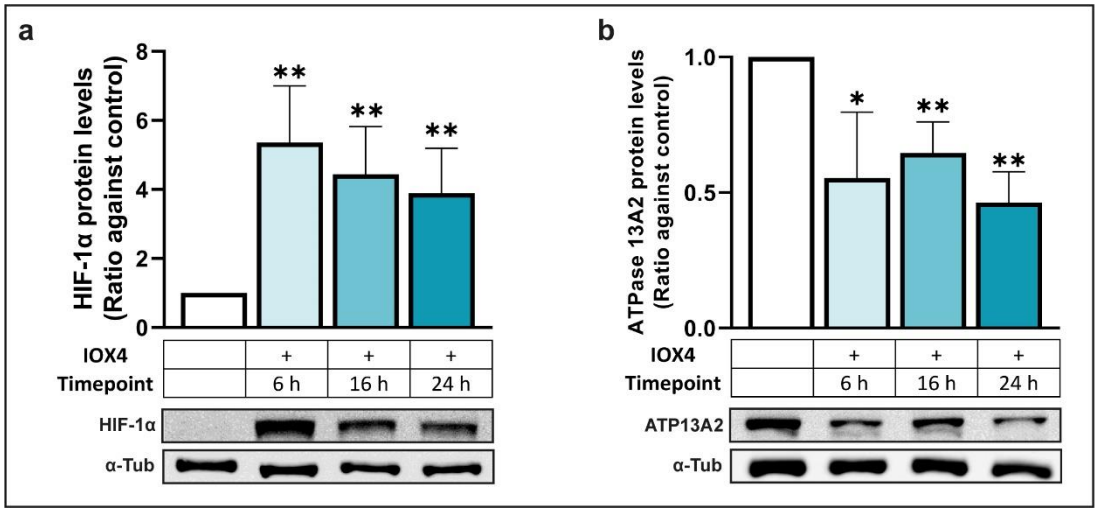

Figure 3.4. IOX4 treatment reduces the levels of ATPase 13A2 in SH-SY5Y cells. a. Representative Western Blot image showing HIF-1α (~120 kDa) and α- Tubulin (~55 kDa, loading control) proteins in lysates from SH-SY5Y cells treated with 10 μM IOX4 for 6, 16 and 24h accompanied densitometric analysis (n=4). **b.** Representative Western Blot image showing ATPase 13A2 (~125 kDa) and α-Tubulin (~55 kDa, loading control) proteins in lysates from SH-SY5Y cells treated with 10 μM IOX4 for 6, 16 and 24h accompanied by densitometric analysis (n=4). Statistical significance was obtained with an unpaired two-tailed Student's t test where $p<0.05$ was recorded as "*" with respect to control.

3.3.4. PD-related protein levels are modified by hypoxia

To further validate the implication of HIF in the alteration of the levels of PD-associated proteins, neuronal cells were cultured under hypoxic conditions. Hypoxia promoted a significant accumulation of HIF-1α in SH-SY5Y cells after 24h while cell viability, measured as MTT reduction, remained unchanged (Fig. 3.5a, b).

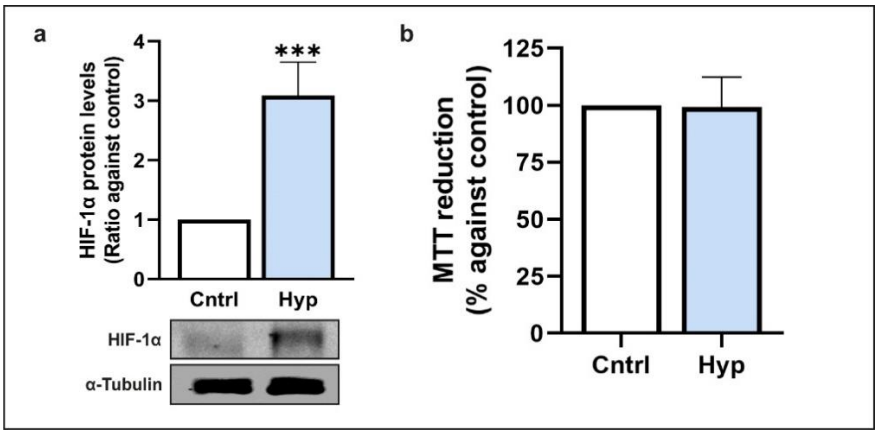

Figure 3.5. Hypoxia induces HIF-1α accumulation in SH-SY5Y cells without impacting cell viability. a. Representative Western Blot image showing HIF-1α (~120 kDa) and α- Tubulin (~55 kDa, loading control) proteins in lysates from SH-SY5Y cells treated with 1% O_2 for 24h accompanied by a plot summarising densitometric analysis of this Western Blot (n=4). **b.** Graph showing MTT reduction in SH-SY5Y cells treated with 1% O_2 for 24h (n=3). Statistical significance was obtained with an unpaired two-tailed Student's t test where $p<0.05$ was recorded as "*" with respect to control.

In concurrence with $CoCl_2$ treatment, hypoxia exposure mirrored the findings obtained, demonstrating significant reductions in the protein levels of ATPase 13A2 and PINK1 after 24h of 1% O_2 (hypoxia) exposure (Fig. 3.6a, c), with the remaining PD-related genes unaffected by the treatment (Fig. 3.6b, d-f). This was directly comparable to $CoCl_2$ treatment (Fig. 3.3a-f) pointing to a role of HIF in modulating the protein levels of ATPase 13A2 and PINK1. Moreover, these findings suggest that the PD-associated proteins studied are unlikely to be direct HIF transcriptional targets in the SH-SY5Y cell line, as they are either unmodified or downregulated after $CoCl_2$ or hypoxia treatment, and HIF primarily acts as a transcriptional activator.

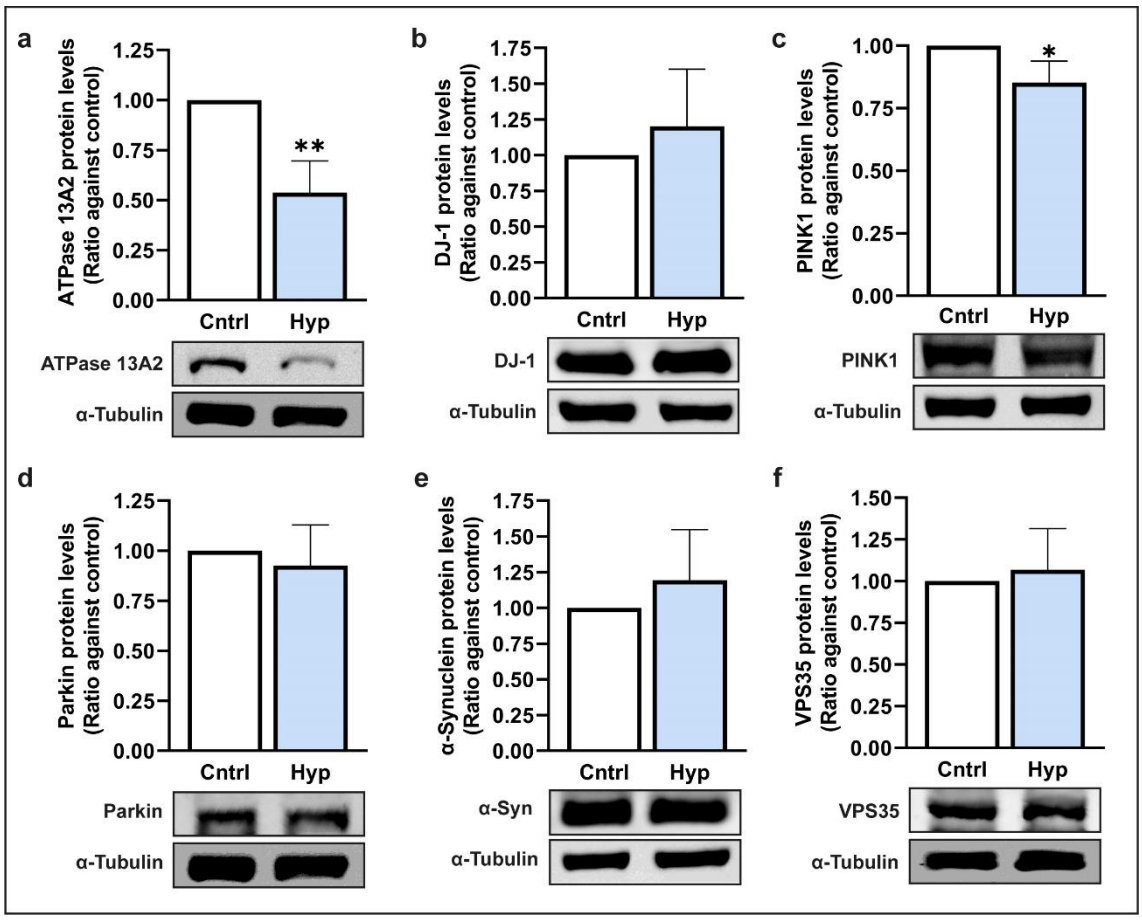

Figure 3.6. Hypoxia treatment reduces the levels of ATPase 13A2 and PINK1 proteins in SH-SY5Y cells. a. Representative Western Blot image showing ATPase 13A2 (~125 kDa) and α- Tubulin (~55 kDa, loading control) proteins in lysates from SH-SY5Y cells treated with 1% O_2 for 24h accompanied by densitometric of this Western Blot (n=4). **b.** Representative Western Blot image showing DJ-1 (~25 kDa) and α- Tubulin (~55 kDa, loading control) proteins in lysates from SH-SY5Y cells treated with 1% O_2 for 24h accompanied by densitometric analysis (n=4). **c.** Representative Western Blot image showing PINK1 (~65 kDa) and α- Tubulin (~55 kDa, loading control) proteins in lysates from SH-SY5Y cells treated with 1% O_2 for 24h accompanied by densitometric analysis (n=4). **d.** Representative Western Blot image showing Parkin (~52 kDa) and α- Tubulin (~55 kDa, loading control) proteins in lysates from SH-SY5Y cells treated with 1% O_2 for 24h accompanied by densitometric analysis (n=4). **e.** Representative Western Blot image showing α-Synuclein (~15 kDa) and α- Tubulin (~55 kDa, loading control) proteins in lysates from SH-SY5Y cells treated with 1% O_2 for 24h accompanied by densitometric analysis (n=4). **f.** Representative Western Blot image showing VPS35 (~92 kDa) and α- Tubulin (~55 kDa, loading control) proteins in lysates from SH-SY5Y cells treated with 1% O_2 for 24h accompanied by densitometric analysis (n=4). Statistical significance was obtained with an unpaired two-tailed Student's t test where $p<0.05$ was recorded as "*" with respect to control.

3.3.5. HIF-α stabilization does not alter the expression of *ATP13A2* and *PINK1*

Consequently, to determine if the reduction in protein levels was due to a decrease in gene expression, the mRNA abundance of *ATP13A2* and *PINK1* was evaluated. No significant effect on gene expression of either *ATP13A2* or *PINK1* genes was observed following $CoCl_2$ treatment, although the known HIF-1α target *SOX9*, included as positive control

of the presence of HIF transcriptional activity, showed significant mRNA increase (Fig. 3.7). Thus, this indicates an indirect effect of HIF in the mechanisms controlling the protein levels of ATPase 13A2 and PINK1 in SH-SY5Y cells that is not dependent on the regulation of their gene expression.

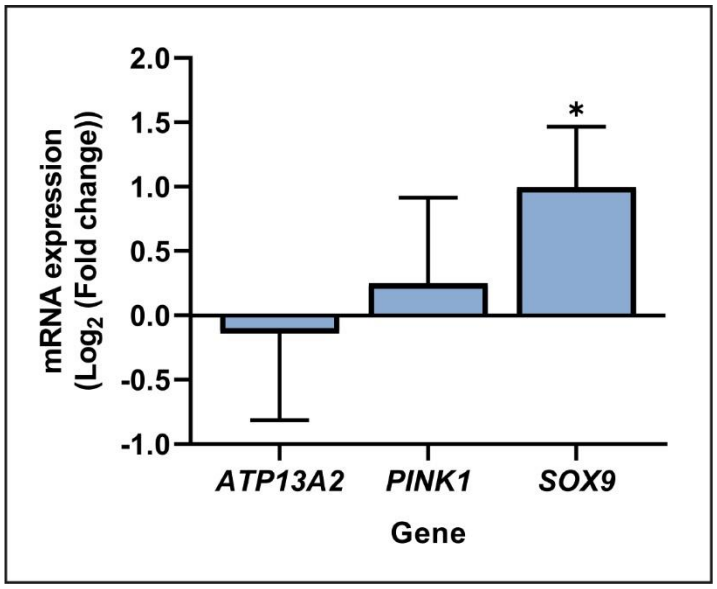

Figure 3.7. $CoCl_2$ does not affect *ATP13A2* and *PINK1* mRNA levels. The graph shows mRNA expression levels normalised to *BACT*, as a fold change against control, of *ATP13A2*, *PINK1* and *SOX9* genes assessed by qRT-PCR in samples from SH-SY5Y cells treated with 100 µM $CoCl_2$ for 24h (n=3). Statistical significance was obtained with an unpaired two-tailed Student's t test where $p<0.05$ was recorded as "*" with respect to control.

3.3.6. HIF-α stabilization modifies the protein levels of PINK1 in dLUHMES

Finally, to determine if the effect of HIF-α stabilization on ATPase 13A2 and PINK1 was cell-type specific, the impact of PHD inhibitors on these proteins was assessed in other cell lines. U-87MG cells show detectable HIF-1α accumulation after 24h of 100µM $CoCl_2$ treatment, similar to SH-SY5Y cells (Fig. 3.8a). However, dLUHMES cells did not show HIF-1α stabilization when treated with $CoCl_2$. This might be related to the specific kinetics of the PHDs in dLUHMES cells, as the specific PHD inhibitor, FG-2216, a 2-OG analogue, was successful in stabilising HIF-1α at the same concentration and was subsequently used in the following experiment (Fig. 3.8b). Interestingly, ATPase 13A2 levels remained unchanged following exposure to PHD inhibitors in both U-87MG and dLUHMES cells, contrary to the findings in SH-SY5Y cells (Fig. 3.8c, d). This potentially indicates that the effect of PHD inhibition on ATPase 13A2 is cell type dependent. Conversely, the significant modest reduction on PINK1 levels demonstrated in SH-SY5Y cells after $CoCl_2$ or hypoxia treatment, was also seen in dLUHMES cells exposed to FG-

2216, although was not replicated in U-87MG cells (Fig. 3.8e, f). Thus, the effect of HIF-α stabilization on PINK1 may be specific to neuronal cells, although the use of an alternative PHD inhibitor in dLUHMES cells complicates definitive confirmation.

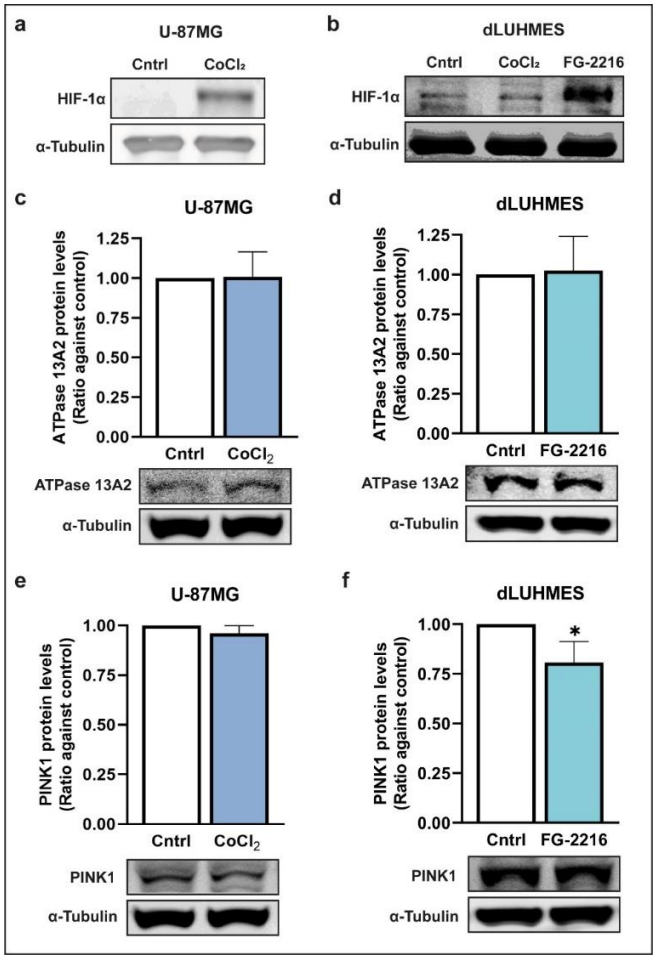

Figure 3.8. Treatment with PHD inhibitors reduces the levels of PINK1 protein in dLUHMES cells but does not modify ATP13A2 protein levels. a. Representative Western Blot image showing HIF-1α (~120 kDa) and α- Tubulin (~55 kDa, loading control) proteins in lysates from U-87MG cells treated with 100 μM $CoCl_2$ for 24h. **b.** Representative Western Blot image showing HIF-1α (~120 kDa) and α- Tubulin (~55 kDa, loading control) proteins in lysates from dLUHMES cells treated with 100 μM $CoCl_2$ or 100 μM FG-2216 for 24h. **c.** Representative Western Blot image showing ATPase 13A2 (~125 kDa) and α- Tubulin (~55 kDa, loading control) proteins in lysates from U-87MG cells treated with 100 μM $CoCl_2$ for 24h accompanied by densitometric analysis (n=3). **d.** Representative Western Blot image showing ATPase 13A2 (~125 kDa) and α- Tubulin (~55 kDa, loading control) proteins in lysates from dLUHMES cells treated with 100 μM FG-2216 for 24h accompanied by densitometric analysis (n=4). **e.** Representative Western Blot image showing PINK1 (~65 kDa) and α- Tubulin (~55 kDa, loading control) proteins in lysates from U-87MG cells treated with 100 μM $CoCl_2$ for 24h accompanied by densitometric analysis (n=3). **f.** Representative Western Blot image showing PINK1 (~65 kDa) and α- Tubulin (~55 kDa, loading control) protein in lysates from dLUHMES cells treated with 100 μM FG-2216 for 24h accompanied by densitometric analysis (n=4). Statistical significance was obtained with an unpaired two-tailed Student's t test where $p<0.05$ was recorded as "*" with respect to control.

3.4.DISCUSSION

Bioinformatic analysis of known PD-related genes revealed that most possess HREs within their promoter regions. However, subsequent evaluation of protein levels demonstrated that expression of the majority remains unaffected, with only ATP13A2 and PINK1 exhibiting downregulation under hypoxic/HIF-1α stabilisation conditions in a specific neuronal cell line.

3.4.1. Bioinformatic evaluation of PD genes as HIF transcriptional targets

This research shows the first systematic bioinformatic analysis of HREs specifically in PD-related genes, using the JASPAR database. All the genes analysed, except *GBA*, showed potential HREs (Table 3.1). However, as mentioned in the introduction, these HREs are ubiquitous within genes but not always active and their functionality should be experimentally determined. Interestingly, the gene with the HRE presenting the highest score, *ATP13A2*, has been shown to have a functional HRE that is bound by HIF-1α in neuronal cells (Xu et al., 2012), and the *LRRK2* gene, transcriptionally induced by HIF-1α in murine cortical neurons, also has several highly scored HREs (Bae et al., 2018). This indicates that the score given by JASPAR, based on how close the sequence is to the motifs of known functional HREs in the genome, can be a useful indicator of potentially active HREs. The functional relationship between PD-associated proteins and HIF-1α was also investigated in the STRING database (Fig. 3.1). Although this study detected the protein-protein interactions of HIF-1α and LRRK2 or Parkin (Liu et al., 2017; Lin et al., 2016), it did not identify a link to the aforementioned HIF-1α transcriptional targets *ATP13A2* and *LRRK2*, which should have been detected via text mining. The other links established via this method were just co-mentions in journal abstracts that do not reference interactions between these proteins. Thus, the STRING database was not found to be effective for detecting potential PD-associated HIF-1α gene targets but could be a valuable resource for the discovery of PD-related proteins interacting with HIF-1α.

3.4.2. Impact of HIF-α stabilization on PD-associated genes

After performing bioinformatic analysis, six genes with varied HRE scores were selected for *in vitro* evaluation. Of these, the protein levels of only two candidate genes were altered by the HIF-α stabilising treatments.

ATPase 13A2 was found to be significantly reduced by PHD inhibition via chemically induced HIF stabilisation or hypoxia treatment specifically in SH-SY5Y cells, although

ATP13A2 mRNA content remained unchanged (Fig. 3.3a; Fig. 3.4b; Fig. 3.6a). Investigation using HIF-1α stabilizing compounds revealed this decrease was specific of this cell type, as U-87MG and dLUHMES cells did not show changes in ATPase 13A2 protein levels, although in dLUHMES cells, this may also be attributed to the use of a different PHD inhibitor (Fig. 3.8c, d). These results point to a regulation of ATPase 13A2 protein levels by an indirect mechanism triggered by HIF-α stabilization. Surprisingly, the *ATP13A2* gene was found to be a HIF-1α transcriptional target by two independent research groups. The first study (Xu et al., 2012) established the presence of functional HREs in the ATP13A2 promoter by luciferase and ChIP assays in HEK293 and MND9 cells exposed to 2% O_2 for 24h. In this study, endogenous *ATP13A2* mRNA level was also found to be increased by qRT-PCR, while protein levels of ATPase 13A2 were not investigated. The second study (Rajagopalan et al.,2016) showed that striatal tissue extracted from a PHD2-KO mice model displayed increased *ATP13A2* mRNA expression and protein levels. Mesencephalic cultures from control mice treated with the PHD2 inhibitor IOX2 also showed increased *ATP13A2* expression. Thus, there is a clear discrepancy between the published investigations and the results reported in this study, which might be due to a variety of reasons. Firstly, the cell lines used in this study differ from the ones used in the cited research papers. Indeed, with the exception of the human HEK293 cell line, the effects of PHD inhibition on *ATP13A2* levels were only tested in murine cells. The results obtained in this investigation show different effects on ATPase 13A2 levels depending on the cell line, which might indicate that the HREs in the *ATP13A2* promoter are not always active and could explain the differences observed. Other circumstances have been shown to modify the capacity of HIF-1α to bind HREs, so elements such as the amount of glucose in the cell media can influence this and could have an impact on the results of these studies (Katavetin et al., 2006). Secondly, differences in the O_2 concentration and/or the concentration/exposure time to chemically induced HIF-1α during culturing could affect HIF-1α accumulation. Studies show that different hypoxia severities and durations, as well as differences in HIF-1α abundance, can elicit diverse transcriptional responses, so this could also contribute to the variances observed between studies (Weiszenstein et al., 2016; Rana et al., 2019). Thirdly, silencing of HIF-1α was not performed in any of these studies, so a contribution of HIF-2α to the effects seen cannot be ruled out. In addition, the hypoxic cells generated in the first study (Xu et al., 2012) were treated with 100μM $CoCl_2$ for 4h before harvest and experimental use, which was not accounted for in the study although the combined exposure to hypoxia and $CoCl_2$ might have off-target effects. The RNA and protein extractions performed in

the study presented here are completed rapidly to avoid HIF-1α degradation and controlled for HIF-1α protein accumulation or HIF-1α gene target expression to ensure the presence of HIF-1α stabilization in the samples (Fig. 3.2b; Fig. 3.4a; Fig. 3.5a; Fig. 3.7; Fig. 3.8a, b). To summarize, further research performed in different cell lines, under diverse HIF-1α stabilization paradigms and with appropriate controls is needed to evaluate the functionality of the HREs in the *ATP13A2* gene and the consequent effects of HIF-1α stabilization on ATPase 13A2 protein expression.

PINK1 protein levels experienced a significant, albeit small, reduction in SH-SY5Y and dLUHMES cells subjected to PHD inhibitory conditions, whilst *PINK1* gene expression remained constant (Fig. 3.3c; Fig. 3.6c; Fig. 3.7; Fig. 3.8f). However, the use of different PHD inhibitors, $CoCl_2$ in SH-SY5Y cells and FG-2216 in dLUHMES cells, introduces a potential challenge in interpreting the combined results. The effect on PINK1 abundance was not recapitulated by U-87MG cells (Fig. 3.8e). This suggests a neuron-specific effect of HIF-1α stabilization on PINK1, possibly through indirect mechanisms, as this is observed in both neuronal cell lines, dLUHMES and SH-SY5Y, regardless of the PHD inhibitor used. Indeed, a decrease in PINK1 protein levels caused by HIF-α-mediated activation of the transcriptional repressor HEY1 after 24h 1% O_2 treatment has been described in hepatocellular carcinoma cells (Kung-Chun Chiu et al., 2019). In differentiated PC12 cells, exposition to 0.5% O_2 for 24 h or 1% O_2 for 48 h caused a decrease in PINK1 abundance (Xu et al., 2018), although the involvement or HIF was not explored. However, increased PINK1 protein levels after O_2 deprivation have also been detected in several cell types in the context of hypoxia-induced mitophagy (Li et al., 2020; Wang et al., 2023). Thus, additional studies are required to elucidate the mechanisms involved in HIF-α mediated reduction of *PINK1* levels in neuronal cells and its biological relevance.

The observed protein level changes in ATP 13A2 and PINK1, which are not mirrored in their mRNA levels, suggest HIF-1α may be exerting an indirect effect by inducing or repressing the expression of genes involved in the regulation of these proteins at the post-transcriptional level. Given the known roles of PINK1 in mitochondrial homeostasis and ATP13A2 in autophagy, both of which are cellular processes modulated by hypoxia, the observed protein level changes could be a consequence of HIF-induced alterations in these very pathways. Understanding the specific factors governing this process is further challenged by the limited overlap in hypoxia-deregulated genes observed between cell types (Yfantis et al., 2023). This finding highlights the dependence of the transcriptional

response to hypoxia on cellular context, as demonstrated in this study. Despite limited knowledge on the specific roles of HIF-1α in neurons versus astrocytes, the varying reliance on mitochondrial respiration and autophagy by these cell types may account for the observed discrepancies in protein level regulation (Juaristi et al., 2019; Kulkarni et al., 2020).

The remaining set of PD-associated genes investigated did not show significant protein level changes in SH-SY5Y cells under 24h $CoCl_2$ or 1% O_2 treatment (Fig. 3.3b, d, e, f; Fig. 3.6b, d, e, f). The possibility that these genes are HIF targets cannot be definitively ruled out, as they might be targets that are transiently altered and subsequently normalised by 24h, be induced by mild hypoxia (lower $CoCl_2$ concentration or at a higher O_2 concentration) or contain inducible HREs only activated in specific circumstances or cell types. It is important to acknowledge that the activity/dimerization of HIF-1α was not investigated so the observed lack of gene activation might be due to insufficient HIF-1α transcriptional activity. Additionally, due to the links already established between the hypoxia response and PD and the widespread use of SH-SY5Y cells in PD research, it is possible that the hypoxia response on PD-associated genes and proteins in this cell line were studied previously but not published due to the prevalent bias towards publishing positive research results against neutral or negative findings in the scientific literature (Nissen et al., 2016).

3.5.CONCLUSION

According to our current understanding, this study constitutes the first structured attempt at identifying HIF transcriptional targets in a set of PD-related genes. This investigation provides a table comprising candidate HREs present in known PD-related genes that can be referred to in subsequent investigations. Although none of the PD-associated proteins analysed showed increased protein levels upon PHD inhibition, indicating they are not hypoxia-inducible targets under these HIF-α stabilization conditions in this specific cell lines, two proteins, ATPase 13A2 and PINK1, showed decreases protein levels in response to HIF-α stabilization in SH-SY5Y cells. The occurrence of this alteration only in certain cell lines further contributes to the recent evidence supporting that HREs can be inducible and that HIF gene targets should be studied in a variety of conditions and cell types. The specific involvement of HIF-1α in this effect should be further investigated by silencing the different HIF-α subunits. The precise mechanisms behind the HIF-

mediated reduction of these proteins could be elucidated by investigating proteins in the HIF targetome that constitute potential inhibitors of ATPase 13A2 or PINK1.

To explore the impact of hypoxia and HIF-1α stabilization on PD in more detail, the impact of these factors on posttranscriptional modifications in PD-related proteins, which can control their activity, should be investigated. It would be of interest to explore the effect of silencing PD-associated genes on HIF-1α stabilization, as disruptions in this mechanism could mean patients with these mutations show an impaired response to hypoxia and are exposed to higher hypoxic damage from pathologies such as TBI. Certainly, the effect hypoxic disorders, including TBI and stroke, have on PD-related gene and protein levels is a topic that would be worth investigating further, but it is beyond the scope of this study. These future investigations would contribute knowledge to determine the role of hypoxia and the HIF-1α response in PD pathology.

In conclusion, this foundational research into the effect of HIF-α stabilization via hypoxia or PHD inhibitors on PD-related genes could have implications for PD. In fact, the research presented shows a reduction in two PD-associated proteins, PINK1 and ATPase 13A2, as a result of the activation of the hypoxia response, which might be related to hypoxic events such as TBI or stroke constituting PD risk factors. In addition, this investigation can help to improve the efficacy of future HIF-1α based therapeutics for PD, which might not be suitable for patients presenting certain mutations.

CHAPTER IV

EFFECT OF PD-RELATED STRESSORS ON HIF-1α LEVELS

4.1. INTRODUCTION

Dysregulation of HIF-1α signalling has been observed in PD patients (Grünblatt et al., 2004; Miller et al., 2006), but the underlying mechanisms are not fully understood. While the effect of HIF-1α on PD-associated pathways has been studied, the impact of PD-related stressors on HIF-1α has not been investigated. The present chapter addresses whether dysfunction of the molecular pathways involved in PD pathogenesis can alter HIF-1α levels, leading to impaired neuronal function and weakened response to hypoxic events that constitute risk factors for PD. This study will utilize both neuronal and astrocytic cell lines to investigate how PD-associated pathway dysfunction differentially affects HIF-1α levels in distinct cell types.

4.1.1. *In vitro* modelling of PD-related pathways

4.1.1.1. Mitochondrial dysfunction

Mitochondrial dysfunction has been widely associated with both sporadic and familial PD pathogenesis (Gao et al., 2022). The involvement of mitochondria in PD has led to the development of well-established experimental models that use mitochondrial toxins to induce the disease. These include two mitochondrial ETC complex I inhibitors, MPTP/MPP+ and rotenone. MPTP neurotoxicity was discovered after a of group people began experiencing PD symptoms following exposure to an illegally synthesised opiate mix. This PD manifestation was traced back to MPTP, which was detected in the drug cocktail. Once in the bloodstream, MPTP can easily cross the blood brain barrier and access the brain, where the enzyme Monoamine Oxidase B, present mostly in astrocytes, transforms MPTP into MPP+. MPP+ can no longer easily diffuse through cell membranes but is incorporated into DAergic neurons thanks to its high affinity to the DA transporter (Mustapha et al., 2020). Rotenone is an organic pesticide and insecticide, produced by the roots of certain plants, and it is highly lipophilic, being able to bypass the blood brain barrier and cell membranes (Johnson et al., 2015). Both toxins cause specific loss of SNpc DAergic neurons and impairment of motor behaviour in animal models. However, only rotenone has been shown to induce aggregation of α-Syn in the SNpc (Jiang et al., 2018). Mitochondrial metabolism can be investigated by measuring O_2 consumption rate with cell respirometers, analysing the activity of ETC complexes with spectrophotometric assays, determining ATP production with fluorescent or bioluminescent reagents and assessing mitochondrial membrane potential with cationic fluorescent dyes like Tetramethylrhodamine methyl ester or JC-1. When examining mitochondrial membrane

potential, it is important to utilise mitochondrial uncouplers as positive control, such as Carbonyl cyanide m-chlorophenylhydrazone (CCCP), which makes the mitochondrial inner membrane leaky to protons (Connolly et al., 2017). PD is also associated with changes in mitochondrial dynamics and mtDNA, which can be investigated by microscopy and PCR respectively (Yin et al., 2022).

4.1.1.2. Oxidative stress

Excessive production of ROS, which can be a consequence of mitochondrial dysfunction, is believed to play a role in PD development and progression. Indeed, the impact of ROS in PD has been primarily investigated in PD models that have been treated with mitochondrial toxins, such as rotenone and MPTP, or have mutations in genes that play a role in mitochondrial homeostasis. Mitochondria are the main producers of ROS but are also very susceptible to them (Puspita et al., 2017). The fact that most oxidants can trigger mitochondrial dysfunction makes it challenging to discern their individual contributions to PD pathogenesis. Nevertheless, multiple compounds that cause increased ROS production have been discovered and can be utilised to study oxidative stress in PD models. Some environmental factors that induce oxidative stress, including exposure to UV light, pesticides and heavy metals, can be replicated in the laboratory (Samet et al., 2018). Several studies have utilised the herbicide paraquat, which produces ROS by suppressing intracellular antioxidant enzymes, to model PD. Similarly, naturally occurring processes in DAergic neurons produce oxidative stress, including DA metabolism, which generates H_2O_2 and superoxide. Indeed, the DA mimic 6-OHDA, widely used to create experimental models of PD, is spontaneously oxidised, producing free radicals (Zeng et al., 2016). Besides, exogenous oxidant compounds can be used to study the mechanisms of oxidative stress present in PD. For example, cells can be treated with Menadione, which generates superoxide and H_2O_2 or 2,2'-Azobis(2-amidinopropane) dihydrochloride (AAPH) which induces the formation of peroxyl radicals (Kelts et al., 2015). ROS can also be induced by chemicals inhibiting antioxidant mechanisms, such as buthionine sulfoximine (BSO), which blocks Glutamate–cysteine ligase, the enzyme that catalyses the rate-determining step in GSH production, or genetic KO of antioxidant enzymes like Catalase or Superoxide Dismutase (Desideri et al., 2019). The effect of ROS on a specific pathway can be evaluated by using antioxidants. Antioxidants can be enzymes, endogenous molecules like GSH, or exogenous compounds like N-Acetylcysteine (NAC) and certain vitamins. Numerous antioxidants have proven

to be beneficial in PD models, including NAC, a precursor to GSH which has undergone Phase II clinical trials for PD treatment (Monti et al., 2019). Vitamins E and C, also named α-tocopherol and Ascorbic Acid (ASC) respectively, exhibit redox properties that allow them to neutralize ROS and have shown promise as neuroprotective agents in PD (Zhao et al., 2019). Intracellular oxidative stress can be measured by utilising fluorogenic probes. These include 5-(and-6)-carboxy-2′,7′-dichlorodihydrofluorescein diacetate (DCFDA), which generates fluorescence upon reaction with H_2O_2, hydroxyl radicals or peroxyl radicals. Similarly, superoxide can be assessed by the fluorescent probe dihydroethidium. The impact of ROS can also be investigated by measuring oxidative changes in proteins, lipids and DNA (Katerji et al., 2019). The antioxidant potential of cell models can be determined by measuring antioxidant enzyme activity and capacity to scavenge ROS (Carocho et al., 2012). These techniques are frequently used in PD research to assess oxidative stress levels caused by PD-related toxins and the efficacy of potential therapeutics.

4.1.1.3. Impaired protein degradation

An impairment to protein degradation has been linked to PD pathophysiology and is believed to contribute to α-Syn accumulation. In PD, both the ubiquitin-proteasome system and autophagy seem to be affected (Lehtonen et al., 2019). Consequently, compounds that have been developed to modulate these pathways can be utilised to study PD. The first proteasome inhibitor that was artificially developed is MG132, a cell-permeable peptide that reversibly binds to threonine residues in the active site of the proteasome. However, MG132 has been shown to have unspecific effects, including the inhibition of calpains and lysosomal cysteine proteases (Sherman et al., 2020). In contrast, Lactacystin (LACT), a non-peptidic natural compound produced by soil bacteria, blocks proteasome activity with high selectivity and without affecting lysosomal enzymes or other proteases. LACT acts by covalently binding and irreversibly inactivating all proteasomal catalytic β-subunits (Ōmura et al., 2019). Due to its characteristics, LACT has been used to study the proteasome inhibition model of PD both in vivo and in vitro. Treatment of DAergic cell lines and primary neurons with LACT triggers apoptosis and aggregation of cytoplasmic α-Syn (Bentea et al., 2017). Similarly, injection of LACT into the SNpc of rodent models causes DAergic neuron degeneration, formation of toxic α-Syn oligomers and motor symptoms (Vernon et al., 2010). In recent years, novel proteasome inhibitors have been developed due to their efficacy in treating certain types

of cancer and innovative proteasome blockers targeted to different proteasome activities are now being explored (Sherman et al., 2010). While proteasome inhibitors should be used with caution, as complete proteasome obstruction is lethal for cells, these compounds remain a valuable tool for the study of PD. Proteasome activity can be measured in proteasome or cell extracts by utilising a peptide or protein substrate linked to a fluorescent or bioluminescent reporter probe that gets cleaved and activated when the substrate is processed by the proteasome (Gan et al., 2019).

Modulation of both macroautophagy and chaperone-mediated autophagy (CMA) has been regarded as a therapeutic target for PD since the discovery that several PD-related genes and toxins cause autophagy dysfunction and consequent α-Syn build-up. Thus, molecules that can induce and supress these autophagic pathways are useful in the investigation of PD. Initiation of macroautophagy is repressed by mTORC1, so inhibitors of these protein, such as rapamycin or starvation, can kickstart autophagy. Autophagy continues through the formation of the phagophore and subsequent autophagosome, which requires the activity of class III PI3-kinases (PI3KIII) and ATG proteins, which can be inhibited by inhibitors like 3-methyladenine (3-MA) or genetic KO respectively. Ultimately, the fusion of the autophagosome with the lysosome and consequent degradation of the autophagic cargo can be supressed by Bafilomycin A1 (BAF) or Chloroquine (CQ) (Mizushima et al., 2010). As inhibition of lysosomal activity by these chemicals can impact other cellular pathways, pharmacological studies should be combined with other experiments, such as the assessment of synthetic autophagy substrate degradation or LC3B-II protein abundance. LC3B-II levels increase upon induction to autophagy as this protein is formed from LC3B-I by the addition of a phosphatidylethanolamine residue by autophagic ATG proteins and attached to nascent phagophores. LC3B-II is degraded after autophagosome-lysosome fusion, so chemically induced autophagy blockade at later stages would also induce LC3B-II accumulation. This molecule constitutes a valuable tool for evaluating autophagy state, especially in combination with compounds that modulate autophagy, and can also be monitored in live cells over time when tagged with a fluorescent molecule. Investigating colocalization of a protein with LC3B-II and evaluating protein levels when utilising different combinations of inhibitors can help determine whether a specific protein is being degraded through macroautophagy (Tanida et al., 2005). In the case of CMA, use of inhibitors of chaperone Hsc70, which binds and direct proteins towards the LAMP-2 receptor in the lysosome, can supress this process. LAMP-2 levels are increased by

compounds that generate ROS, such as 6-aminonicotinamide, and downregulated by antioxidants (Hubert et al., 2022). However, fast-acting chemical agents that can specifically suppress CMA have not yet been developed. To investigate CMA flux, assays that study lysosomal levels of CMA proteins, quantity of CMA-active lysosomes or turnover rate of known CMA targets can be utilised. In order to determine whether a protein is a CMA substrate, its interaction with LAMP2A and Hsc70 can be studied by immunoprecipitation (Pate et al., 2015). Disruption of lysosomal protein degradation in animal models by toxins or genetic KO of autophagy-related genes recapitulates many PD features, including α-Syn aggregation, loss of DAergic neurons and motor dysfunction (Jiang et al., 2018). Indeed, autophagy inducers like rapamycin have been shown to be protective against PD, while use of autophagy inhibitors such as BAF can induce the formation of α-Syn inclusions that trigger cell apoptosis (Malagelada et al., 2010; Klucken et al., 2012).

4.1.2. Regulation of HIF-1α from transcription to degradation

4.1.2.1. *HIF1A* gene expression

Although HIF-1α regulation in hypoxia is mainly posttranslational, a swift but brief increase in *HIF1A* mRNA abundance in response to low O_2 has been detected in several cell types (Görlach et al., 2009). Investigation into the epigenetic changes elicited by hypoxia shows that, while intermittent hypoxia increases histone H3 lysine demethylation near the HIF1A locus with concomitant increase of *HIF1A* expression, chronic O_2 deprivation causes hypermethylation of this histone (Martinez et al., 2022). Indeed, additional mechanisms, such as activation of transcriptional repressors that mediate the downregulation of *HIF1A* mRNA production, are induced in sustained hypoxia to counteract excessive HIF-1α accumulation (Pierre et al., 2015; Cavadas et al., 2015). The expression of the *HIF1A* gene is also tightly regulated by TFs and chromatin modifications. The *HIF1A* promoter has an antioxidant response element motif that can be bound by NRF2, which upregulates *HIF1A* expression (Lacher et al., 2018). Similarly, ROS-induced binding of NFκB to the *HIF1A* promoter increases *HIF1A* mRNA levels (Bonello et al., 2007). A variety of stimuli can induce the activity of other TFs, including STAT3, STAT1 and SP1, that control *HIF1A* gene transcription rate in normoxia (Niu et al., 2008; Yao et al., 2022).

4.1.2.2. HIF-1α protein synthesis

The stability of the *HIF1A* mRNA determines the quantity of transcript that is accessible to ribosomes for protein synthesis. The 3′-untranslated region of the *HIF1A* mRNA has numerous conserved AU-rich elements that are known to regulate the rapid degradation of mRNAs (Sheflin et al., 2004). Indeed, multiple factors that can interact with these sequences specifically reduce *HIF1A* mRNA half-life, including RNA binding proteins, micro RNAs (miRNA) and long non-coding RNAs (lncRNAs) (Loh et al., 2020; Chamboredon et al., 2011; Bruning et al., 2011; Uchida et al., 2004). On the contrary, certain RNA binding proteins can promote *HIF1A* mRNA stability (Sheflin et al., 2004). Although activation of some of these inhibitory mechanisms has been associated with hypoxia-mediated *HIF1A* mRNA decay, the induction of this process by non-hypoxic stressors has not been explored.

The regulation of HIF-1α levels is thought to be heavily influenced by its translation, which is estimated to account for 40-50% of the increase in HIF-1α levels (Galbán et al., 2009). In fact, the rise in HIF-1α biosynthesis is a notable exception to the general decrease in translation that occurs in hypoxic cells. In normoxia, *HIF1A* mRNA translation is kept to a minimum and controlled mainly by mTOR influence on the canonical cap-dependent translation pathway (Knaup et al., 2009). However, a variety of signalling molecules like growth factors and cytokines can promote *HIF1A* mRNA translation in normoxic conditions (Zhou et al., 2006). In hypoxia, HIF-1α biosynthesis is believed to be linked to the presence of internal ribosomal entry site elements in the *HIF1A* mRNA, which are not affected by the global repression of transcription elicited by hypoxia and allow for cap-independent translation to occur. Similarly, several RNA binding proteins can also promote *HIF1A* mRNA translation (Koh et al., 2008).

4.1.2.3. HIF-1α protein stability

Once HIF-1α has been synthesised its stability is strictly regulated by the PHD/pVHL/proteasome system. The stability of PHDs and pVHL is in turn controlled by specific E3 ubiquitin ligases (Fong et al., 2008; Jung et al., 2006). PHDs can also be induced at the transcriptional level, as PHD2 and PHD3 are HIF-1α target genes, which serves as a negative feedback loop under hypoxia and ensures rapid HIF-1α degradation upon normoxia (Stiehl et al., 2006). Interestingly, accessibility of pVHL E3 ligase complex to HIF-1α can be stimulated by regulatory proteins in order to increase HIF-1α degradation (Baek et al., 2005; Baek et al., 2007). Thus, factors affecting the

PHD/pVHL/proteasome system can have an impact on HIF-1α accumulation in hypoxia or in the presence of PHD/pVHL inhibition.

Although VHL was first discovered and seems to be the main E3 ubiquitin ligase controlling HIF-1α degradation, several recent studies have uncovered alternative E3 ubiquitin ligases that are able to polyubiquitinate HIF and direct it towards degradation independently of O_2 gradient and the PHD/VHL system. For example, E3 ubiquitin ligases Parkin, MDM2, hypoxia-associated factor (HAF) and C-terminus of Hsc70-interacting protein (CHIP) have been found to direct HIF-1α to proteasomal degradation (Liu et al., 2017; Joshi et al., 2014; Koh et al., 2008; Bento et al., 2010). Proteins that induce the recruitment of the E3 ubiquitin ligase machinery to HIF-1α, including the receptor of activated protein kinase (PK)C (RACK1), Glycogen synthase kinase 3 (GSK3) and Polo-like kinase 3 (PLK3) also promote HIF-1α degradation via the proteasome (Liu et al., 2007; Flugel et al., 2007; Xu et al., 2010). Remarkably, degradation of HIF-1α by autophagy has recently been reported. HIF-1α contains a non-canonical KFERQ-motif, which targets proteins for degradation via CMA. Degradation of HIF-1α through CMA can be facilitated by E3 ubiquitin ligase CHIP and Cyclin dependent kinase 2 (Cdk2) irrespectively of O_2 tension (Ferreira et al., 2015; Hubbi et al., 2014). In addition, HIF-1α has been shown to be degraded by macroautophagy in the presence of the Q6 hypoxia-targeted drug and a mTORC1/2 inhibitor (Liu et al., 2014; Zheng et al., 2015). However, this is just one part of the puzzle, as HIF-1α stability is heavily regulated by a plethora of post-translational modifications, which are also involved in the activity of some of the aforementioned proteins. For example, GSK3 and PLK3 phosphorylate HIF-1α to promote its degradation. Other proteins like Cdk1, Cdk5, and ATM can phosphorylate HIF-1α at distinct sites to promote stabilisation. HIF-1α stability can also be compromised or induced by acetylation, methylation, SUMOylation, S-Nitrosylation, S-Glutathionylation and Neddylation (Albanese et al., 2021). Remarkably, lack of acetylation, methylation, or SUMOylation on specific HIF-1α amino acids appears to promote its stability, whereas the presence of these modifications triggers HIF-1α degradation (Semenza, 2017). These findings provide evidence that the degradation of HIF-1α is a complex process that involves both the proteasome and autophagy, although the factors that influence the choice of degradation pathway for HIF-1α are a matter of ongoing research.

4.1.3. Aims of the chapter

This chapter focuses on characterizing changes in HIF-1α levels induced by PD-associated pathway dysfunction. HIF-1α dysregulation is implicated in impaired neuronal function and a weakened response to hypoxic events such as TBI and OSA, which constitute risk factors for PD. By examining whether PD-related stressors affect the cellular response to hypoxia through HIF-1α, we can gain insights into the vulnerability of DAergic neurons in the disease. The pathways investigated include:

1) Mitochondrial dysfunction
2) Oxidative stress
3) Protein degradation impairment

4.2. METHODOLOGY

Western Blot and qRT-PCR were used to measure changes in HIF-1α protein levels and gene expression respectively in SH-SY5Y, U87-MG and dLUHMES cells. HIF-1α was stabilized by different PHD inhibitors in the presence of PD-related stressors used simultaneously, inducing mitochondrial damage, increased ROS and protein degradation impairment. A variety of techniques were utilised to assess the impact of these treatments on the cells, including measuring cell viability, ATP levels, mitochondrial membrane depolarisation, proteasome activity, GSH content and ROS production. Chapter II can be referred to for full details on methodology.

4.3. RESULTS

4.3.1. IMPACT OF MITOCHONDRIAL DYSFUNCTION ON HIF-1α

4.3.1.1. Mitochondrial toxins reduce HIF-1α levels in SH-SY5Y and U-87MG cells

In order to investigate the effect of mitochondrial dysfunction in HIF-1α protein levels, we employed several mitochondrial toxins, including two inhibitors of ETC Complex I, Rotenone and MPP+, and a mitochondrial uncoupler, CCCP. SH-SY5Y and U-87MG cells were exposed to these mitochondrial toxins in the presence of $CoCl_2$ to evaluate HIF-1α accumulation, as HIF-1α is undetectable in normoxic conditions. Interestingly, the effect of these chemicals is similar in both cell lines, with lower concentrations of rotenone and CCCP, as well as MPP+, causing a reduction in HIF-1α protein abundance despite $CoCl_2$-induced PHD inhibition (Fig. 4.1a-d). Analysis of cell viability demonstrates that rotenone is more effective at reducing cellular metabolic activity than MPP+ (Fig. 4.1e). In addition, evaluation of ATP levels in SH-SY5Y cells shows a reduction in ATP content after all treatments, but MPP+ caused a significantly less pronounced decrease than Rotenone and CCCP (Fig. 4.1f). It is worth noting that $CoCl_2$ alone provokes a reduction in ATP production without impacting cell viability. Thus, mitochondrial toxins, when used at a dose that triggers mild mitochondrial damage, can lower HIF-1α accumulation in $CoCl_2$-treated SH-SY5Y and U-87MG cells. Consequently, as MPP+ caused the greatest decrease in HIF-1α levels, it was used as a model for the following experiments.

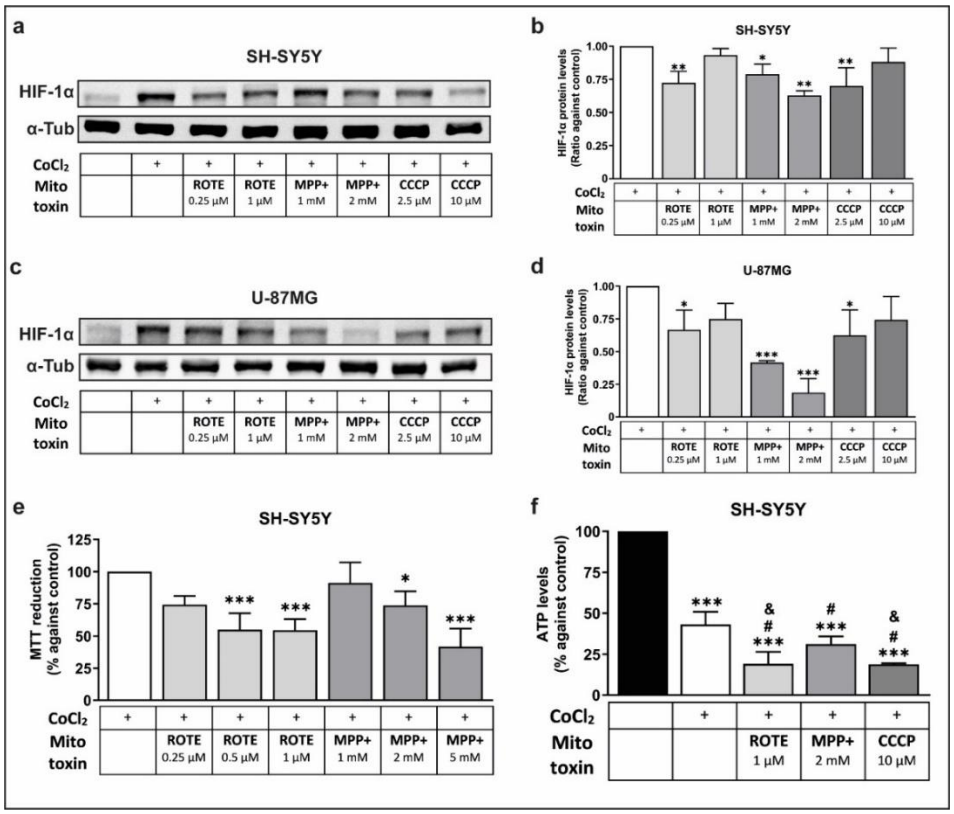

Figure 4.1. Mitochondrial toxins reduce $CoCl_2$-mediated HIF-1α accumulation in SH-SY5Y and U-87MG cells and lower viability and ATP levels. a. Representative Western Blot image showing HIF-1α (~120 kDa) and α-Tubulin (~55 kDa, loading control) proteins in lysates from SH-SY5Y cells treated with 100μM $CoCl_2$ for 24h in combination with Rotenone (0.25 μM or 1 μM), MPP+ (1 mM or 2 mM) or CCCP (2.5 μM or 10 μM). **b.** Plot summarising densitometric analysis of the a. Western Blot (n=3). **c.** Representative Western Blot image showing HIF-1α (~120 kDa) and α-Tubulin (~55 kDa, loading control) proteins in lysates from U-87MG cells treated with treated with 100μM $CoCl_2$ for 24h in combination with Rotenone (0.25 μM or 1 μM), MPP+ (1 mM or 2 mM) or CCCP (2.5 μM or 10 μM). **d.** Plot summarising densitometric analysis of the c. Western Blot (n=3). **e.** Plot displaying MTT reduction in SH-SY5Y cells treated with $CoCl_2$ and Rotenone (0.25 μM, 0.5 μM or 1 μM) or MPP+ (1 mM, 2 mM or 5 mM) for 24h (n=3). **f.** Graph showing ATP content in lysates from SH-SY5Y cells treated with 100 μM $CoCl_2$ (CC) in combination with 1 μM rotenone, 2 mM MPP+ or 10 μM CCCP for 24h (n=3). Statistical analysis was performed using a one-way ANOVA followed with Dunnett's post-hoc test where $p<0.05$ was recorded as "*" with respect to control ($CoCl_2$ for b, d and e), "#" with respect to $CoCl_2$ in plot f and "&" when comparing to $CoCl_2$ and MPP+ combined treatment in plot f.

4.3.1.2. Antioxidants lower HIF-1α levels in the presence of MPP+

As ROS have been implicated in the control of HIF-1α abundance and MPP+ is known to produce oxidative stress, we evaluated whether the use of antioxidants reverses MPP+-mediated reduction of HIF-1α protein levels. This will allow to determine if the effect of MPP+ is linked to its capacity to generate ROS or is solely dependent on its ability to induce mitochondrial dysfunction. SH-SY5Y and U-87MG cells were treated with $CoCl_2$ and MPP+ in the presence of ROS scavengers ASC, NAC and GSH. Interestingly, treatment with an antioxidant in conjunction with MPP+ significantly reduces HIF-1α protein levels when compared against MPP+ treatment alone in both cell lines (Fig. 4.2a-d). This indicates that the effect observed is unlikely to be caused directly by ROS, and that a lack of oxidative stress can enhance the MPP+ effect by exacerbating the decrease in HIF-1α accumulation.

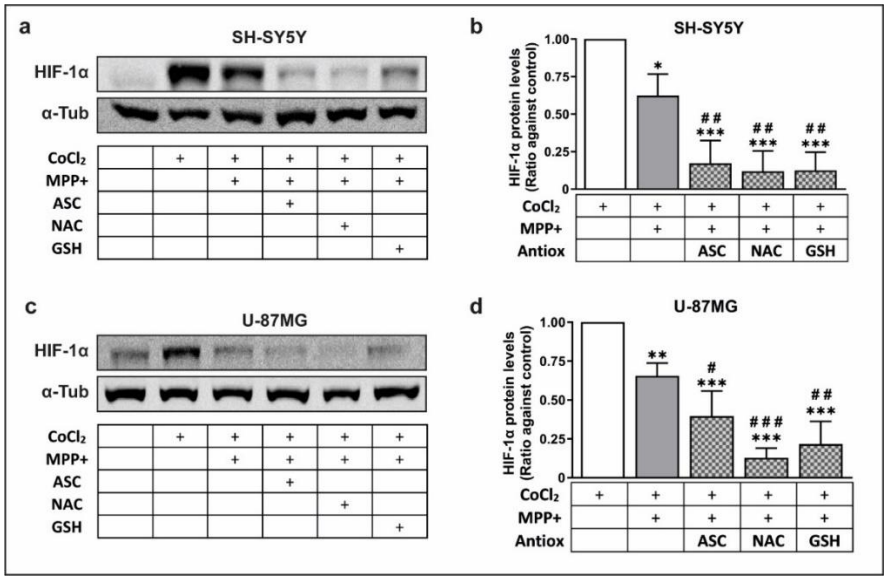

Figure 4.2. Antioxidants ASC, NAC and GSH accentuate MPP+-mediated decrease on HIF-1α levels in SH-SY5Y and U-87MG cells. a. Representative Western Blot image showing HIF-1α (~120 kDa) and α-Tubulin (~55 kDa, loading control) proteins in lysates from SH-SY5Y cells treated with 100μM $CoCl_2$ for 24h in combination with 2 mM MPP+ and 1 mM of antioxidants ASC, NAC or GSH. **b.** Plot summarising densitometric analysis of the a. Western Blot (n=3). **c.** Representative Western Blot image showing HIF-1α (~120 kDa) and α-Tubulin (~55 kDa, loading control) proteins in lysates from U-87MG cells treated with 100μM $CoCl_2$ for 24h in combination with 2 mM MPP+ and 1 mM of antioxidants ASC, NAC or GSH. **d.** Plot summarising densitometric analysis of the c. Western Blot (n=3). Statistical analysis was performed using a one-way ANOVA followed with Dunnett's post-hoc test where $p<0.05$ was recorded as "*" with respect to control ($CoCl_2$) and "#" when comparing to combined treatment ($CoCl_2$ and MPP+).

4.3.1.3. The effect of MPP+ on HIF-1α is independent of the PHD inhibition method

To rule out the possibility that MPP+ is specifically disrupting the mechanism of action of $CoCl_2$, the effect of MPP+ on HIF-1α stabilization was assessed using an alternative PHD inhibitor, the 2-OG mimic FG-2216. The results show that MPP+ reduces HIF-1α protein accumulation in the presence of FG-2216 in both SH-SY5Y and U-87MG cells (Fig. 4.3a-d), which is consistent with the outcome of the study on $CoCl_2$, demonstrating that the influence of MPP+ on HIF-1α levels is not affected by the HIF-1α stabilising strategy utilised.

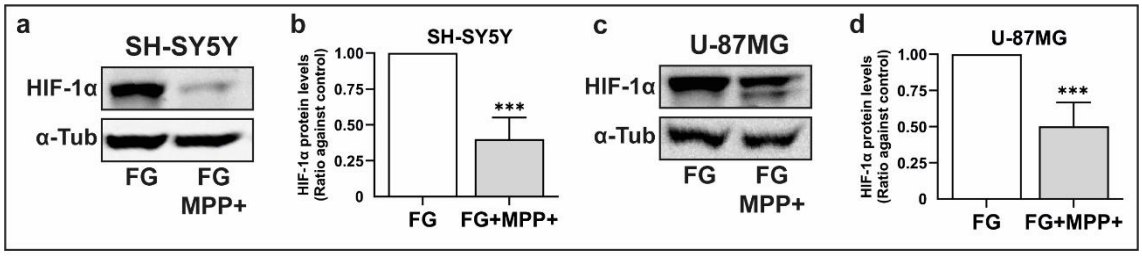

Figure 4.3. The effect of MPP+ on HIF-1α levels is maintained in the presence of alternative PHD inhibitor FG-2216 in SH-SY5Y and U-87MG cells. a. Representative Western Blot image showing HIF-1α (~120 kDa) and α-Tubulin (~55 kDa, loading control) proteins in lysates from SH-SY5Y cells treated with 100μM FG-2216 (FG) for 24h in combination with 2 mM MPP+. **b.** Plot summarising densitometric analysis of the a. Western Blot (n=4). **c.** Representative Western Blot image showing HIF-1α (~120 kDa) and α-Tubulin (~55 kDa, loading control) proteins in lysates from U-87MG cells treated with 100μM FG-2216 (FG) for 24h in combination with 2 mM MPP+. **d.** Plot summarising densitometric analysis of the c. Western Blot (n=4). Statistical analysis was performed using an unpaired two-tailed Student's t test where $p<0.05$ was recorded as "*" with respect to control (FG).

4.3.1.4. MPP+ induces HIF-1α autophagic clearance and reduces *HIF1A* expression

Both $CoCl_2$ and FG-2216 inhibit PHDs, so it is conceivable to hypothesise that MPP+ may affect HIF-1α regulation upstream of PHD activity, including *HIF1A* mRNA expression and turnover, or directly impact HIF-1α stability independently of PHDs. Evaluation of HIF-1α stabilization by $CoCl_2$ in the presence of MPP+ over time showed a significant decrease in $CoCl_2$-induced HIF-1α protein levels upon exposure to MPP+

for all timepoints investigated in both SH-SY5Y and U-87MG cells (Fig. 4.4a-d). This implies that MPP+ can effect both *HIF1A* transcription and HIF-1α degradation, most likely through mechanisms common to both cell lines. To study the clearance pathway of HIF-1α in this experimental setting, SH-SY5Y cells incubated with $CoCl_2$ and MPP+ and cotreated with proteasome blocker LACT or autophagy inhibitor CQ were used. Although the MPP+-mediated reduction in HIF-1α protein was not rescued by treatment with LACT, exposure to CQ returned HIF-1α protein levels to baseline (Fig. 4.4e). These findings suggest that MPP+ reduces HIF-1α levels by destabilising HIF-1α, despite PHD inhibition, whilst increasing its degradation via autophagy. Given that HIF-1α typically undergoes degradation by the proteasome, it is reasonable to speculate that the reduction in ATP levels induced by MPP+ could lead to decreased proteasome activity, thereby shifting HIF-1α degradation towards autophagy. Indeed, MPP+ treatment in the presence of $CoCl_2$ resulted in a significant decrease of 25% in proteasome activity compared to the $CoCl_2$ control (Fig. 4.4f). Thus, autophagy can become a dominant pathway for HIF-1α degradation when proteasome activity is impaired by MPP+, even in the presence of PHD inhibition.

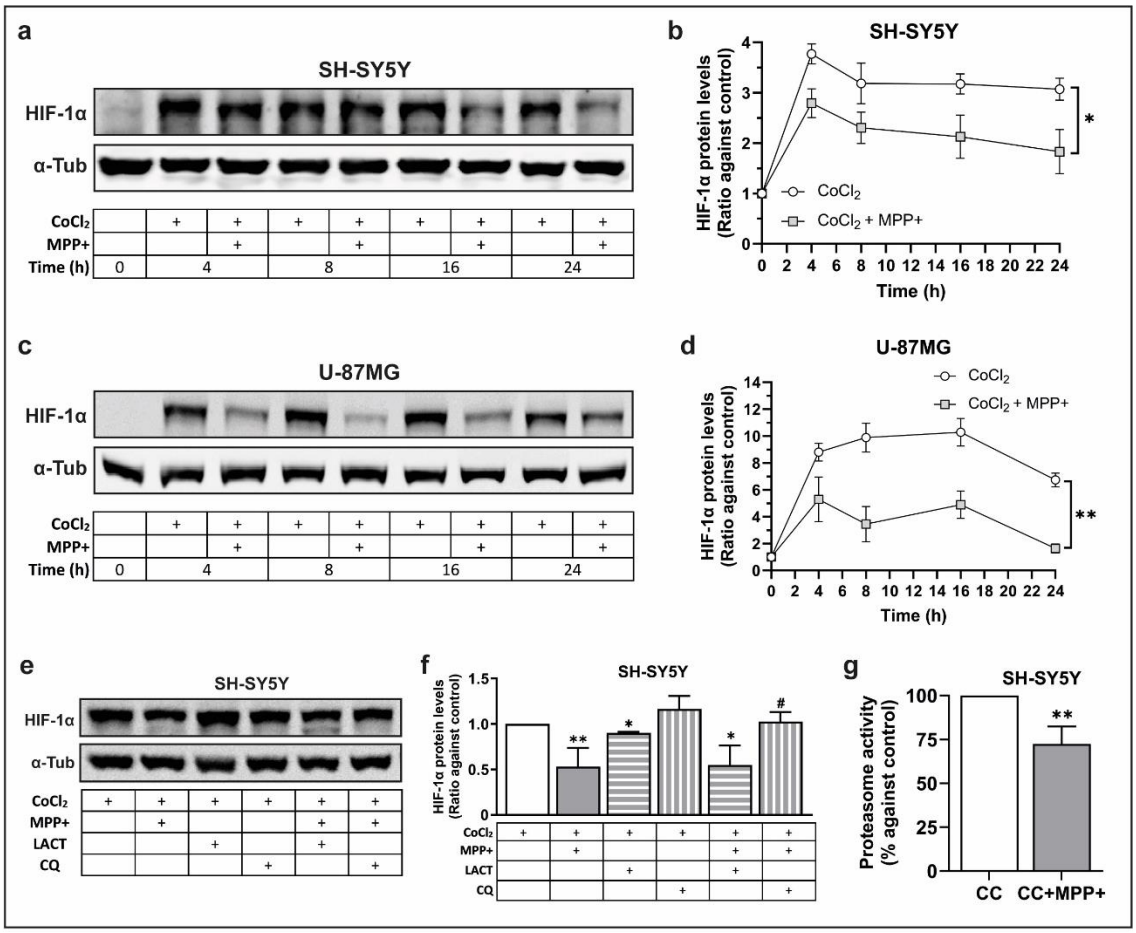

Figure 4.4. Exposure to MPP+ modifies the degradation pattern of HIF-1α in SH-SY5Y and U-87MG cells and reduces proteasome activity. a. Representative Western Blot image showing HIF-1α (~120 kDa) and α-Tubulin (~55 kDa, loading control) proteins in lysates from SH-SY5Y cells treated with 100μM $CoCl_2$ alone or in combination with 2 mM MPP+ at different timepoints. **b.** Plot summarising densitometric analysis of the a. Western Blot (n=3). **c.** Representative Western Blot image showing HIF-1α (~120 kDa) and α-Tubulin (~55 kDa, loading control) proteins in lysates from U-87MG cells treated with 100μM $CoCl_2$ alone or in combination with 2 mM MPP+ at different timepoints. **d.** Plot summarising densitometric analysis of the c. Western Blot (n=3). **e.** Representative Western Blot image showing HIF-1α (~120 kDa) and α-Tubulin (~55 kDa, loading control) proteins in lysates from SH-SY5Y cells treated with 100μM $CoCl_2$ alone or in combination with 2 mM MPP+ and 0.5 μM LACT or 200 μM CQ for 24h. **f.** Plot summarising densitometric analysis of the e. Western Blot (n=4).**g.** Graph displaying proteasome activity in SH-SY5Y cells samples treated with 100 μM $CoCl_2$ (CC) in combination with 2 mM MPP+ for 24h (n=3). Statistical analysis was performed using a one-way ANOVA followed with Dunnett's post-hoc test for b, d and f and an unpaired two-tailed Student's t test for g. $p<0.05$ was recorded as "*" with respect to control ($CoCl_2$), "#" when comparing to combined treatment ($CoCl_2$ and MPP+).

After confirming the impact of MPP+ on the degradation of HIF-1α, it was necessary to investigate whether MPP+ was also affecting HIF1A mRNA dynamics. Analysis of *HIF1A* mRNA expression in $CoCl_2$-treated SH-SY5Y cells exposed to MPP+ showed a significant reduction in *HIF1A* mRNA levels (Fig. 4.5a). This is likely due to MPP+ blocking Complex I in the ETC, reducing O_2 utilisation by mitochondria and thereby rising intracellular O_2 levels. Since hypoxia can modify chromatin to facilitate *HIF1A* transcription, changes in O_2 levels elicited by MPP+ could affect chromatin structure and reduce *HIF1A* transcription. In fact, MPP+ exposure significantly lowers mitochondrial membrane potential in SH-SY5Y cells (Fig. 4.5b, c), which impacts the capacity of the mitochondria to consume O_2 and produce ATP. Thus, MPP+ seems to decrease HIF-1α accumulation in the presence of PHD inhibition by reducing *HIF1A* mRNA content and promoting HIF-1α degradation via autophagy.

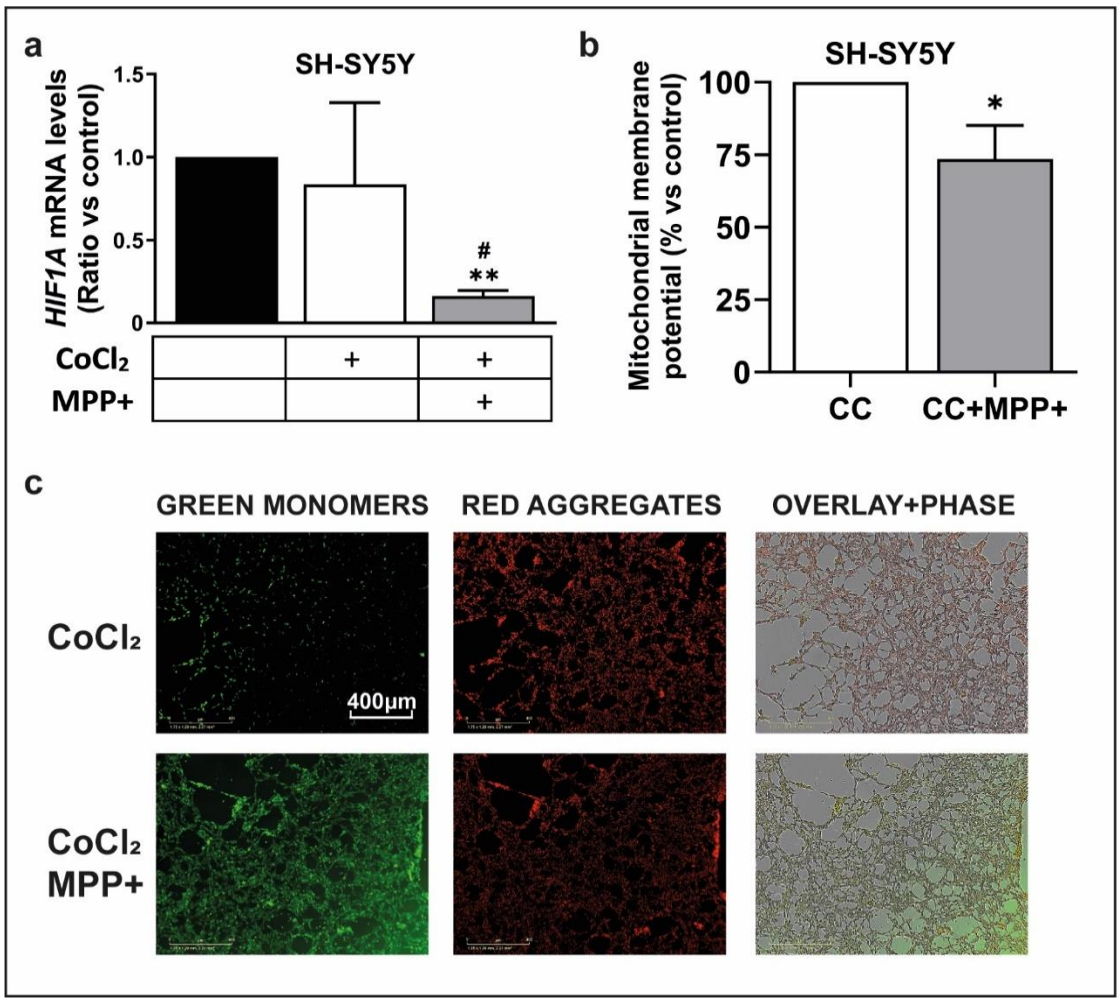

Figure 4.5. MPP+ treatment reduces *HIF1A* mRNA expression and lowers mitochondrial membrane potential in SH-SY5Y cells. a. Graph showing mRNA expression levels of *HIF1A* assessed by qRT-PCR in samples from SH-SY5Y cells treated with 100µM $CoCl_2$ alone or in combination with 2 mM MPP+ for 24h (n=4). **b.** Graph displaying mitochondrial membrane potential measured as ratio of green monomers to red aggregates of the fluorescent probe JC-1 based on the images taken with the Incucyte S3 system of SH-SY5Y cells treated with 100µM $CoCl_2$ (CC) alone or in combination with 2 mM MPP+ for 24h (n=3). **c.** Representative microscopy images acquired with the Incucyte S3 system showing fluorescence from the JC-1 probe in SH-SY5Y cells under shown treatments for 24h. Scale bar indicates 400 µm. Statistical analysis was performed using a one-way ANOVA followed with Dunnett's post-hoc test for a and an unpaired two-tailed Student's t test for b. $p<0.05$ was recorded as "*" with respect to control ($CoCl_2$) and "#" when comparing to combined treatment ($CoCl_2$ and MPP+).

4.3.2. REGULATION OF HIF-1α BY OXIDATIVE STRESS

4.3.2.1. ROS-inducing agents AAPH and BSO lower HIF-1α levels in SH-SY5Y cells

To investigate the impact of oxidative stress on HIF-1α stabilisation, it was necessary to evaluate changes in HIF-1α levels in human SH-SY5Y neuroblastoma cells and human U87-MG glioblastoma cells in response to ROS-generating compounds. DA, AAPH, and BSO were utilised to produce distinct ROS production profiles whilst $CoCl_2$ was used to stabilize HIF-1α in normal oxygen conditions. Indeed, $CoCl_2$ stabilized HIF-1α in SH-

SY5Y cells and this stabilization was maintained in the presence of DA. However, AAPH treatment resulted in the most significant reduction in HIF-1α levels, exceeding 80% compared to the control, so it was chosen for subsequent experiments. This effect was also seen, albeit to a lesser extent, with BSO, which caused a 20% reduction in HIF-1α levels (Fig. 4.6a, b). In contrast, neither ROS inducer significantly modified $CoCl_2$-mediated HIF-1α stabilization in U87-MG cells (Fig. 4.6c, d). This difference might be attributable to variations in cellular antioxidant capacity between neurons and astrocytes. To assess this, the levels of ubiquitous ROS-scavenging molecule GSH were measured after treatment with $CoCl_2$ alone or in combination with AAPH in both cell types. In SH-SY5Y cells, GSH levels were significantly decreased in the presence of AAPH, while GSH content in U-87MG cells remained unchanged (Fig. 4.6e, f). Although the MTT viability assay showed that AAPH caused a significant decrease in cell metabolic activity, this does not explain the drastic reduction in HIF-1α levels (Fig. 4.6g). The results of this study collectively suggest that AAPH-induced ROS play a role in the destabilization of HIF-1α in $CoCl_2$-treated SH-SY5Y cells.

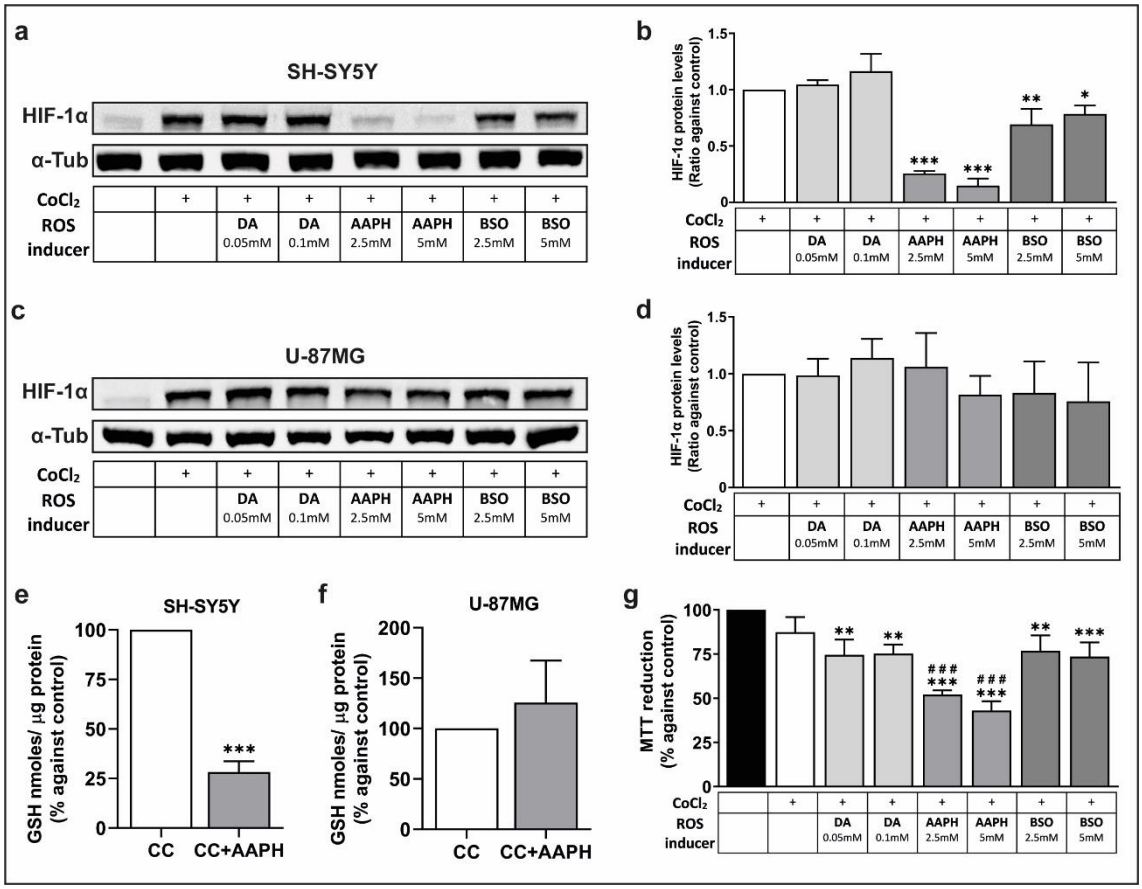

Figure 4.6. AAPH reduces $CoCl_2$-mediated HIF-1α stabilization and lowers GSH content exclusively in SH-SY5Y cells. a. Representative Western Blot image showing HIF-1α (~120 kDa) and α-Tubulin (~55 kDa, loading control) proteins in lysates from SH-SY5Y cells treated with 100μM $CoCl_2$ for 24h in combination with DA (0.05 mM or 0.1 mM), AAPH (2.5 mM or 5 mM) or BSO (2.5 mM or 5 mM). **b.** Plot summarising densitometric analysis of the a. Western Blot (n=3). **c.** Representative Western Blot image showing HIF-1α (~120 kDa) and α-Tubulin (~55 kDa, loading control) proteins in lysates from U-87MG cells treated with 100μM $CoCl_2$ for 24h in combination with DA (0.05 mM or 0.1 mM), AAPH (2.5 mM or 5 mM) or BSO (2.5 mM or 5 mM). **d.** Plot summarising densitometric analysis of the c. Western Blot (n=3). **e.** Graph showing total GSH levels measured in SH-SY5Y cell extracts after 24h treatment with 100μM $CoCl_2$ alone (CC) or in combination with 2.5 mM AAPH (n=3). **f.** Graph showing total GSH levels measured in U-87MG cell extracts after 24h treatment with 100μM $CoCl_2$ alone (CC) or in combination with 2.5 mM AAPH (n=3). **g.** Plot displaying MTT reduction in SH-SY5Y cells treated with $CoCl_2$ and ROS-inducing compounds for 24h (n=3). Statistical analysis was performed using a one-way ANOVA followed with Dunnett's post-hoc test for b, d and g and an unpaired two-tailed Student's t test for e and f. $p<0.05$ was recorded as "*" with respect to control ($CoCl_2$ for b, d, e and f) and "#" with respect to $CoCl_2$ in plot g.

4.3.2.2. AAPH impairs HIF-1α stabilization in dLUHMES

As the impact of AAPH on HIF-1α levels appeared to be limited to neuronal cells, it would be reasonable to anticipate a comparable reduction in the stabilization of HIF-1α in other neuronal models. Since SH-SY5Y cells are undifferentiated and retain some non-neuronal characteristics, we considered it crucial to verify that the effect of AAPH is also observed in a model that more closely resembles primary neurons. To validate this hypothesis and confirm the generalizability of the observed effect in other neuronal lines beyond SH-SY5Y cells, LUHMES cells that had been differentiated into postmitotic neurons were used. dLUHMES were treated with FG-2216, either alone or in combination with AAPH, since $CoCl_2$ treatment was ineffective in stabilizing HIF-1α in this cell line as previously shown. Treatment with AAPH completely reversed the stabilization of HIF-1α by FG-2216 (Fig. 4.7a-c), comparable to the effect seen in SH-SY5Y cells, suggesting that the mechanism by which AAPH inhibits HIF-1α accumulation was not cell line-specific.

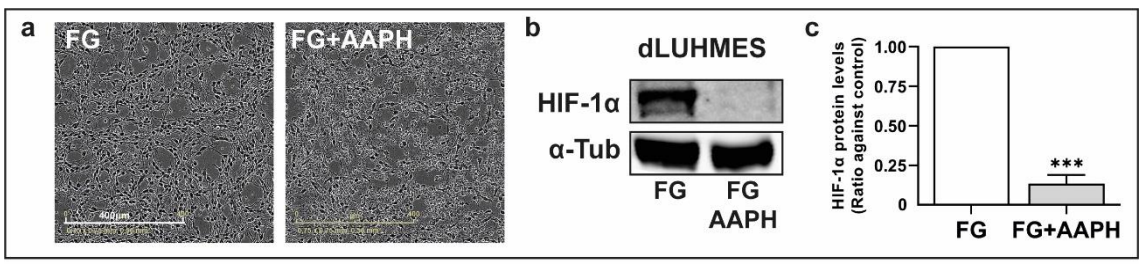

Figure 4.7. FG-2216-stabilized HIF-1α levels are decreased by AAPH in differentiated LUHMES. **a.** Representative microscopy images showing differentiated LUHMES cells treated with 100μM FG-2216 alone (FG) or in combination with 2.5 mM AAPH for 24h. Scale bar indicates 400 μm. **b.** Representative Western Blot image showing HIF-1α (~120 kDa) and α-Tubulin (~55 kDa, loading control) proteins in lysates from dLUHMES cells treated with 100μM FG-2216 (FG) for 24h in combination with 2.5 mM AAPH **c.** Plot summarising densitometric analysis of the c. Western Blot (n=3). Statistical analysis was performed using an unpaired two-tailed Student's t test where $p<0.05$ was recorded as "*" with respect to control.

4.3.2.3. Antioxidants mitigate the AAPH-mediated decrease in HIF-1α levels

To establish a direct causal relationship between the ROS generated by AAPH and the reduction in HIF-1α levels, we sought to determine if the observed decrease in HIF-1α is indeed a primary consequence of AAPH-induced oxidative stress and not a secondary effect resulting from the drug's interaction with other signalling pathways that regulate HIF-1α. To determine the role of AAPH-induced ROS, SH-SY5Y cells were used as a neuronal model system and treated with a range of antioxidants, including ASC, NAC and GSH, in the presence of AAPH. NAC and GSH were both able to rescue the reduction in HIF-1α levels caused by AAPH, while ASC was not (Fig. 4.8a, b). This indicates that ROS are likely to be involved in HIF-1α stability regulation. The ability of NAC to elevate GSH levels and to replicate the rescuing effect observed with GSH on AAPH-mediated reduction of HIF-1α accumulation indicates that the ROS generated by AAPH are effectively neutralised by GSH. Since ASC is a cofactor for PHD enzymes and its combined effect with $CoCl_2$ on PHD activity and subsequent HIF-1α levels is uncertain, we chose to exclude ASC from further experiments. Interestingly, the effect observed with the antioxidants was not due to changes in cell survival. This was evident from the MTT viability assay, which showed no significant difference in cell viability between AAPH-treated cells in the presence or absence of antioxidants (Fig. 4.8c). Nonetheless, investigation of ROS production by SH-SY5Y cells showed that the AAPH-mediated reduction in HIF-1α levels was accompanied by an increase in ROS levels. Treatment of SH-SY5Y cells with $CoCl_2$ resulted in a modest decrease in ROS levels, which may be attributed to the ability of HIF-1α to curb excessive oxidative stress. Conversely, the addition of AAPH to cells in the presence of $CoCl_2$ resulted in elevated ROS production by 50% compared to the control. However, the addition of the antioxidants NAC and GSH, but not ASC, significantly reduced ROS levels, returning them to baseline (Fig. 4.8d, e). The inverse correlation between the changes in ROS production and HIF-1α accumulation further supports the hypothesis that AAPH-induced increase in ROS may be involved in the decline of HIF-1α levels.

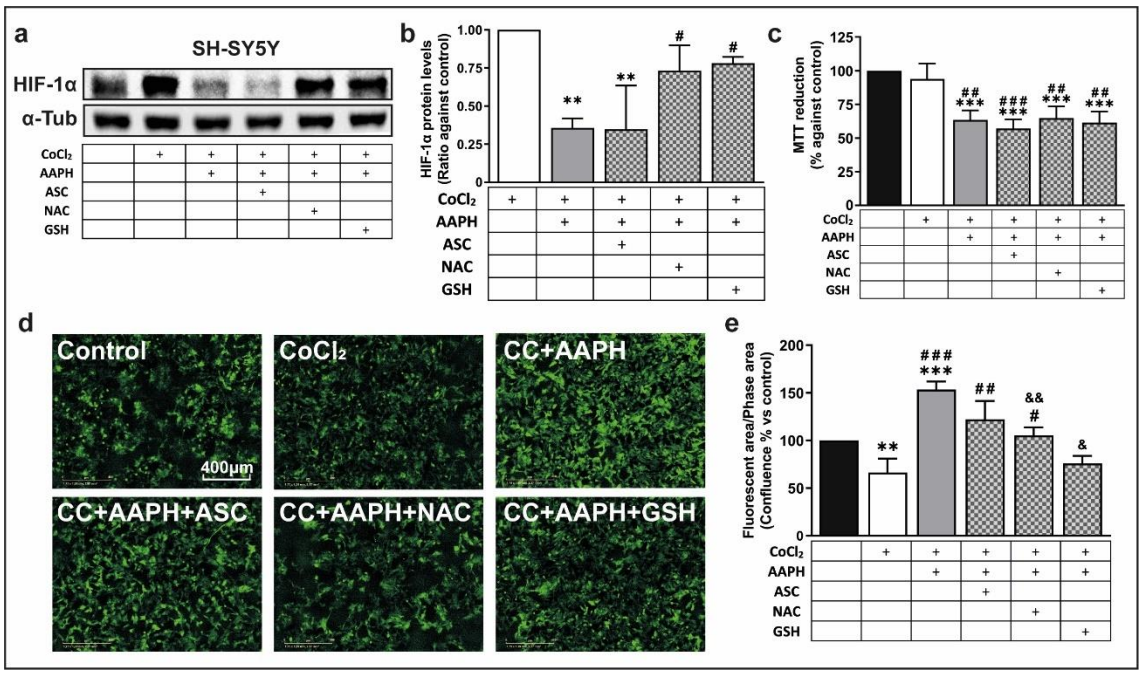

Figure 4.8. The antioxidant compounds NAC and GSH were able to rescue the decrease in HIF-1α levels caused by AAPH in $CoCl_2$-treated SH-SY5Y cells. a. Representative Western Blot image showing HIF-1α (~120 kDa) and α-Tubulin (~55 kDa, loading control) proteins in lysates from SH-SY5Y cells treated with 100µM $CoCl_2$ for 24h in combination with 2.5 mM AAPH and 1 mM of antioxidants ASC, NAC and GSH. **b.** Plot summarising densitometric analysis of the a. Western Blot (n=3). **c.** Plot displaying MTT reduction in SH-SY5Y cells treated with $CoCl_2$ and AAPH in combination with antioxidant compounds for 24h (n=3). **d.** Representative microscopy images acquired with the Incucyte S3 system showing ROS production as green fluorescence detected by the 2,7-DCDFA probe normalized to phase confluence in SH-SY5Y cells under shown treatments for 24h. Scale bar indicates 400 µm. **e.** Plot showing the quantification of green fluorescence area/phase area percentage based on the images taken with the Incucyte S3 system (n=3). Statistical analysis was performed using a one-way ANOVA followed with Dunnett's post-hoc test where $p<0.05$ was recorded as "*" with respect to control ($CoCl_2$ for b), "#" with respect to single treatment ($CoCl_2$) in plots c and e or combined treatment ($CoCl_2$ and AAPH) in plot b, and "&" when comparing to combined treatment ($CoCl_2$ and AAPH) for plot e.

4.3.2.4. The effect of AAPH is preserved in different HIF-1α stabilisation pathways

To determine whether the effect of AAPH was specific to a HIF-1α stabilisation mechanism, $CoCl_2$ was substituted with different HIF-1α stabilising agents that work through distinct pathways, such as 2-OG replacement (FG-2216), iron chelation (ML-228), or directly via hypoxia (1% O_2). This investigation will elucidate whether the effect of AAPH solely influences $CoCl_2$-mediated HIF-1α stabilization or if there are off-target interactions between these two compounds. Remarkably, the decrease in HIF-1α levels caused by AAPH and the rescue effect of the antioxidants NAC and GSH were also observed under these conditions (Fig. 4.9a-f). The decrease in HIF-1α levels provoked by AAPH in hypoxia was less pronounced than in normoxia which may be due to the diminished ability of AAPH to generate ROS under long-term O_2 deprivation.

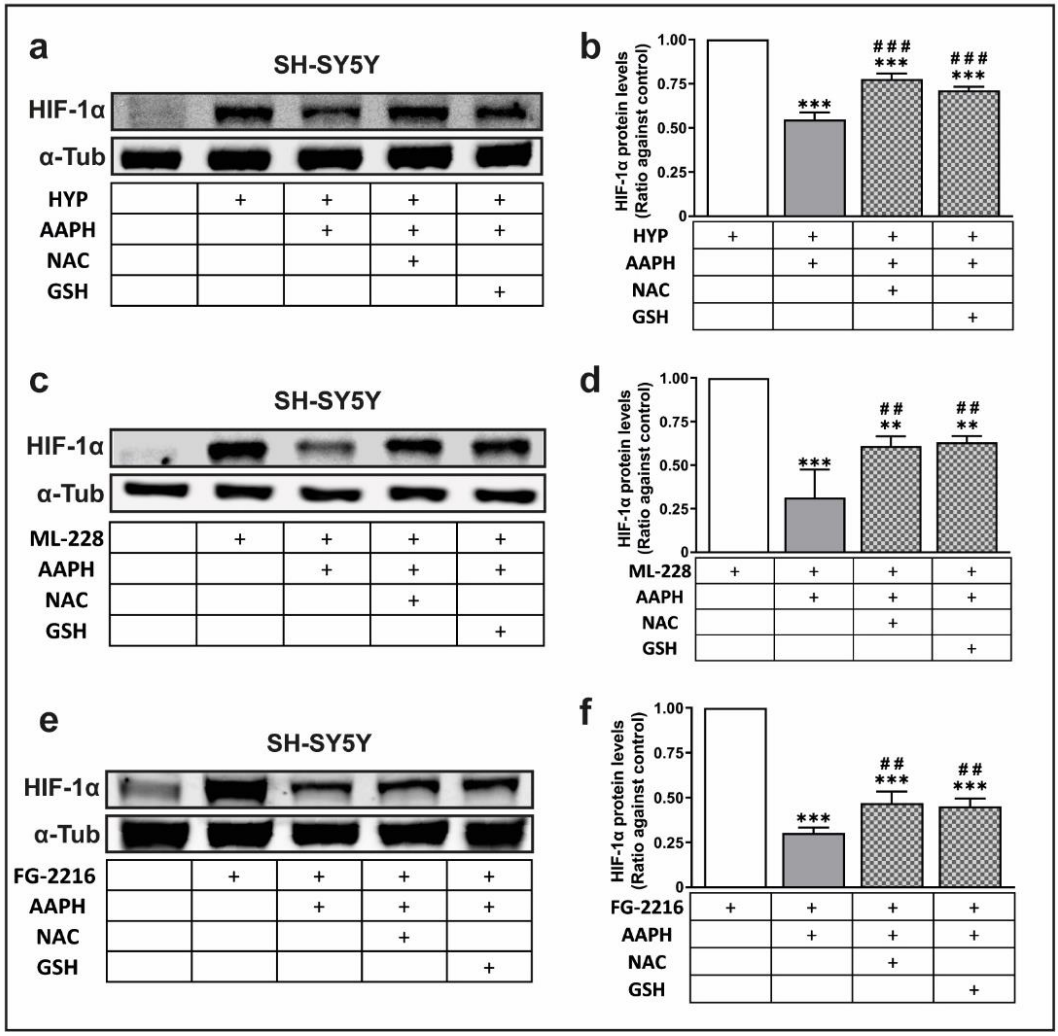

Figure 4.9. The effect of AAPH, NAC, and GSH on HIF-1α levels is independent of the different HIF-1α-stabilizing strategies used in SH-SY5Y cells. a. Representative Western Blot image showing HIF-1α (~120 kDa) and α-Tubulin (~55 kDa, loading control) proteins in lysates from SH-SY5Y cells treated with 1% O_2 for 24h in combination with 2.5 mM AAPH and 1 mM of antioxidants NAC and GSH. **b.** Plot summarising densitometric analysis of the a. Western Blot (n=3). **c.** Representative Western Blot image showing HIF-1α (~120 kDa) and α-Tubulin (~55 kDa, loading control) proteins in lysates from SH-SY5Y cells treated with 0.5 μM ML-228 for 24h in combination with 2.5 mM AAPH and 1 mM of antioxidants NAC and GSH. **d.** Plot summarising densitometric analysis of the c. Western Blot (n=3). **e.** Representative Western Blot image showing HIF-1α (~120 kDa) and α-Tubulin (~55 kDa, loading control) proteins in lysates from SH-SY5Y cells treated with 100μM FG-2216 for 24h in combination with 2.5 mM AAPH and 1 mM of antioxidants NAC and GSH. **f.** Plot summarising densitometric analysis of the d. Western Blot (n=3). Statistical analysis was performed using a one-way ANOVA followed with Dunnett's post-hoc test where $p<0.05$ was recorded as "*" with respect to control (HYP/ML-228/FG-2216) and "#" when comparing to combined treatment (HYP/ML-228/FG-2216 and AAPH).

4.3.2.5. AAPH promotes the degradation of HIF-1α through autophagy

HIF-1α undergoes regulation across various levels, encompassing transcription, translation, and protein stability. Therefore, the ROS generated by AAPH could potentially impact any of these stages. A time-course analysis of the effects of AAPH on HIF-1α stabilization by $CoCl_2$ in SH-SY5Y cells showed that the abundance of HIF-1α

protein does not vary at early timepoints in the presence of AAPH but started to decrease significantly after 16 hours of AAPH treatment (Fig. 4.10a, b). This experiment provides evidence that AAPH may be altering the rate at which HIF-1α is degraded. Since the main pathway controlling HIF-1α stability, the PHD/VHL/proteasome system, is inhibited by $CoCl_2$, we investigated whether AAPH-induced ROS affect HIF-1α degradation via an alternative mechanism. To investigate this, $CoCl_2$-treated SH-SY5Y cells were incubated with protein degradation inhibitors in the presence and absence of AAPH and GSH. As GSH proved more potent in reducing ROS and rescuing AAPH-induced reduction in HIF-1α levels, it was used as antioxidant in this experiment. The proteasome inhibitor LACT and the autophagy inhibitor CQ were employed to determine the contribution of these pathways to HIF-1α degradation. The findings indicated that the inclusion of either GSH or CQ substantially mitigated the reduction in HIF-1α levels induced by AAPH, restoring HIF-1α to approximately 25% or 50%, respectively, of the $CoCl_2$ control value. In contrast, LACT showed no discernible effect. Interestingly, the co-administration of GSH and CQ further reversed the reduction of HIF-1α accumulation by AAPH, increasing HIF-1α levels to approximately 75% of control (Fig. 4.10c, d). These findings suggest that AAPH induces HIF-1α degradation via autophagy. We hypothesised that this effect might be related to proteasome dysfunction elicited by AAPH. Indeed, proteasome activity in SH-SY5Y cells was reduced by 15% in the presence of AAPH (Fig. 4.10e). This decline in proteasome activity, albeit small, might be enough to divert part of the HIF-1α pool towards autophagy mediated degradation. AAPH has been shown to cause ROS-mediated mitochondrial depolarization, which can lead to a drop in proteasome activity due to decreased ATP levels. Indeed, investigation of ATP content in SH-SY5Y cells confirmed that ATP levels were significantly reduced in the presence of AAPH (Fig. 4.10f). Thus, AAPH-mediated enhancement of HIF-1α degradation via autophagy might be related to impaired proteasome activity, which could be explained by lower ATP production. The lack of change in *HIF1A* mRNA expression in $CoCl_2$-treated SH-SY5Y cells exposed to AAPH alone or in combination with GSH further supports the idea that AAPH exclusively impacts HIF-1α stabilization (Fig. 4.10g).

These results collectively provide evidence that ROS produced by AAPH can induce autophagy-mediated degradation of HIF-1α, independent of the PHD/VHL/proteasome system, and that this effect might be related to AAPH-mediated disruption of proteasome activity.

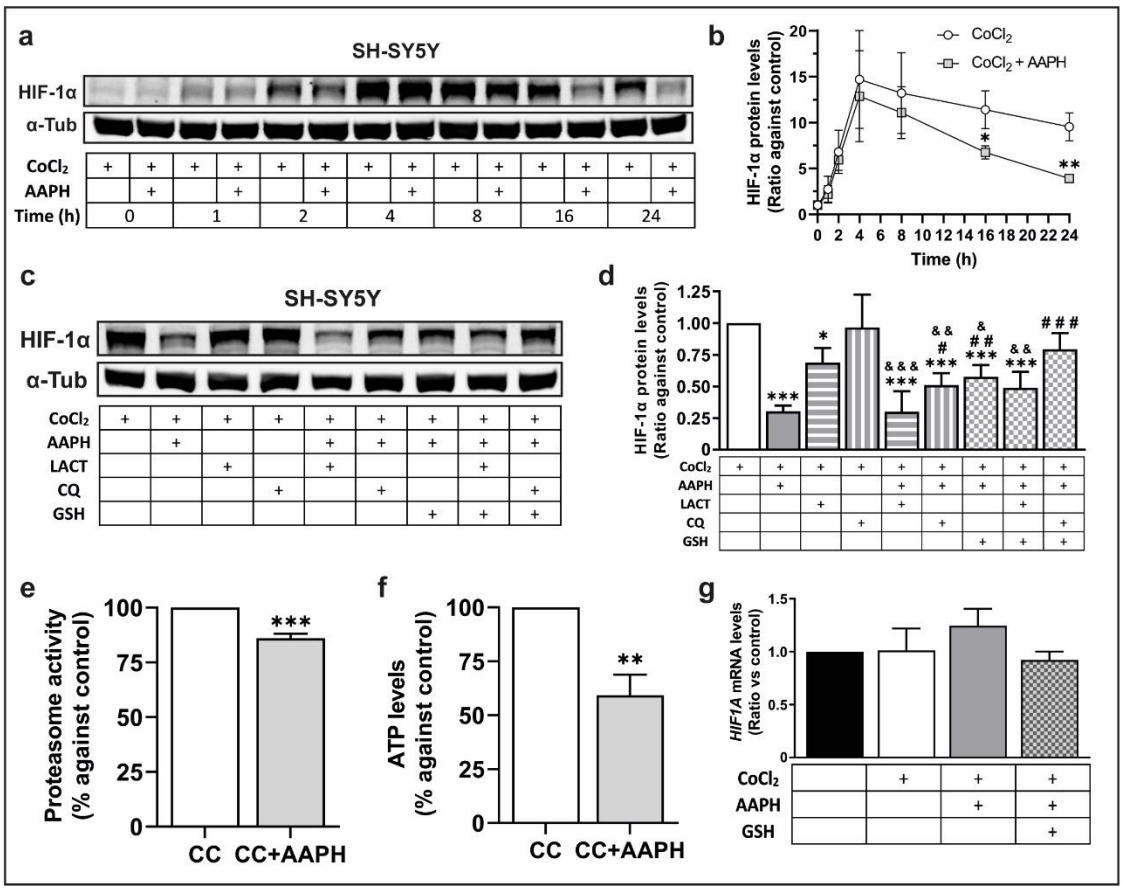

Figure 4.10. Exposure to AAPH alters the degradation pattern of HIF-1α and the activity of the proteasome in SH-SY5Y cells. a. Representative Western Blot image showing HIF-1α (~120 kDa) and α-Tubulin (~55 kDa, loading control) proteins in lysates from SH-SY5Y cells treated with 100μM $CoCl_2$ alone or in combination with 2.5 mM AAPH at different timepoints. **b.** Plot summarising densitometric analysis of the a. Western Blot (n=3). **c.** Representative Western Blot image showing HIF-1α (~120 kDa) and α-Tubulin (~55 kDa, loading control) proteins in lysates from SH-SY5Y cells treated with 100μM $CoCl_2$ alone or in combination with 2.5 mM AAPH and 0.5 μM LACT, 200 μM CQ or 1 mM GSH for 24h. **d.** Plot summarising densitometric analysis of the c. Western Blot (n=5). **e.** Graph displaying proteasome activity in SH-SY5Y cells samples treated with 100 μM $CoCl_2$ (CC) in combination with 2.5 mM AAPH for 24h (n=3). **f.** Graph showing ATP content in lysates from SH-SY5Y cells treated with 100 μM $CoCl_2$ (CC) in combination with 2.5 mM AAPH for 24h (n=3). **g.** Graph showing mRNA expression levels of *HIF1A* assessed by qRT-PCR in samples from SH-SY5Y cells treated with 100μM $CoCl_2$ alone or in combination with 2.5 mM AAPH and 1 mM GSH for 24h (n=4). Statistical analysis was performed using a one-way ANOVA followed with Dunnett's post-hoc test for d and g and an unpaired two-tailed Student's t test for b, e and f. $p<0.05$ was recorded as "*" with respect to control ($CoCl_2$), "#" with respect to combined treatment ($CoCl_2$ and AAPH) and "&" when comparing to multiple treatment ($CoCl_2$, AAPH, CQ and GSH) in plot d.

4.3.3. INFLUENCE OF PROTEIN DEGRADATION IMPAIRMENT ON HIF-1α

4.3.3.1. $CoCl_2$ induces autophagy without affecting proteasome activity

To further investigate how impairment of protein degradation affects HIF-α, it was necessary to explore the impact of stabilizing HIF-α with $CoCl_2$ on the rate of autophagy and proteasome activity. This step allows us to determine the baseline activity of these

pathways upon HIF-1α stabilization by $CoCl_2$, establishing a reference point before further manipulation with autophagy and proteasome inhibitors. Analysis of the autophagosome marker LC3B-II by Western Blot showed significantly increased protein levels throughout the course of $CoCl_2$ treatment in both SH-SY5Y and U-87MG (Fig. 4.11a-c). Conversely, proteasome activity remained unchanged in the presence of $CoCl_2$ (Fig. 4.11d). This indicates the possibility that HIF-α induces autophagy under these conditions.

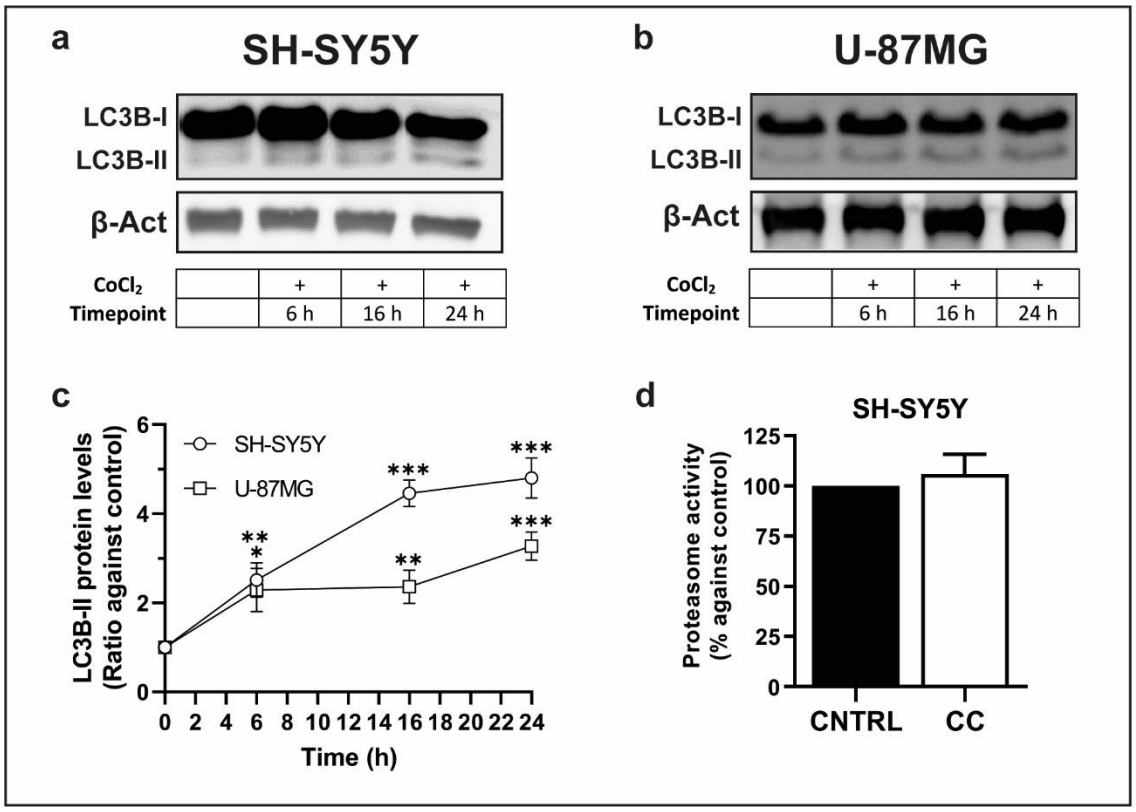

Figure 4.11. $CoCl_2$ treatment promotes autophagy but does not affect proteasome activity. a. Representative Western Blot image showing HIF-1α (~120 kDa) and β-Actin (~45 kDa, loading control) proteins in lysates from SH-SY5Y cells treated with 100μM $CoCl_2$ for 6, 16 or 24 hours. **b.** Representative Western Blot image showing HIF-1α (~120 kDa) and β-Actin (~45 kDa, loading control) proteins in lysates from U-87MG cells treated with 100μM $CoCl_2$ for 6, 16 or 24 hours. **c.** Plot summarising densitometric analysis of the a. and b. Western Blots (n=3). **d.** Graph showing proteasome activity in SH-SY5Y cells treated with 100 μM $CoCl_2$ (CC) for 24h (n=3). Statistical analysis was performed using an unpaired two-tailed Student's t test where $p<0.05$ was recorded as "*" with respect to control.

4.3.3.2. Proteasome and autophagy inhibitors modify HIF-1α accumulation in SH-SY5Y cells

In order to evaluate the impact of protein degradation impairment on HIF-1α accumulation, HIF-1α protein levels were investigated after treatment with proteasome or autophagy inhibitors in the presence of $CoCl_2$, revealing whether these inhibitors

amplify, block, or alter the stabilization process of HIF-1α. In SH-SY5Y cells, proteasome inhibitor MG132 reduced the levels of HIF-1α at the highest dose used while autophagy inhibitor BAF, although not CQ, increased HIF-1α levels (Fig. 4.12a, b). However, the use of these inhibitors did not significantly impact HIF-1α levels in U-87MG cells (Fig. 4.12c, d). Autophagy inhibitors CQ and BAF, which block the fusion of the autophagosome with the lysosome, are anticipated to cause the same impact on HIF-1α accumulation, so the levels of autophagic marker LC3B-II were analysed to determine potential differences in autophagy induction by the different inhibitors. Treatment with MG132 caused increased autophagy, likely to compensate for proteasome disruption, with a similar increase in LC3B-II levels observed in both cell lines (Fig. 4.12e-h). As anticipated, both CQ and BAF generated considerable LC3B-II accumulation. This was due to the creation of autophagic vesicles containing LC3B-II induced by $CoCl_2$ - mediated HIF-1α stabilization. However, the fusion of these vesicles with the lysosome and the subsequent recycling of LC3B-II were inhibited (Fig. 4.12e-h). Interestingly, LC3B-II accumulation under these conditions was higher in SH-SY5Y cells than U-87MG cells, with a 15-fold and a 5-fold increase respectively. This might indicate that SH-SY5Y cells have a higher rate of autophagy than U-87MG cells, which could explain some of the differences encountered in the results.

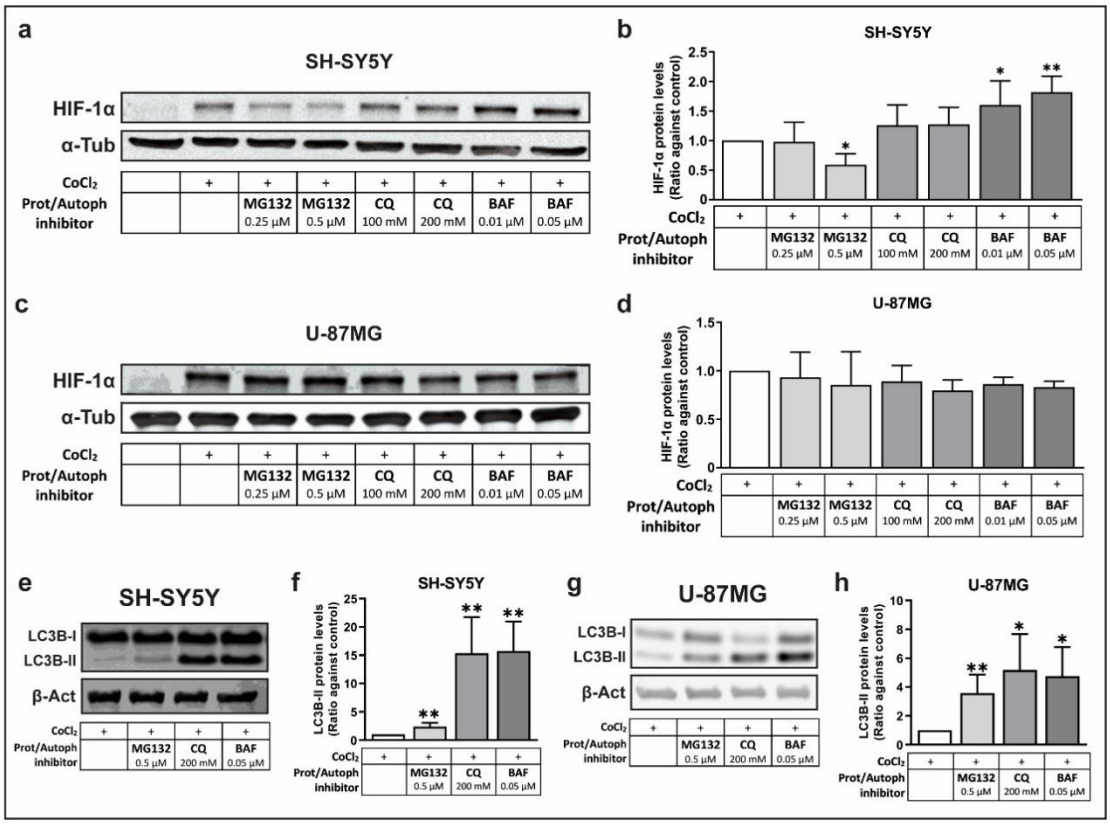

Figure 4.12. HIF-1α levels are impacted by MG132 and BAF in $CoCl_2$-treated SH-SY5Y cells. a. Representative Western Blot image showing HIF-1α (~120 kDa) and α- Tubulin (~55 kDa, loading control) proteins in lysates from SH-SY5Y cells treated with 100μM $CoCl_2$ for 24h in combination with MG132 (0.25 μM or 0.5 μM), CQ (100 μM or 200 μM) or BAF (0.01 μM or 0.05 μM). **b.** Plot summarising densitometric analysis of the a. Western Blot (n=3). **c.** Representative Western Blot image showing HIF-1α (~120 kDa) and α-Tubulin (~55 kDa, loading control) proteins in lysates from U-87MG cells treated with 100μM $CoCl_2$ for 24h in combination with MG132 (0.25 μM or 0.5 μM), CQ (100 μM or 200 μM) or BAF (0.01 μM or 0.05 μM). **d.** Plot summarising densitometric analysis of the c. Western Blot (n=3). **e.** Representative Western Blot image showing LC3B (~14,16 kDa) and β-Actin (~45 kDa, loading control) proteins in lysates from SH-SY5Y cells treated with 100μM $CoCl_2$ for 24h in combination with MG132 (0.5 μM), CQ (200 μM) or BAF (0.05 μM). **f.** Plot summarising densitometric analysis of the e. Western Blot (n=3). **g.** Representative Western Blot image showing LC3B (~14,16 kDa) and β-Actin (~45 kDa, loading control) proteins in lysates from U-87MG cells treated with 100μM $CoCl_2$ for 24h in combination with MG132 (0.5 μM), CQ (200 μM) or BAF (0.05 μM). **h.** Plot summarising densitometric analysis of the g. Western Blot (n=3). Statistical analysis was performed using a one-way ANOVA followed with Dunnett's post-hoc test for b and d and an unpaired two-tailed Student's t test for f and h. $p<0.05$ was recorded as "*" with respect to control.

It is tempting to hypothesise that if $CoCl_2$-stabilised HIF-1α was degraded by autophagy, the effects observed when treating with autophagy inhibitors CQ and BAF, which block the same step in the autophagic pathway, would be similar. However, although BAF increased HIF-1α protein levels in SH-SH5Y cells, CQ did not have a significant effect. BAF has been found to stabilize HIF-1α in normoxia in colon cancer cell lines by causing a partial depolarization of mitochondria that increases O_2 consumption by mitochondrial metabolism (Zhdanov et al., 2012). Hence, it was decided to investigate the effect of both BAF and CQ on HIF-1α stabilization in the presence or absence of $CoCl_2$, as well as in combination with mitochondrial complex I inhibitor MPP+. The results corroborate the cited research, showing that BAF can induce HIF-1α accumulation in normoxia in both SH-SY5Y and U-87MG cells (Fig. 4.13a-d). BAF-mediated HIF-1α accumulation reached the same level as $CoCl_2$-mediated HIF-1α stabilization in SH-SY5Y cells but was significantly lower in U-87MG cells. This might explain why the combined effect of BAF and $CoCl_2$ contributes to a significant increase on HIF-1α accumulation compared to $CoCl_2$ alone in SH-SY5Y cells. CQ did not stabilize HIF-1α in normoxia, indicating that the increase in HIF-1α levels elicited by BAF was independent of autophagy inhibition and related to the off-target effects of this chemical. Cotreatment with MPP+ appeared to abolish the influence of BAF on HIF-1α levels, which would support previous research that demonstrates that BAF stabilises HIF-1α through increasing mitochondrial respiration, which is blocked by MPP+ (Fig. 4.13a-d).

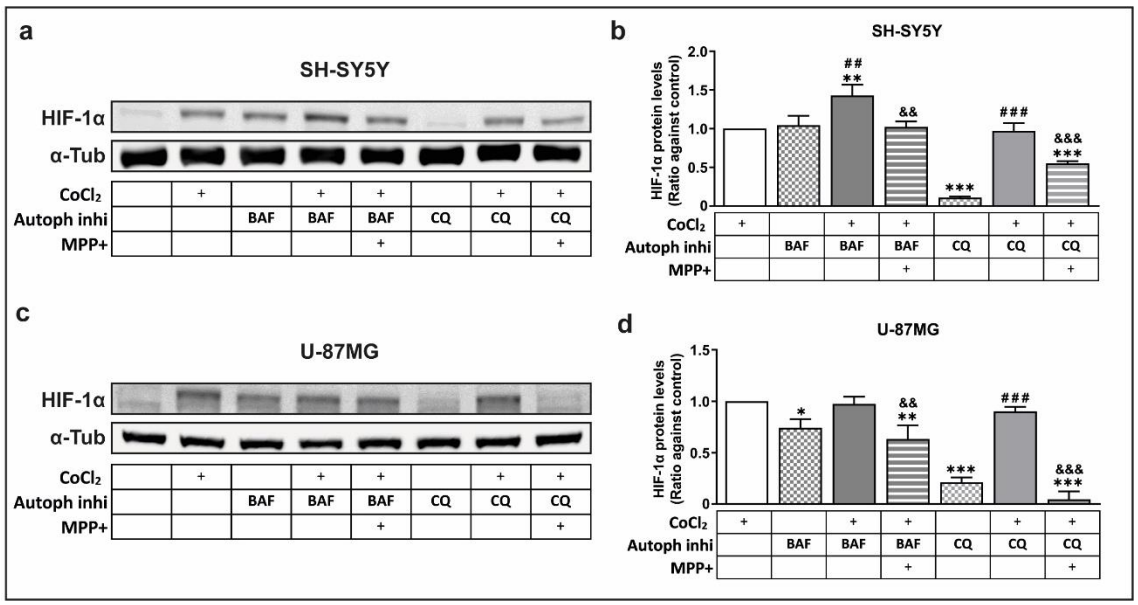

Figure 4.13. BAF stabilizes HIF-1α in SH-SY5Y and U-87MG cells. a. Representative Western Blot image showing HIF-1α (~120 kDa) and α- Tubulin (~55 kDa, loading control) proteins in lysates from SH-SY5Y cells treated with 200 μM CQ or 0.05 μM BAF in the presence or absence of 100 μM $CoCl_2$ and 2 mM MPP+ for 24h. **b.** Plot summarising densitometric analysis of the a. Western Blot (n=3). **c.** Representative Western Blot image showing HIF-1α (~120 kDa) and α-Tubulin (~55 kDa, loading control) proteins in lysates from U-87MG cells treated with 200 μM CQ or 0.05 μM BAF in the presence or absence of 100 μM $CoCl_2$ and 2 mM MPP+ for 24h. **d.** Plot summarising densitometric analysis of the c. Western Blot (n=3). Statistical analysis was performed using a one-way ANOVA followed with Dunnett's post-hoc test where $p<0.05$ was recorded as "*" with respect to control ($CoCl_2$), "#" with respect to single treatments (BAF/CQ) and "&" when comparing to combined treatments ($CoCl_2$+BAF/CQ).

To comprehensively explore the role of autophagy in HIF-1α stabilization and rule out potential off-target effects arising from specific interactions between $CoCl_2$ and the other autophagy inhibitors utilised, we employed 3-MA, an inhibitor that acts upstream of autophagic vesicle formation. 3-MA, similarly to CQ, does not stabilize HIF-1α in normoxia, suggesting that this protein is not targeted for autophagic degradation under basal conditions in both SH-SY5Y and U-87MG cell lines (Fig. 4.14a-d). However, 3-MA does increase the levels of HIF-1α under $CoCl_2$ treatment (Fig. 4.14a-d). As the presence of HIF-1α in the macroautophagic pathway would also be detected by downstream inhibition through CQ, it is possible that this is an off-target effect of 3-MA, which is a general inhibitor of type III Phosphatidylinositol 3-kinases (PI3K).

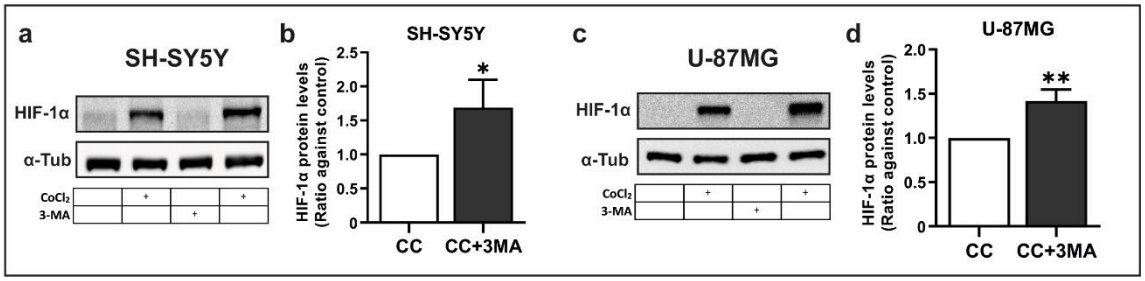

Figure 4.14. HIF-1α levels are increased by 3-MA in $CoCl_2$-treated SH-SY5Y and U-87MG cells. **a.** Representative Western Blot image showing HIF-1α (~120 kDa) and α- Tubulin (~55 kDa, loading control) proteins in lysates from SH-SY5Y cells treated with 100μM $CoCl_2$ (CC) for 24h in combination with 5 mM 3-MA. **b.** Plot summarising densitometric analysis of the a. Western Blot (n=3). **c.** Representative Western Blot image showing HIF-1α (~120 kDa) and α-Tubulin (~55 kDa, loading control) proteins in lysates from U-87MG cells treated with 100μM $CoCl_2$ (CC) for 24h in combination with 5 mM 3-MA**. d.** Plot summarising densitometric analysis of the c. Western Blot (n=3). Statistical analysis was performed using an unpaired two-tailed Student's t test where $p<0.05$ was recorded as "*" with respect to control.

To establish the role of proteasome inhibition in the regulation of HIF-1α levels, a different proteasome inhibitor, LACT, was utilised. Replicating the effects obtained with MG132, LACT caused a reduction in HIF-1α stabilization in SH-SY5Y cells while having no effect on HIF-1α levels in U-87MG cells (Fig. 4.15a-d). LC3-II levels were additionally assessed in cells subjected to LACT treatment, with an aim to validate whether the effect of proteasome inhibition was consistent across cell lines. Indeed, LACT, similarly to MG132, caused a comparable rise in LC3-II levels in both cell lines (Fig. 4.15e-h). In conclusion, proteasome inhibition by either MG132 or LACT caused a decrease in $CoCl_2$-mediated HIF-1α accumulation in SH-SY5Y cells only. The divergent outcomes of proteasome disruption in the two cell lines are not likely to be linked to differences in the potency of inhibitors, as these provoked a similar increase in LC3-II in both cell lines.

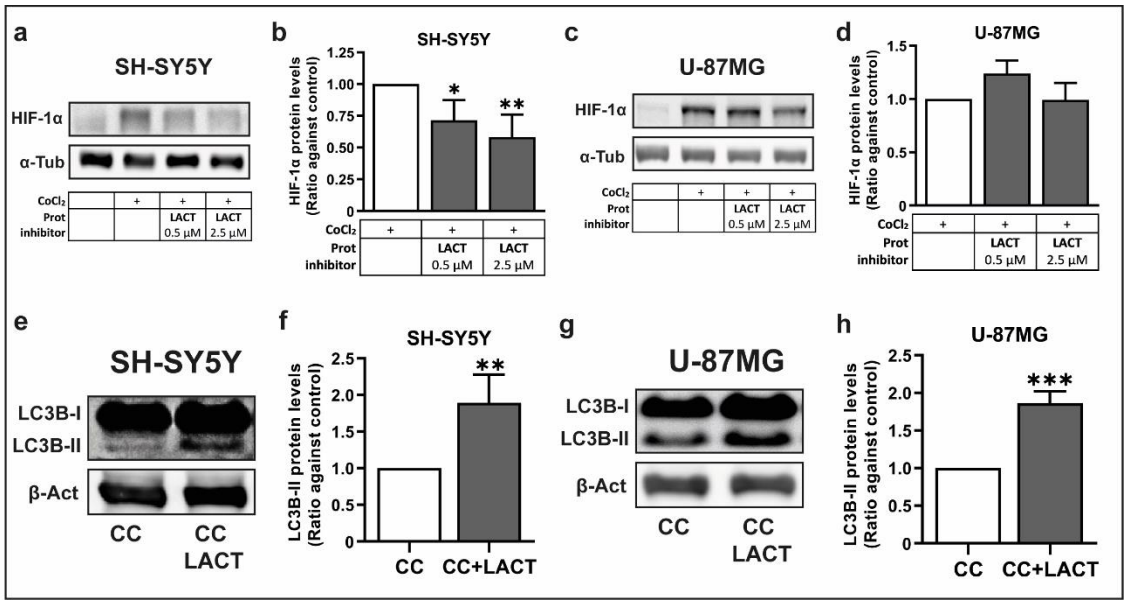

Figure 4.15. LACT reduces HIF-1α stabilization in $CoCl_2$-treated SH-SY5Y cells. a. Representative Western Blot image showing HIF-1α (~120 kDa) and α- Tubulin (~55 kDa, loading control) proteins in lysates from SH-SY5Y cells treated with 100μM $CoCl_2$ (CC) for 24h in combination with LACT (0.5 μM or 2.5 μM). **b.** Plot summarising densitometric analysis of the a. Western Blot (n=4). **c.** Representative Western Blot image showing HIF-1α (~120 kDa) and α-Tubulin (~55 kDa, loading control) proteins in lysates from U-87MG cells treated with 100μM $CoCl_2$ for 24h in combination with LACT (0.5 μM or 2.5 μM). **d.** Plot summarising densitometric analysis of the c. Western Blot (n=4). **e.** Representative Western Blot image showing LC3B (~14,16 kDa) and β-Actin (~45 kDa, loading control) proteins in lysates from SH-SY5Y cells treated with 100μM $CoCl_2$ and 2.5 μM LACT for 24 **f.** Plot summarising densitometric analysis of the e. Western Blot (n=3). **g.** Representative Western Blot image showing LC3B (~14,16 kDa) and β-Actin (~45 kDa, loading control) proteins in lysates from U-87MG cells treated with 100μM $CoCl_2$ and 2.5 μM LACT for 24h. **h.** Plot summarising densitometric analysis of the g. Western Blot (n=3). Statistical analysis was performed using a one-way ANOVA followed with Dunnett's post-hoc test for b and d and an unpaired two-tailed Student's t test for f and h. $p<0.05$ was recorded as "*" with respect to control.

4.3.3.3. Proteasome inhibition triggers HIF-1α degradation via autophagy

As the findings of this study indicate that disrupting proteasome activity can diminish HIF-1α stability resulting from PHD inhibition, it was necessary to explore whether HIF-1α can be eliminated through autophagy under these conditions. Indeed, incubation of $CoCl_2$-treated SH-SY5Y cells with LACT significantly decreased HIF-1α levels, which remain unaffected by CQ treatment (Fig. 4.16a, b). However, treatment with a combination of LACT and CQ in the presence of $CoCl_2$ caused a substantial accumulation of HIF-1α, which was significant against all individual treatments (Fig. 4.16a, b). This treatment cocktail will cause increased autophagy due to HIF-1α stabilisation by $CoCl_2$ and LACT-mediated proteasome inhibition, while blocking the breakdown of the autophagosomal cargo by CQ. This results in an increase in the levels of the contents of the autophagosome, which appears to include HIF-1α. Additionally, LACT treatment in the presence of $CoCl_2$ demonstrated a significant 50% reduction in proteasome activity in SH-SY5Y cells, which mimicked the decrease in HIF-1α levels following LACT treatment (Fig. 4.16c). Thus, this data indicates that, while HIF-1α is not degraded by autophagy under basal conditions or when stabilized by PHD inactivation, the presence of proteasome inhibition triggers an increased HIF-1α clearance through autophagy.

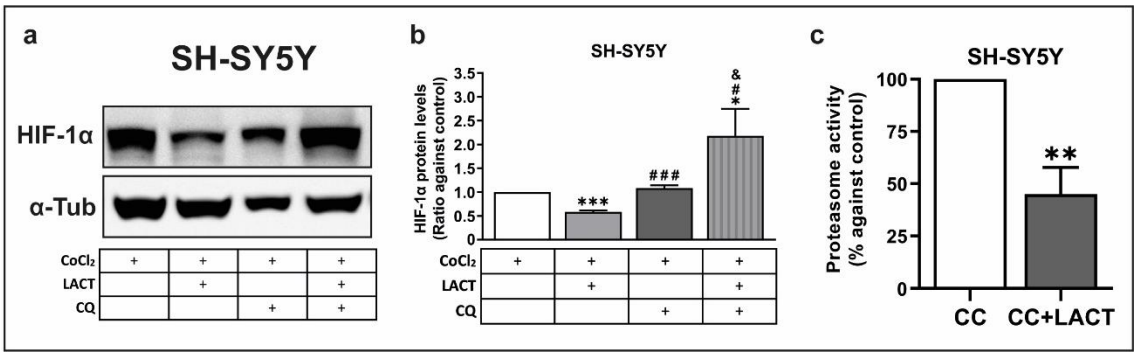

Figure 4.16. LACT-mediated reduction of HIF-1α stabilization in $CoCl_2$-treated SH-SY5Y cells is rescued by CQ treatment. a. Representative Western Blot image showing HIF-1α (~120 kDa) and α-Tubulin (~55 kDa, loading control) proteins in lysates from SH-SY5Y cells treated with 100μM $CoCl_2$ in the presence of 2.5 μM LACT, 200 μM CQ or both for 24 hours. **b.** Plot summarising densitometric analysis of the a. and b. Western Blots (n=3). **c.** Graph displaying proteasome activity in SH-SY5Y cells samples treated with 100 μM $CoCl_2$ (CC) in combination with 2.5 μM LACT for 24h (n=3). Statistical analysis for graph b was performed using a one-way ANOVA followed with Dunnett's post-hoc where $p<0.05$ was recorded as "*" with respect to control ($CoCl_2$), "#" with respect to CQ and "&" when comparing to BAF. Statistical analysis for graph c was performed using an unpaired two-tailed Student's t test where $p<0.05$ was recorded as "*" with respect to control.

4.3.4. MODULATION OF BASAL HIF-1α BY PD-RELATED STRESSORS

To identify the differences in the effects of PD-related stressors on HIF-1α protein levels in the presence and absence of PHD inhibition, an additional analysis of the abundance of HIF-1α protein in basal normoxic conditions was conducted. Exposure of SH-SY5Y cells to ROS-generating compounds BSO and AAPH, as well as proteasome inhibitors, LACT and MG, stabilised HIF-1α (Fig. 4.17a, b). The effect of these compounds appears to be contingent upon the presence of PHD inhibition. Previous experiments have shown that when these chemicals are combined with PHD inhibitors, they trigger a reduction in HIF-1α levels instead of an increase. Interestingly, although MPP+ caused a reduction in HIF-1α protein accumulation and *HIF1A* mRNA expression in the presence of PHD inhibition, it did not have a significant effect on basal HIF-1α levels (Fig. 4.17a, b). Of note, $CoCl_2$, which was added as a control for the stabilization of HIF-1α in normoxia, was the most effective agent at stabilising HIF-1α protein levels. This study underscores the importance of effective PHD inhibitors like $CoCl_2$ for HIF-1α research. The undetectable levels of HIF-1α under basal normoxic conditions demonstrate the necessity of these tools to stabilise HIF-1α and study its regulation.

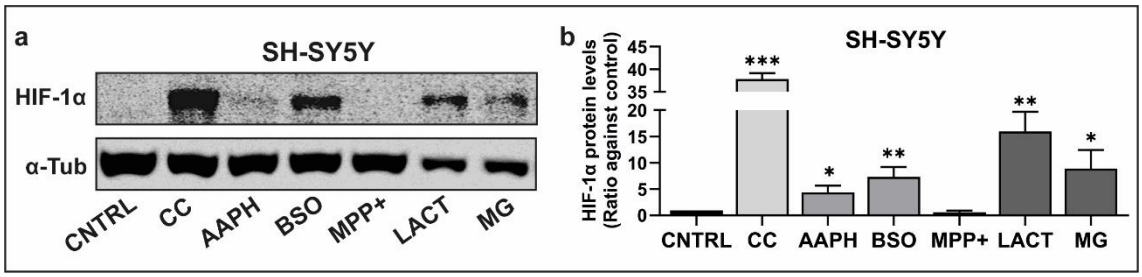

Figure 4.17. HIF-1α is stabilized in normoxia by AAPH, BSO, LACT and MG treatments in SH-SY5Y cells. a. Representative Western Blot image showing HIF-1α (~120 kDa) and α- Tubulin (~55 kDa, loading control) proteins in lysates from SH-SY5Y cells treated with 100μM $CoCl_2$, 2.5 mM AAPH, 2.5 mM BSO, 2 mM MPP+, 2.5 μM LACT and 0.5 μM MG132 for 24 hours. **b.** Plot summarising densitometric analysis of the a. Western Blot (n=3). Statistical analysis was performed using an unpaired two-tailed Student's t test where $p<0.05$ was recorded as "*" with respect to control.

4.4. DISCUSSION

This study demonstrates that PD-associated pathway dysfunction, including mitochondrial dysfunction, increased oxidative stress and proteasome blockade, can lead to decreased HIF-1α levels despite PHD inhibition. This reduction may compromise the response to specific hypoxic events that constitute risk factors for PD development.

4.4.1. Impact of mitochondrial dysfunction on HIF-1α

The role of mitochondria in stabilizing HIF-1α in hypoxia has been extensively studied, but there is no consensus on the contribution of mitochondrial ROS and metabolism to this process (Thomas et al., 2019). However, the effect of mitochondrial dysfunction on HIF-1α levels in the presence of pharmacological PHD inhibition has not been explored. In this study, we show that inhibitors of complex I, rotenone and MPP+, and a mitochondrial uncoupler, CCCP can reduce HIF-1α protein accumulation in SH-SY5Y and U-87MG cells when PHDs are inhibited through exposure to $CoCl_2$ (Fig. 4.1a-d). The effect of MPP+ on HIF-1α is replicated in cells treated with FG-2216, a PHD inhibitor that blocks access of 2-OG to the PHD active site (Fig. 4.3a-d). These findings are consistent with studies that show that MPP+ reduces HIF-1α in the presence of VHL suppressor Orexin-A and PHD inhibitor FG-4592 (Li et al., 2018; Feng et al., 2014), although the molecular basis of this phenomenon is not explored. Studies have indicated that Complex I inhibitors, including rotenone and MPP+, can hinder HIF-1α stabilisation even under hypoxic conditions, so it would be valuable to investigate whether this effect can be replicated in other neural cell lines (Agani, 2002 et al.; Chua et al., 2011; Bastian et al., 2017; Kumar et al., 2021). In these studies, the ability of Complex I inhibitors to block HIF-1α stabilisation is linked to an increase in intracellular O_2 levels due to a decreased use of O_2 by the ETC, which reactivates PHDs. However, this investigation reveals that Complex I inhibitors induce this effect even in the presence of chemical PHD inhibition. Despite increased intracellular O_2 levels, potentially enabling PHDs to operate more efficiently, their catalytic centre remains inhibited and their capacity to direct HIF-1α towards degradation would continue to be obstructed.

Subsequent research into the role of MPP+ in this process demonstrated that antioxidants ASC, NAC and GSH did not lead to the restoration of HIF-1α levels; instead, they exacerbated the effect (Fig. 4.2a-d). This indicates that the MPP+-induced increase in mitochondrial ROS production is not responsible for the reduction in HIF-1α levels and that lowering ROS seemingly potentiates the MPP+ effect. Interestingly, antioxidants

have been shown to reduce HIF-1α levels by counteracting ROS-mediated PHD inhibition (Gao et al., 2007). This study shows a negative effect of MPP+ and antioxidants on HIF-1α levels in the presence of PHD inhibitors in two different cell lines, indicating this might constitute a conserved process that is likely independent of the PHD/VHL/Proteasome system. We therefore proposed that HIF-1α could be controlled by MPP+ at the transcriptional level, and our findings supported this hypothesis by showing that MPP+ treatment decreased the expression of *HIF1A* mRNA in SH-SY5Y cells (Fig.4.5a). Previous publications investigating ETC Complex I inhibition and HIF-1α levels failed to assess *HIF1A* expression, so this effect could have been missed. Both MPP+, acting as a complex I inhibitor, and HIF-1α, acting as a suppressor of oxidative metabolism, cause a reduction in mitochondrial O_2 consumption with a concomitant decrease in ATP levels as demonstrated in this study (Fig.4.1f). However, this treatment combination might increase intracellular O_2 levels. Low O_2 tension controls chromatin structure to support *HIF1A* expression so increases in O_2 levels could reverse the changes in chromatin structure that are necessary for *HIF1A* expression, even under normoxia (Batie et al., 2019). In the case of MPP+, the ROS produced by this compound might be able to mitigate this effect as the *HIF1A* promoter contains elements controlled by ROS-induced TFs (Lacher et al., 2018). We suggest that increased intracellular O_2 levels can cause a decrease in *HIF1A* mRNA content, but this effect is limited, as oxidative stress can still induce *HIF1A* expression. However, the dissipation of MPP+-induced ROS by antioxidants may further repress *HIF1A*, which is evident in the baseline HIF-1α levels obtained when treating the cells with a combination of $CoCl_2$, MPP+, and different antioxidants (Fig. 4.2a-d). This could be proved by an additional experiment including antioxidant compounds in the investigation of HIF-1α levels by qRT-pCR. Further research, including investigation of intracellular O_2 tension and changes in chromatin dynamics, would be necessary to fully confirm this hypothesis. This investigation does not rule out the possibility that unknown transcriptional repressors or factors regulating *HIF1A* mRNA stability controlled by fluctuations in O_2 levels or ROS may be involved in the effect of MPP+.

Remarkably, MPP+ can influence HIF-1α levels in a variety of ways, not just through translation. Utilisation of autophagy inhibitor CQ effectively rescues the MPP+-induced reduction in HIF-1α stabilised by $CoCl_2$, indicating that this complex I inhibitor triggers the degradation of HIF-1α via autophagy, as proteasome inhibitor LACT has no effect (Fig4.4e, f). We hypothesised that this change in HIF-1α degradation pattern could be

related to a reduction in proteasome activity as both ATP depletion and ROS are known disruptors of the proteasome system in neural cells (Höglinger et al., 2003). Indeed, our data is consistent with previous studies, showing that MPP+ exposure in SH-SY5Y cells leads to a significant reduction in proteasome activity (Caneda-Ferron et al., 2008). Thus, the reduction in proteasome activity caused by MPP+ could activate molecular pathways that lead to the degradation of HIF-1α through autophagy.

4.4.2. Regulation of HIF-1α by oxidative stress

The effects of ROS on HIF-1α protein are a matter of scientific debate, as both destabilisation and stabilisation of HIF-1α by ROS have been reported. This research investigates a novel mechanism of HIF-1α regulation by ROS in the presence of PHD inhibition. The ROS inducer AAPH, significantly reduces drug/hypoxia-mediated HIF-1α stabilisation in neuronal cell lines, SH-SY5Y and dLUHMES, but not in the astrocyte model, U87-MG (Fig.4.6a-d; Fig4.7b, c; Fig4.9a-d). This seems to be related to a higher antioxidant capacity of astrocytes with respect to neurons, which has been reported in the literature (Chen et al., 2020) and is further supported by our experiments. These results show lower levels of the ROS-scavenger, GSH, in SH-SY5Y versus U87-MG cells upon exposure to AAPH (Fig.4.6e, f). This observation is complemented by differences in the expression and activity of antioxidant enzymes after AAPH treatment in SH-SY5Y compared to U87-MG cells. The use of antioxidants NAC and GSH reverses the AAPH-induced increase in ROS and reduction in HIF-1α levels, indicating that ROS are involved in this process (Fig.4.8a, b, d, e; Fig.4.9a-f). Indeed, the destabilisation of HIF-1α under hypoxia has also been reported to occur in the presence of ROS produced by H_2O_2 (Niecknig et al., 2012), BSO (Jin et al., 2011; Badawi et al., 2012) and Nitric Oxide (NO) (Mateo et al., 2003; Callapina et al., 2005; Berchner-Pfannschmidt et al., 2007; Cattaneo et al., 2012) via modulation of PHD activity. However, in this current investigation, AAPH-mediated ROS generation triggered the degradation of HIF-1α despite the use of PHD inhibitors, indicating that this process is independent of the canonical PHD/VHL/proteasome HIF-1α regulation pathway. While the proteasome blocker LACT does not have an effect on HIF-1α levels, autophagy inhibitor CQ attenuates the impact of AAPH on HIF-1α and in combination with GSH restores HIF-1α levels to baseline (Fig.4.10). Thus, we can speculate that AAPH facilitates HIF-1α degradation via autophagy when proteasome activity is affected. Indeed, ROS can impair proteasome activity by causing oxidative posttranslational modifications of proteasome subunits and

increasing the burden of oxidized proteins in the cell (Lefaki et al., 2017). Furthermore, proteasome activity is decreased in the presence of AAPH (Fig.4.10e), as also demonstrated by other studies (Hota et al., 2010). The effects of AAPH on the proteasome may not be solely mediated by ROS, as AAPH also causes ATP depletion (Fig.4.10f). Although AAPH does not significantly modify *HIF1A* expression, a minor increase can be discerned (Fig.4.10g). These findings indicate that when PHDs are supressed and proteasome activity is reduced, HIF-1α is degraded by autophagy. Additional research would be needed to determine the molecular mechanisms involved in this pathway and whether proteasomal inhibition is the trigger for the changes in HIF-1α degradation. For example, the formation of disulphide bonds in HIF-1α by oxidant enzymes has recently been reported as an important step for HIF-1α degradation via chaperone-mediated autophagy (Kobayashi et al., 2021). It is conceivable that a similar pathway is activated under these conditions, leading to the modification of HIF-1α by peroxyl radicals from AAPH and its subsequent degradation by autophagy. This would merit further investigation.

It is surprising that antioxidants have opposite effects on HIF-1α levels depending on the pathway inhibited, despite the fact that MPP+ and AAPH both produce ROS. This disparity can be caused by AAPH and MPP+ producing different types of ROS. We also speculate that the distinct mechanisms by which these compounds influence gene expression can be responsible for this result. While MPP+ diminishes the expression of the *HIF1A* gene, which could be exacerbated by antioxidants, AAPH causes a detectable, although not significant, increase in *HIF1A* mRNA content, which is attenuated by GSH. These findings suggest that these chemicals have different mechanisms of action, but that proteasome inhibition that is common to both leads to the degradation of HIF-1α by autophagy when PHDs are inhibited.

4.4.3. Influence of protein degradation impairment on HIF-1α

The proteasome is the main mechanism by which HIF-1α is degraded and its levels kept low in cells under normoxia (Huang et al., 1998). In recent years, there has been growing evidence that autophagy can also contribute to the degradation of HIF-1α under certain conditions, such as in response to cellular stress (Ferreira et al., 2015). We have shown that mitochondrial dysfunction and increased ROS can promote the degradation of HIF-1α by autophagy in the presence of PHD inhibitors. Subsequently, we hypothesised that

the impact of these factors on proteasome activity, may be the underlying cause of the redirection of HIF-1α degradation. To verify this, we directly investigated the influence of protein degradation pathway suppression on $CoCl_2$-stabilised HIF-1α levels. Notably, it is intriguing that proteasome inhibitors MG132 and LACT reduce HIF-1α levels in SH-SY5Y, but not in U-87MG cells (Fig.4.12a-d; Fig.4.15a-d). Given that proteasome inhibitors induce a comparable compensatory increase in the autophagy marker LC3B-II in both cell lines employed (Fig.4.12e-h; Fig.4.15e-h), our hypothesis is that SH-SY5Y cells may exhibit a higher susceptibility to proteasome suppression than U-87MG cells. Indeed, a study in primary rat cultures shows that neurons have lower basal proteasome activity than astrocytes alongside differences in the regulation of autophagy between these cell types (Tydlacka et al., 2008; Kulkarni et al., 2019). Consequently, the disruption of proteasome activity may serve as a more pronounced stress signal in neurons than in astrocytes, resulting in distinct responses.

Studies on autophagy have produced mixed results, depending on the specific compound used. The autophagy inhibitor BAF, which blocks lysosomal degradation, can stabilize HIF-1α in normoxia in SH-SY5Y and U-87MG cell lines (Fig.4.13a-d), which supports the findings of a previous study in human colon cancer cells (Zhdanov et al., 2012). Surprisingly, BAF is still used to investigate autophagy, despite this study raising questions about its suitability for this purpose. The use of BAF could be distorting the findings of studies, since HIF-1α can promote autophagy and regulate several proteins involved in this pathway (Wang et al., 2017). The autophagy inhibitor CQ, which blocks the same step in autophagy as BAF, does not affect HIF-1α levels (Fig.4.13a-d). On the contrary, inhibition of autophagy upstream of autophagosome formation by 3-MA in the presence of $CoCl_2$ further increases HIF-1α accumulation (Fig.4.14a-d). 3-MA is primarily an inhibitor of class III PI3Ks, but it has also been shown to block class I PI3Ks, which can modify HIF-1α levels (Wu et al., 2010; Jiang et al., 2001). To confirm these findings, the use of alternative autophagy inhibitors, as well as autophagy inducers such as rapamycin, should be considered. Interestingly, a previous study showed that serum deprivation, which increases autophagy flux, reduces $CoCl_2$-mediated HIF-1α stabilisation (Ferreira et al., 2015). These studies should be completed with the knockdown of autophagy genes in order to definitively determine whether HIF-1α is degraded by autophagy in the presence of PHD inhibition. Suppression of autophagy can lead to increased proteasome degradation, which could conceal a potential induction of HIF-1α accumulation by autophagy inhibition. However, the inhibition of the

PHD/VHL/Proteasome pathway by $CoCl_2$ makes this explanation improbable for this observation.

The combination of the autophagy suppressor, CQ and proteasomal inhibitor, LACT in SH-SY5Y cells triggers a substantial accumulation of HIF-1α, indicating that in the presence proteasome inhibition, HIF-1α is degraded by autophagy (Fig.4.16a-c). This experiment should be repeated in hypoxic conditions to evaluate whether this is a common mechanism during PHD inhibition. This research implies that proteasome inhibition is a critical stressor that regulates HIF-1α stability. As HIF-1α is conventionally degraded by the proteasome, inhibition of this pathway may act as a stress signal to regulate excessive HIF-1α accumulation. Thus, the elimination of HIF-1α via autophagy may exist as a protective mechanism against excessive HIF-1α levels, resulting from PHD inhibition. It is challenging to determine whether HIF-1α is degraded by macroautophagy or chaperone-mediated autophagy, as both have been reported, but specific and selective chaperone-mediated autophagy inhibitors are not yet available. In order to investigate this, the interaction of HIF-1α with chaperone-mediated autophagy associated proteins should be assessed.

Taken together, these results demonstrate that conditions that decrease proteasome activity, including mitochondrial damage, increased ROS or direct proteasome inhibition, trigger HIF-1α degradation via autophagy independently of the PHD/VHL system. To confirm that the treatments are not reversing PHD inhibition, PHD activity would need to be assessed.

4.4.4. Modulation of native HIF-1α by PD-related stressors

It is well-known that HIF-1α is not only responsive to changes in O_2 levels, but also to a variety of factors that can stabilize HIF-1α even in normal oxygen conditions (Kuschel et al., 2012). Thus, we decided to investigate whether the compounds utilised for this study are also affecting basal HIF-1α levels in SH-SY5Y cells. As expected, proteasome inhibition by either MG or LACT stabilises HIF-1α (Fig.4.17a, b). These findings, together with previous results showing that autophagy inhibitors CQ and 3-MA did not alter basal HIF-1α levels, provide further evidence that the proteasome is the predominant pathway for degrading HIF-1α in normoxia and that its inhibition is sufficient to generate detectable HIF-1α levels. Interestingly, both AAPH and BSO stabilise HIF-1α (Fig.4.17a, b). The stabilization of HIF-1a by ROS producers has been the subject of much scrutiny,

but this is the first study to demonstrate that these specific oxidant compounds can stabilize HIF-1α in normoxia. It would be worthwhile to investigate whether this is consequence of ROS-inducible elements present within the *HIF1A* promoter, an inhibition of PHDs, suppression of proteasome activity or an alternative mechanism. MPP+ alone does not modify HIF-1α levels, indicating that its ability to generate ROS is inferior to that of AAPH and BSO (Fig.4.17a, b). This could account for the differences in the effects of MPP+ and AAPH when using antioxidants. It is essential to bear in mind that while compounds that induce proteasome inhibition and oxidative stress stabilize HIF-1α in normoxic environments, their effect is markedly different when PHDs are inhibited.

4.5. CONCLUSION

The main goal of this study was to investigate the impact of PD-related stressors on HIF-1α levels in the presence of PHD inhibition. In the past, the effects of stressors on HIF-1α levels have only been investigated in normal or hypoxic conditions, as it was thought that the presence of a chemical PHD inhibitor would stabilize HIF-1α and make it resistant to external factors. This study, however, reveals how different factors can have a major impact on HIF-1α levels by altering upstream elements, such as mRNA levels, or by directly destabilizing HIF-1α through mechanisms that do not involve PHDs. Of note, while we focused on HIF-1α protein levels, to gain a more comprehensive understanding of HIF-1α functionality as a TF, future studies should investigate its activation through dimerization with HIF-1β and binding to transcriptional cofactors. Besides, we have also demonstrated that the effects of these stressors can be dependent on cell type by comparing the effects between neuronal and astrocyte models.

The complex interplay of conditions, proteins, RNAs, chromatin changes, and post-translational modifications that regulate HIF-1α levels makes it challenging to identify the factors involved in the disruption of HIF-1α stabilization mediated by stressors associated with PD. Nevertheless, these findings allow us to propose a possible mechanism driving this process. In normoxia, when PHDs are not inhibited, HIF-1α is degraded by the proteasome, avoiding its accumulation. Upon PHD inhibition, which can be caused by hypoxia or alterations in different pathways/metabolite levels, proteasome mediated degradation of HIF-1α is suppressed, but remains responsive in the event of sudden increases in O_2 levels or PHD reactivation. However, the present study shows that diverse PD-related stressors that ultimately converge on reduced proteasome activity,

target HIF-1α for degradation through autophagy, possibly as a mechanism to prevent its accumulation when no longer required. The identification of the stress-activated proteins that might be involved in directing HIF-1α towards autophagic degradation is a promising avenue for future research. In addition, to strengthen the clinical relevance of these findings, future studies should examine HIF-1α levels in brain samples from PD patients or animal models, as well as in patient-derived DAergic neurons generated from iPSCs.

In conclusion, we present novel evidence that three pathways that are generally involved in neurodegeneration, and specifically PD, can disrupt the accumulation of HIF-1α. This could have an impact on the response of neuronal cells to hypoxic events and changes to normal physiological processes. Therefore, the observed reduction in HIF-1α levels due to PD-associated pathway dysfunction could explain why hypoxic insults like TBI are risk factors for PD. This finding also suggests potential limitations for the efficacy of PHD inhibitors as a therapeutic approach in PD.

CHAPTER V

THE THERAPEUTIC POTENTIAL OF HIF-1α STABILIZATION IN A CELLULAR MODEL OF PD

5.1. INTRODUCTION

This chapter investigates a range of HIF-1α stabilizing drugs with different mechanisms of action, some of which have demonstrated neuroprotective potential in animal models of PD (Lestón Pinilla et al., 2021). The broad therapeutic potential of HIF-1α stabilizers, not only for neurodegeneration but also for other diseases, is fuelling the continuous search for novel HIF-1α inducers, most of which have not yet been evaluated for their use as a therapeutic in PD. Thus, we sought to identify recently developed HIF-1α stabilising drugs that exhibit neuroprotective effects in a cellular PD model. This chapter presents the first comprehensive evaluation of the therapeutic potential of two HIF-1α stabilizers, IOX4 and ML228, in rotenone-treated SH-SY5Y by studying a number of parameters, including apoptosis markers, mitochondrial function, ROS production and autophagy.

5.1.1. Apoptosis in PD

Apoptosis is a form of highly regulated programmed cell death dependent on ATP for the activation of caspase proteins that control this process (Elmore et al., 2007). Caspase induction initiates the degradation of intracellular components and the onset of morphological changes such as cell shrinkage, chromatin condensation and DNA fragmentation, which ultimately result in cell death (Li et al., 2008). Apoptosis can be triggered by either intrinsic or extrinsic signals, which lead to two seemingly independent pathways that eventually converge.

Intrinsic apoptosis (Fig.5.1) can be induced by an array of cellular stresses including genotoxic damage, ER stress, growth factor deprivation, hypoxia, mitochondrial dysfunction, oxidative stress and oncogene activation (Elmore et al., 2007). These stressors signal through several intracellular pathways which can regulate the initiation of apoptosis, such as the mitogen-activated protein kinase (MAPK) pathway via phosphorylation of p38, c-Jun N-terminal kinases (JNKs) and Extracellular signal-regulated kinases (ERKs) (Yue et al., 2020), or the unfolded protein response via downstream activation of pro-apoptotic C/EBP homologous protein (CHOP) (Hertz et al., 2012). The key event of the apoptotic process is the permeabilization of the mitochondrial outer membrane, which is controlled by the balance of a set of pro-apoptotic and anti-apoptotic proteins from the Bcl-2 family. Upon apoptotic stimuli, Bcl-2-associated X (BAX), which is cytosolic in basal conditions, translocates to the mitochondria and associates with Bcl-2-antagonist/killer 1 (BAK) to disrupt of the mitochondrial outer

membrane integrity via pore formation (Cosentino et al., 2017). Anti-apoptotic proteins BCL-2 and BCL-XL can prevent the activation of BAX/BAK after a death signal, while pro-apoptotic sensitizer BAD can block the function of BCL-2 and BCL-XL (Kale et al., 2017). If the balance tips towards apoptosis induction, mitochondria outer membrane permeabilization occurs and results in the release of a set of factors such as cytochrome c, second mitochondrial activator of caspases (Smac) and apoptosis inducing factor mitochondrial 1 (AIF) (Tait et al., 2013). Smac promotes apoptosis by antagonizing the anti-apoptotic function of inhibitor of apoptosis (IAP) proteins, such as XIAP and cIAP1/2, which inhibit caspase activation (Verhagen et al., 2000). In the cytosol, cytochrome c oligomerizes with Apoptotic Peptidase Activating Factor 1 (Apaf-1) and pro-caspase 9 to form the apoptosome, a multimeric complex that provides a platform for the activation of caspase 9 (Bao et al., 2006). Caspase-9 is an initiator caspase that triggers the apoptotic cascade by cleaving and activating effector caspases-3 and -7, which are the executioners of apoptosis (Wilson et al., 1998). Compelling evidence from both patients and experimental models suggests that intrinsic apoptosis plays a key role in DAergic neuron loss in PD. In fact, upregulation of pro-apoptotic proteins accompanied by downregulation of anti-apoptotic proteins has been reported. Lewy bodies from PD patients are immunoreactive for cytochrome c, Apaf-1, and cleaved caspase-9 (Kawamoto et al., 2014). Similarly, postmortem human brain samples from PD patients exhibit increased caspase-3 activation and BAX expression compared to controls (Tatton et al., 2000). Inactivation of XIAP has been reported in animal models of PD and in patient samples (Tsang et al., 2008). Caspase activation by PD-related toxins has been detected in animal and cellular models, and caspase inhibition has been shown to rescue cell death (Holville et al., 2019). These studies provide strong evidence that abnormal activation of the intrinsic apoptotic pathway may be a key mechanism in the neurodegeneration associated with PD.

The extrinsic apoptosis cascade (Fig.5.1) is initiated by the interaction of a death ligand with a death receptor from the tumor necrosis factor (TNF) receptor superfamily. Ligands include TNF, Fas and TNF-related apoptosis inducing ligand (TRAIL). TNF receptor activation induces a signalling pathway that leads to the autoproteolytic cleavage of procaspase-8 and -10, which become activated. In turn, these caspases promote the activation of executioner caspases-3 and-7. In addition, caspases -8 and -10 can cleave Bid to its active truncated form, tBID, which promotes BAX/BAK-mediated mitochondrial outer membrane permeabilization and consequent release of Smac and

cytochrome c (Korsmeyer et al., 2000). The contribution of extrinsic apoptosis to the pathogenesis of PD remains unclear. Clinical investigations show that a higher percentage of DAergic neurons in the SNpc of PD patients present caspase-8 activation and TNF receptor expression than controls (Mogi et al., 2000; Hartmann et al., 2001). However, caspase-8 inhibitors fail to protect PD animal models against mitochondrial toxins (Hartmann et al., 2001). Thus, further research is required to elucidate the role of extrinsic apoptosis in PD.

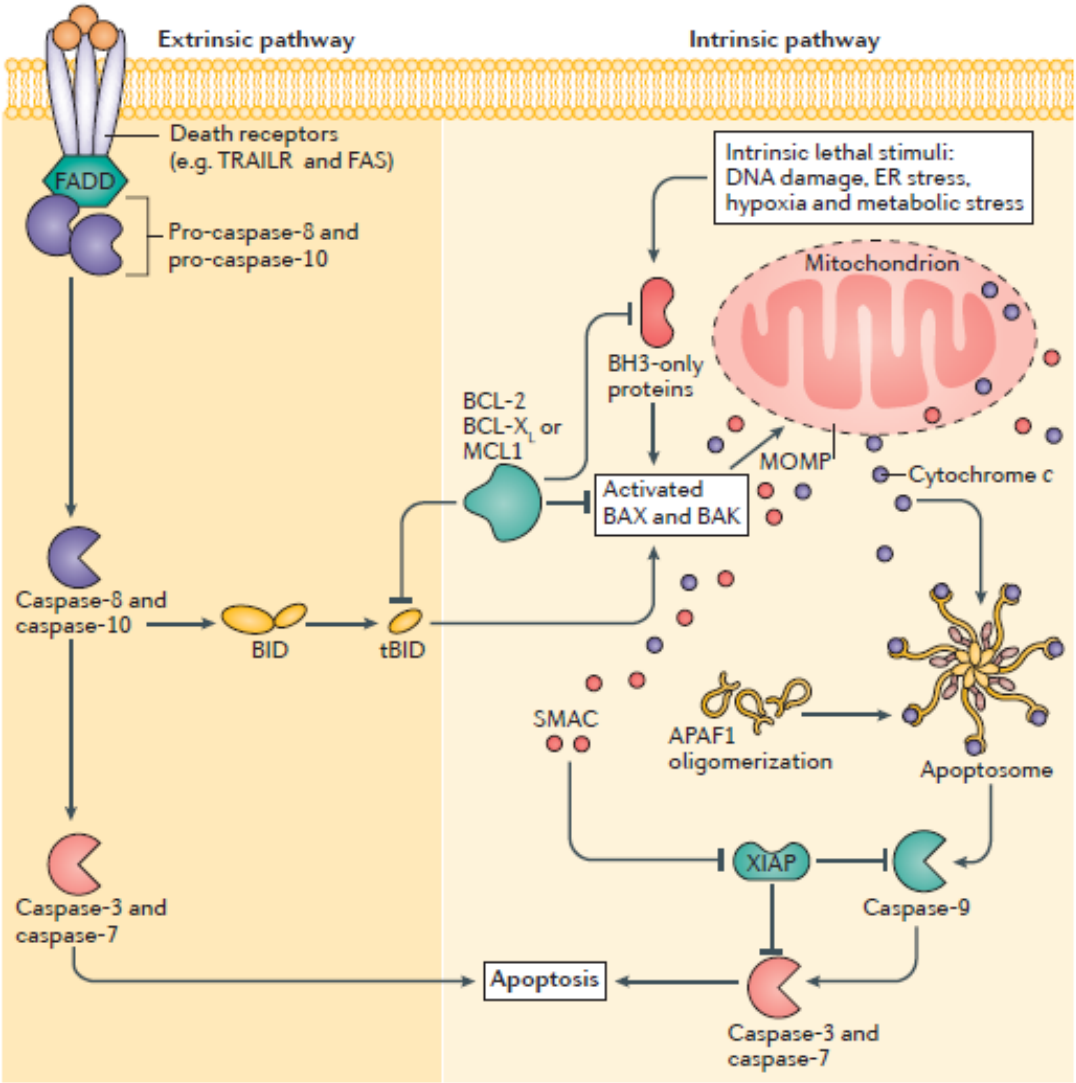

Figure 5.1. Intrinsic and extrinsic apoptosis pathways. The intrinsic apoptosis pathway can be initiated by a series of stressors, resulting in activation of BAX/BAK, which produce pores in the mitochondrial outer membrane. Induction of BAX/BAK is controlled by anti-apoptotic factors such as Bcl-2. Mitochondrial outer membrane permeabilisation triggers the release of different proteins, including cytochrome c, which associates with Apaf-1 and pro-caspase-9 to form the apoptosome. Apoptosome assembly promotes the activation of Caspase-9, which in turn proteolitically activates executioner caspases -3 and -7 to induce apoptosis. The extrinsic apoptotic pathway is induced by specific interactions between ligands and plasma membrane receptors, which result in the activation of Caspase-8 and -10. These caspases can cleave BID, which promotes BAX/BAK activation, acting as a point of contact between apoptotic mechanisms. Caspase-8 and -10 can also directly activate caspases -3 and -7, which leads to apoptosis (Ichim, 2016).

In addition to intrinsic apoptosis, there is also evidence for the presence of other programmed cell death mechanisms in PD, such as necroptosis and parthanatos (Dionisio et al., 2021). However, the investigation of these alternative pathways is beyond the scope of this study.

5.1.2. The SH-SY5Y rotenone model of PD

Rotenone has been utilised in a range of immortalised cells, such as PC12, LUHMES and SH-SY5Y to model PD in vitro. In SH-SY5Y cells, rotenone decreases cell viability in a dose and time-dependent manner triggering activation of Caspase-9 and Caspase-3 (Condello et al., 2011; Ma et al., 2018). In addition, enhanced cleavage of PARP, a caspase substrate, has been reported (Ma, 2018). Changes in apoptotic protein levels and activity are also detected, including decreased Bcl-2, increased Bak, Bax, and phosphorylated Bad, and mitochondrial release of cytochrome c (Condello et al., 2011; Park et al., 2013; Jang et al., 2014; Li et al., 2022). Rotenone-mediated induction of apoptosis seems to be triggered by phosphorylation of MAP kinases p38 and JNK1/2 (Newhouse et al., 2004; Ma et al., 2018; Park et al., 2013). However, the role of ERK1/2 activation in this process is uncertain, with conflicting evidence from different studies (Newhouse et al., 2004 Ma et al., 2018). Rotenone is also known to elevate ER stress markers, such as CHOP (Wu et al., 2014; Ramalingam et al., 2019). As expected, rotenone causes a decrease in mitochondrial respiration and ATP production accompanied by substantial loss of mitochondrial membrane potential (Li et al., 2022; Condello et al., 2011). Mitochondrial content and mitochondrial DNA copy number are negatively affected as well (Simões et al., 2022). Coincidentally, rotenone reduced the levels of PGC-1α and TFAM, which are involved in mitochondrial biogenesis and DNA transcription respectively (Lu et al., 2018; Han et al., 2022). Rotenone increases overall and mitochondrial ROS production (Ma et al., 2018; Li et al., 2022). In consequence, reduced GSH levels and increases in protein carbonylation and lipid peroxidation have been detected in rotenone-treated SH-SY5Y cells (Cabeza-Arvelaiz et al., 2012; González-Burgos et al., 2017; Zhang et al., 2018). Increases in catalase and SOD2 activity, as well as nuclear translocation of the antioxidant response transcription factor NF-κB, have been reported, suggesting a cellular response to oxidative stress (Condello et al., 2011; Barreca et al., 2017). Rotenone can disrupt the upstream regulation of autophagy by inducing mTOR and inhibiting Beclin-1 and AMPK phosphorylation (Jang et al., 2014; Jang et al., 2015), which results in a decrease of autophagy marker LC3B-II (Li et al., 2020; Zhang et al., 2018). Proteasome inactivation and accumulation of oxidized proteins are additional hallmarks of rotenone-induced

toxicity (Shamoto-Nagai et al., 2003). In addition, rotenone causes an increase in α-syn protein levels (Han et al., 2022; Li et al., 2020; Jang et al., 2015).

Beyond its canonical effects., rotenone also affects other pathways that have been implicated in PD to a lesser extent. For example, rotenone increases cyclin-dependent kinase inhibitor p21 protein levels and changes the expression of cyclin genes (Cabeza-Arvelaiz et al., 2012) with concomitant deregulation of cell cycle progression (Wang et al., 2005; Yu et al., 2013). Rotenone can also cause DNA damage (Barreca et al., 2017), as indicated by increased expression of genes involved in sensing and repairing DNA strand breaks (Cabeza-Arvelaiz et al., 2012), as well as elevated levels of p53, a protein that controls these mechanisms (Wang et al., 2019; Li et al., 2022). In addition, increased intracellular Ca^{2+} levels have been detected in rotenone-treated cells, which is thought to play a role in rotenone-mediated apoptosis (Wang et al., 2005; Park et al., 2013, Yu et al., 2013). Thus, the rotenone SH-SY5Y model recapitulates important molecular features of PD. As this study investigates novel drugs not previously tested, the well-characterized DAergic SH-SY5Y cell line offers a valuable starting point. This line has a documented history of producing reliable and reproducible results, allowing to study the specific effect of these drugs in the cellular mechanisms of PD. This initial investigation will provide a foundation for further studies using more complex models.

5.1.3. Differentiation of SH-SY5Y cells

Although immortalised SH-SY5Y cells have been widely used to model neurodegeneration, they exhibit some key differences from human neurons. For example, they often have underdeveloped neurites, divide continuously and lack some neuronal markers (Kovalevich et al., 2016). To address the limitations of immortalized neuronal cell lines, researchers have developed protocols to induce these cells into a mature neuronal phenotype. The most common method involves reducing the serum concentration in the culture medium and supplementing it with all-trans-retinoic acid (RA) for at least 3 days, which significantly promotes neurite outgrowth and neuronal marker expression (Lopes et al., 2010). RA is a derivative of vitamin A1 (all-trans-retinol) that is produced through two sequential oxidation reactions (Kedishvili et al., 2016). RA exerts its effects by binding to specific ligand-activated transcription factors that orchestrate the expression of different genes involved in the differentiation of a variety of cell types (Mey et al., 2004). In addition to its effects on gene expression, RA also

modifies molecular pathways such as ERK1/2 and phosphatidylinositol 3-kinase/Akt, which are thought to be involved in RA function as well (Lopez-Carballo et al., 2002; Khatib et al., 2019). Differentiation with RA increases the levels of mature neuron markers, such as Synaptophysin, βIII-Tubulin, TH and neuron specific enolase (Lopes et al., 2010). Upon differentiation, SH-SY5Y cells also exhibit cytoskeletal rearrangement and decreased proliferation due to cell cycle withdrawal (Zhang et al., 2021).

In addition to RA, a variety of other agents can be used to differentiate SH-SY5Y cells into mature human neurons, such as phorbol esters, dbcAMP, and specific neurotrophins such as BDNF. RA stimulates the expression of tyrosine kinase receptor B (NTrkB), which is activated by BDNF and triggers downstream neurotrophic signalling cascades (Encinas et al., 2002). Sequential exposure to RA and BDNF produces a uniform population of neurons with extended neurites and minimal proliferation (Encinas et al., 2002; Hromadkova et al., 2020). Diverse differentiation methods can induce SH-SY5Y to adopt a variety of neuron subtypes, such as adrenergic, cholinergic, and DAergic, with new methods still being developed to differentiate these cells into other subtypes (Martin et al., 2022). Interestingly, both DAergic and cholinergic characteristics have been reported in neurons differentiated with RA alone or in combination with BDNF (Xicoy et al., 2017). Despite the need for further clarification of specific phenotypes, differentiated SH-SY5Y cells provide a neuronal model that presents numerous features from human post-mitotic mature neurons.

5.1.4. Aims of the chapter

This chapter aims to explore the therapeutic potential of HIF-1α stabilizing drugs in PD-related cell models presenting mitochondrial dysfunction caused by rotenone. The neuroprotective effect of these compounds is evaluated by assessing:

1) Viability and apoptosis
2) Mitochondrial function
3) Oxidative stress
4) Protein degradation impairment
5) Cell cycle progression
6) Ca^{2+} levels
7) Changes in gene expression

These parameters are altered as part of the neurodegenerative process, so their evaluation is critical in both understanding the pathophysiology of PD and assessing potential neuroprotective interventions.

5.2. METHODOLOGY

Western Blot was utilised to detect HIF-1α protein stabilisation in mitotic SH-SY5Y and U87-MG treated with HIF-1α inducers. A range of techniques were utilised to assess the beneficial effect of these treatments against rotenone toxicity. Cell viability was evaluated by Incucyte confluence analysis and MTT assay, while apoptosis was measured as activation of Caspase-3 and -7. Viability measurements will be performed in both neuronal and astrocytic cell lines to assess differences in the response to HIF-1α stabilising drugs, as well as in differentiated SH-SY5Y. Mitochondrial function was investigated by quantifying ATP levels with a bioluminescence-based kit and mitochondrial membrane potential with the JC-1 probe. Alterations to mitochondrial morphology were explored by fluorescent microscopy. Production of ROS was assessed using the 2,7-DCFDA dye and autophagy flux was measured as increase in GFP-LC3 levels. Alterations to cell cycle progression were investigated by flow cytometry whilst changes in intracellular Ca^{2+} content were evaluated with a fluorescent probe. Markers for apoptosis, mitochondrial homeostasis, autophagy and cell cycle regulation were investigated by Western Blot. Proteasome characterisation with an apoptosis array and RNA expression profiling with a nCounter Human Neuropathology Panel were utilised to identify novel proteins and genes that are involved in the studied process. The full details of the methods used in this chapter can be found in Chapter II.

5.3. RESULTS

5.3.1. EVALUATION OF HIF-1α STABILISING DRUGS

5.3.1.1. HIF-1α inducers vary in their ability to stabilise HIF-1α

To investigate the potential neuroprotective role of HIF-1α in rotenone-induced toxicity, we selected commercially available HIF-1α stabilizers not previously tested in our PD cell model. We assessed their ability to induce HIF-1α accumulation in normoxia and to improve cell viability in rotenone-treated cells. The selected drugs include IOX4, VH298 and GSK1278863 (GSK, Daprodustat). IOX4 is a tricyclic triazole-containing potent PHD inhibitor that selectively competes with 2-OG (Chan et al., 2015). VH298 is part of a novel set of HIF-1α inducers that block pVHL with high affinity, triggering the accumulation of hydroxylated HIF-1α (Frost et al., 2016). GSK1278863 is a pyrimidinetrione-glycinamide 2-OG mimic (Dhillon et al., 2020). Firstly, SH-SY5Y were treated with different concentrations of these compounds to evaluate HIF-1α stabilisation. $CoCl_2$ treatment was used as positive control. IOX4 potently stabilises HIF-1α at concentrations of 10-200 μM while higher concentrations of VH298 are needed to stabilize HIF-1α, as HIF-1α is only detected at a concentration range of 50 to 200 μM (Fig. 5.2a, c). In turn, GSK1278863 stabilized HIF-1α at 10 and 25 μM, but was evidently cytotoxic at higher doses after 4 hours of incubation, so its investigation was not pursued (Fig. 5.2e). Of the three compounds, IOX4 is the only one that seems more effective at stabilizing HIF-1α than $CoCl_2$.

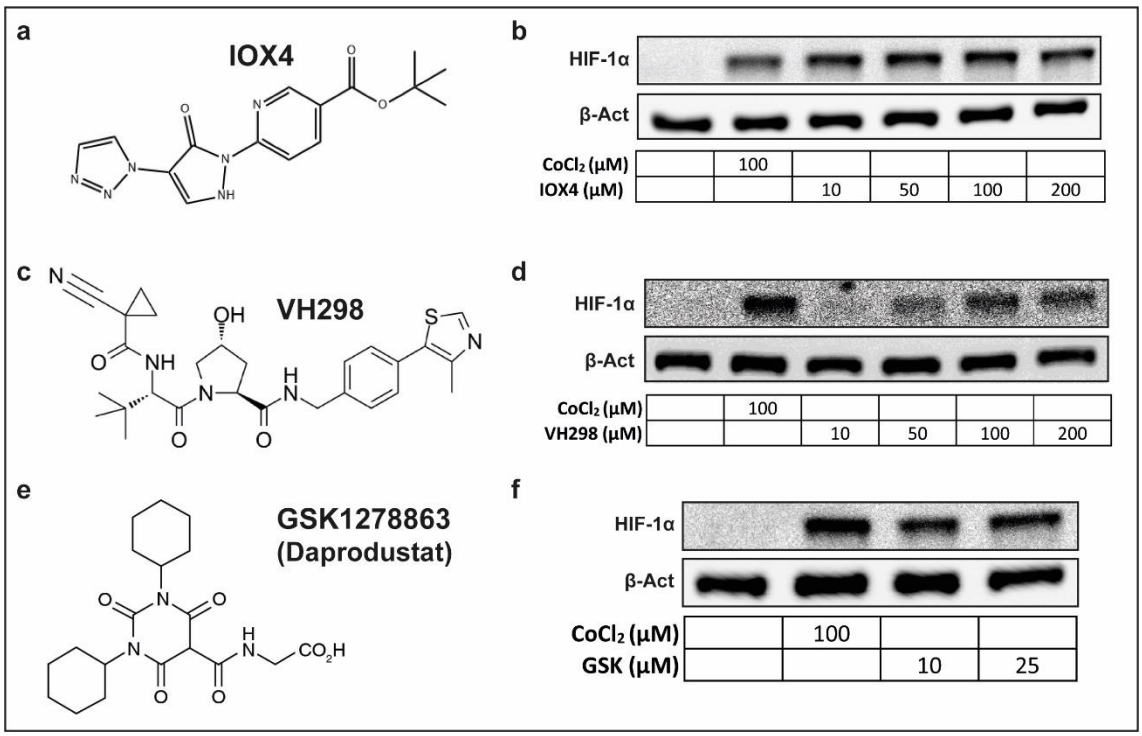

Figure 5.2. HIF-1α stabilizers vary in their potency. a. Illustration depicting the chemical structure of IOX4. **b.** Representative Western Blot image showing HIF-1α (~120 kDa) and β-Actin (~45 kDa, loading control) proteins in lysates from SH-SY5Y cells treated with different concentrations of IOX4 for 4h. **c.** Illustration depicting the chemical structure of VH298. **d.** Representative Western Blot image showing HIF-1α (~120 kDa) and β-Actin (~45 kDa, loading control) proteins in lysates from SH-SY5Y cells treated with different concentrations of VH298 for 4h. **e.** Illustration depicting the chemical structure of GSK1278863. **f.** Representative Western Blot image showing HIF-1α (~120 kDa) and β-Actin (~45 kDa, loading control) proteins in lysates from SH-SY5Y cells treated with different concentrations of GSK1278863 for 4h.

5.3.1.2. IOX4 sustains SH-SY5Y cell confluence in the presence of rotenone

We next investigated the neuroprotective potential of IOX4 and VH298 in SH-SY5Y cells exposed to mitochondrial ETC complex I inhibitor rotenone. Preliminary experiments showed that VH298 did not affect cell confluence in the presence of rotenone, but cotreatment with IOX4 resulted in a sustained growth (Fig. 5.3a, b). Considering this evidence, our research focused on IOX4.

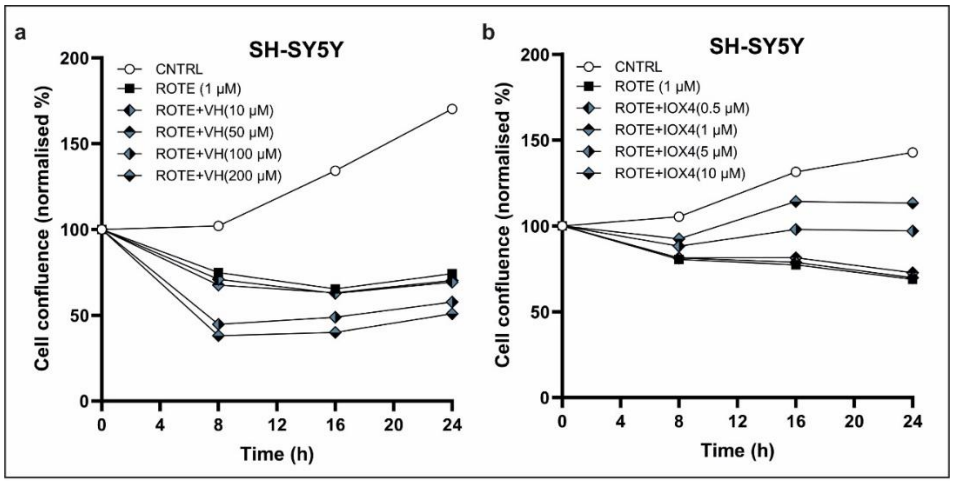

Figure 5.3. IOX4, but not VH298, attenuates the rotenone-induced decrease in cell confluence. a. Plot displaying the quantification of phase cell confluence of SH-SY5Y cells treated with 1 μM Rotenone and different VH298 concentrations during 24h acquired with the Incucyte S3 live cell analysis system (n=1). **b.** Plot displaying the quantification of phase cell confluence of SH-SY5Y cells treated with 1 μM Rotenone and different IOX4 concentrations during 24h acquired with the Incucyte S3 live cell analysis system (n=1).

5.3.2. THE STUDY OF HIF-1α INDUCER IOX4

5.3.2.1. IOX4 protects SH-SY5Y cells against rotenone-mediated damage

To further investigate the potential protective effect of IOX4 against rotenone-mediated cytotoxicity, we treated SH-SY5Y and U-87MG cells with different combinations of IOX4 and rotenone. In SH-SY5Y cells, a significant 50% drop in cell confluence is observed after 24 hours of rotenone treatment (Fig. 5.4a, b). Exposure to 0.5 μM IOX4 had no impact on cell viability, while 2.5 μM IOX4 decreased cell number after 24 hours

(Fig. 5.4a). Cotreatment with 2.5 μM IOX4 resulted in a modest increase in cell number, while neither 0.5 μM nor 2.5 μM IOX4 significantly affected cell viability (Fig. 5.4a). Increasing IOX4 concentration to 5 μM or 10 μM significantly attenuated the drop in cell confluence caused by rotenone (Fig. 5.4b). This is a substantial mitigation of the effects of rotenone on cell confluence that is likely associated with HIF-1α stabilization, as the beneficial effect is only observed at IOX4 concentrations that stimulate potent HIF-1α stabilisation. However, treatment with these concentrations of IOX4 in the absence of rotenone reduces cell confluence from 24 h (Fig. 5.4b). Microscopy images acquired at the 24h timepoint show that IOX4 counteracts the rotenone-mediated alterations in cell morphology (Fig. 5.4c). Assessment of HIF-1α levels shows that HIF-1α accumulation is still detectable after 24 hours and remains relatively constant at concentrations from 10 to 100 μM (Fig. 5.4d). In contrast, IOX4 treatment did not prevent the rotenone-induced decrease in U-87MG cell confluence, although IOX4 treatment alone affected cell number (Fig. 5.4e). Microscopy images confirm these results, indicating that IOX4 did not reverse the morphological changes induced by rotenone in these cells (Fig. 5.4f).

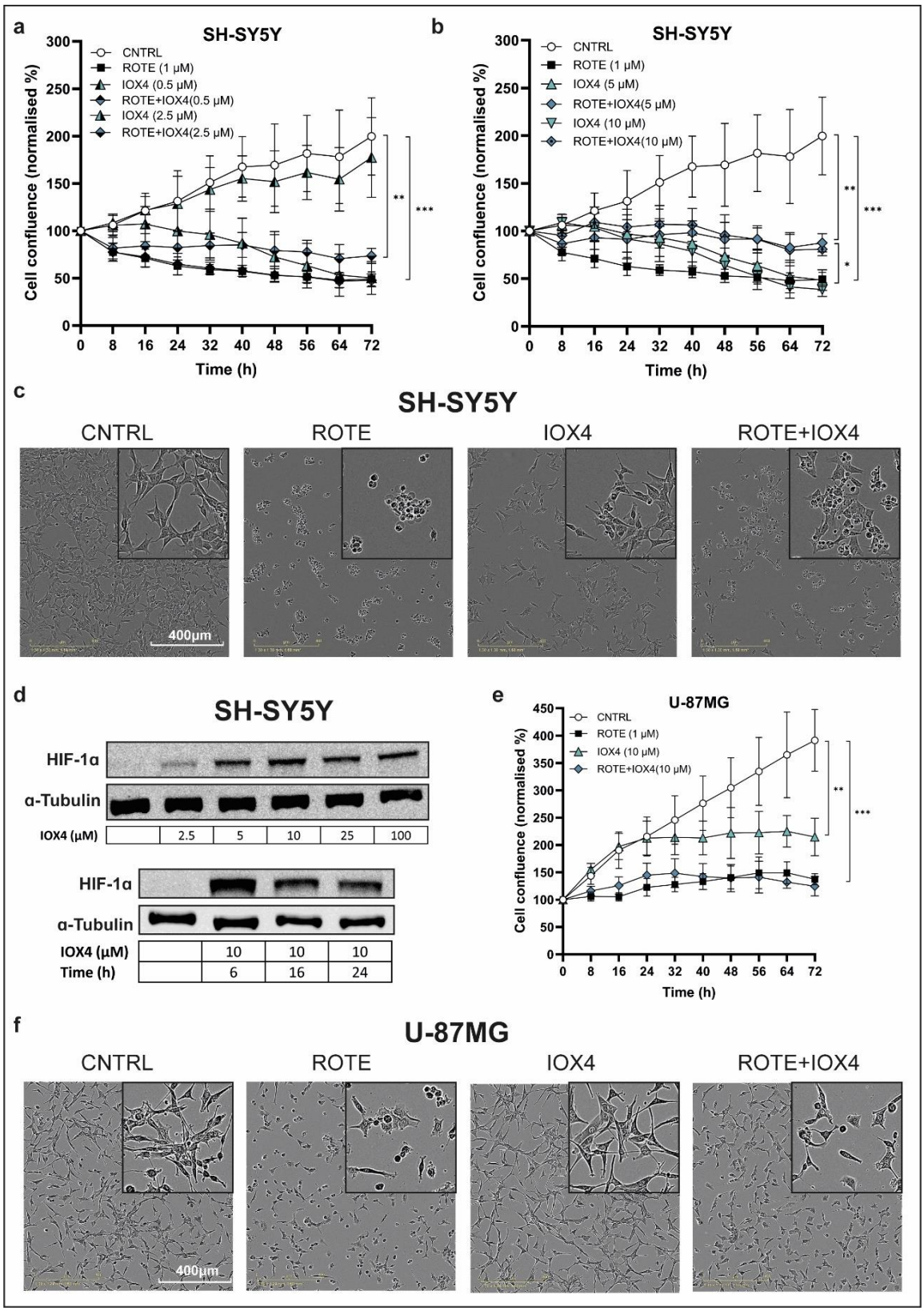
a
SH-SY5Y
CNTRL
ROTE (1 μM)
IOX4 (0.5 μM)
ROTE+IOX4(0.5 μM)
IOX4 (2.5 μM)
ROTE+IOX4(2.5 μM)
Cell confluence (normalised %)
Time (h)
b
SH-SY5Y
CNTRL
ROTE (1 μM)
IOX4 (5 μM)
ROTE+IOX4(5 μM)
IOX4 (10 μM)
ROTE+IOX4(10 μM)
Cell confluence (normalised %)
Time (h)
c
SH-SY5Y
CNTRL
ROTE
IOX4
ROTE+IOX4
400μm
d
SH-SY5Y
HIF-1α
α-Tubulin
IOX4 (μM)
2.5
5
10
25
100
HIF-1α
α-Tubulin
IOX4 (μM)
Time (h)
10
6
10
16
10
24
e
U-87MG
CNTRL
ROTE (1 μM)
IOX4 (10 μM)
ROTE+IOX4(10 μM)
Cell confluence (normalised %)
Time (h)
f
U-87MG
CNTRL
ROTE
IOX4
ROTE+IOX4
400μm

Figure 5.4. IOX4 specifically attenuates the rotenone-mediated decrease in cell confluence in SH-SY5Y cells. a. Plot displaying the quantification of phase cell confluence of SH-SY5Y cells treated with 1 μM Rotenone and 0.5 or 2.5 μM IOX4 separately or combined during 72h acquired with the Incucyte S3 live cell analysis system (n=4). **b.** Plot displaying the quantification of phase cell confluence of SH-SY5Y cells treated with 1 μM Rotenone and 5 or 10 μM IOX4 separately or combined during 72h acquired with the Incucyte S3 live cell analysis system (n=4). **c.** Representative microscopy images acquired with the Incucyte S3 system showing SH-SY5Y cells treated with 1 μM Rotenone and 10 μM IOX4 separately or combined for 24h. Scale bar indicates 400 μm. **d.** Representative Western Blot images showing HIF-1α (~120 kDa) and α-Tubulin (~55 kDa, loading control) proteins in lysates from SH-SY5Y cells treated as stated. **e.** Plot displaying the quantification of phase cell confluence of U-87MG cells treated with 1 μM Rotenone and 10 μM IOX4 separately or combined during 72h acquired with the Incucyte S3 live cell analysis system (n=4) **f.** Representative microscopy images acquired with the Incucyte S3 system showing U-87MG cells treated with 1 μM Rotenone and 10 μM IOX4 separately or combined for 24h. Scale bar indicates 400 μm. Statistical analysis was performed using a two-way ANOVA followed with Tukey's post-hoc test where $p<0.05$ was recorded as "*".

We hypothesized that the protective effect of IOX4 on SH-SY5Y cells may also be evident in differentiated SH-SY5Y cells (5 days RA, dSH-SY5Y), and therefore investigated this possibility. Using dSH-SY5Y cells provides a more relevant model for studying neuronal processes, as these cells can present different gene expression, drug responses and morphology compared to non-differentiated cells. To validate this model, we evaluated the expression of the neuronal markers βIII-tubulin and synaptophysin, which are significantly upregulated in differentiated SH-SY5Y cells relative to mitotic SH-SY5Y cells (Fig. 5.5a, b). Microscope images show that differentiated cells present an elongated morphology with increased number of neurites (Fig. 5.5c). dSH-SY5Y cell proliferation is also reduced compared to mitotic cells (Fig. 5.4a, b; Fig. 5.5d). In dSH-SY5Y cells rotenone had a less severe effect on cell confluence, reducing it to about 75% (Fig. 5.5d). Cotreatment with IOX4 significantly alleviates the rotenone-induced decrease in cell confluence over 72 hours (Fig. 5.5d).

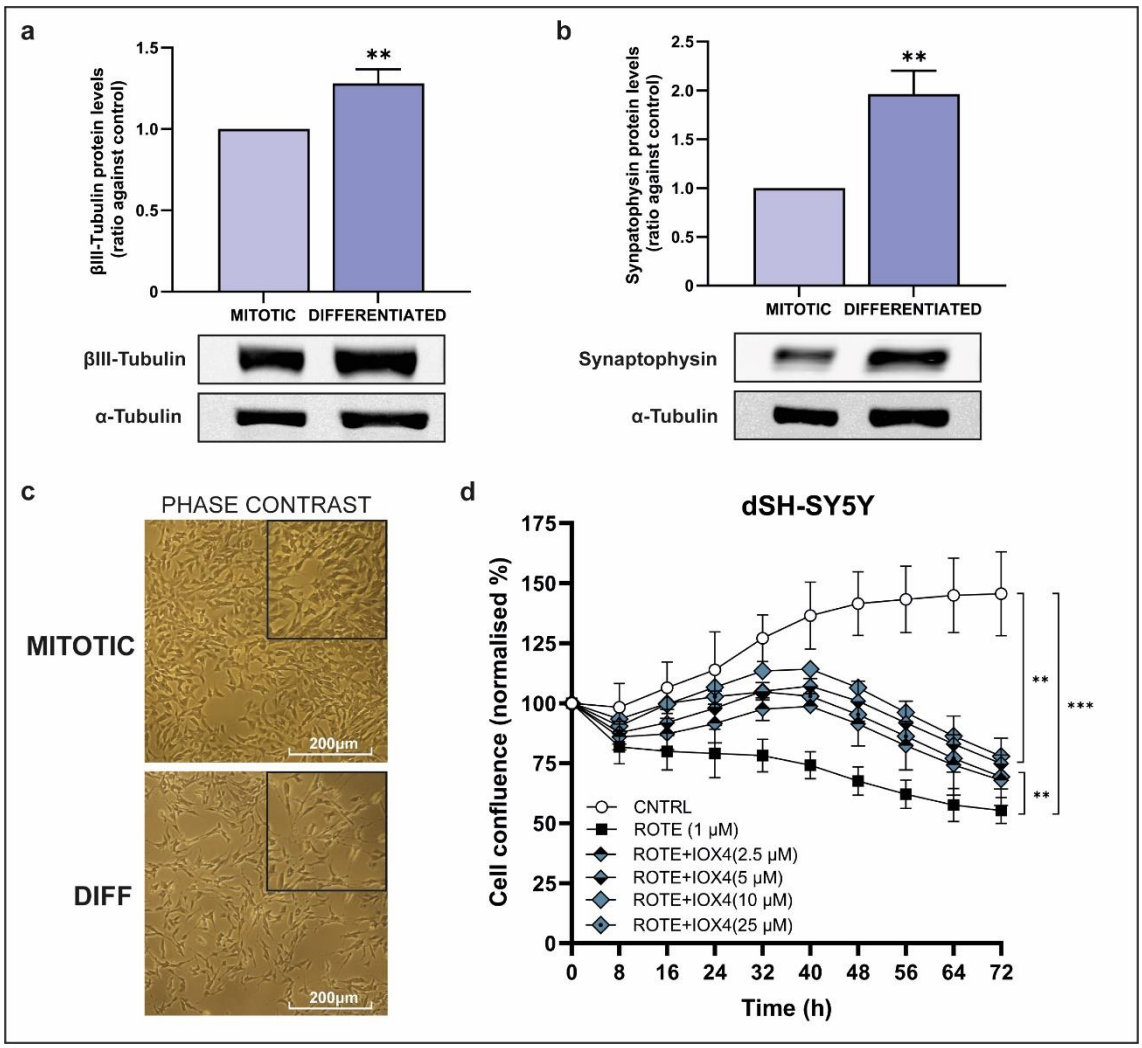

Figure 5.5. IOX4 remains effective in protecting differentiated SH-SY5Y cells from rotenone-mediated cytotoxicity. a. Representative Western Blot image showing βIII-Tubulin (~50 kDa) and α-Tubulin (~55 kDa, loading control) proteins in lysates from mitotic and differentiated SH-SY5Y cells accompanied by densitometric analysis (n=3). **b.** Representative Western Blot image showing Synaptophysin (~38 kDa) and α-Tubulin (~55 kDa, loading control) proteins in lysates from mitotic and differentiated SH-SY5Y cells accompanied by densitometric analysis (n=3). **c.** Representative phase contrast images of mitotic and differentiated SH-SY5Y. **d.** Plot displaying the quantification of phase cell confluence of differentiated SH-SY5Y cells treated with 1 µM Rotenone and the specified IOX4 concentrations combined during 72h acquired with the Incucyte S3 live cell analysis system (n=5). Statistical analysis for graph a and b was performed using an unpaired two-tailed Student's t test where $p<0.05$ was recorded as "*" with respect to control. Statistical analysis for plot d was performed using a two-way ANOVA followed with Tukey's post-hoc test where $p<0.05$ was recorded as "*".

5.3.2.2. IOX4 blocks rotenone-induced apoptosis

To investigate whether the protective effects of IOX4 on mitotic SH-SY5Y cells, which were more evident than in differentiated cells, were mediated by alterations in apoptosis, we analysed the expression of apoptotic markers. IOX4 significantly counteracts rotenone-induced apoptosis, as demonstrated by the reduction in cleaved Caspase-3 levels (Fig.5.6a). However, a small increase in cleaved Caspase-3 could also be observed in cells treated with IOX4 only. Evaluation of caspase-3/7 activation using a fluorescent dye over

72 hours indicates that rotenone robustly triggers caspase-3/7 activity, while IOX4 treatment results in a small, albeit statistically insignificant, increase in caspase-3/7 activity (Fig. 5.6b, c). Strikingly, IOX4 co-treatment significantly abrogates caspase-3/7 activation in rotenone-treated cells (Fig. 5.6b, c).

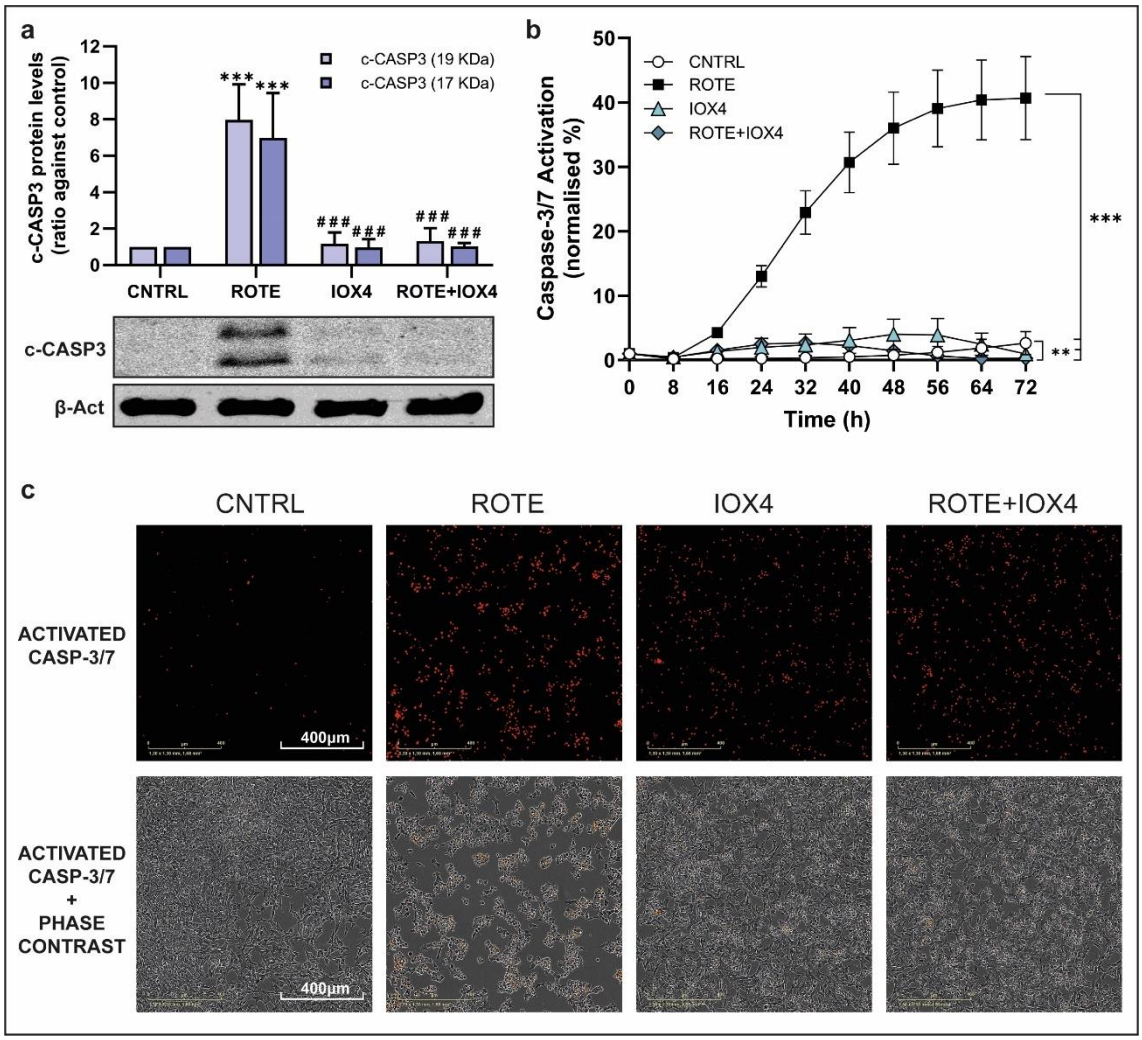

Figure 5.6. IOX4 reduces Caspase-3/7 activation caused by rotenone in SH-SY5Y cells. a. Representative Western Blot image showing cleaved Caspase-3 (~17,19 kDa) and β-Actin (~45 kDa, loading control) proteins in lysates from SH-SY5Y cells treated with 1 μM Rotenone and 10 μM IOX4 separately or combined for 24 hours accompanied by densitometric analysis (n=3). **b.** Plot displaying the quantification of Incucyte Caspase-3/7 Red Dye fluorescence normalized to phase cell confluence of SH-SY5Y cells treated as previously stated during 72h acquired with the Incucyte S3 live cell analysis system (n=4). **c.** Representative microscopy images acquired with the Incucyte S3 system showing SH-SY5Y cells treated as previously stated for 24h in the presence of the Incucyte Caspase-3/7 Red Dye. Scale bar indicates 400 μm. Statistical analysis for graph a was performed using a one-way ANOVA followed with Dunnett's post-hoc where $p<0.05$ was recorded as "*" with respect to control and "#" with respect to rotenone. Statistical analysis for graph b was performed using a two-way ANOVA followed with Tukey's post-hoc test where $p<0.05$ was recorded as "*".

5.3.2.3. IOX4 induces ATP depletion and mitochondrial membrane depolarisation

Rotenone critically impacts mitochondria as a mitochondrial ETC complex I inhibitor and HIF-1α downregulates OXPHOS. Surprisingly, both rotenone and IOX4 treatment over

24 or 28 hours significantly reduce ATP levels compared to untreated cells (Fig. 5.7a, b). The combination of these treatments results in a substantial reduction in ATP content (Fig. 5.7a, b). Our findings suggest that the protective effect of IOX4 is not due to an increase in ATP levels, and that reduced ATP levels are not the primary mechanism by which IOX4 treatment exerts its negative effects, as co-treated cells have similar ATP levels but higher cell confluence.

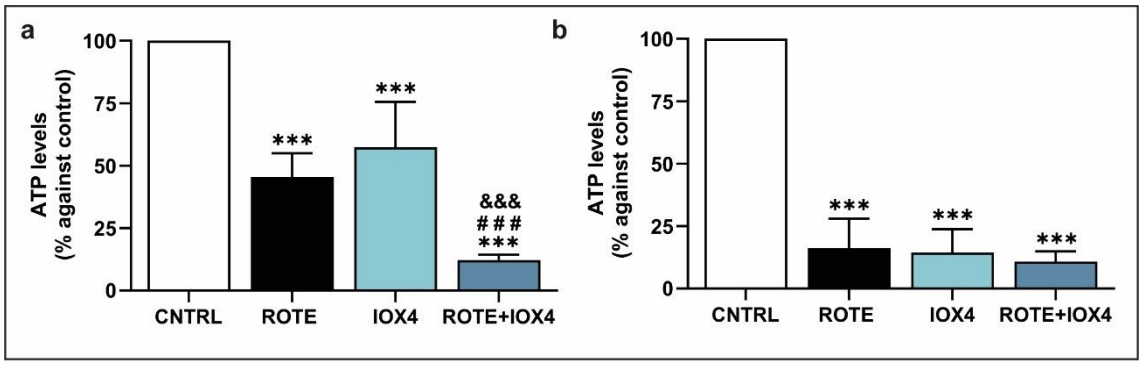

Figure 5.7. IOX4 and rotenone reduce ATP levels. a. Graph displaying ATP content in lysates from SH-SY5Y cells treated with 1 μM Rotenone and 10 μM IOX4 separately or combined for 24h (n=5). **b.** Graph displaying ATP content in lysates from SH-SY5Y cells treated with 1 μM Rotenone and 10 μM IOX4 separately or combined for 48h (n=5). Statistical analysis was performed using a one-way ANOVA followed with Dunnett's post-hoc where $p<0.05$ was recorded as "*" with respect to control, "#" with respect to rotenone and "&" when comparing to IOX4.

The ETC plays a critical role in maintaining mitochondrial membrane potential by generating a proton gradient across the inner mitochondrial membrane. Consequently, rotenone significantly decreased mitochondrial membrane potential in SH-SY5Y cells (Fig. 5.8a-c). Surprisingly, IOX4 can also depolarise the mitochondrial membrane, with a mild effect at 24h but a pronounced effect at 48h (Fig. 5.8a-c). Despite this fact, combination of rotenone and IOX4 treatments significantly increase membrane potential when compared to cells treated with rotenone only (Fig. 5.8a-c). These changes mirror the effects of IOX4 in cell viability, where IOX4 treatment improves survival when combined with rotenone but proves toxic on its own.

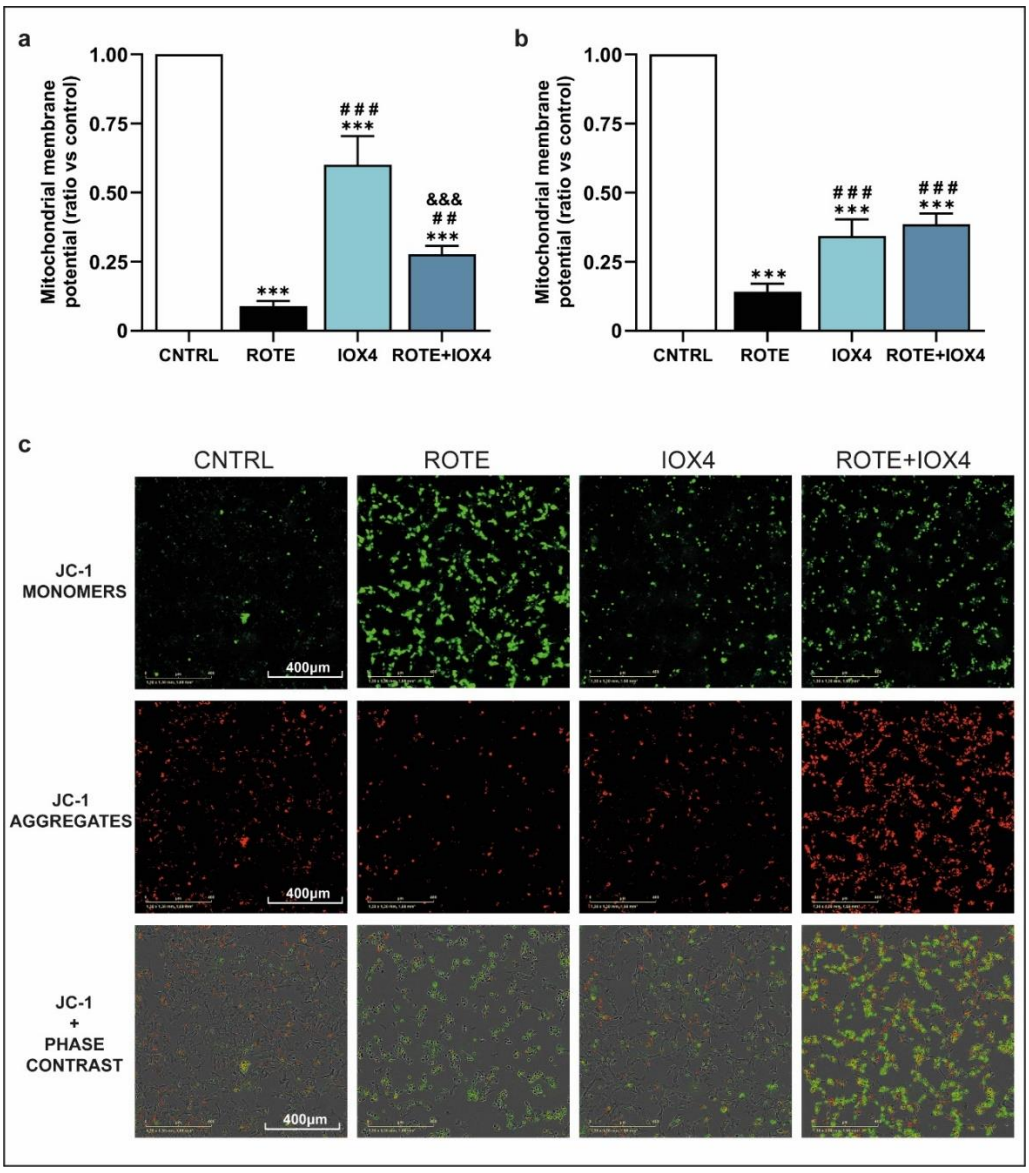

Figure 5.8. Both rotenone and IOX4 reduce mitochondrial membrane potential. a. Graph displaying mitochondrial membrane potential measured as ratio of green monomers to red aggregates of the fluorescent probe JC-1 based on the images taken with the Incucyte S3 system of SH-SY5Y cells treated with 1 µM Rotenone and 10 µM IOX4 separately or combined for 24h (n=4). **b.** Graph displaying mitochondrial membrane potential measured as ratio of green monomers to red aggregates of the fluorescent probe JC-1 based on the images taken with the Incucyte S3 system of SH-SY5Y cells treated as previously stated for 48h (n=3). **c.** Representative microscopy images acquired with the Incucyte S3 system showing fluorescence from the JC-1 probe in SH-SY5Y cells under shown treatments for 24h. Scale bar indicates 400 µm. Statistical analysis was performed using a one-way ANOVA followed with Dunnett's post-hoc where $p<0.05$ was recorded as "*" with respect to control, "#" with respect to rotenone and "&" when comparing to IOX4.

Mitochondrial network homeostasis is maintained by a delicate balance between mitochondrial fission and fusion, which is regulated by a complex network of proteins. Remarkably, treatment with IOX4 downregulated the levels of Mitofusin-1 (MFN1) and -2 (MFN2), as well as the phosphorylation at Ser616 of Drp1, although Drp1 total levels

remain unchanged (Fig. 5.9a-c). In contrast to rotenone treatment, which only reduced S-OPA1 levels, IOX4 treatment reduced both OPA1 isoforms (Fig. 5.9c). IOX4 appeared to slightly decrease HUMMR levels although this reduction was not statistically significant (Fig. 5.9d). These findings indicate that IOX4 profoundly impacts mitochondrial dynamics, which might be related to its side effects.

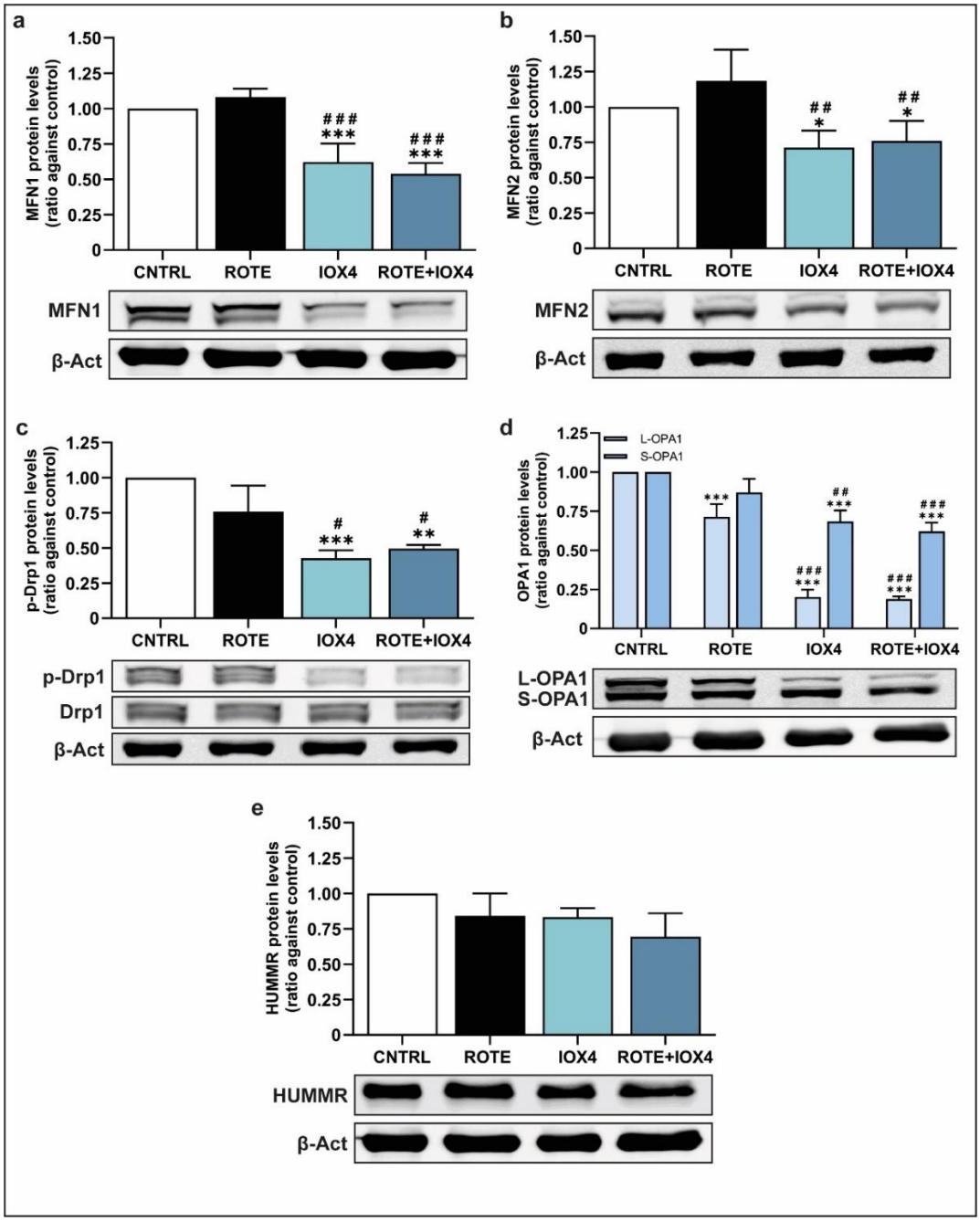

Figure 5.9. IOX4 modifies the levels of an array of proteins involved in mitochondrial dynamics. **a.** Representative Western Blot image showing MFN1 (~82 kDa) and β-Actin (~45 kDa, loading control) proteins in lysates from SH-SY5Y cells treated with 1 μM Rotenone and 10 μM IOX4 separately or combined for 24h accompanied by densitometric analysis (n=3). **b.** Representative Western Blot image showing MFN2 (~80 kDa) and β-Actin (~45 kDa, loading control) proteins in lysates from SH-SY5Y cells treated as previously stated accompanied by densitometric analysis (n=3). **c.** Representative Western Blot image showing p-Drp1 (S616) and Drp1 (~80 kDa) as well as β-Actin (~45 kDa, loading control) proteins in lysates from SH-SY5Y cells treated as previously stated accompanied by densitometric analysis (n=3) **d.** Representative Western Blot image showing OPA1 (~80,100 kDa) and β-Actin (~45 kDa, loading control) proteins in lysates from SH-SY5Y cells treated as previously stated accompanied by densitometric analysis (n=3). **e.** Representative Western Blot image showing HUMMR (~50 kDa) and β-Actin (~45 kDa, loading control) proteins in lysates from SH-SY5Y cells treated as previously stated accompanied by densitometric analysis (n=3). Statistical analysis was performed using a one-way ANOVA followed with Dunnett's post-hoc where $p<0.05$ was recorded as "*" with respect to control and "#" with respect to rotenone.

5.3.2.4. IOX4 attenuates the increased ROS triggered by rotenone

When mitochondrial function, membrane potential, and dynamics are disrupted, ROS generation can be altered. Rotenone treatment of SH-SY5Y cells resulted in a significant and pronounced increase in ROS production (Fig. 5.10a, b). IOX4 prevented rotenone from elevating ROS levels, returning ROS production to baseline (Fig. 5.10a, b). Thus, IOX4 may protect cells from rotenone toxicity by reducing oxidative stress.

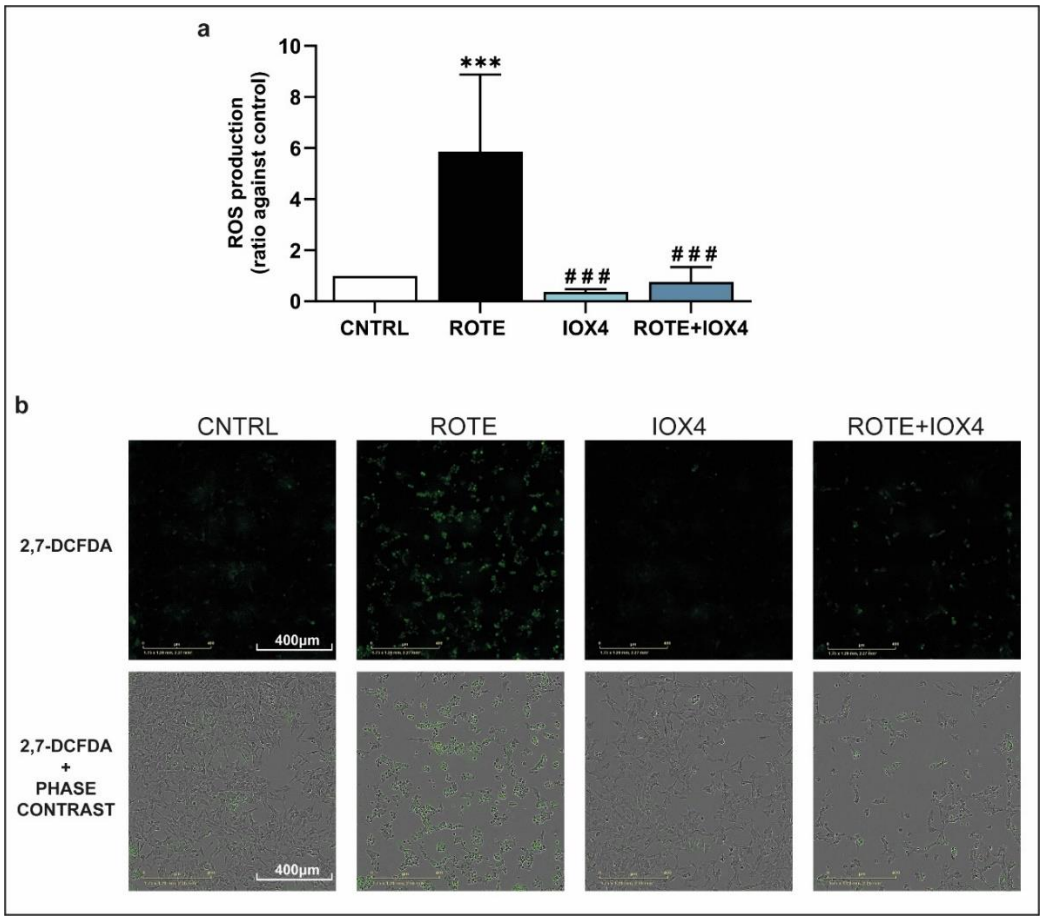

Figure 5.10. IXO4 mitigates rotenone-induced ROS overproduction. a. Plot showing the quantification of 2,7-DCDFA green fluorescence area/phase confluence area percentage based on the images taken with the Incucyte S3 system of SH-SY5Y cells treated with 1 μM Rotenone and 10 μM IOX4 separately or combined for 24h (n=4). **b.** Representative microscopy images acquired with the Incucyte S3 system showing ROS production as green fluorescence detected by the 2,7-DCDFA probe and phase confluence of SH-SY5Y cells under shown treatments for 24h. Scale bar indicates 400 μm. Statistical analysis was performed using a one-way ANOVA followed with Dunnett's post-hoc where $p<0.05$ was recorded as "*" with respect to control and "#" when comparing to rotenone.

5.3.2.5. IOX4 induces changes in p53 and Heat shock proteins

To identify the proteins involved in both the beneficial and detrimental effects of IOX4, we used a proteome array to profile a panel of cellular stress proteins. As anticipated, HIF-1α was stabilized to a greater extent than HIF-2α, but both proteins exhibited a noticeable increase (Fig. 5.11a, b). Carbonic anhydrase 9 (CA9), a known HIF-1α target gene, was also upregulated (Fig. 5.11a, b). Notably, rotenone and IOX4 induce similar changes in some proteins, including p53 phosphorylation at Ser46 and Heat shock protein Hsp60 downregulation, which may be linked to the adverse effects of IOX4 (Fig. 5.11a, b). In addition, IOX4 induces some unique changes, such as increased levels of cell cycle regulator p27 and phosphorylation of Hsp27 at Ser78/82 (Fig. 5.11a, b). Although this study provided valuable insights into the effects of IOX4 on SH-SY5Y cells, its induction of mitochondrial toxicity and cell growth inhibition led us to discontinue its investigation and focus on other HIF-1α stabilizing drugs that may exhibit only the beneficial effects of IOX4.

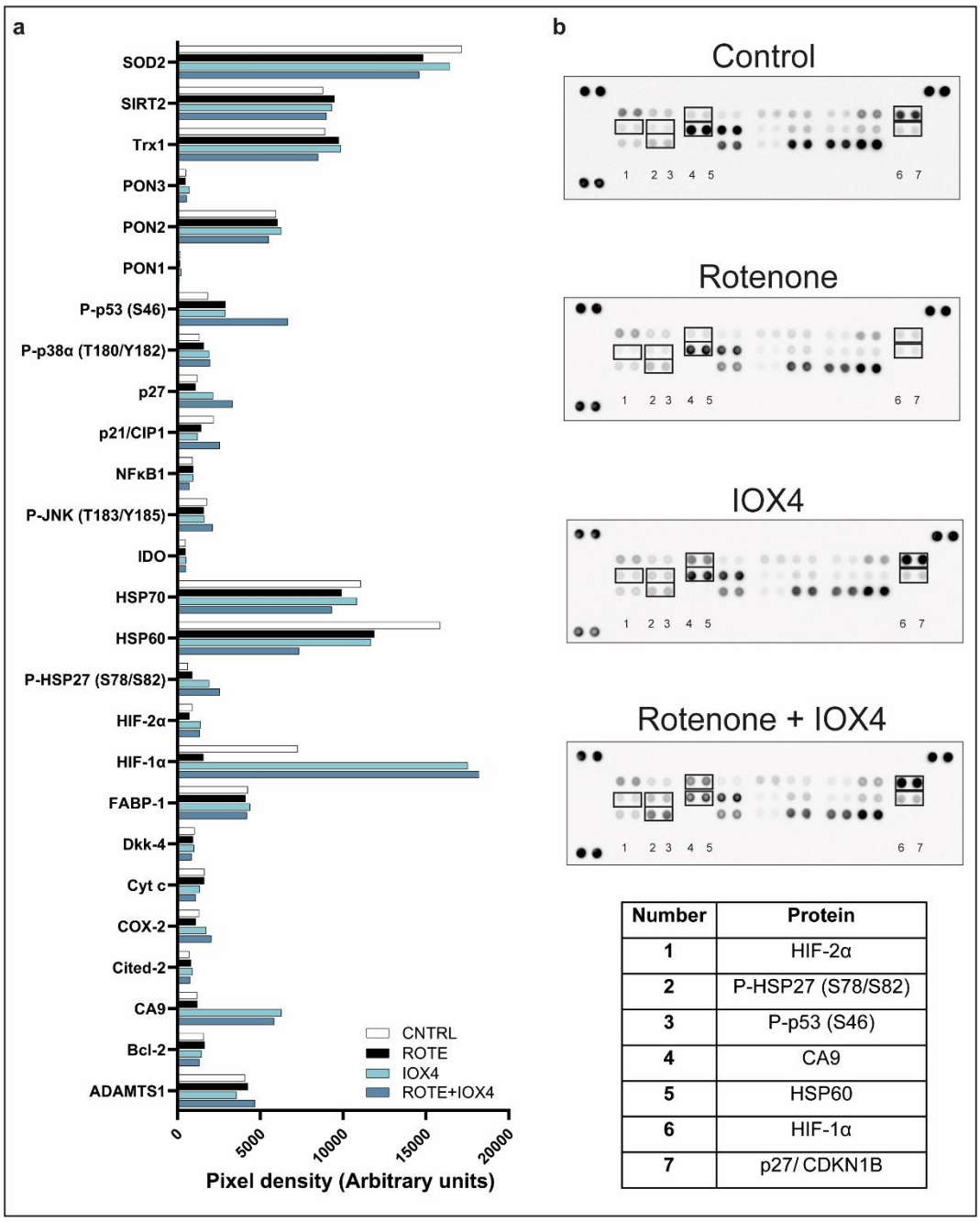

Figure 5.11. IOX4 modulates the levels and phosphorylation state of p53 and HSPs. a. Plot summarising densitometric analysis of the Proteome Profiler Human Apoptosis Array of lysates from SH-SY5Y cells treated with 1 μM Rotenone and 10 μM IOX4 separately or combined for 24h (n=1). **b.** Proteome Profiler Human Apoptosis Array membrane images for all groups analysed accompanied by a table highlighting the location of proteins of interest.

5.3.3. THE STUDY OF HIF-1α INDUCER ML228

5.3.3.1. ML228 stabilises HIF-1α in SH-SY5Y and U-87MG cells

Encouraged by the potential of targeting HIF-1α in this PD model, and given the limitations of previously explored drugs, we set out to investigate a different novel HIF-1α stabilising drug, ML228 (Fig. 5.12a). ML228 is a lipophilic triazine that is believed to stabilise HIF-1α by chelating iron (Theriault, 2012). Firstly, the effect of ML228 on SH-SY5Y cell confluence over 72h was investigated. Low concentrations of ML228 (0.1, 0.5 μM) do not seem to impact cell number, while increasing the concentration can slow down (2.5 μM) or reduce (5, 10 μM) cell growth after 24h (Fig. 5.12b). Analysis of HIF-1α levels in SH-SY5Y and U-87MG cells treated with different concentrations of ML228 for 24 hours shows significantly increased HIF-1α protein accumulation, at concentrations of 0.5 μM or higher in SH-SY5Y cells and 2.5 μM or higher in U-87MG cells (Fig. 5.12c, d).

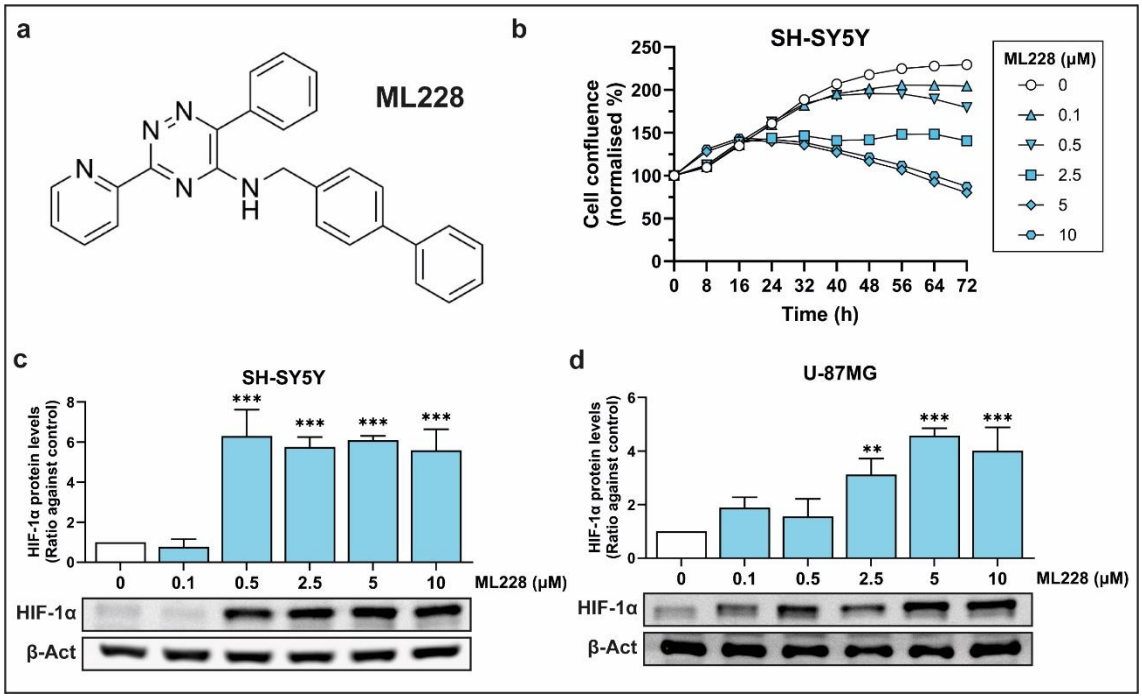

Figure 5.12. ML228 induces HIF-1α accumulation in SH-SY5Y and U-87MG cells. a. Illustration depicting the chemical structure of ML228. **b.** Plot displaying the quantification of phase cell confluence of SH-SY5Y cells treated with different ML228 concentrations during 72h acquired with the Incucyte S3 live cell analysis system (n=1). **c.** Representative Western Blot image showing HIF-1α (~120 kDa) and β-Actin (~45 kDa, loading control) proteins in lysates from SH-SY5Y cells treated with different ML228 concentrations for 24h accompanied by densitometric analysis (n=3). **d.** Representative Western Blot image showing HIF-1α (~120 kDa) and β-Actin (~45 kDa, loading control) proteins in lysates from U-87MG cells treated with different ML228 concentrations for 24h accompanied by densitometric analysis (n=3). Statistical analysis was performed using a one-way ANOVA followed with Dunnett's post-hoc test where $p<0.05$ was recorded as "*" with respect to control.

5.3.3.2. ML228 protects SH-SY5Y cells against rotenone-mediated alterations in cell number, morphology and metabolism

After the initial evaluation of ML228, its potential protective effect against rotenone-mediated decrease in cell number was investigated. In SH-SY5Y cells, it was decided to utilise two concentrations that have no impact on cell confluence, 0.1 and 0.5 μM, while only 0.5 μM was shown to stabilise HIF-1α. Analysis of cell confluence shows a significant reduction of approximately 50% after 24 hours of rotenone treatment (Fig. 5.13a, b). Although 0.1 μM ML228 had no effect on rotenone-mediated decrease on cell number, addition of 0.5 μM ML228 increased cell confluence up to 50% when compared to rotenone only treatment (Fig. 5.13a, b). The effect of 0.5 μM ML228 is significant from 16 hours onwards and remains significant at the end of the study at 72 hours (Fig. 5.1b). This constitutes a substantial attenuation of the impact of rotenone on cell levels, and it is likely to be linked to HIF-1α stabilisation, as the beneficial effect is only observed for ML228 concentrations that induce HIF-1α accumulation. As the maximum effect of ML228 can be observed at 24h, this timepoint was chosen for further evaluation. Microscopy images acquired during this investigation demonstrate that ML228 also reverses the alternations in cell morphology induced by rotenone (Fig. 5.13c). Conversely, the treatment of U-87MG cells with 0.5μM does not rescue the decrease in cell number caused by rotenone (Fig. 5.13d). As this concentration only induced a small increase on HIF-1α levels, higher concentrations of ML228 were also investigated. However, treatment with either 2.5 or 5 μM ML228 had no effect on rotenone-mediated reduction in cell confluence (Fig. 5.13e) and microscopy images corroborate the data, as 2.5 μM ML228 does not abrogate morphological changes (Fig. 5.13f).

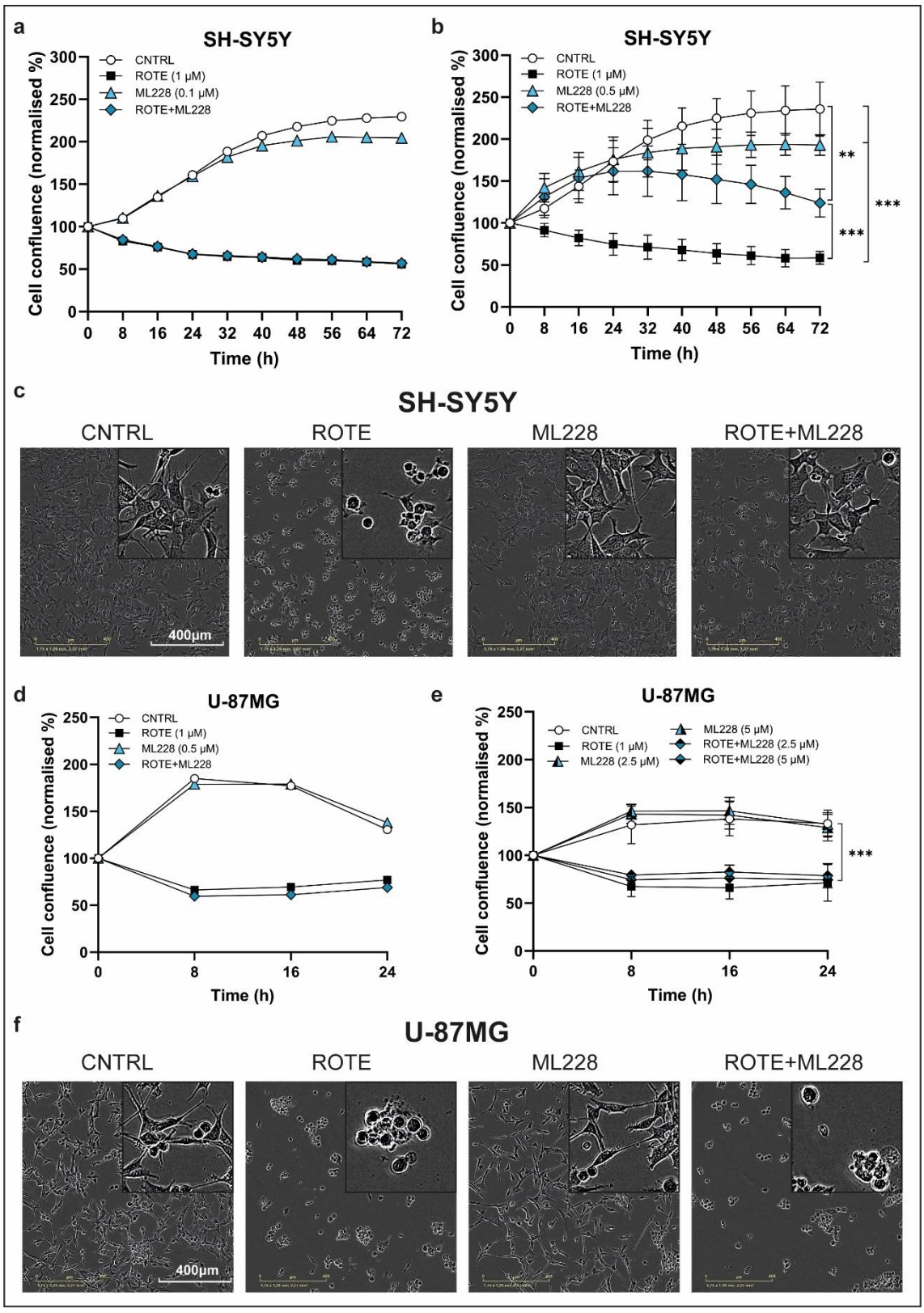
a
SH-SY5Y
CNTRL
ROTE (1 µM)
ML228 (0.1 µM)
ROTE+ML228
Cell confluence (normalised %)
Time (h)
b
SH-SY5Y
CNTRL
ROTE (1 µM)
ML228 (0.5 µM)
ROTE+ML228
**
***
***
Cell confluence (normalised %)
Time (h)
c
SH-SY5Y
CNTRL
ROTE
ML228
ROTE+ML228
400µm
d
U-87MG
CNTRL
ROTE (1 µM)
ML228 (0.5 µM)
ROTE+ML228
Cell confluence (normalised %)
Time (h)
e
U-87MG
CNTRL
ROTE (1 µM)
ML228 (2.5 µM)
ML228 (5 µM)
ROTE+ML228 (2.5 µM)
ROTE+ML228 (5 µM)
***
Cell confluence (normalised %)
Time (h)
f
U-87MG
CNTRL
ROTE
ML228
ROTE+ML228
400µm

Figure 5.13. ML228 reduces the impact of rotenone on cell confluence in SH-SY5Y cells exclusively. a. Plot displaying the quantification of phase cell confluence of SH-SY5Y cells treated with 1 µM Rotenone and 0.1 µM ML228 separately or combined during 72h acquired with the Incucyte S3 live cell analysis system (n=1). **b.** Plot displaying the quantification of phase cell confluence of SH-SY5Y cells treated with 1 µM Rotenone and 0.5 µM ML228 separately or combined during 72h acquired with the Incucyte S3 live cell analysis system (n=5). **c.** Representative microscopy images acquired with the Incucyte S3 system showing SH-SY5Y cells treated with 1 µM Rotenone and 0.5 µM ML228 separately or combined for 24h. Scale bar indicates 400 µm. **d.** Plot displaying the quantification of phase cell confluence of U-87MG cells treated with 1 µM Rotenone and 0.5 µM ML228 separately or combined during 72h acquired with the Incucyte S3 live cell analysis system (n=1). **e.** Plot displaying the quantification of phase cell confluence of U-87MG cells treated with 1 µM Rotenone and 2.5 or 5 µM ML228 separately or combined during 72h acquired with the Incucyte S3 live cell analysis system (n=4). **f.** Representative microscopy images acquired with the Incucyte S3 system showing U-87MG cells treated with 1 µM Rotenone and 2.5 µM ML228 separately or combined for 24h. Scale bar indicates 400 µm. Statistical analysis was performed using a two-way ANOVA followed with Tukey's post-hoc test where $p<0.05$ was recorded as "*".

To further evaluate the effect of ML228 on cell morphology, we analysed microscopy images with the Neurotrack software to detect neurites in SH-SY5Y cells (Lee et al., 2022). The analysis of cell morphology, especially in neuronal cells like SH-SY5Y, can reveal valuable information about cellular health, and if ML228 promotes neurite outgrowth or prevents neurite degeneration, it suggests that the drug may have neuroprotective properties. At 24 hours, rotenone was found to induce neurite retraction, while cotreatment with ML228 significantly prevented this effect (Fig. 5.14a), as can be clearly observed in the microscopy images (Fig. 5.14b). Thus, ML228 protects against loss of neurites and cytoplasmic retraction, maintaining a higher percentage of cells in the standard SH-SY5Y elongated shape with neurite extensions.

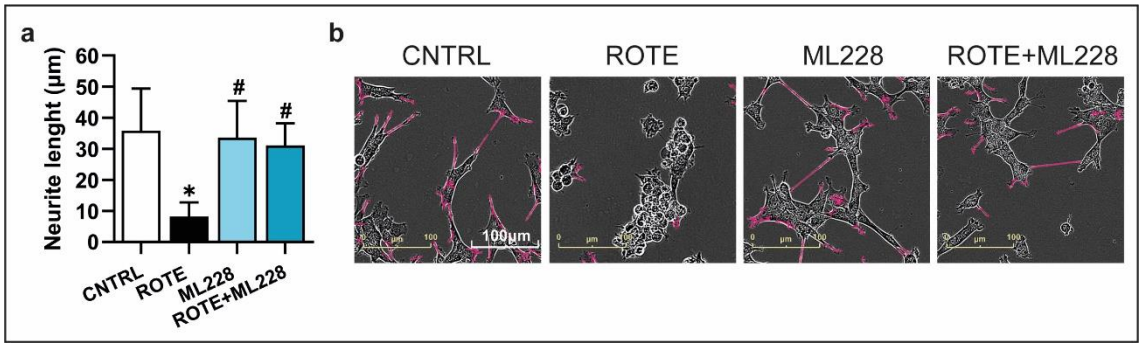

Figure 5.14. ML228 maintains cell morphology and neurite extension in rotenone-treated SH-SY5Y cells. a. Plot summarising neurite analysis of microscopy images of SH-SY5Y cells treated with 1 µM Rotenone and 0.5 µM ML228 separately or combined for 24h processed with the Incucyte Neurotrack software module (n=4) **b.** Representative microscopy images acquired with the Incucyte S3 system (20X objective) showing SH-SY5Y cells treated with 1 µM Rotenone and 0.5 µM ML228 separately or combined for 24h. The pink overlay represents the Incucyte Neurotrack mask utilized to calculate neurite length. Scale bar indicates 100 µm Statistical analysis was performed using a one-way ANOVA followed with Dunnett's post-hoc test where $p<0.05$ was recorded as "*" with respect to control and "#" when comparing to rotenone.

Since the Incucyte analysis only provides information on cell confluence, it is necessary to investigate whether the effect of ML228 and the differences between cell lines translated to alterations in cell metabolism. Indeed, rotenone causes a substantial drop in MTT reduction, used as a measure of cellular metabolic activity, of 50% in SH-SY5Y cells and 40% in U-87MG cells (Fig. 5.15a, b). MTT reduction is not altered by ML228, in line with the findings of the cell confluence analysis (Fig. 5.15a, b). When combining rotenone with ML228, the decrease in MTT reduction caused by rotenone is attenuated to a 25% only in SH-SY5Y cells, with no effect detected in U-87MG cells, mirroring the results obtained previously (Fig. 5.15a, b).

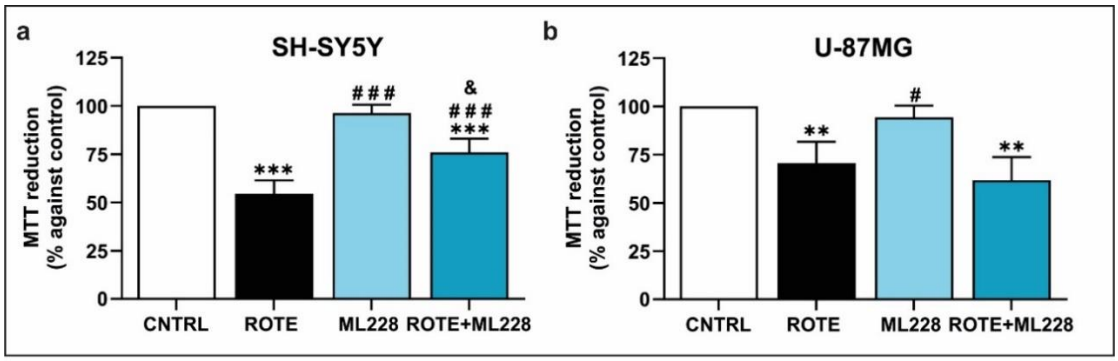

Figure 5.15. ML228 protects against the reduction in cellular metabolic activity caused by rotenone exclusively in SH-SY5Y cells. a. Plot displaying MTT reduction in SH-SY5Y cells treated with 1 μM Rotenone and 0.5 μM ML228 separately or combined for 24h (n=5). **b.** Plot displaying MTT reduction in SH-SY5Y cells treated with 1 μM Rotenone and 0.5 μM ML228 separately or combined for 24h (n=3). Statistical analysis was performed using a one-way ANOVA followed with Dunnett's post-hoc test where $p<0.05$ was recorded as "*" with respect to control, "#" with respect to rotenone and "&" when comparing to ML228.

Because the protective effect of ML228 was only seen in SH-SY5Y cells, we investigated whether this effect could be replicated in differentiated SH-SY5Y cells. By employing various differentiation protocols, SH-SY5Y cells can be induced to develop into neuronal phenotypes with varying degrees of maturity, enabling the assessment of drug effects across different stages of neuronal development and the identification of potential treatment limitations. In differentiated SH-SY5Y cells (5 days RA, dSH-SY5Y), ML228 had no considerable impact on cell number although a modest increase in early timepoints can be observed (Fig. 5.16a). The combination of rotenone with ML228 significantly attenuates the decrease in cell confluence caused by rotenone throughout 72h (Fig. 5.16a). However, the protective effect of ML228 is diminished in fully differentiated SH-SY5Y cells (5 days RA followed by 3 days Brain derived neurotrophic factor (BDNF), fdSH-SY5Y). In these cells, the effect of ML228 is only significant at the 16 and 24h timepoints, and treatment with ML228 alone seems to cause toxicity after 24h (Fig. 5.16b). These findings indicate that ML228 activates protective mechanisms against rotenone, likely

through HIF-1α, that are present for at least 24h in mitotic SH-SY5Y cells as well as dSH-SY5Y and fdSH-SY5Y cells.

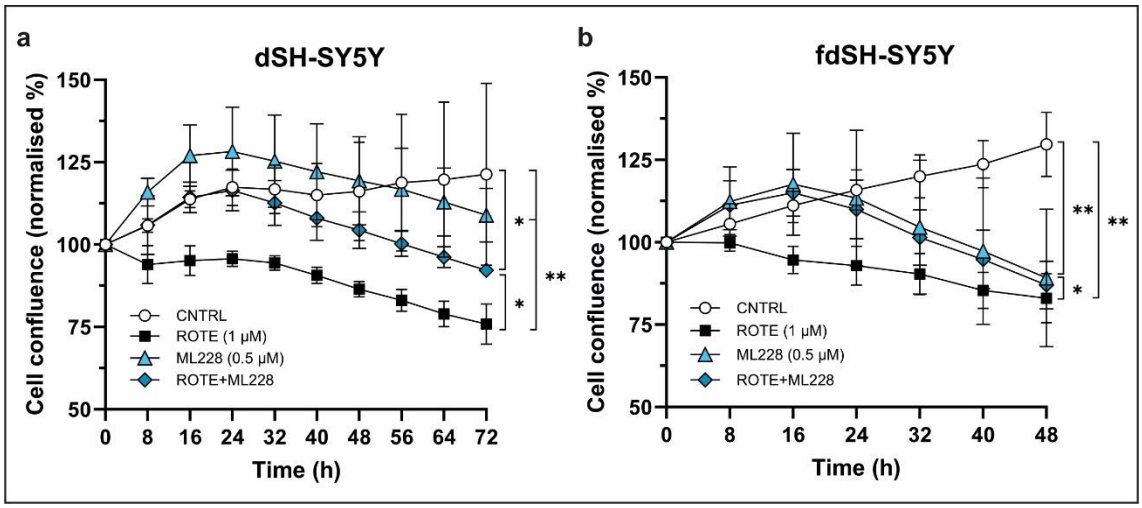

Figure 5.16. The protective effect of ML228 against rotenone is preserved in differentiated SH-SY5Y cells. a. Plot displaying the quantification of phase cell confluence of SH-SY5Y cells treated with 1 µM Rotenone and 0.5 µM ML228 separately or combined during 72h acquired with the Incucyte S3 live cell analysis system (n=4). **b.** Plot displaying the quantification of phase cell confluence of SH-SY5Y cells treated with 1 µM Rotenone and 0.5 µM ML228 separately or combined during 72h acquired with the Incucyte S3 live cell analysis system (n=4). Statistical analysis was performed using a two-way ANOVA followed with Tukey's post-hoc test where $p<0.05$ was recorded as "*".

To confirm that HIF-1α is involved in the protective effect of ML228 against rotenone, we evaluated the performance of ML228 in conjunction with a HIF-1α inhibitor, which blocks HIF-1α accumulation and consequent changes in gene expression (Fig. 5.17a). Different concentrations were evaluated and 5 and 10 µM were selected as they induced a potent reduction of HIF-1α levels (Fig. 5.17b). Analysis of cell confluence during 72h shows that the HIF-1α inhibitor alone did not alter cell number or affect the growth curves of cells treated with rotenone or ML228 (Fig. 5.17c, e). However, when added to the cells treated with both rotenone and ML228, it attenuates the increase of cell confluence elicited by ML228 in the presence of rotenone (Fig. 5.17c, e). Close-up study of three representative timepoints demonstrates that the efficacy of ML228 in protecting against the drop in cell number caused by rotenone is significantly diminished by the HIF-1α inhibitor for three representative timepoints and two different inhibitor concentrations (Fig. 5.17d, f). However, the effect of ML228 is not completely abolished by the use of the HIF-1α inhibitor (Fig. 5.17d, f). These results provide evidence that the stabilisation of HIF-1α by ML228 is at least partially responsible for the protective effect of ML228 against rotenone.

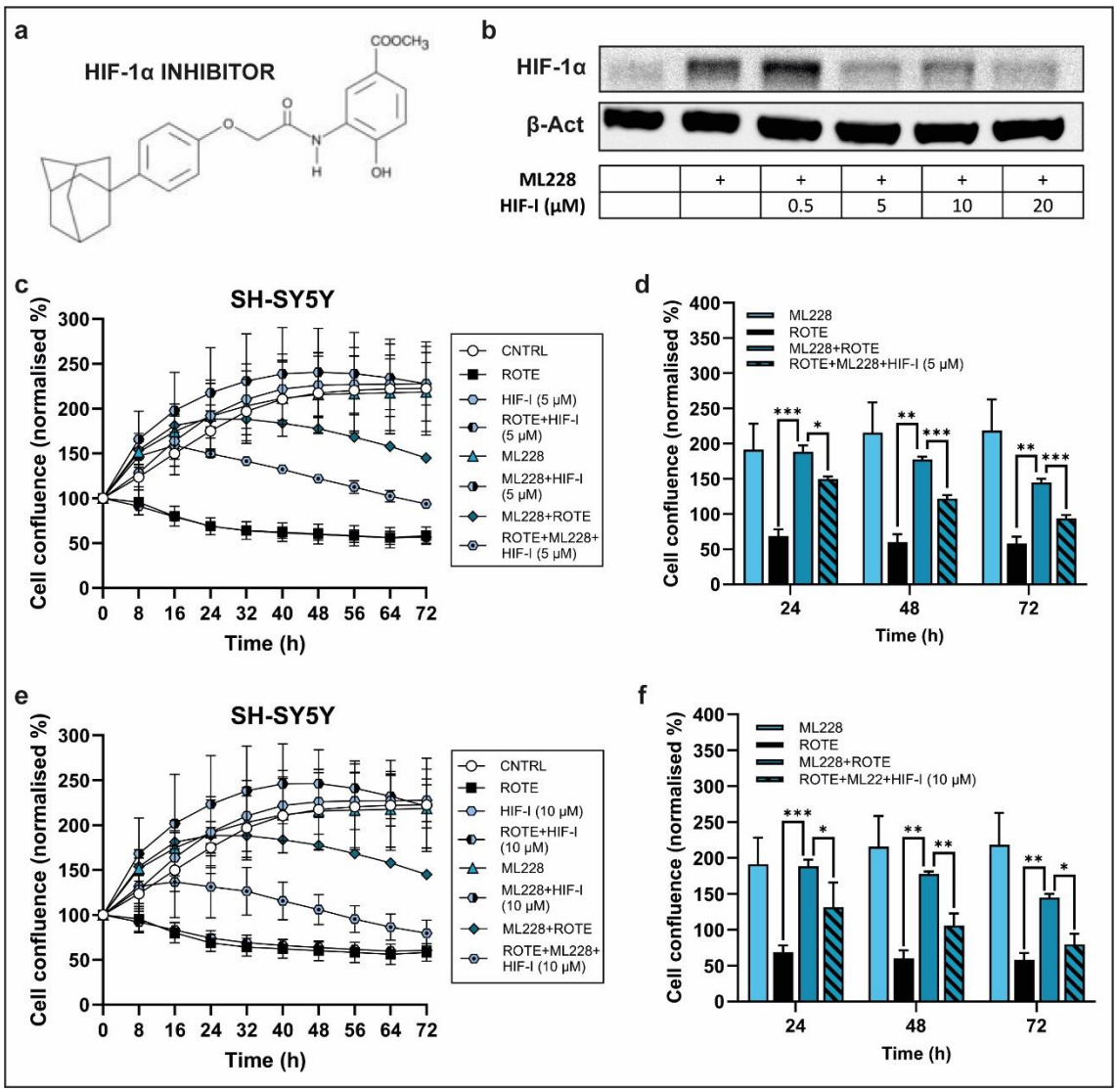

Figure 5.17. Blocking HIF-1α signalling diminishes the ability of ML228 to counteract rotenone toxicity. a. Illustration depicting the chemical structure of the HIF-1α inhibitor sc-205346. **b.** Representative Western Blot image showing HIF-1α (~120 kDa) and β-Actin (~45 kDa, loading control) proteins in lysates from SH-SY5Y cells treated with different HIF-1α inhibitor concentrations in the presence of 0.5 μM ML228 for 24h (n=2). **c.** Plot displaying the quantification of phase cell confluence of SH-SY5Y cells treated with 1 μM Rotenone and 0.5 μM ML228 separately or combined in the presence or absence of 5 μM HIF-1α inhibitor during 72h acquired with the Incucyte S3 live cell analysis system (n=4). **d.** Plot summarising quantification of phase cell confluence at representative timepoints of the c. graph (n=4). **e.** Plot displaying the quantification of phase cell confluence of SH-SY5Y cells treated with 1 μM Rotenone and 0.5 μM ML228 separately or combined in the presence or absence of 10 μM HIF-1α inhibitor during 72h acquired with the Incucyte S3 live cell analysis system (n=4). **f.** Plot summarising quantification of phase cell confluence at representative timepoints of the e. graph (n=4). Statistical analysis was performed using a two-way ANOVA followed with Tukey's post-hoc test where $p<0.05$ was recorded as "*". Statistical significance was excluded from the c and e graphs for

5.3.3.3. ML228 attenuates rotenone-induced apoptosis

As the findings of this study suggest that ML228 can improve cell confluence, morphology and metabolic activity in rotenone-treated SH-SY5Y cells, it was decided to investigate whether this was related to changes in apoptosis. Rotenone treatment increases the levels of cleaved Caspase-3, which is significantly reduced by cotreatment with

ML228 (Fig. 5.18a). Similarly, analysis of Caspase-3/7 activation with a fluorescent dye over 72h shows widespread activation in the presence of rotenone. Remarkably, addition of ML228 to rotenone-treated cells significantly blunts Caspase-3/7 activation since this process is triggered by rotenone at 24h (Fig. 5.18b, c). While rotenone treatment amounts to a 40% of cells presenting activation of Caspase-3/7 at 72h, only 10% of cells cotreated with ML228 are positive for Caspase-3/7 activation (Fig. 5.18b). These numbers are very similar to the results obtained previously on cell confluence and cell metabolism assays, where rotenone caused a reduction of these parameters to about a 50% while cotreatment with ML228 partially mitigated this decrease, improving these factors in 25%.

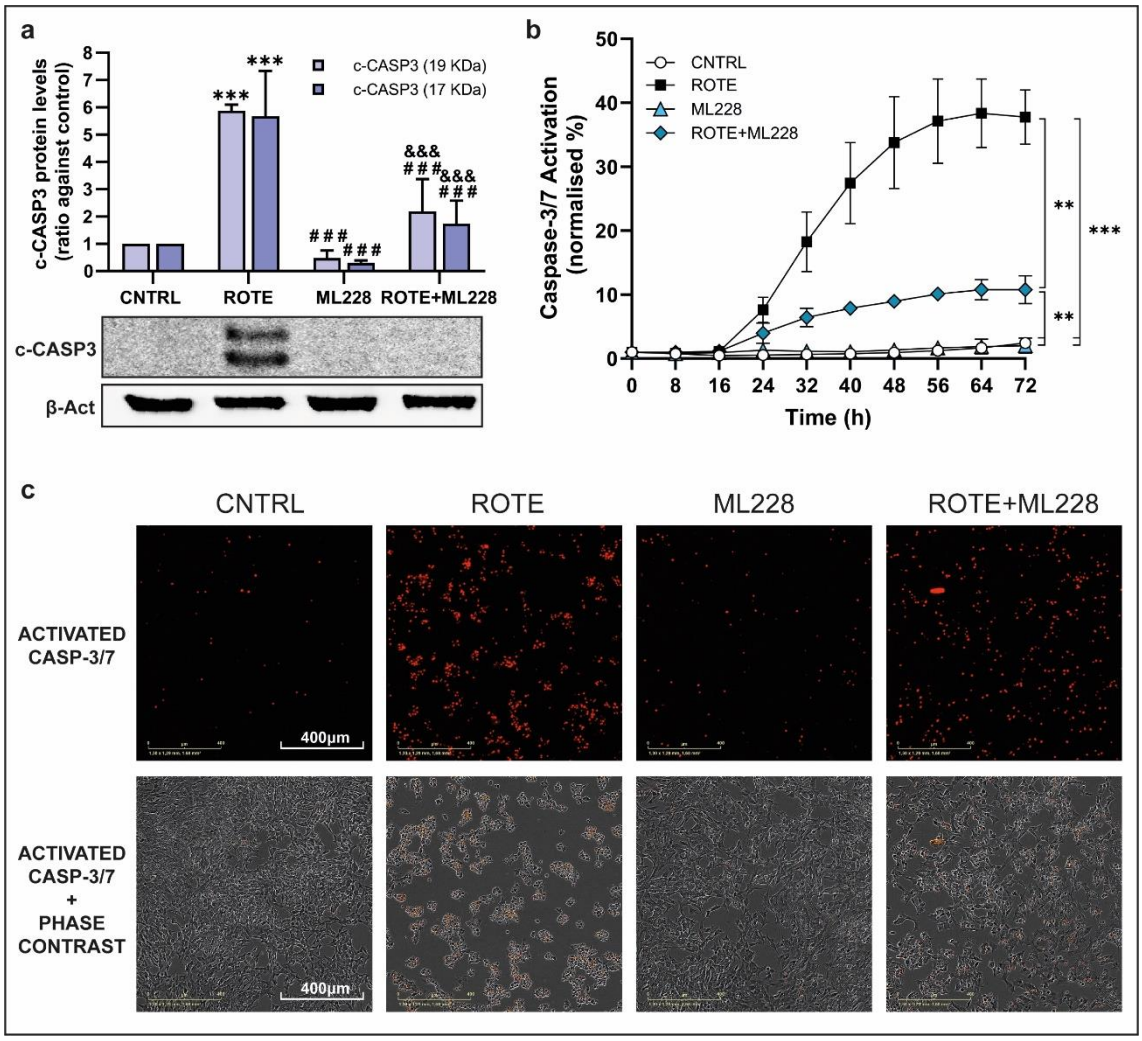

Figure 5.18. ML228 reduces Caspase-3/7 activation triggered by rotenone in SH-SY5Y cells. a. Representative Western Blot image showing cleaved Caspase-3 (~17,19 kDa) and β-Actin (~45 kDa, loading control) proteins in lysates from SH-SY5Y cells treated with 1 μM Rotenone and 0.5 μM ML228 separately or combined for 24 hours accompanied by densitometric analysis (n=3). **b.** Plot displaying the quantification of Incucyte Caspase-3/7 Red Dye fluorescence normalized to phase cell confluence of SH-SY5Y cells treated with 1 μM Rotenone and 0.5 μM ML228 separately or combined during 72h acquired with the Incucyte S3 live cell analysis system (n=4). **c.** Representative microscopy images acquired with the Incucyte S3 system showing SH-SY5Y cells treated with 1 μM Rotenone and 0.5 μM ML228 separately or combined for 24h in the presence of the Incucyte Caspase-3/7 Red Dye. Scale bar indicates 400 μm. Statistical analysis for graph a was performed using a one-way ANOVA followed with Dunnett's post-hoc where $p<0.05$ was recorded as "*" with respect to control, "#" with respect to rotenone and "&" when comparing to ML228. Statistical analysis for graph b was performed using a two-way ANOVA followed with Tukey's post-hoc test where $p<0.05$ was recorded as "*".

As Caspase-3/7 activation is the final stage of apoptosis, we investigated upstream apoptosis markers to identify the step at which ML228 is intervening. The release of Cytochrome c from the mitochondria, a turning point in apoptosis, was increased in the presence of rotenone, while cotreatment with ML228 significantly increases Cytochrome c levels in mitochondria (Fig. 5.19a). This suggests that ML228 might be acting via the pathways that control the initiation of apoptosis, such as the MAPKs. A prominent MAPK that has been linked to inducing cell survival and downregulating apoptosis is ERK1/2, which is activated by phosphorylation of threonine and tyrosine residues within its regulatory site (Lu, 2006). Interestingly, phosphorylation of ERK1/2 at the Thr183 and Tyr185 residues in the activation loop is increased in the presence of ML228 (Fig. 5.19b), which might be linked to the protective effect of ML228 against rotenone-mediated apoptosis.

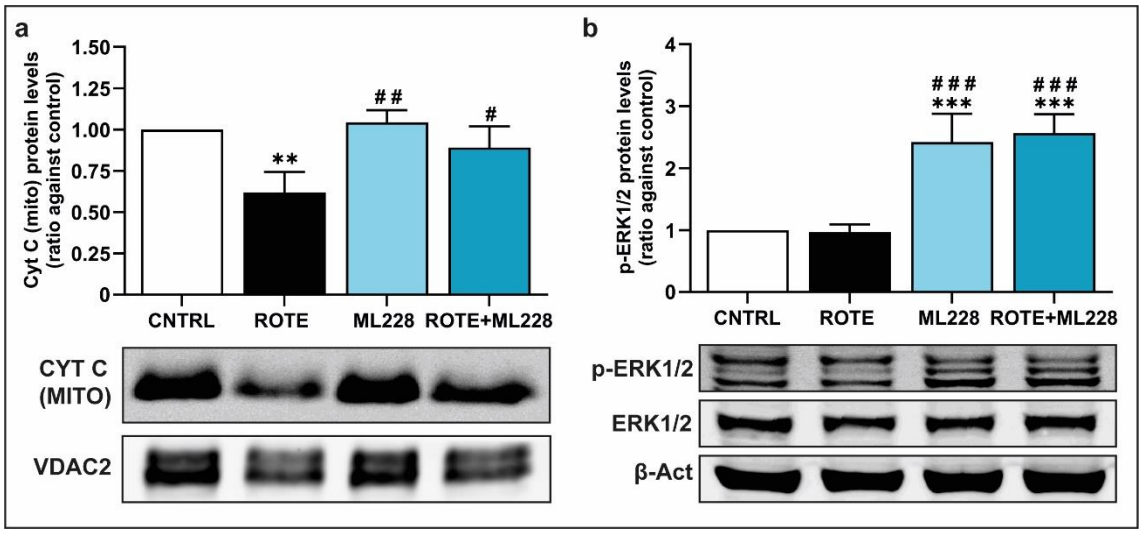

Figure 5.19. ML228 maintains mitochondrial cytochrome c levels and increases phosphorylation of ERK1/2. a. Representative Western Blot image showing cytochrome c (~14 kDa) and VDAC2 (~32 kDa, loading control for mitochondria) proteins in mitochondrial extracts from SH-SY5Y cells treated with 1 μM Rotenone and 0.5 μM ML228 separately or combined for 24h accompanied by densitometric analysis (n=3). **b.** Representative Western Blot image showing p-ERK1/2 (T183/Y185) (~42,44 kDa), ERK1/2 (~42,44 kDa) and β-Actin (~45 kDa, loading control) proteins in lysates from SH-SY5Y cells treated with treated with 1 μM Rotenone and 0.5 μM ML228 separately or combined for 24h accompanied by densitometric analysis (n=3). Statistical analysis was performed using a one-way ANOVA followed with Dunnett's post-hoc where $p<0.05$ was recorded as "*" with respect to control and "#" with respect to rotenone.

5.3.3.4. ML228 increases glycolytic metabolism and rescues rotenone-induced drop in mitochondrial membrane potential

Rotenone critically impacts mitochondria as a ETC complex I inhibitor. Thus, we assessed the effect of ML228 on several mitochondrial parameters in the presence of rotenone to evaluate whether the increase in cell survival observed is linked to an improvement in mitochondrial fitness. Indeed, we evaluated whether the alterations to cell viability are correlated with changes in energy production as ATP. As expected, ATP levels are significantly decreased in cells treated with ML228 or rotenone with respect to control (Fig. 5.20). Combination of these treatments causes a dramatic reduction on ATP content (Fig. 5.20). These findings suggest that the protective effect of ML228 is not related to an increase in ATP levels.

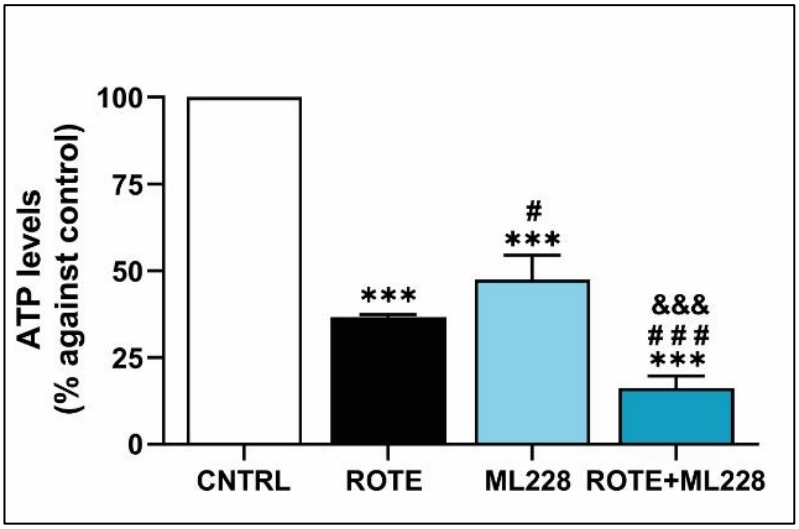

Figure 5.20. ML228 and rotenone reduce ATP levels. Graph displaying ATP content in lysates from SH-SY5Y cells treated with 1 μM Rotenone and 0.5 μM ML228 separately or combined for 24h (n=4). Statistical analysis was performed using a one-way ANOVA followed with Dunnett's post-hoc where $p<0.05$ was recorded as "*" with respect to control, "#" with respect to rotenone and "&" when comparing to ML228.

The contribution of glycolysis and OXPHOS to the protective effect of ML228 against rotenone was further investigated using oligomycin and 2-Deoxyglucose (2-DG), which blocks the glycolytic pathway. Analysis of cell confluence demonstrates that both oligomycin and 2-DG cause a decrease in cell number, with oligomycin impact being more pronounced (Fig. 5.21a). This correlates with the data obtained previously which shows that SH-SY5Y cells primarily obtain their energy from OXPHOS. These treatments also decrease cell confluence in cells treated with rotenone, ML228 or both, which is consistent with the preliminary findings showing residual OXPHOS and increased glycolysis in these cells (Fig. 5.21a). In absence of additional treatments, ML228 causes a substantial improvement on cell number in rotenone-treated cells. While this effect is maintained in the presence of oligomycin, addition of 2-DG significantly abrogates ML228-mediated increase in cell confluence (Fig. 5.21a). These findings imply that, although ML228 does not increase ATP levels, the maintenance of energy production via glycolysis is essential for ML228 to exert its protective effect against rotenone. Remarkably, ML228 also prevents the oligomycin-induced loss of cells. This suggests that ML228 may be able to protect cells from ETC blockade regardless of the underlying cause.

ETC disruption can cause loss of proton shuttling across the inner mitochondrial membrane resulting in mitochondrial membrane depolarisation. Indeed, treatment with rotenone significantly decreased mitochondrial membrane potential in SH-SY5Y cells (Fig. 5.21b). Although a similar proportion of cells positive for mitochondrial membrane depolarisation is observed when combining rotenone and ML228 treatments, a higher number of cells is maintained in a healthy mitochondrial membrane potential range (Fig. 5.21b, c). Thus, ML228 can partially reverse the impact of rotenone on mitochondrial membrane potential.

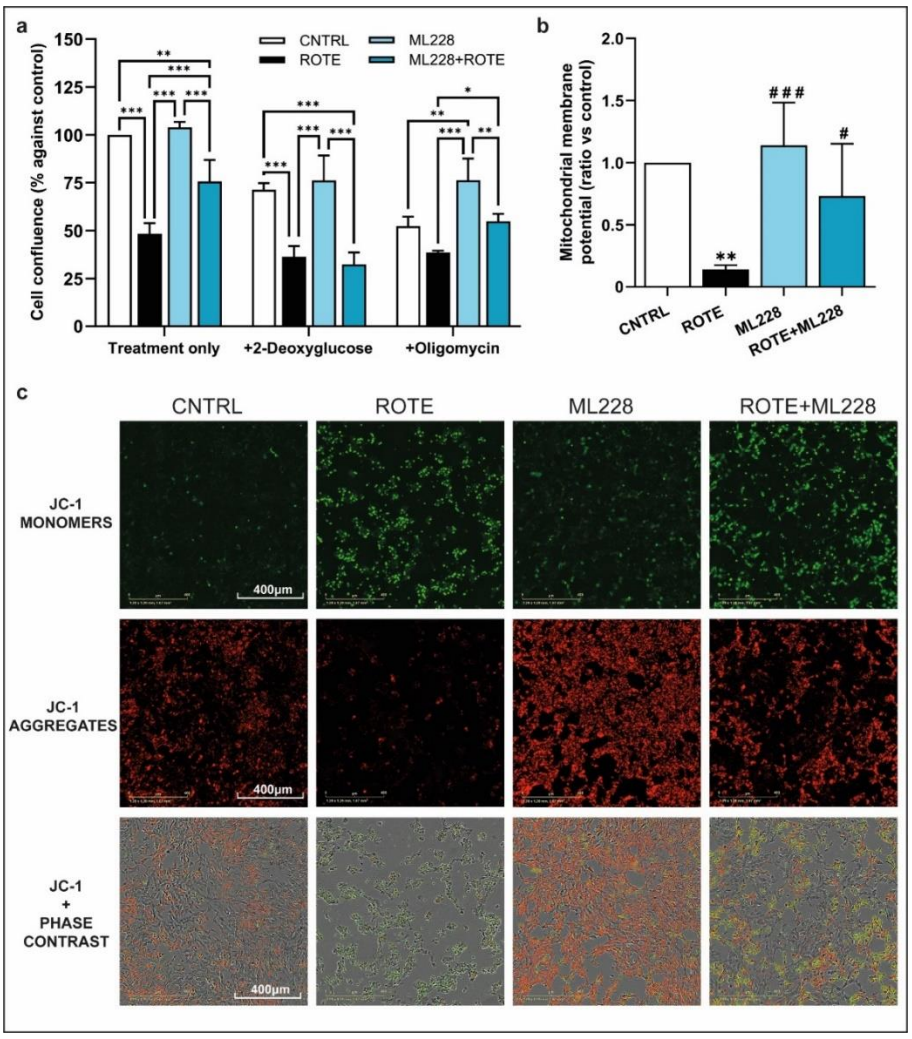

Figure 5.21. ML228 may protect cells against rotenone by maintaining glycolysis and mitochondrial membrane potential. a. Plot displaying the quantification of phase cell confluence of SH-SY5Y cells treated with 1 µM Rotenone and 0.5 µM ML228 separately or combined in the presence or absence of 5 µM oligomycin or 10 mM 2-DG for 24h acquired with the Incucyte S3 live cell analysis system (n=3). **b.** Graph displaying mitochondrial membrane potential measured as ratio of green monomers to red aggregates of the fluorescent probe JC-1 based on the images taken with the Incucyte S3 system of SH-SY5Y cells treated with 1 µM Rotenone and 0.5 µM ML228 separately or combined for 24h (n=4). **c.** Representative microscopy images acquired with the Incucyte S3 system showing fluorescence from the JC-1 probe in SH-SY5Y cells under shown treatments for 24h. Scale bar indicates 400 µm. Statistical analysis for graph a was performed using a two-way ANOVA followed with Tukey's post-hoc test where $p<0.05$ was recorded as "*". Statistical analysis for graph b was performed using a one-way ANOVA followed with Dunnett's post-hoc where $p<0.05$ was recorded as "*" with respect to control and "#" with respect to rotenone.

Disruptions in ATP production and mitochondrial membrane potential can be accompanied by structural alterations of the mitochondrial network. Consequently, we used fluorescent microscopy to examine mitochondrial morphology parameters in SH-SY5Y cells expressing mCherry-labelled mitochondria. Control cells show the typical extended filamentous mitochondrial network. Mitochondria in cells treated with ML228 present similar features to control cells (Fig. 5.22a, b). However, rotenone-treated cells

present a shattered and collapsed mitochondrial network, with few mitochondria that present a round shape, although cotreatment with ML228 appears to increase mitochondrial density (Fig. 5.22a, b). These changes are reflected in the analysis of morphological parameters. Indeed, the area and perimeter occupied by mitochondria are significantly reduced in rotenone-treated cells, but ML228 is able to reverse this effect, increasing both parameters (Fig. 5.22c, d). Similarly, rotenone treatment significantly reduces aspect ratio, a measure of mitochondrial elongation, but cotreatment with ML228 attenuates this effect (Fig. 5.22e). No changes are observed between treatments when analysing mitochondrial circularity (Fig. 5.22f), which might be due to the reduced number of mitochondria in rotenone-treated cells. Since this measure is not normalized to mitochondrial number and rounded mitochondria are still present in healthy cells, the total number of round-shaped mitochondria can be the same. These results provide evidence that ML228 can reverse rotenone-induced alterations in mitochondrial density and elongation.

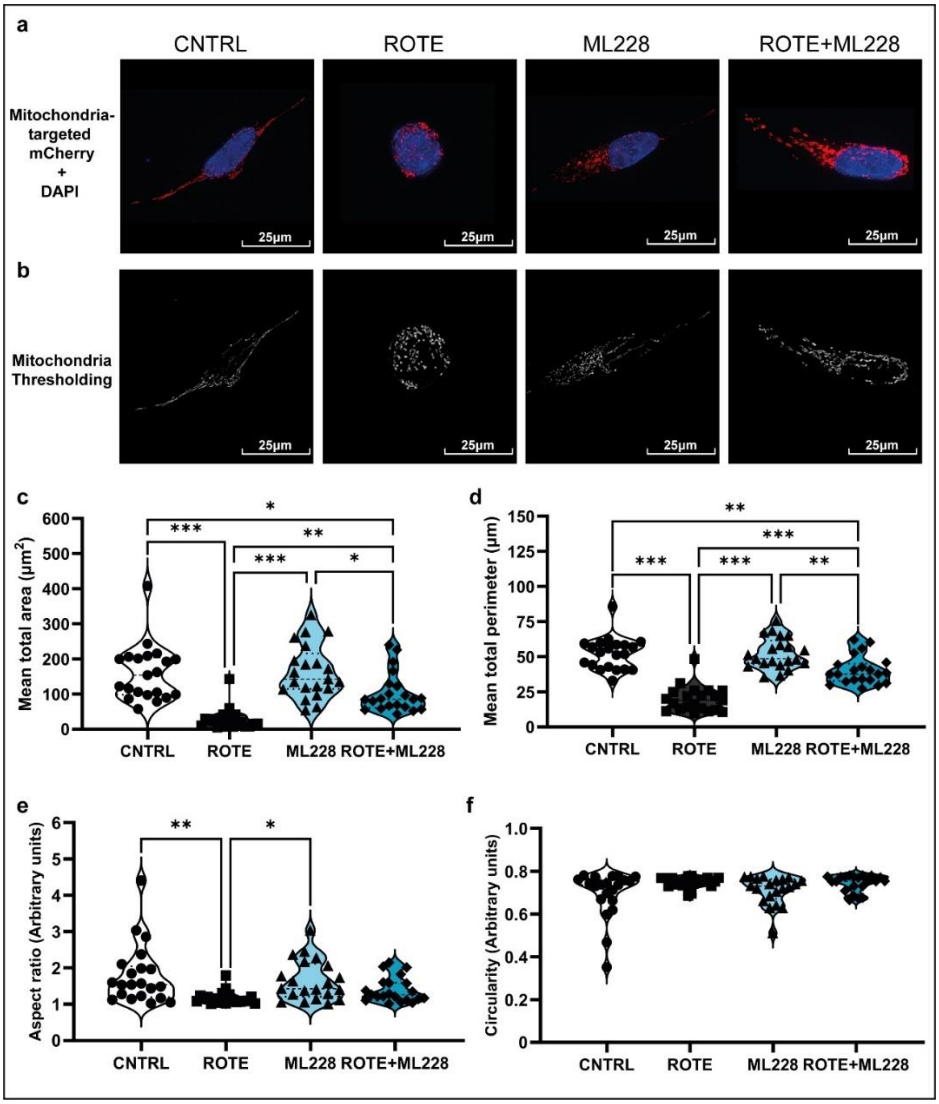

Figure 5.22. ML228 can rescue rotenone-induced mitochondrial loss and fragmentation. a. Representative microscopy images acquired with the Leica Thunder Live Cell microscope (100X objective) of SH-SY5Y cells with mCherry-labeled mitochondria and DAPI staining treated with 1 μM Rotenone and 0.5 μM ML228 separately or combined for 24h. Scale bar indicates 25 μm. **b.** Images showing the objects identified by application of image thresholding to microscopy images from a. **c, d, e, f.** Quantitative morphological analysis of mitochondria in each of the treatment categories (n=3, 7 images analysed from each independent repeat for a total of 21) for mean total area **(c)** mean total perimeter **(d),** aspect ratio **(e)** and circularity **(f).** Statistical analysis was performed using a one-way ANOVA followed with Dunnett's post-hoc where $p<0.05$ was recorded as "*".

Mitochondrial network homeostasis is orchestrated by a complex interplay of proteins. Thus, disruptions in mitochondrial dynamics can be mirrored by changes in the levels of certain proteins. However, the levels of Mitofusins-1 and -2, which control mitochondrial fusion, remain unaltered (Fig. 5.23a, b). Interestingly, a reduction in S-OPA1, but not L-OPA1, was detected in both rotenone and ML228-treated cells (Fig. 5.23c) Given the reduced number of mitochondria in rotenone-treated cells observed in the previous study, we hypothesized that mitophagy may be involved. Recruitment of Parkin to the mitochondria, which can indicate increased mitophagy, is not modified by the treatments (Fig. 5.23d). These findings indicate that the regulation of mitochondrial dynamics by ML228 does not require changes in the levels of these specific proteins.

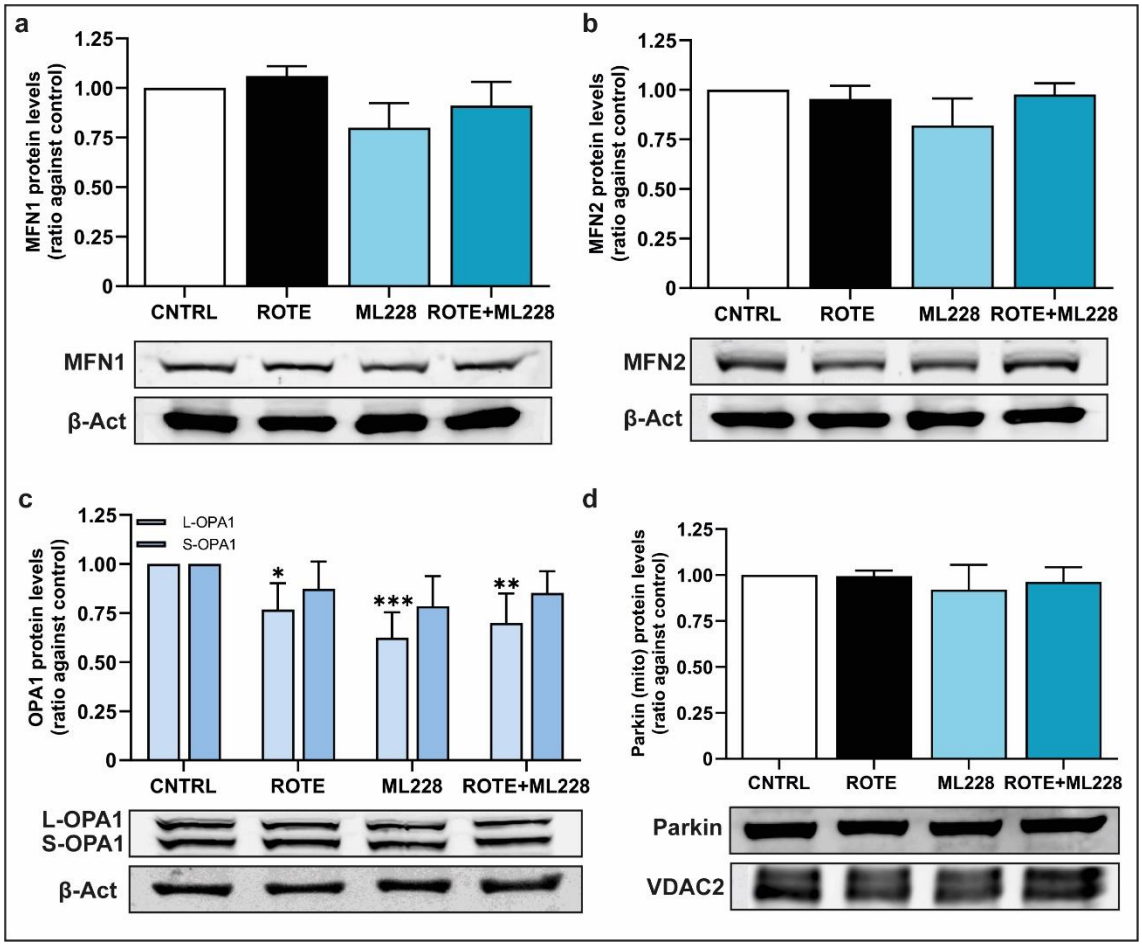

Figure 5.23. Rotenone and ML228 decrease the levels of S-OPA1 while having no effect on MFN1/2 or mitochondrial Parkin abundance. a. Representative Western Blot image showing MFN1 (~82 kDa) and β-Actin (~45 kDa, loading control) proteins in lysates from SH-SY5Y cells treated with 1 μM Rotenone and 0.5 μM ML228 separately or combined for 24h accompanied by densitometric analysis (n=3). **b.** Representative Western Blot image showing MFN2 (~80 kDa) and β-Actin (~45 kDa, loading control) proteins in lysates from SH-SY5Y cells treated as previously stated accompanied by densitometric analysis (n=3). **c.** Representative Western Blot image showing OPA1 (~80,100 kDa) and β-Actin (~45 kDa, loading control) proteins in lysates from SH-SY5Y cells treated as previously stated accompanied by densitometric analysis (n=3). **d.** Representative Western Blot image showing Parkin (~50 kDa) and VDAC2 (~32 kDa, loading control for mitochondria) proteins in mitochondrial extracts from SH-SY5Y cells treated as previously stated accompanied by densitometric analysis (n=3). Statistical analysis was performed using a one-way ANOVA followed with Dunnett's post-hoc where $p<0.05$ was recorded as "*" with respect to control.

5.3.3.5. ML228 mitigates ROS increase triggered by rotenone

Disruption of ETC, mitochondrial membrane potential and mitochondrial dynamics can lead to changes in ROS production. Investigation of ROS production in SH-SY5Y cells treated with rotenone shows a significant marked increase in ROS (Fig. 5.24a, b). ML228 prevents rotenone-mediated ROS elevation, maintaining ROS production close to control levels (Fig. 5.24a, b). The ability of ML228 to reduce oxidative stress caused by rotenone might be linked to its role in preventing rotenone cellular damage.

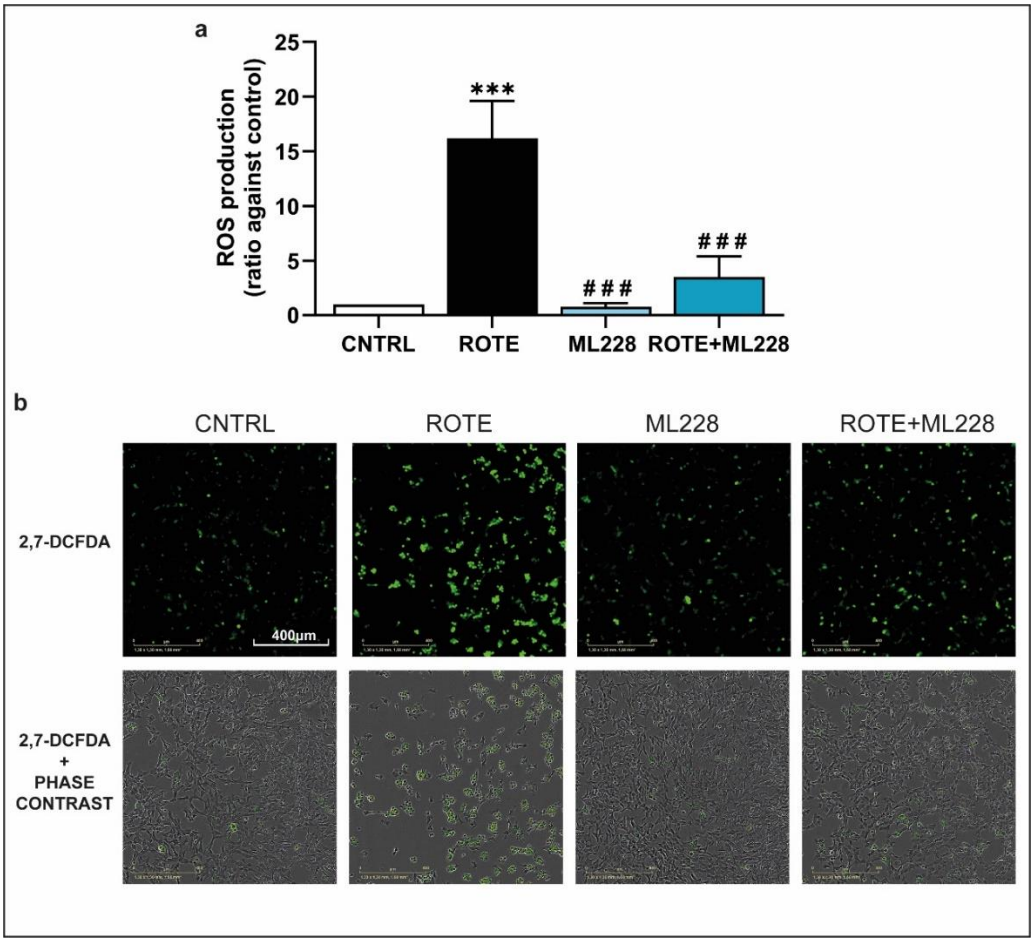

Figure 5.24. ML228 attenuates rotenone-induced ROS overproduction. a. Plot showing the quantification of 2,7-DCDFA green fluorescence area/phase confluence area percentage based on the images taken with the Incucyte S3 system of SH-SY5Y cells treated with 1 μM Rotenone and 0.5 μM ML228 separately or combined for 24h (n=4). **b.** Representative microscopy images acquired with the Incucyte S3 system showing ROS production as green fluorescence detected by the 2,7-DCDFA probe and phase confluence of SH-SY5Y cells under shown treatments for 24h. Scale bar indicates 400 μm. Statistical analysis was performed using a one-way ANOVA followed with Dunnett's post-hoc where $p<0.05$ was recorded as "*" with respect to control and "#" when comparing to rotenone.

5.3.3.6. ML228 preserves autophagy in the presence of rotenone

Having analysed mitochondrial function and oxidative stress, we turned our attention to the other factor that is believed to be involved in PD pathogenesis, protein degradation. The levels of autophagy marker LC3-II are slightly reduced by rotenone treatment while being significantly increased in cells treated with ML228 (Fig. 5.25a). Total LC3 levels were investigated during 72h in SH-SY5Y cells expressing GFP-labelled LC3. GFP-LC3 levels remain constant for the first 24h but show a significant decrease in rotenone-treated cells and a substantial increase in ML228-treated cells (Fig. 5.25b, c). Combination of rotenone and ML228 returns GFP-LC3B levels to control (Fig. 5.25b, c). Together, detection of increased LC3B-II at 24h and elevation of total LC3B from 24h onwards point to an increase in autophagy induced by ML228. These results suggest that rotenone-mediated suppression of autophagy can be rescued by ML228, which can contribute to the beneficial effect of ML228 against rotenone.

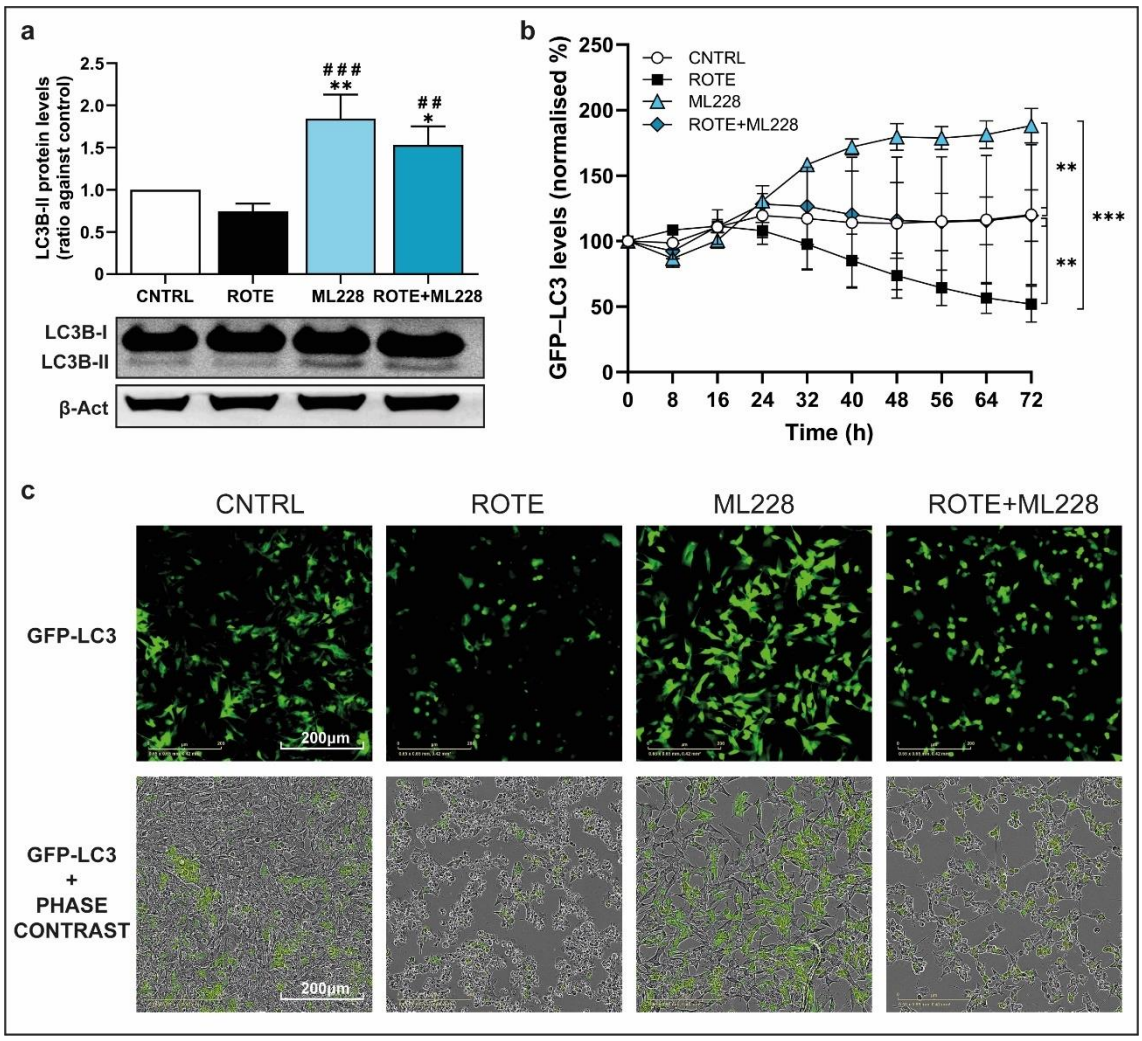

Figure 5.25. ML228 counteracts rotenone-mediated reduction of autophagy. a. Representative Western Blot image showing LC3B (~14,16 kDa) and β-Actin (~45 kDa, loading control) proteins in lysates from SH-SY5Y cells treated with 1 µM Rotenone and 0.5 µM ML228 separately or combined for 24h (n=3). **b.** Graph displaying LC3-GFP protein levels over 72h measured as percentage of green fluorescence to phase confluence based on the images taken with the Incucyte S3 system of SH-SY5Y cells treated with cells treated as previously stated (n=4). **c.** Representative microscopy images acquired with the Incucyte S3 system (20X objective) showing fluorescence from LC3-GFP protein in SH-SY5Y cells treated as previously stated for 72h. Scale bar indicates 200 µm. Statistical analysis for graph a was performed using a one-way ANOVA followed with Dunnett's post-hoc where $p<0.05$ was recorded as "*" with respect to control and "#" with respect to rotenone. Statistical analysis for graph b was performed using a two-way ANOVA followed with Tukey's post-hoc test where $p<0.05$ was recorded as "*".

5.3.3.7. ML228 restores cell cycle homeostasis in rotenone-treated cells

To explore the potential involvement of other pathways in the mechanism of action of ML228, we utilised a proteome array to profile the levels of a variety of proteins. The previously reported changes in HIF-1α and Cleaved-Caspase 3 abundance can be observed in this study as well (Fig. 5.26a, b). No drastic alterations in apoptosis-related proteins are observed in the presence of rotenone, although a discrete reduction on antiapoptotic c-IAP1/2 can be detected, which is corrected by cotreatment with ML228 (Fig. 5.26a, b). Interestingly, we noticed that several proteins involved in the control of

cell cycle progression, including p21, p27 and phosphorylated p53, were increased upon combined ML228 and rotenone treatment (Fig. 5.26a, b).

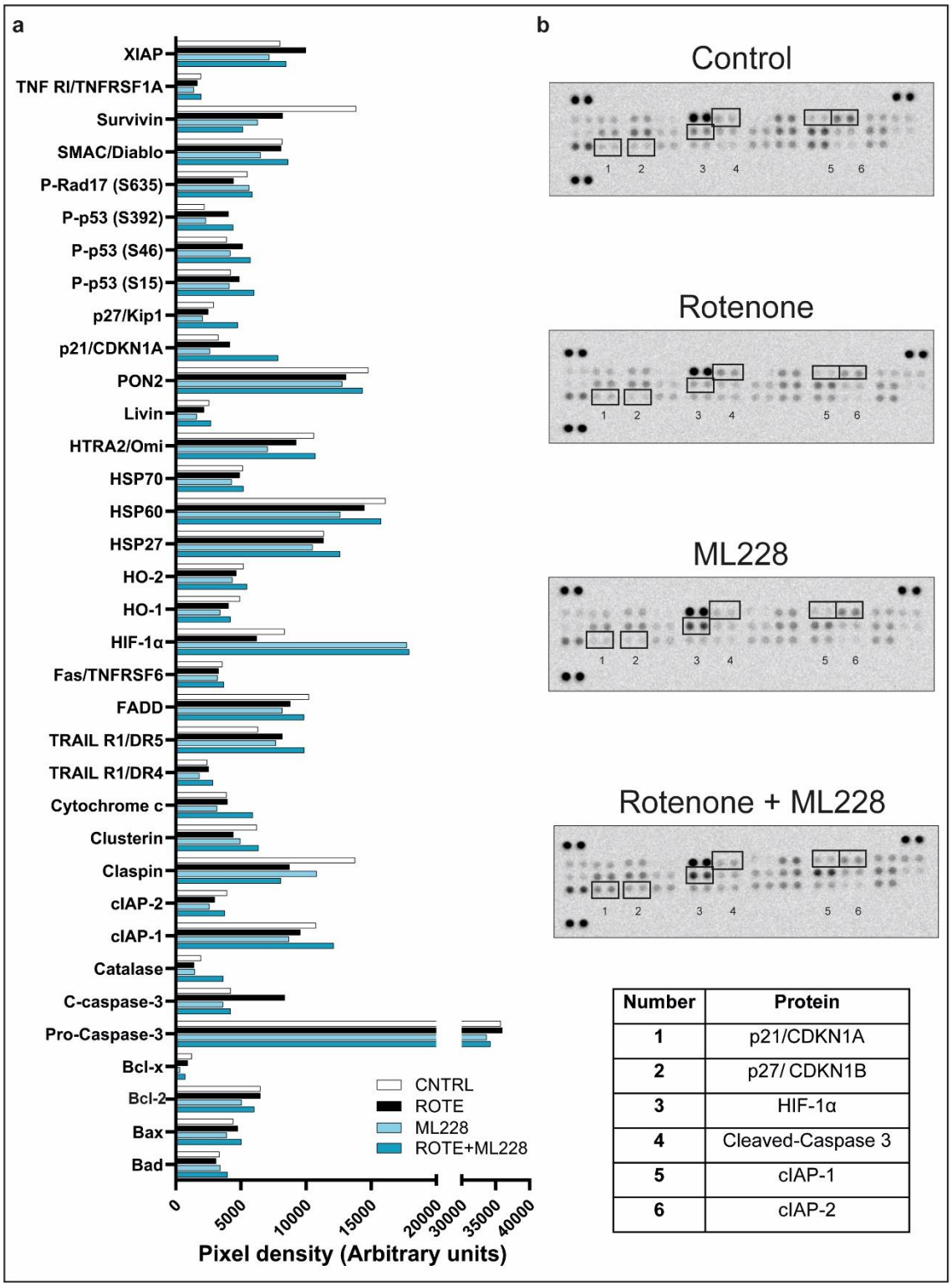

Number	Protein
1	p21/CDKN1A
2	p27/ CDKN1B
3	HIF-1α
4	Cleaved-Caspase 3
5	cIAP-1
6	cIAP-2

Figure 5.26. ML228 modulates the levels of cell cycle regulatory proteins. a. Plot summarising densitometric analysis of the Proteome Profiler Human Apoptosis Array of lysates from SH-SY5Y cells treated with 1 µM Rotenone and 0.5 µM ML228 separately or combined for 24h (n=1). **b.** Proteome Profiler Human Apoptosis Array membrane images for all groups analysed accompanied by a table highlighting the location of proteins of interest.

To confirm the results obtained with the proteome array, we investigated the levels of cell cycle regulatory proteins p21 and p27. p21 blocks the activity of the cyclin-CDK1, -CDK2 and -CDK4/6 complexes, which control progression through the G1, S and G2/M phases of the cell cycle and p27 mainly targets cyclin-CDK2 complexes, blocking G1/S transition (Amani, 2021). In SH-SY5Y cells, p21 levels are significantly elevated by both rotenone and ML228 treatments, while p27 is only increased in cells exposed to ML228 (Fig. 5.27a, b). These changes in protein levels can directly alter the distribution of cells across the different phases of the cell cycle. Indeed, rotenone treatment increased the cells in early apoptosis, while drastically reducing the cells in G1 phase and increasing the percentage of cells going through S phase (Fig. 5.27c, d). ML228-treated cells, as expected due to the upregulation of p27 levels, shows a significant accumulation of cells in the G1 phase, and reduced flow of cells through the S and G2/M phases (Fig. 5.27c, d). Combination of both treatments restores the proportion of cells in the G1 and G2/M phases to baseline levels, although a modest increase in the percentage of cells going through S phase is still present (Fig. 5.27c, d). In accordance with our previous results, ML228 significantly mitigates rotenone-induced apoptosis, as demonstrated by the reduced number of cells in the early apoptotic phase upon cotreatment (Fig. 5.27c, d). The alterations in cell cycle induced by ML228 may play a role in its ability to protect against rotenone toxicity.

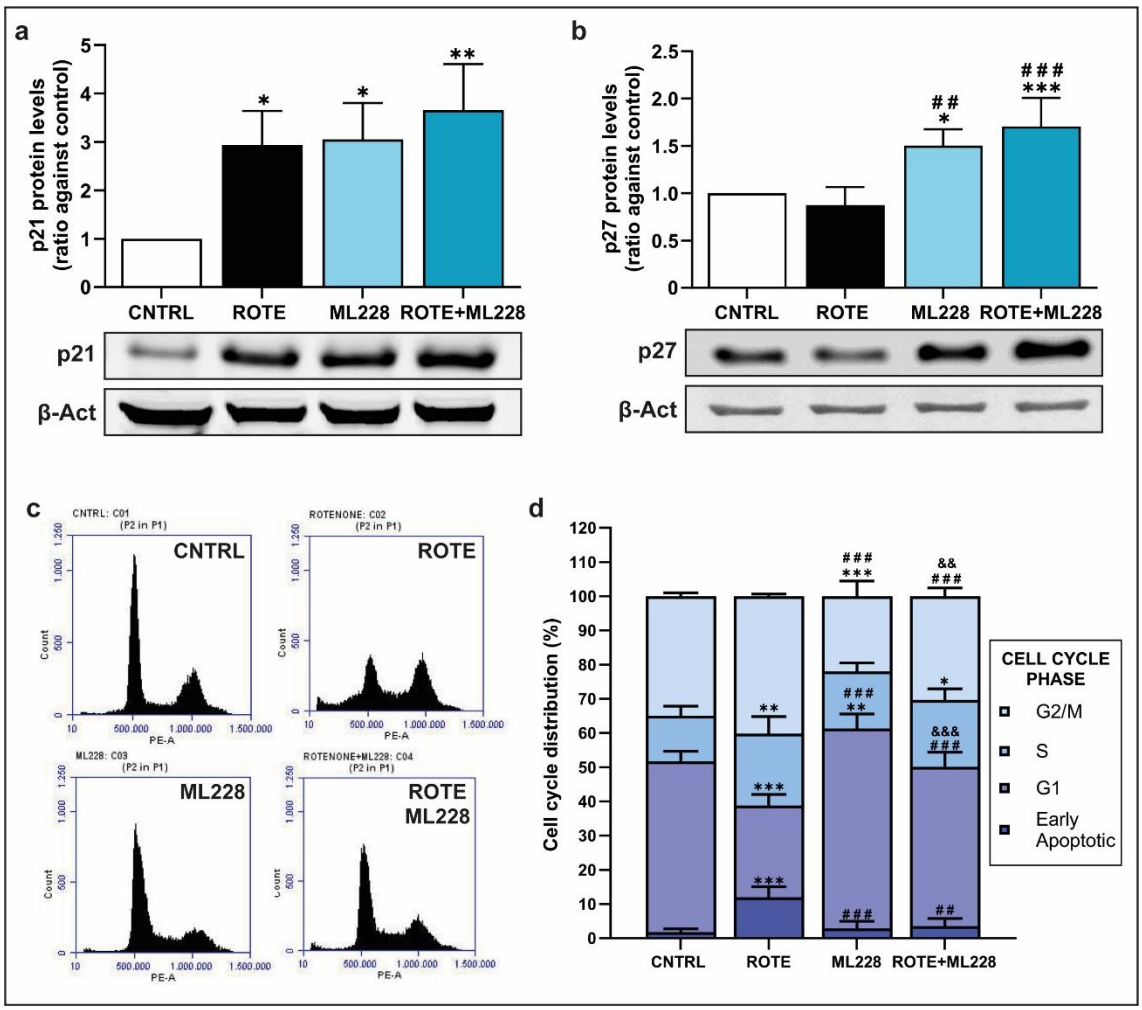

Figure 5.27. ML228 upregulates p21 and p27 levels and normalises cell cycle progression in rotenone-treated cells. a. Representative Western Blot image showing p27 (~27 kDa) and β-Actin (~45 kDa, loading control) proteins in lysates from SH-SY5Y cells treated with 1 µM Rotenone and 0.5 µM ML228 separately or combined for 24h accompanied by densitometric analysis (n=3). **b.** Representative Western Blot image showing p21 (~21 kDa) and β-Actin (~45 kDa, loading control) proteins in lysates from SH-SY5Y cells treated as previously stated accompanied by densitometric analysis (n=3). **c.** Flow cytometry histogram displaying distribution of cells in different phases of the cell cycle in SH-SY5Y cells samples treated as previously stated. **d.** Plot showing flow cytometry data after gating for different phases of the cell cycle (n=4). Statistical analysis for graph a and b was performed using a one-way ANOVA followed with Dunnett's post-hoc where $p<0.05$ was recorded as "*" with respect to control and "#" with respect to rotenone. Statistical analysis for graph d was performed using a two-way ANOVA followed with Tukey's post-hoc test where $p<0.05$ was recorded as "*" with respect to control, "#" with respect to rotenone and "&" when comparing to ML228.

5.3.3.8. Transcriptomic analysis reveals that ML228 blocks the rotenone-induced intracellular Ca^{2+} surge

To gain a better understanding of the pathways involved in the protective effect of ML228 against rotenone toxicity, we compared transcriptomes from fdSH-SY5Y cells treated with rotenone and ML228 alone or combined obtained using a Nanostring nCounter Neuropathology panel. This section will focus on the transcriptomic differences between

rotenone-treated samples and samples treated with rotenone and ML228, as the ML228 transcriptome will be analysed in depth in the following chapter.

Rotenone exclusively deregulates 18 genes, while the remaining genes overlap with the ML228 transcriptomes (Fig. 5.28a). Firstly, we investigated the mRNA levels of this group of genes to evaluate noteworthy changes. These include genes that encode proteins with functions in the ubiquitin–proteasome system (*CUL3*, *VCP*), regulation of gene expression (*MTA1*, *FMR1*, *BRMS1L*) and oxidative stress response (*NFE2L2*, *NME5*) (Fig. 5.28b). Interestingly, reduced levels of pro-apoptotic Bid are also observed (Fig. 5.28b). Then, we examined the expression of genes that overlap between rotenone-treated cells and cells treated with rotenone and ML228. Of note, the expression of multiple members of the extrinsic apoptotic pathway, including *TNSFR10A*, *FAS*, *TNSFR12A* and *TNSFR10A* is increased by rotenone and further elevated in samples treated with the combination treatment (Fig. 5.28c). Genes involved in the ER stress response, such as *DDIT3* and *ATF4*, are also increased in rotenone-treated cells while cotreatment with ML228 slightly downregulates their expression (Fig. 5.28c). Out of all the genes analysed, only five were found to be differentially expressed between the two treatment groups (*ATP6V0E1*, *NSF*, *UNC13A*, *FAM126A* and *PGAM1*) (Fig. 5.28c). The previously mentioned genes are downregulated by rotenone, but their expression is significantly rescued after treatment with ML228. Conversely, ML228 cotreatment reverses the rotenone-induced upregulation of *PRKCA*, which participates in multiple cellular processes (Fig. 5.28c). These findings suggest that, in fdSH-SY5Y cells, rotenone induces the extrinsic apoptotic pathway, possibly via activation of the ER stress response, which is moderately attenuated by ML228 cotreatment. Comparing the transcriptomes of the two treatment groups revealed that ML228 restores the expression of genes involved in vesicular transport, myelination, and glycolysis, which may underlie its protective effect against rotenone-induced damage.

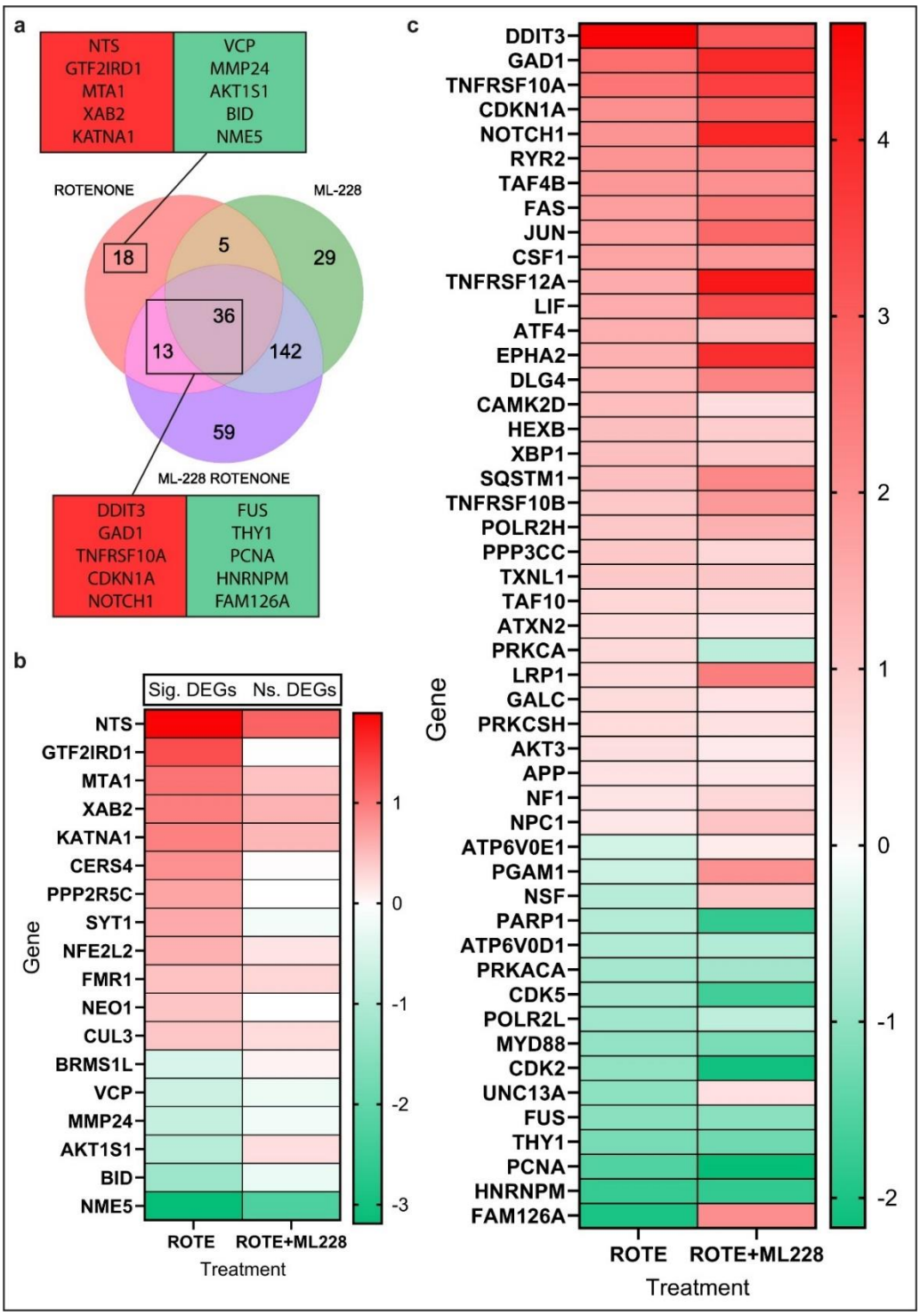

Figure 5.28. Treatment with ML228 modifies the expression of a set of differentially expressed genes (DEGs) induced by rotenone in fdSH-SY5Y. a. Venn Diagram showing the overlap between DEGs in fdSH-SY5Y cells treated with 1 μM Rotenone and 0.5 μM ML228 separately or combined for 24h. **b.** The heatmap shows the fold change in the expression of genes compared to control in the stated treatment groups. The DEGs shown correspond to significant genes present only in the rotenone group and their expression in the combined treatment group. **c.** The heatmap shows the fold change in the expression of genes compared to control in the stated treatment groups. The DEGs shown correspond to significant genes present in both the rotenone and the combined treatment groups.

We noticed that multiple genes involved in Ca^{2+} signalling were deregulated in this study, including several involved in controlling Ca^{2+} entry through membrane channels

(*CACNB2*, *CACNA1D*) and intracellular Ca^{2+} buffering (*S100B*, *CALB1*) (Fig. 5.29a). As Ca^{2+} has been linked to rotenone-mediated apoptosis, we aimed to determine whether the genetic changes induced by ML228 affected Ca^{2+} levels in SH-SY5Y cells. Consistent with expectations, rotenone treatment elevated intracellular Ca^{2+} levels (Fig. 5.29b, c). ML228 alone did not affect Ca^{2+} levels, but it prevented the rotenone-induced increase in intracellular Ca^{2+} (Fig. 5.29b, c). In conclusion, ML228-mediated reduction in Ca^{2+} levels through the modification of genes involved in Ca^{2+} trafficking could be a mechanism by which ML228 inhibits apoptosis in rotenone-treated SH-SY5Y cells.

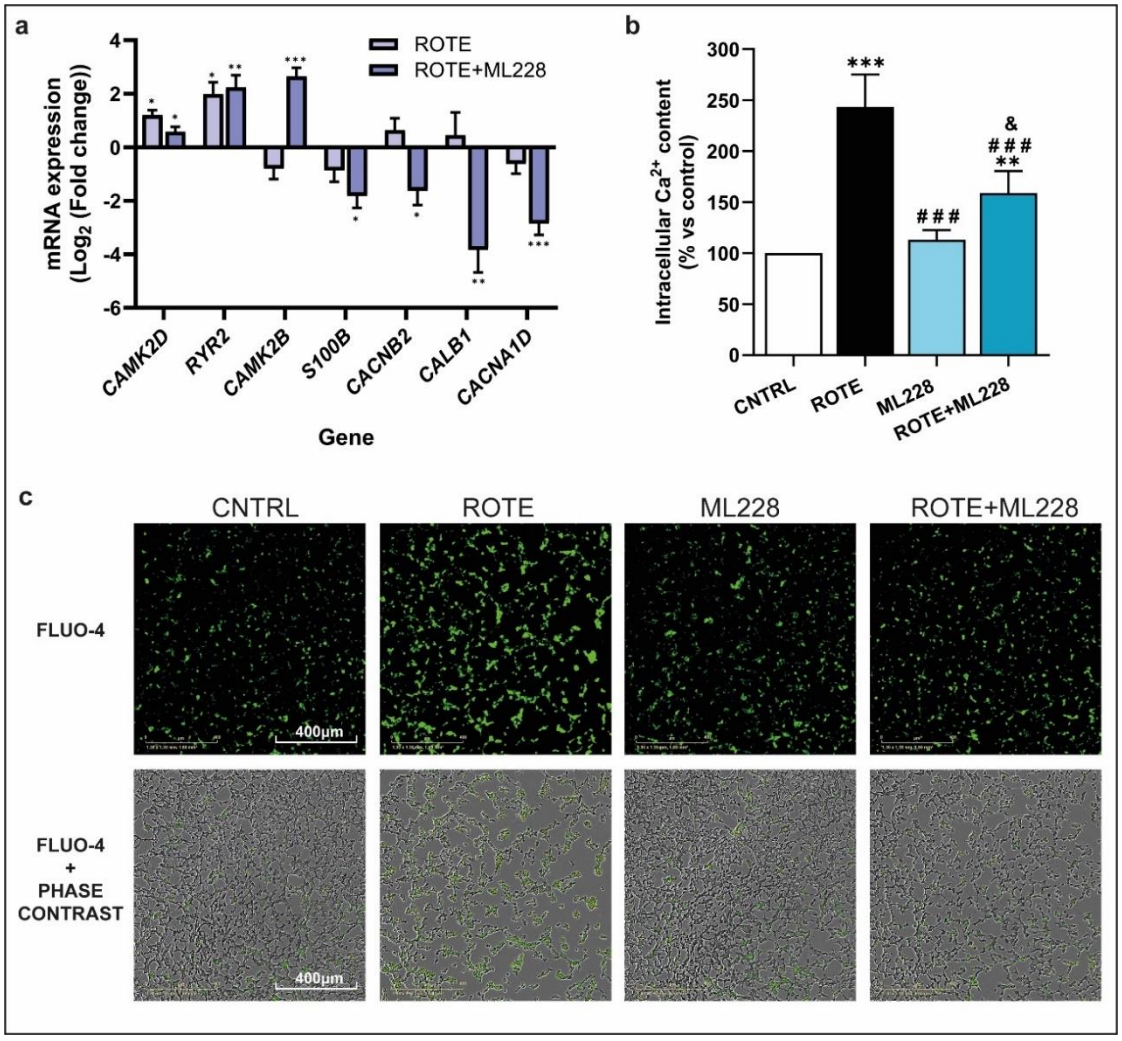

Figure 5.29. ML228 antagonizes the rotenone-mediated increase in intracellular Ca^{2+} content. a. Graph that shows mRNA expression levels, as a fold change against control, of a set of genes related to Ca^{2+} homeostasis, assessed by Nanostring nCounter in samples from fdSH-SY5Y treated with 1 µM Rotenone alone or combined with 0.5 µM ML228. **b.** Graph showing Ca^{2+} levels against control for SH-SY5Y cells treated with 1 µM Rotenone and 0.5 µM ML228 separately or combined for 24h. This is calculated as Mean fluorescence intensity of Ca^{2+} probe Fluo-4 normalized to cell phase area confluence obtained with Incucyte S3 software (n=4). **c.** Representative images from the Incucyte S3 Software that show cells treated as stated and used to calculate the previously reported Ca^{2+} levels. Scale bar indicates 400 µm. Statistical analysis was performed using a one-way ANOVA followed with Dunnett's post-hoc where $p<0.05$ was recorded as "*" with respect to control, "#" with respect to rotenone and "&" when comparing to ML228.

5.4. DISCUSSION

This study explores the protective effects of various HIF-1α stabilizing drugs against rotenone-induced toxicity in SH-SY5Y cells, utilised as PD model, uncovering the novel PHD inhibitor ML228 as a promising candidate for further investigation.

5.4.1. Evaluation of HIF-1α stabilising drugs

Several drugs were selected to probe their capacity to stabilize HIF-1α and protect SH-SY5Y cells from rotenone toxicity. As discussed in the chapter introduction, rotenone is widely used to model PD and has no impact on HIF-1α levels in this experimental setup, as shown in the previous chapter. We found that ML228 and IOX4 induced HIF-1α stabilization at lower concentrations (0.5 and 2.5 μM, respectively) than VH298 and GSK1278863 (Fig. 5.2b, d, f; Fig. 5.12c) and significantly improved cell viability in rotenone-treated SH-SY5Y (Fig. 5.4b; Fig. 5.13b). Consistent with previous reports in cancer cell lines, HIF-1α accumulation was detected with VH298 concentrations of 50 μM or higher (Frost et al., 2016). Similarly, previous studies have shown that VH298 induces lower levels of HIF-1α than PHD inhibitors like FG-4592 at the same concentrations (Frost et al., 2016) and that IOX4 is more potent that GSK1278863 (Yeh et al., 2017). In our study, HIF-1α levels in cells treated with 50-200 μM VH298 were lower than those in cells treated with 100 μM $CoCl_2$. VH298 has been shown to increase the expression of HIF-1α canonical target genes (Fros et al., 2016). However, VH298 is a pVHL inhibitor, so unlike PHD inhibitors, it stabilizes HIF-1α in its hydroxylated form. This could affect its interaction with transcriptional coactivators and subsequent gene expression. While VH298 has only been used in a few studies not related to PD, inhibition of pVHL by other means has been shown to be neuroprotective in PD animal models, although the role of HIF-1α was not investigated (Chen et al., 2019; Liang et al., 2023). However, VH298 did not show significant protection against rotenone damage in SH-SY5Y cells (Fig. 5.3b). The 2-OG analogue GSK1278863 has been approved in Japan to treat anemia caused by chronic kidney disease (Dhillon et al., 2020). In line with previous studies in cancer cell lines, 25 μM GSK1278863 induces considerable HIF-1α stabilization (Ariazi et al., 2017). However, higher concentrations of GSK1278863 caused widespread death of SH-SY5Y cells after only 4 hours of treatment, so we did not pursue its study further for this project. Since only compounds that induce potent HIF-1α stabilization protect SH-SY5Y cells from rotenone toxicity, it is possible that HIF-1α accumulation must reach a certain threshold to have a neuroprotective effect.

5.4.2. Comparison of IOX4 and ML228 as potential therapeutic agents in a PD cellular model

The beneficial effects of IOX4 and ML228 against rotenone were thoroughly investigated to elucidate the mechanisms underlying their neuroprotective properties. These compounds have been used in few studies, none of which focused on neurodegeneration. IOX4 blocks 2-OG access to the active site of PHDs, resulting in potent and selective PHD inhibition (Chan et al., 2015). In a panel of several PHD inhibitors, IOX4 induced the highest increase in the expression of HIF-1α targets (Yeh et al., 2017). Intraperitoneal injection of IOX4 into mice induces HIF-1α stabilization in the brain, suggesting that this compound can cross the blood-brain barrier (Chan et al., 2015). ML228 stabilizes HIF-1α likely by chelating iron in the active site of PHDs (Theriault et al., 2012). Interestingly, studies have utilized ML228 to improve neuronal survival after transient global ischemia and spinal cord injury in rats (Liu et al., 2016; Chen et al., 2017). Both IOX4 and ML228 improved cell confluence and morphology in rotenone-treated SH-SY5Y cells, but not U-87MG cells (Fig. 5.4; Fig. 5.13). Similarly, ML228 protected SH-SY5Y cells from the rotenone-induced decline in metabolic activity, with no effect on U-87MG cells (Fig. 5.15). This may be due to the different roles of HIF-1α in neurons and astrocytes. Indeed, one study found that loss of HIF-1α made primary neurons more vulnerable to hypoxic damage, while it improved survival in astrocytes (Vangeison et al., 2008). It would be of great interest to fully explore the differential effects of these specific PHD inhibitors on neurons and astrocytes. The neuroprotective effects of these compounds were maintained in differentiated SH-SY5Y cells (Fig. 5.5d; Fig. 5.16a). In fully differentiated SH-SY5Y cells, ML228 rescued the cytotoxicity elicited by rotenone up to 24 hours, but reduced cell confluence at later timepoints (Fig. 5.16b). This may be related to the treatment of these cells with RA and BDNF, as differentiation has been shown to change the sensitivity of SH-SY5Y to certain drugs (De Conto et al., 2021). Interactions between the chemicals used for differentiation may also play a role, as RA has been shown to increase HIF-1α levels (Fernández-Martínez et al., 2012) and there also might be potential unknown drug interactions between ML228 and RA/BDNF. ML228 also counteracted the marked reduction in neurite length caused by rotenone treatment (Fig. 5.14). Since DAergic axon degeneration occurs prior to neuronal death in both PD patients and rotenone-induced PD models (Tagliaferro et al., 2016), maintenance of neurite extension by ML228 suggests an improvement in neuronal health. The involvement of HIF-1α in the neuroprotective characteristics of ML228 was evaluated by using a HIF-1α inhibitor. This inhibitor reduced HIF-1α stabilisation, which significantly diminished the protective effect of

ML228 against rotenone (Fig. 5.17). Thus, neuroprotection mediated by ML228 is dependent on HIF-1α, although other factors, such as HIF-2α, may also play a role, as the inhibitor did not completely abrogate the effect of ML228.

Of note, although co-treatment with IOX4 improved cell number in rotenone-treated cells, IOX4 used alone caused significant toxicity from 24 hours. Investigation of caspase-3/7 activation showed that both ML228 and IOX4 could blunt caspase cleavage induced by rotenone, while slight caspase activation was detected in IOX4-treated cells (Fig. 5.6; Fig. 5.18). HIF-1α inducers Agmantine, Orexin-A and Lactoferrin are also capable of reducing Caspase-3 activation in animal and cellular PD models presenting mitochondrial dysfunction (Leston Pinilla et al., 2021). Further research into mechanisms involved in apoptosis demonstrated that ML228 can prevent the rotenone-mediated loss of mitochondrial cytochrome c and induce the phosphorylation of ERK1/2 (Fig. 5.19). Activation of ERK1/2 has been linked to increased survival in PD models (Bohush et al., 2018). Our findings indicate that these PHD inhibitors increase cell viability in rotenone-treated SH-SY5Y cells by blocking apoptosis. Since mitochondria are central to apoptosis, we evaluated a series of mitochondrial parameters. Both drugs caused a significant decrease in ATP levels (Fig. 5.7; Fig. 5.20), likely due to HIF-1α-mediated reduction in mitochondrial oxygen consumption and activation of glycolysis, which produces ATP less efficiently (Papandreou et al., 2006). In fact, assessment of the effect of ML228 in the presence of inhibitors of OXPHOS and glycolysis showed that glycolysis is necessary for the protective effect of ML228 (Fig. 5.21a). Interestingly, enhancement of glycolysis via stimulation of PGK1 activity prevented neuronal death in mice, rats, flies, and iPSCs that were used to model PD using toxins or genetic engineering (Cai et al., 2019).

Given that oxidative energy production depends on the proton gradient across the inner mitochondrial membrane maintained by the activity of the ETC, and rotenone blocks ETC complex I, we assessed mitochondrial membrane potential. As expected, rotenone induced a substantial decrease in mitochondrial membrane potential, which was rescued by cotreatment with either IOX4 or ML228 (Fig. 5.8; Fig. 5.21b, c). Prior research indicates that mitochondria-targeted HIF-1α can restore loss of mitochondrial membrane potential (Li et al., 2019) and multiple PHD inhibitors improve this parameter in PD models presenting mitochondrial damage (Li et al., 2018; Rajagopalan et al., 2016). Unlike ML228, IOX4 treatment alone caused a loss of mitochondrial membrane potential and a decrease in the levels of proteins involved in controlling mitochondrial dynamics,

including OPA1, Mfn1, Mfn2, and p-Drp1 (Fig. 5.9). Mfn1/2 control mitochondrial fusion while phosphorylation of Drp-1 at Ser616 induces mitochondrial fission (Ni et al., 2015). In turn, rotenone and ML228 exclusively alter the levels of s-OPA1 (Fig. 5.23). OPA1 regulates mitochondrial inner membrane fusion and cristae structure and presents long and short isoforms, whose balance is key to mitochondrial homeostasis (Del Dotto et al., 2017). Thus, the loss of both OPA1 isoforms as well as other proteins linked to mitochondrial dynamics elicited by IOX4 might be linked to its detrimental effect. Morphological changes in mitochondria due to this protein deficits can be assessed by transmission electron microscopy. Further investigation on the impact of ML228 on mitochondrial function revealed that this compound can rescue rotenone-mediated reduction in mitochondrial area, perimeter and elongation (Fig. 5.22). As mitochondrial health is linked to ROS production, we examined oxidative stress levels and found that these were increased in rotenone-treated SH-SY5Y but were returned to baseline by both IOX4 and ML228 treatments (Fig. 5.10; Fig. 5.24). HIF-1α can downregulate ROS generation by modulating ETC activity (Fukuda et al., 2007). With the objective to characterise the pathways affected by IOX4, we performed a proteome array for proteins involved in cellular stress, which showed alterations to proteins involved in the response to stressful environments, such as heat shock protein HSP60 and p53 (Fig. 5.11). While the exact mechanism underlying the harmful effects of IOX4 remains to be determined, these findings suggests that IOX4 has complex effects on mitochondrial function, and that its therapeutic benefits need to be weighed against its potential for mitochondrial toxicity. In summary, both IOX4 and ML228 offer neuroprotection against rotenone, likely through HIF-1α stabilization, by improving cell viability and reducing ROS. However, while IOX4 has complex effects on mitochondria, including some detrimental ones, ML228 exhibits a more favourable profile with better mitochondrial function and no signs of intrinsic cytotoxicity. These contrasting effects might be due to the distinct mechanisms of action and potencies of the two drugs. IOX4 has been shown to be highly potent and likely acts through direct PHD inhibition, potentially leading to excessive HIF-1α activation (Chan et al., 2015). In contrast, ML228 functions via iron chelation, which can offer additional off-target benefits and might induce a more moderate HIF-1α response (Theriault et al., 2012).

ML228 was selected for further investigation as a potential therapeutic candidate. The results of this research show that ML228 appears to induce autophagy through increasing the levels of LC3B and LC3B-II (Fig. 5.25a-c). HIF-1α likely contributes to this effect,

as it can regulate the expression of several proteins involved in the autophagic pathway (Daskalaki et al., 2018). In fact, increased LC3-II levels in the presence of HIF-1α stabilization have been reported in several cell and animal models, including SH-SY5Y cells (Guo et al., 2017; Lu et al., 2018). It would be interesting to investigate the levels of specific autophagy proteins to assess the specific changes elicited by HIF-1α stabilization in this context. PD has been linked to autophagy deficits, and autophagy-enhancing strategies, like rapamycin treatment or pharmacological AMPK activation, have been shown to be neuroprotective in PD models (Moors et al., 2017). In SH-SY5Y cells, autophagy inducers such as rapamycin protect against rotenone-mediated cell death, while autophagy inhibitors such as chloroquine increase rotenone toxicity (Xiong et al., 2011). Our findings, in conjunction with available literature, strongly suggest that the neuroprotective effect of ML228 might be dependent on its ability to induce autophagy.

In order to identify additional pathways involved in the neuroprotective effect of ML228, we performed a proteome analysis using an array containing proteins related to apoptosis. Despite the lack of significant changes in proteins directly linked to apoptosis, proteins related to cell cycle control were differentially expressed. Indeed, both rotenone and ML228 increased the levels of p21, while p27 was only elevated by ML228 (Fig. 5.27a, b). Increased levels of p21 in rotenone-treated SH-SY5Y cells have been described beforehand (Ho et al., 2021) while p21 and p27 have been identified as HIF-1α targets (Goda et al., 2003). Interestingly, both p21 and p27 can repress the expression of α-Syn (Gallastegui et al., 2018). Rotenone impacts on the cell cycle by increasing the number of apoptotic cells while reducing cells in proliferative state and triggering the accumulation of cells in the later stages of the cell cycle (Fig. 5.27c, d). Rotenone exposure has been shown to alter cell cycle distribution in previous studies, producing changes similar to those observed in this project (Wang et al., 2014). Cotreatment with ML228 reduces the number of apoptotic cells and restores the fraction of cells in the G1 and G2/M phases while increasing the percentage of cells going through the replicative S phase (Fig. 5.27c, d). Recent investigations have linked cell cycle deregulation to DAergic neuron loss in PD (Joseph et al., 2020). In addition, PD-related genes *PINK1* and *DJ1* seem to control cell cycle progression and loss of either gene can lead to abnormal cell cycle re-entry (O'Flanagan et al., 2014; López-Grueso et al., 2023). Since neurons are typically in a quiescent state known as G_0 phase, the role of ML228 in cell cycle dynamics should be investigated in primary neurons (Frade et al., 2015).

Nevertheless, ML228 may enhance survival by remodelling cell cycle progression in SH-SY5Y cells.

To further characterise the role of ML228 in mitigating rotenone-mediated neurotoxicity, we performed a transcriptomic analysis of fdSH-SY5Y cells under these treatments. Interestingly, although rotenone has been predominantly linked to the intrinsic apoptotic pathway, rotenone activates several genes encoding death receptors involved in the extrinsic apoptotic pathway, as well as genes participating in the ubiquitin-proteasome system, the untranslated protein response, oxidative stress and gene transcription (Fig. 5.28). This data indicates that activation of the extrinsic apoptotic pathway, likely via the untranslated protein response, should be considered when studying rotenone-based PD models. This response is not significantly changed by HIF-1α, although it reduces the increase elicited by rotenone in genes involved in ER stress. Similarly, Adaptaquin, a HIF-1α inducer, can downregulate the activation of proteins involved in the untranslated protein response in cellular and mouse models of PD (Aime et al., 2020). We investigated the genes that are differentially regulated in co-treated cells compared to rotenone-treated cells and identified 5 genes that play a role in vesicle trafficking (*ATP6V0E1*, *NSF* and *UNC13A*), myelination (*FAM126A*), glycolysis (*PGAM1*), and signalling cascades (*PRKCA*) that were differentially regulated. Remarkably, some of these genes have been linked to PD. Indeed, *NSF* has been reported as a potential genetic risk factor for PD (Liu et al., 2011) and bioinformatic approaches have identified *UNC13A* as a gene of interest in PD (Chandrasekaran et al., 2013). Investigation of these pathways could shed light on the pathogenesis of PD and lead to new therapeutic strategies. Additionally, several changes in the expression of proteins involved in calcium trafficking were observed. ML228 does not alter intracellular Ca^{2+} levels on its own, but it can reduce the increase in intracellular calcium caused by rotenone (Fig. 5.29). To elucidate the mechanism of action of ML228, we could study the exact changes in Ca^{2+}-related proteins that may be involved in this process. As elevated intracellular Ca^{2+} is linked to rotenone-mediated apoptosis (Yu et al., 2013), reduction of Ca^{2+} accumulation by ML228 could be linked to its ability to inhibit apoptotic mechanisms.

Although multiple effects of ML228 overlap with other HIF-1α-stabilizing drugs, such as downregulation of apoptotic mechanisms and ROS production, our study also reveals modulation of factors not previously associated with this class of compounds, such as neurite extension, mitochondrial morphology, cell cycle regulation, and Ca^{2+} trafficking.

5.5. CONCLUSION

Although multiple PHD inhibitors are being developed for the treatment for a variety of diseases, their therapeutic potential in PD has not been evaluated. With no disease-modifying drugs for PD yet available, it is of the utmost importance to explore new therapeutic approaches. In this chapter, we provide the first evidence that PHD inhibitors IOX4 and ML228 have neuroprotective effects in rotenone-treated SH-SY5Y cells, a preclinical cell model of PD. ML228 is the most effective compound at protecting against rotenone cytotoxicity and improves a broad range of parameters affected by this PD-related toxin, including apoptosis, ROS production, mitochondrial homeostasis, autophagy, cell cycle progression, and Ca^{2+} levels. Importantly, the neuroprotective effect of ML228 is dependent on HIF-1α stabilisation.

HIF-1α is a pleiotropic TF that can control a variety of pathways that are dysregulated in PD patients, as this study has shown. This has also been cited as a downside of HIF-1α-based therapeutics. However, the recent approval of HIF-1α-stabilising drugs for human use and the number of these drugs in clinical trials demonstrate that they are safe and effective (Miao et al., 2022). At the very least, research using HIF-1α stabilizers will allow the research field to assess multiple candidate pathways that show therapeutic potential in PD, as opposed to investigating them individually.

In conclusion, ML228 shows promising neuroprotective effects in a rotenone-based *in vitro* PD model, and further testing is needed to assess its potential in the treatment of PD. Evaluating the neuroprotective effects of ML228 in other PD models, such as iPSCs and animals, would support its development as a PD therapeutic.

CHAPTER VI

THE TRANCRIPTIONAL RESPONSE TO HIF-1α STABILISATION IN NEURONAL CELLS

6.1.INTRODUCTION

HIF-1α, as previously discussed, controls genes in a wide variety of pathways. The importance of HIF-1α in the NS has only recently been recognized, and as a result, most of its target genes have been investigated in other specific contexts, such as cardiovascular disease and cancer. Given that the expression of HIF-1α target genes can be further regulated by several factors including cell type, it is important to evaluate the induction of known HIF-1α target genes in different NS cell types. Although the genes constituting the core response to hypoxia via HIF-1α have been precisely investigated, non-canonical HIF-1α targets continue to be discovered. Thus, it is of importance to study the complete transcriptional response to HIF-1α in cells of neuronal origin in order to uncover the specific role of this important TF on neural physiological functions as well as in neuropathologies, such as PD.

6.1.1. Transcriptomics

The study of the entire transcriptome through analysing total mRNA counts became possible thanks to the advent of transcriptomics technologies in the 1990s. To date, the most used transcriptomics techniques include microarrays, which utilize a fixed collection of hybridization probes targeted to preset sequences, and RNA-Seq, which utilize high-throughput sequencing to read all the transcripts present in each sample (Lowe et al., 2017). Some variations of these techniques are beginning to emerge. The Nanostring nCounter is a type of microarray capable of quantifying the expression of a panel of up to 800 mRNAs simultaneously by hybridization of target transcripts to colour-coded gene-specific probes that are microscopically imaged and counted with a digital analyser (Fig 6.1). The number of colour barcodes detected for each mRNA is counted and compared against housekeeping mRNA controls, providing the fold change in the expression of the genes analysed (Geiss et al., 2008).

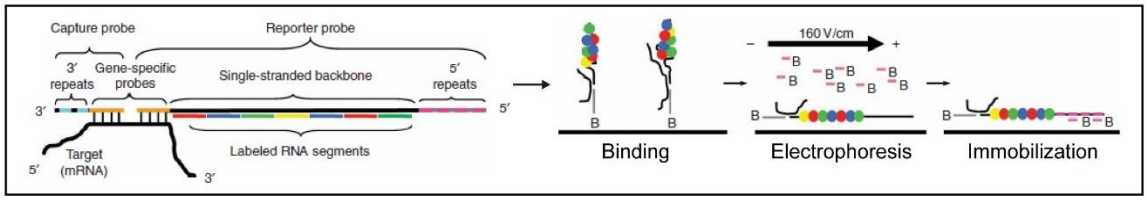

Figure 6.1. Overview of Nanostring nCounter technology. The series of images represent the steps in Nanostring nCounter protocol: mRNA binding to the colour-coded probe, binding of the mRNA-probe complexes to the capture slide and alignment of the mRNA-probe pairs by electrophoresis for subsequent imaging (Geiss et al., 2008).

This technique was chosen as it presents several advantages, including high sensitivity, quick sample preparation and processing, direct reading of native RNA counts allowing for accurate quantification, the use of a targeted neuropathology-related mRNA panel, and simple but powerful data analysis protocol. Indeed, this technique allows to directly detect mRNA transcript levels, avoiding the variability attached to the RNA to cDNA conversion step in RNA-Seq and qRT-PCR. In addition, no previous experience is needed to use this technology, while specific expertise is needed for library preparation, sequencing and data analysis in RNA-Seq (Narrandes and Xu, 2018).

As mentioned, the HIF-1α transcriptome has been investigated before, but this has been mostly performed in different research contexts than the one of interest in this project. Indeed, several RNA-Seq and ChIP-Seq studies look at the transcriptome of cancer cells under hypoxic conditions (Schödel et al., 2011; Andrysik et al., 2021). Interestingly, an investigation exploring the role of hypoxia in neuroblastoma using SKNBE2 cells highlights pathways involved in neuronal homeostasis, such as axon guidance, as targets of HIF-1α (Cimmino et al., 2019). An additional RNA-Seq study compares the transcriptomes of HeLa cells treated with different PHD inhibitors, showing that more than 65% of the upregulated genes are shared with the hypoxia signature (Frost et al., 2019). However, research specifically investigating the function of HIF-1α in the NS remains limited, with current studies employing mouse neurons. These studies emphasize the involvement of HIF-1α in hypoxia-induced adaptations of energy metabolism but also hint at its broader influence on neuronal processes like neurotransmitter release (Zhang et al., 2023). In the study carried out in this chapter, the use of a targeted neuropathology gene panel and differentiated SH-SY5Y cells shifts the focus to pathways specifically active in the NS, as the study of the whole genome by RNA-Seq can mask important gene expression changes in under-represented pathways. Thus, the application of the Nanostring nCounter technology using a Neuropathology panel on samples of differentiated neuroblastoma cells exposed to different HIF-1α stabilizing paradigms will permit the discovery of differentially expressed genes that constitute potential HIF-1α targets in the NS and will help establish novel NS pathways where HIF-1α plays important regulatory roles. Of note, to study the transcriptional targets of HIF-1α, which is rapidly degraded under normoxic conditions, it is essential to use HIF-1α stabilizing drugs (PHD/VHL inhibitors) or hypoxic conditions. Traditional approaches like gene knockout or overexpression are not suitable for HIF-1α, as its it is not constitutively present in cells and its levels are primarily regulated at the protein level.

6.1.2. TF Binding Motifs analysis

A preliminary approach to determine whether a differentially expressed gene (DEG) is a target of a specific TF, such as HIF-1α, is to evaluate the presence of functional TF binding sites like HREs with bioinformatic tools. The open access and high-quality bioinformatic software JASPAR, as aforementioned, can be utilised to map the promoters of genes of interest to find consensus TF binding sequences (Castro-Mondragon et al., 2022). An additional resource that may be used to screen for functional TF binding motifs is cross-species genomic sequence alignment to identify the promoter regions containing TF binding motifs that have been conserved throughout evolution. This can be carried out with specific software such as Basic Local Alignment Search Tool (BLAST) (McGinnis and Madden, 2004). The presence of a highly similar TF binding motif between different lineages can indicate that this sequence has functional importance (Kim et al., 2010)

6.1.3. Interaction databases

When investigating a TF such as HIF-1α, it is important to know if the DEG is a direct target of this TF, which can be explored using interaction databases. These databases pull information from a variety of sources to generate a unique map of interactions between genes or proteins. To investigate the relationship between a TF and a potential target, it is necessary to employ a database that includes expression interactions, showing the TFs controlling the expression of a given protein, like Pathway Commons (Rodchenkov et al., 2020).

6.1.4. Pathway enrichment analysis

The Nanostring data analysis software provides a DEG classification into gene sets. However, in order to identify the actual biological pathways that the DEGs detected by RNA profiling belong to, it is necessary to perform Pathway Enrichment Analysis. This bioinformatic method associates a set gene list to specific biological pathways, statistically determining the pathways that are overrepresented. There are two main databases that can be utilised to carry out this analysis, Gene ontology (GO), which hierarchically allocates genes to a set of predefined categories depending on its molecular function, biological process and cellular localization, and Kyoto Encyclopedia of Genes and Genomes (KEGG), which groups lists of genes into pathways (Chicco and Agapito, 2022). These two classification methods, as well as many additional ones, can be

compared using Enrichr, a software application integrating different approaches to obtain enrichment results (Xie et al., 2021). The principal difference between these two methods is the classifications that they contain, with KEGG presenting <200 module pathways and GO terms totaling >38 000 (Altman et al., 2013; Balakrishnan et al., 2013). Thus, GO biological process annotations capture in more detail the wide variety of biological pathways. However, as GO enriched categories may be highly redundant, the server REVIGO can be utilised to cluster the obtained GO terms based on semantic similarity (Supek et al., 2011). Acquiring a curated and representative list of overrepresented GO biological processes is key to precisely pinpoint the pathways enriched in the data and evaluate HIF-1α role in these processes.

6.1.5. Validation of transcriptomic profiling

Although Nanostring nCounter RNA profiling is an extremely robust and reliable method, and data obtained is supported by internal quality controls alongside post-sample bioinformatic analysis, it is commonplace to perform laboratory-based experiments to further confirm the validity and relevance of the data acquired from transcriptomics techniques (Chuaqui et al., 2002). These include qRT-PCR to confirm changes in gene expression, ChIP or luciferase reporter assays to validate the functionality of TF binding sites and/or Western Blot to explore differences in protein levels.

6.1.6. Aims of the chapter

While the previous chapter utilised transcriptomics to identify key genes in the HIF-1α protective response to rotenone toxicity, this investigation focuses on the transcriptional response mediated by HIF-1α in the NS. To achieve this, we will perform transcriptomic analysis using a targeted neuropathology panel on differentiated SH-SY5Y cells treated with diverse PHD inhibitors. Employing dSH-SY5Y cells offers a relevant model system, as they exhibit a more mature neuronal phenotype. This enhanced physiological relevance allows for a more accurate investigation of HIF-1α target genes within neuronal pathways. Following transcriptomic analysis, validation assays and literature review will be used to link key candidate genes to PD. Ultimately, the aim of this research is to investigate the HIF-1α transcriptome in neuronal cells in order to:

1) Identify potential HIF-1α target genes in the NS and their link to PD.
2) Uncover novel HIF-1α associated pathways of relevance in NS biological functions and neuropathologies, with special emphasis on PD.

6.2.METHODOLOGY

RNA expression profiling was used to explore the changes in gene expression in neuronal cells under HIF-1α stabilizing treatments. This was carried out with a nCounter Human Neuropathology Panel in the NanoString nCounter equipment. RNA samples utilized were extracted from dSH-SY5Y cells treated with ML228, IOX4, VH298 or 1% O_2 for 24h, with non-treated normoxic dSH-SY5Y cells used as control. As mentioned in the previous chapter, each drug stabilises HIF-1α through a distinct mechanism: ML228 via iron chelation, IOX4 through direct PHD inhibition, and VH298 by inhibiting VHL. By using PHD inhibitors with diverse mechanisms, we can identify commonly deregulated genes with a high probability of being bona-fide HIF-1α targets. The data obtained was analysed with the nSolver 4.0 software to obtain the DEGs and visualized on the Nanostring Advanced Analysis online platform. Bioinformatic analysis of the functionality of HREs was carried out using the JASPAR, BLAST and Pathway Commons software. Enrichment analysis using the Enrichr resource was performed to determine overrepresented GO Biological Processes. At least two genes of interest per GO term, with previously unexplored or preliminary links to HIF-1α, were validated by qRT-PCR utilising the same samples as those used for the transcriptomic analysis. Western Blot was used subsequently to evaluate whether changes in gene expression translated to modifications in protein levels. Fluctuations in Ca^{2+} levels were investigated with a commercially available kit. The full details of the methods used in this chapter can be found in Chapter II.

6.3. RESULTS

6.3.1. ML228, IOX4 and hypoxia change global differential expression of genes

To study the effect of HIF-1α-mediated transcriptional response on genes and pathways involved in the NS, RNA was extracted from fdSH-SY5Y treated with different HIF-1α stabilizing drugs and subjected to RNA profiling analysis. The drugs and respective concentrations were selected from the HIF-1α-stabilising drug evaluation performed in the previous chapter. The results are represented in volcano plots, showing that the samples from ML228, IOX4 and hypoxia treated cells show significant changes in gene expression profiles, ranging between 12 and 375 for hypoxia and IOX4, respectively, compared to control (normoxia). In contrast, 50 μM VH298 treatment did not show any changes in gene expression (Fig. 6.2a-d). Several canonical targets of HIF-1α were induced by ML228, IOX4 and hypoxia, including *VEGF*, *BNIP3* and *PGK1*, as well as previously unknown potential targets of HIF-1α such as *SNCB*, *NOL3* and *NAGLU* (Fig. 6.2e). While hypoxia only modified the expression of a small number of genes, ML228 and IOX4 had a more substantial effect on gene expression, significantly modifying the response 161 common genes between them which could be potential HIF-1α targets and of interest for further analysis (Fig. 6.2e).

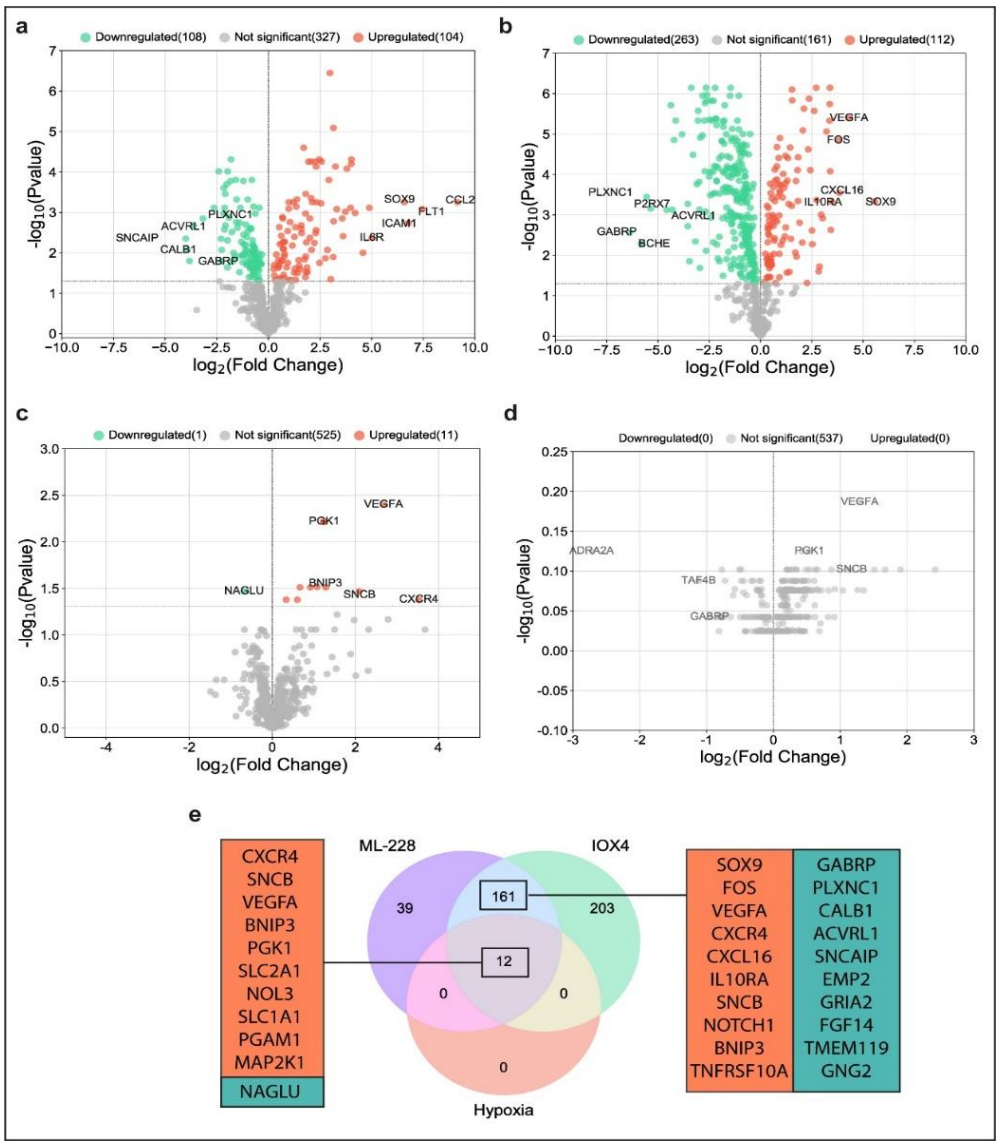

Figure 6.2. DEGs under different HIF-1α stabilizing treatments in fdSH-SY5Y. All Volcano plots present the fold changes and p-values of DEGs with the top 5 upregulated and downregulated labelled with the gene name**. a.** Volcano plot representing DEGs after 24h 0.5 μM ML228 treatment. **b.** Volcano plot representing DEGs after 24h 10 μM IOX4 treatment. **c.** Volcano plot representing DEGs after 24h 1% O_2 treatment. **d.** Volcano plot representing DEGs after 24h 50 μM VH298 treatment. **e.** Venn Diagram showing the overlap between DEGs in different treatments.

Subsequently, GO biological process enrichment analysis was performed to predict pathways associated with HIF-1α using the DEGs that overlap between the ML228 and IOX4 treated dSH-SY5Y samples. These were curated with the REVIGO software and the top 20 are shown in a bubble plot below. These GO terms include known functions of HIF-1α in pathways such as apoptosis or autophagy, while uncovering novel potential roles of HIF-1α in processes such as axonogenesis (Fig. 6.3). The different GO terms and corresponding DEGs were grouped into broader pathways (SI Table 8.7) and are

discussed in the following sections, along with the DEGs in related pathways included in the Nanostring gene set classification (SI Table 8.8).

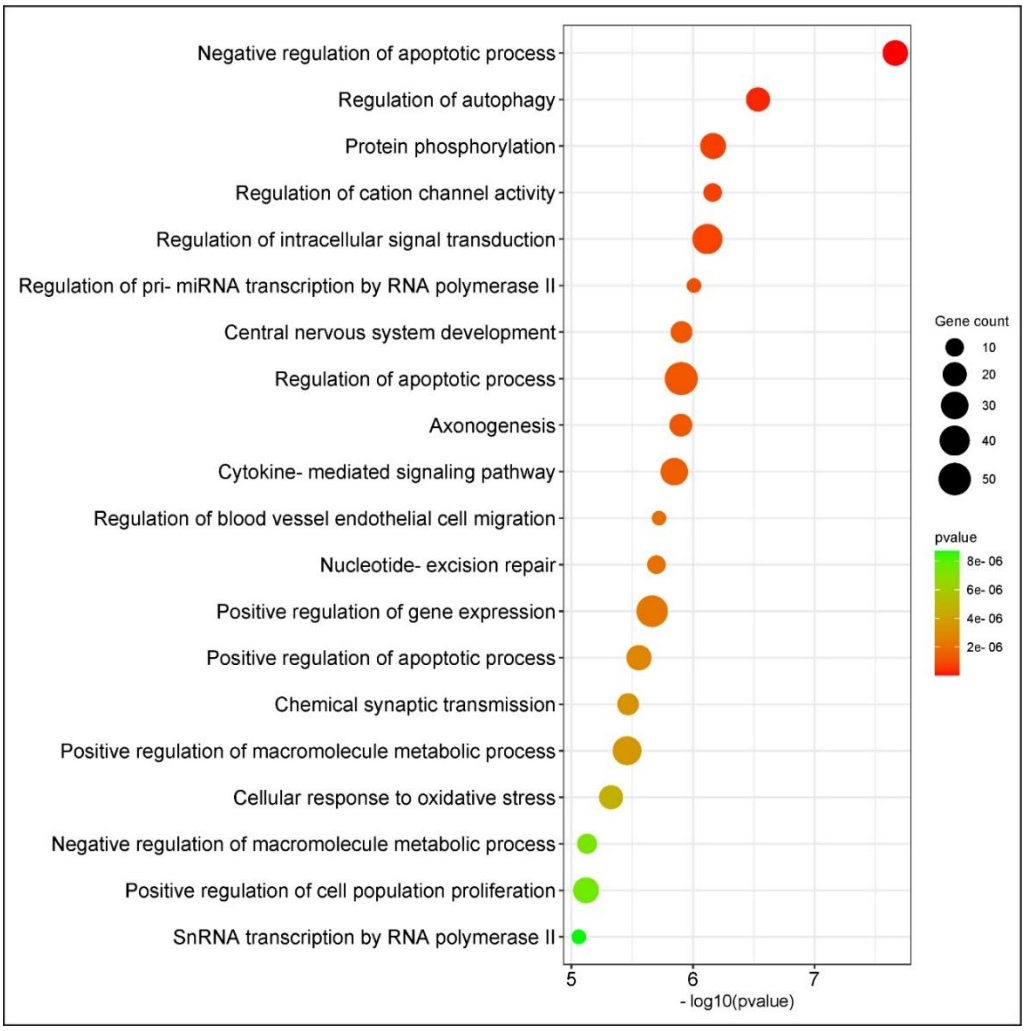

Figure 6.3. GO biological process enrichment utilising common DEGs in ML228 and IOX4 treated dSH-SY5Y. The bubble plot represents the REVIGO-curated GO biological process enrichment analysis, in which colours show the adjusted p-value and bubble size denotes gene counts. GO biological process terms are sorted by p-value.

6.3.2. Differential expression of genes involved in apoptosis

The DEGs included in the GO terms and in Nanostring gene sets related to apoptosis (SI Table 8.8) are presented on the following heatmaps (Fig. 6.4a, b). Treatments stabilising HIF-1α appear to influence both pro-apoptotic and anti-apoptotic genes. Indeed, increased expression of several members of the apoptosis-inducing TNF receptor superfamily, including *TNFRSF10A*, *TNFRSF10B*, and *TNFRSF12A* and *FAS* were observed, while levels of the downstream apoptosis effector *CASP6* were significantly reduced. Conversely, genes promoting survival such as *VEGFA*, *EGR1* and *NOL3* showed an increased fold change, with some anti-apoptotic genes showing a reduction, such as *HMGB1* and *NTRK1*. Some genes at the crossroads between cell death and survival,

including the ones controlling the cell cycle like *CDKN1A* and *CDK5*, also exhibited differential expression upon HIF-1α-stabilising treatments. qRT-PCR analysis demonstrates that the variation in the expression of the genes *NOL3* and *CDK5* corresponded to the results obtained in the transcriptomic analysis (Fig. 6.4c).

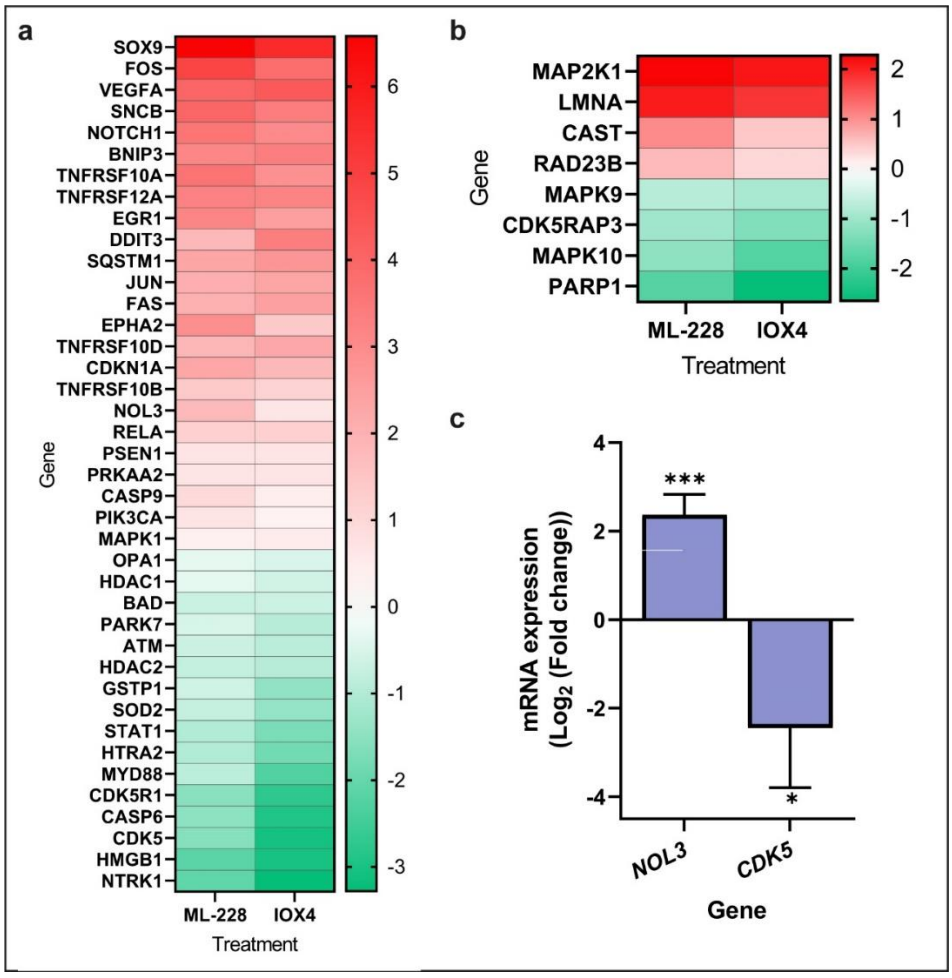

Figure 6.4. Common DEGs involved in apoptosis in ML228 and IOX4 treated fdSH-SY5Y. The heatmaps show the fold change in the expression of genes compared to control. **a.** Heatmap that includes DEGs in GO terms related to apoptosis. **b.** Heatmap that includes DEGs in Nanostring gene sets related to apoptosis. **c.** Graph that shows mRNA expression levels, as a fold change against control, of *NOL3* and *CDK5* assessed by qRT-PCR in samples from fdSH-SY5Y treated with ML-228 for 24h against control (n=3). Statistical analysis was performed using an unpaired two-tailed Student's t test where $p<0.05$ was recorded as "*".

6.3.3. Differential expression of genes involved in autophagy

The DEGs included in the GO terms and in Nanostring gene sets related to autophagy (SI Table 8.8) are presented on the following heatmaps (Fig. 6.5a, b). Activation of autophagy through the AMPK-mTOR-PI3K axis (*PRKAA2*, *MTOR*, *PIK3CA*, *PIK3CB*), as well as increases in downstream autophagy effector *SQSTM1* were evident. The mitophagy-related genes *BNIP3* and *OPTN* were also elevated by the treatments. Profiling data

showed changes to genes contributing to lysosomal function, such as V-type proton ATPase subunits *ATP6V1A*, *ATP6V0E2* and *ATP6V1G2* and genes involved in lipid metabolism in these organelles, such as *GBA*, *NAGLU*, *PPT1*, *GUSB* and *NPC1*. qRT-PCR analysis demonstrated that the variation in the expression of the genes *NPC1* and *NAGLU* corresponded to the results obtained in the transcriptomic analysis (Fig. 6.5c).

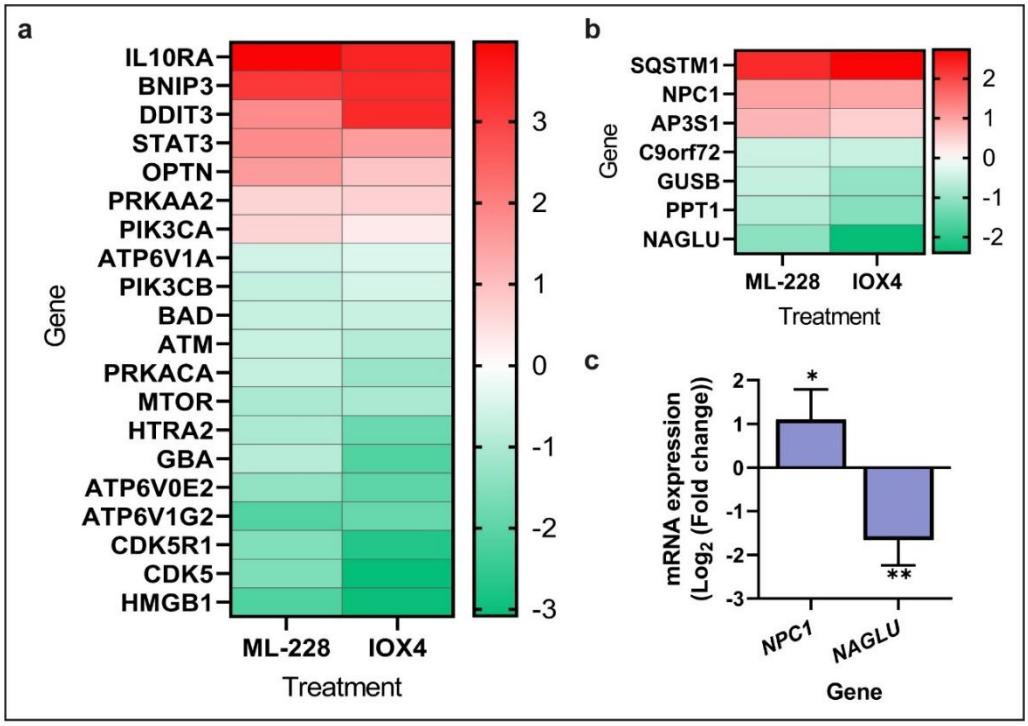

Figure 6.5. Common DEGs involved in autophagy in ML228 and IOX4 treated fdSH-SY5Y. The heatmaps show the fold change in the expression of genes compared to control. **a.** Heatmap that includes DEGs in GO terms related to autophagy. **b.** Heatmap that includes DEGs in Nanostring gene sets related to autophagy. **c.** Graph that shows mRNA expression levels, as a fold change against control, of *NPC1* and *NAGLU* assessed by qRT-PCR in samples from fdSH-SY5Y treated with ML-228 for 24h (n=3). Statistical analysis was performed using an unpaired two-tailed Student's t test where $p<0.05$ was recorded as "*".

6.3.4. Differential expression of genes involved in cell signalling

The DEGs included in the GO terms and in Nanostring gene sets related to cell signalling (Table 8.8) are presented on the following heatmaps (Fig 6.6 a, b). The treatments modified the expression of genes involved in multiple signalling cascades. These comprise transmembrane receptors such as *TGFBR2*, *ACVRL1*, *NOTCH1* and *NOTCH4* and ligands *VEGFA*, *FGF2*, *FGF14* and *LIF*. In addition, multiple genes related to intracellular signal transduction showed altered expression, including members of the PI3K pathway (*INPP4A*, *PLCB3*, *PIK3CB*, *PIK3CA*), mitogen-activated protein kinases (*MAP2K1*, *MAPK10*, *MAPK9*, *MAPK1*) cyclin-dependent kinases (*CDK2*, *CDK5*, *CDK5R1*, *CDK5RAP3*, *CDK7*) AGC kinase family members (*PRKACA*, *PRKCQ*) and

transcription factors (*EGR1*, *STAT1*, *STAT3*). qRT-PCR analysis demonstrated that the variation in the expression of the genes *EGR1* and *LIF* corresponded to the results obtained in the transcriptomic analysis (Fig. 6.6c).

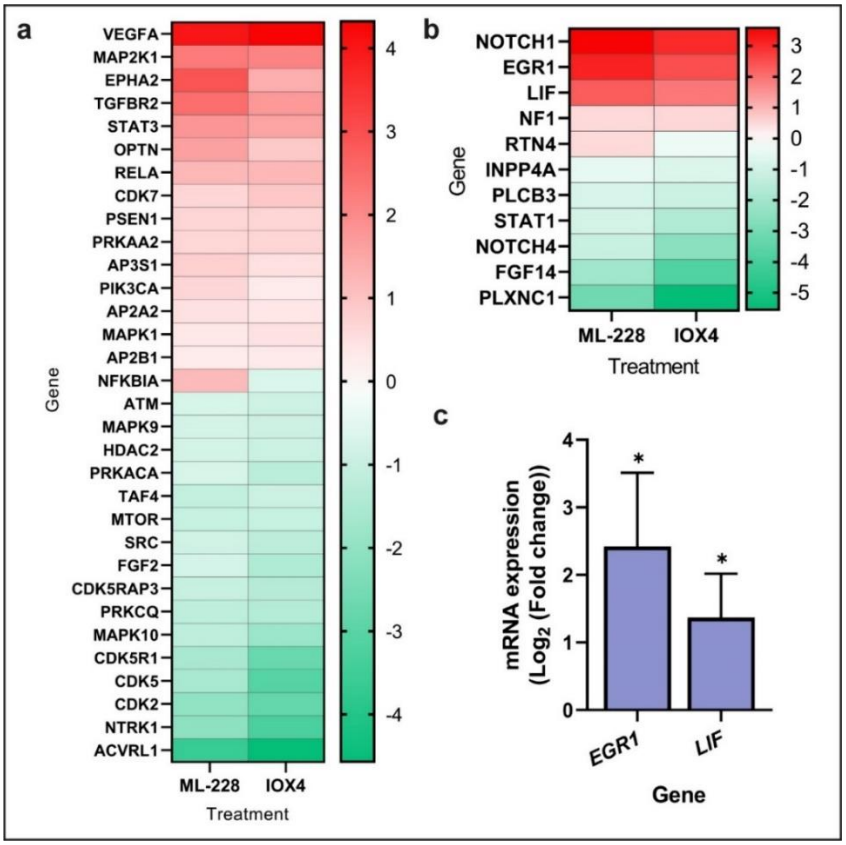

Figure 6.6. Common DEGs involved in cell signalling in ML228 and IOX4 treated fdSH-SY5Y. The heatmaps show the fold change in the expression of genes compared to control. **a.** Heatmap that includes DEGs in GO terms related to cell signalling. **b.** Heatmap that includes DEGs in Nanostring gene sets related to cell signalling. **c.** Graph that shows mRNA expression levels, as a fold change against control, of *EGR1* and *LIF* assessed by qRT-PCR in samples from fdSH-SY5Y treated with ML-228 for 24h (n=3). Statistical analysis was performed using an unpaired two-tailed Student's t test where $p<0.05$ was recorded as "*".

6.3.5. Differential expression of genes involved in cation channel function

The DEGs included in the GO terms and in Nanostring gene sets related to cation channel function (SI Table 8.8) are presented on the following heatmaps (Fig. 6.7a, b). The levels of several genes involved in regulating cation channel activity were modified by the treatments. The HIF-1α stabilising drugs altered the expression of specific L-type Ca^{2+} voltage-gated channel subunits, such as *CACNA1D* and *CACNB2*, and Ca^{2+}/calmodulin-dependent protein kinase II subunits, such as *CAMK2B* and *CAMK2D* (Fig 6.7 a). In contrast, genes related to the trafficking of other cations, such as Na^{+} and K^{+}, were present in the panel but not modified by the treatments, pointing to a specific regulation of Ca^{2+}

homeostasis by HIF-1α. Cation channels are also regulated by cation availability, so the expression of alternative genes controlling Ca^{2+} levels were investigated. Interestingly, several genes that encode Ca^{2+} binding proteins were modified, such as *RYR2*, *S100B* and *CALB1* (Fig. 6.7b). qRT-PCR analysis demonstrated that the variation in the expression of the genes *CAMK2B*, *CACNA1D* and *CALB1* corresponded to the results obtained in the transcriptomic analysis (Fig. 6.6c). While multiple genes related to Ca^{2+} trafficking appeared modified by ML228 and IOX4 treatments, no changes in total intracellular Ca^{2+} levels were observed (Fig. 6.7d, e). However, changes in Ca^{2+} localization or mobilisation cannot be ruled out.

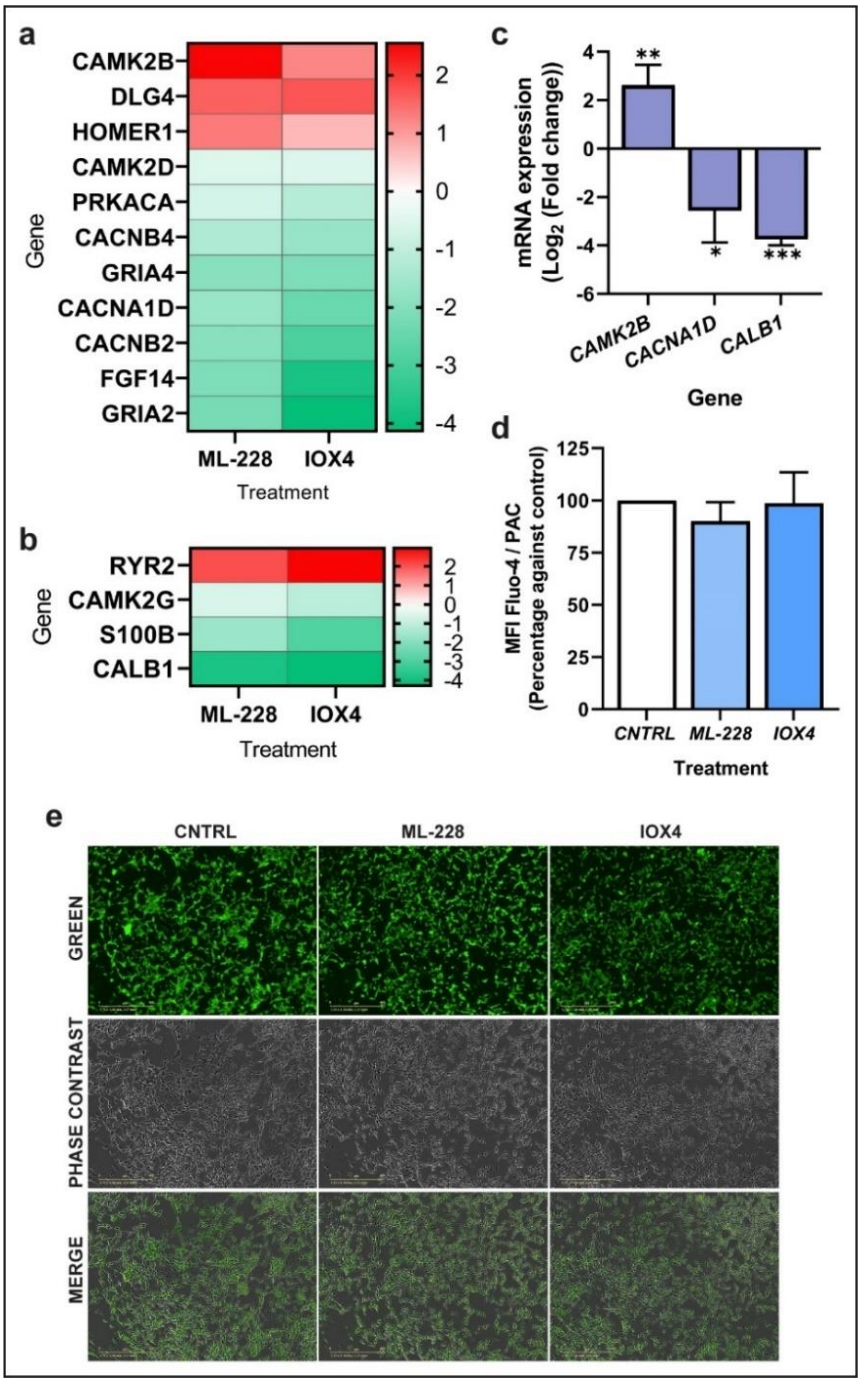

Figure 6.7. Common DEGs involved in cation channel function in ML228 and IOX4 treated fdSH-SY5Y. The heatmaps show the fold change in the expression of genes compared to control. **a.** Heatmap that includes DEGs in GO terms related to cation channel function. **b.** Heatmap that includes DEGs in Nanostring gene sets related to cation channel function. **c.** Graph that shows mRNA expression levels, as a fold change against control, of *CAMK2B, CACNA1D and CALB1* assessed by qRT-PCR in samples from fdSH-SY5Y treated with ML-228 for 24h (n=3). **d**. Graph showing Ca^{2+} levels against control for fdSH-SY5Y cells treated with either ML-228 or IOX4 for 24h.This is calculated as Mean fluorescence intensity of Ca^{2+} probe Fluo-4 normalized to cell phase area confluence obtained with Incucyte S3 software (n=4). **e**. Representative images from the Incucyte S3 Software that show cells treated as stated and used to calculate the previously reported Ca^{2+} levels. Statistical analysis was performed using an unpaired two-tailed Student's t test where $p<0.05$ was recorded as "*".

6.3.6. Differential expression of genes involved in neuronal development and activity

The DEGs included in the GO terms and in Nanostring gene sets related to neuronal development and activity (SI Table 8.8) are presented on the following heatmaps (Fig. 6.8a, b). These encompassed genes controlling NS development and homeostasis, including transcription factors such as *SOX9*, growth factors like *VEGFA* and receptors including *CXCR4* and *NOTCH1*. They also included genes involved in neuronal functions, including synaptic transmission (*SNCB*, *GAD1*, *DLG4*, *SLC1A1*), neurotransmitter signal transduction (*GLRB*, *ADORA2A*, *GRIA2*, *GRIA4*, *GABRP*), vesicle trafficking (*SNCB*, *RAB3A*), axonal structure modifications (*PLXNC1*, *SPCTNB2*) and myelination (*MYRF*, *ATRN*, *FAM126A*). qRT-PCR analysis demonstrated that the variation in the expression of the neurotransmitter receptors *GRIA3*, *ADORA2A*, GR*IA2* and *GABRP*, as well as the changes in other genes contributing to neuronal homeostasis such as *SOX9*, *GAD1*, *SCL1A1* and *FAM126A* corresponded to the results obtained in the transcriptomic analysis (Fig. 6.8c, d).

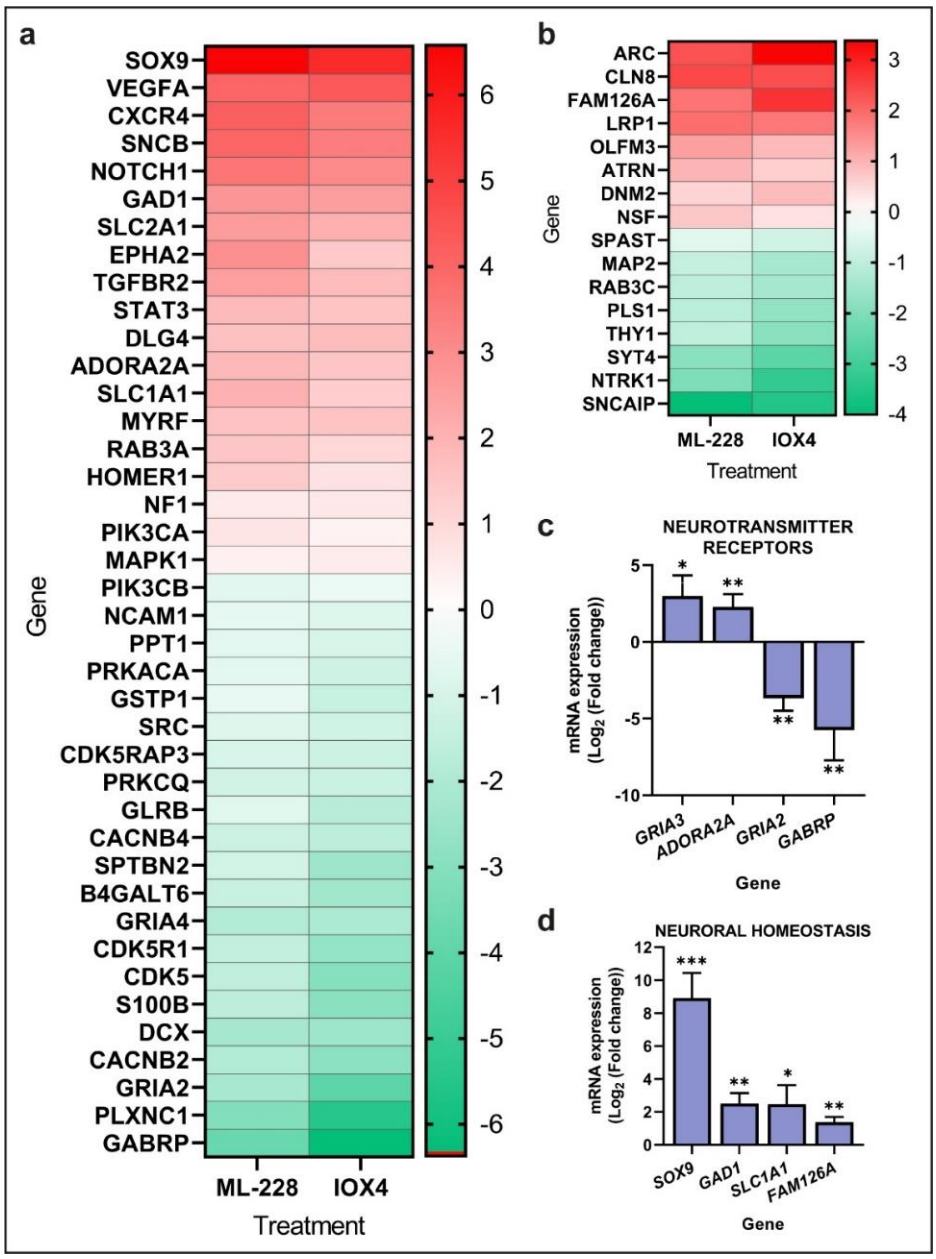

Figure 6.8. Common DEGs involved in neuronal development and activity in ML228 and IOX4 treated fdSH-SY5Y. The heatmaps show the fold change in the expression of genes compared to control. **a.** Heatmap that includes DEGs in GO terms related to neuronal development and activity. **b.** Heatmap that includes DEGs in Nanostring gene sets related to neuronal development and activity. **c.** Graph that shows mRNA expression levels, as a fold change against control, of *GRIA3, ADORA2A, GRIA2 and GABRP,* assessed by qRT-PCR in samples from fdSH-SY5Y treated with ML-228 for 24h (n=3). **d**. Graph that shows mRNA expression levels, as a fold change against control, of *SOX9, GAD1, SCL1A1 and FAM126A,* assessed by qRT-PCR in samples from fdSH-SY5Y treated with ML-228 for 24h (n=3). Statistical analysis was performed using an unpaired two-tailed Student's t test where $p<0.05$ was recorded as "*".

Interestingly, the mRNA expression of the genes *SNCB* and *SNCAIP*, codifying for β-Synuclein (β-Syn) and Synphilin-1 (Sph-1) proteins respectively, appeared to be strongly regulated by HIF-1α stabilizing treatments. For instance, ML228, IOX4 and hypoxia significantly increased *SNCB* expression whilst ML228 and IOX4 reduced *SNCAIP* expression (Fig. 6.9a). The regulation of these two proteins appears important for PD as β-Synuclein can reduce aggregation of α-Syn, a hallmark of PD, while Synphilin-1 can promote this aggregation process (Brown et al., 2016; Eyal et al., 2006a). Given their potential role in PD, these proteins were studied in more detail. qRT-PCR analysis demonstrates that the variation in the expression of both genes corresponded to the results obtained in the transcriptomic analysis (Fig. 6.9b). Western Blot analysis showed that both ML228 and IOX4 significantly increased β-Synuclein protein expression and reduced Synphilin-1 protein levels in dSH-SY5Y, replicating the effect of the treatments on *SNCB* and *SNCAIP* at the transcriptional level (Fig. 6.9c, d). Indeed, HIF-1α appears as an expression interaction partner of *SNCB* in the database Pathway Commons (Fig. 6.9e). This information was obtained from a Gene Set Enrichment Analysis list of genes having at least one occurrence of the motif matching the *HIF1A* TF binding site. After screening of the *SNCB* promoter against HREs using the JASPAR database and comparing these TF binding sequences against those in other primate species with the BLAST software, a candidate promoter sequence that contains a HRE which is conserved across species was identified (Fig. 6.9f).

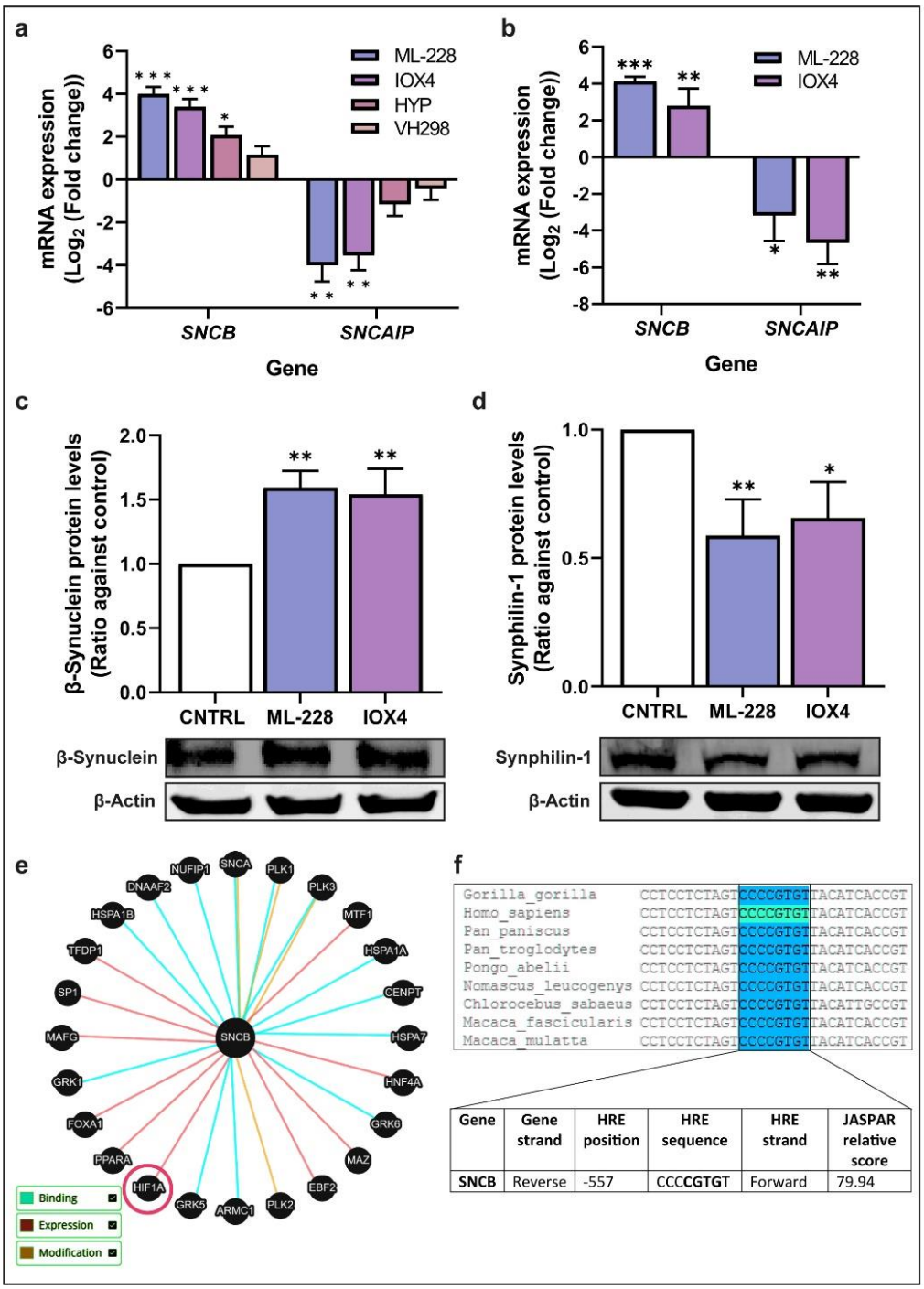

Gene	Gene strand	HRE position	HRE sequence	HRE strand	JASPAR relative score
SNCB	Reverse	-557	CCCCGTGT	Forward	79.94

Figure 6.9. Identification of *SNCB* as potential target of HIF-1α in fdSH-SY5Y. **a.** Graph that shows mRNA expression levels, as a fold change against control, of *SNCB* and *SNCAIP,* assessed by Nanostring nCounter in samples from fdSH-SY5Y treated with ML-228, IOX4, 1% O_2 or VH298 for 24h (n=3). **b.** Graph that shows mRNA expression levels, as a fold change against control, of *SNCB* and *SNCAIP,* assessed by qRT-PCR in samples from fdSH-SY5Y treated with ML-228 or IOX4 for 24h (n=3). **c**. Graph that demonstrates protein levels, as ratio against control, of β-Synuclein in samples from fdSH-SY5Y treated with ML-228 or IOX4 for 24h (n=3). **d**. Graph that demonstrates protein levels, as ratio against control, of Synphilin-1 in samples from fdSH-SY5Y treated with ML-228 or IOX4 for 24h (n=3). **e**. Scheme obtained from Pathway Commons depicting the main 25 interactions of *SNCB,* where *HIF1A* is highlighted. **f**. Image of the alignment of a specific section of the *Homo Sapiens SNCB* gene containing a potential HRE with 8 primate species, accompanied by the information about the specified HRE obtained from JASPAR database. Statistical analysis was performed using an unpaired two-tailed Student's t test where p<0.05 was recorded as "*".

6.3.7. Differential expression of genes involved in the immune response

The DEGs included in the GO terms and in Nanostring gene sets related to the immune response (SI Table 8.8) are presented on the following heatmaps (Fig. 6.10a, b). As mentioned, HIF-1α is crucial for the correct functioning of the cells of the immune system, and several of its known targets, such as chemokine ligands (*CCL5, CXCL16*) and cytokine receptors (*CXCR4*, *IL10RA*, *TNFRSF12A*) were shown to be overexpressed following treatment. Due to modification in the expression of the glycolytic gene *PGK1* and taking into consideration that the glycolytic metabolism pathway is key for immune cell activation (Ganeshan and Chawla, 2014), the expression of other genes involved in glucose metabolism were investigated. This highlighted changes in the expression of other glycolytic genes such as *SLC1A1*, *PGAM1* and *DLAT* (Fig 6.10 c). qRT-PCR analysis demonstrated that the variation in the expression of the genes *IL10RA*, *CXCR4* and *PGAM1* corresponded to the results obtained in the transcriptomic analysis (Fig. 6.10d).

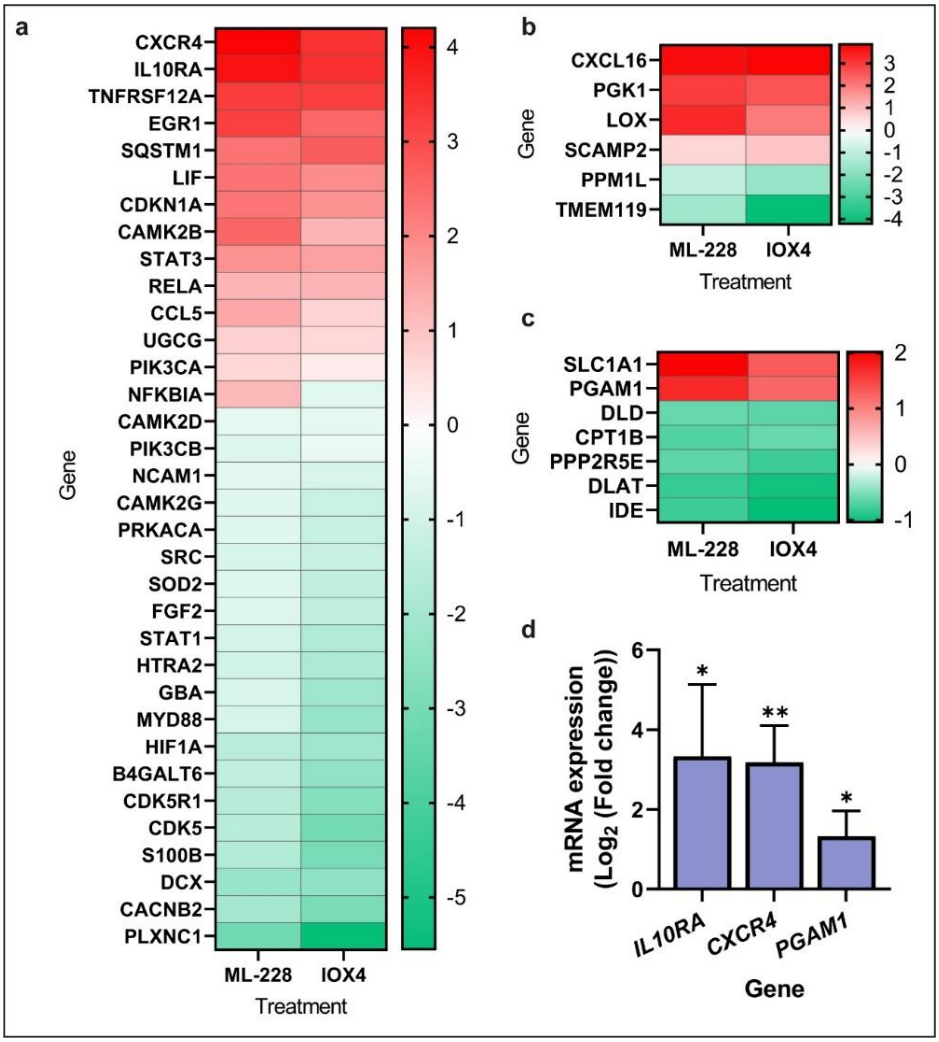

Figure 6.10. Common DEGs involved in the immune response in ML228 and IOX4 treated fdSH-SY5Y. The heatmaps show the fold change in the expression of genes compared to control. **a.** Heatmap that includes DEGs in GO terms related to the immune response. **b.** Heatmap that includes DEGs in Nanostring gene sets related to the immune response. **c.** Graph that shows mRNA expression levels, as a fold change against control, of *IL10RA* and *CXCR4* and *PGAM1* assessed by qRT-PCR in samples from fdSH-SY5Y treated with ML-228 for 24h (n=3). Statistical analysis was performed using an unpaired two-tailed Student's t test where $p<0.05$ was recorded as "*".

6.3.8. Differential expression of genes involved in transcription

The DEGs included in the GO terms and in Nanostring gene sets related to transcription (Appendix Table) are presented on the following heatmaps (Fig 6.11 a, b). As a TF, it is no surprise that by inducing HIF-1α response, there would be changes in genes involved in Chromatin remodelling (*DOT1L*, *HDAC2*, *PHF19*, *HMGB1*, *PHF2*, *ATXN7*), RNA Polymerase II activity (*GTF2H3*, *TAF4*), subunits of RNA Polymerase II (*POLR2H*, *POLR2L*) and other TFs (*FOS*, *JUN*, *STAT3, STAT1, HIF1A*). Intriguingly, the enrichment analysis highlighted that there were genes modified by the treatments that participate in mRNA splicing (*DDX23*, *HNRNPM*, *LSM2*), transcription of spliceosome components Small nuclear RNAs (snRNAs) (*CDK7*, *SP1*, *GTF2B*) and primary miRNA transcription (*EGR1*, *SOX9*, *FGF2*). qRT-PCR analysis demonstrated that the variation in the expression of the genes *DOT1L* and *PHF19* corresponded to the results obtained in the transcriptomic analysis (Fig 6.11 c).

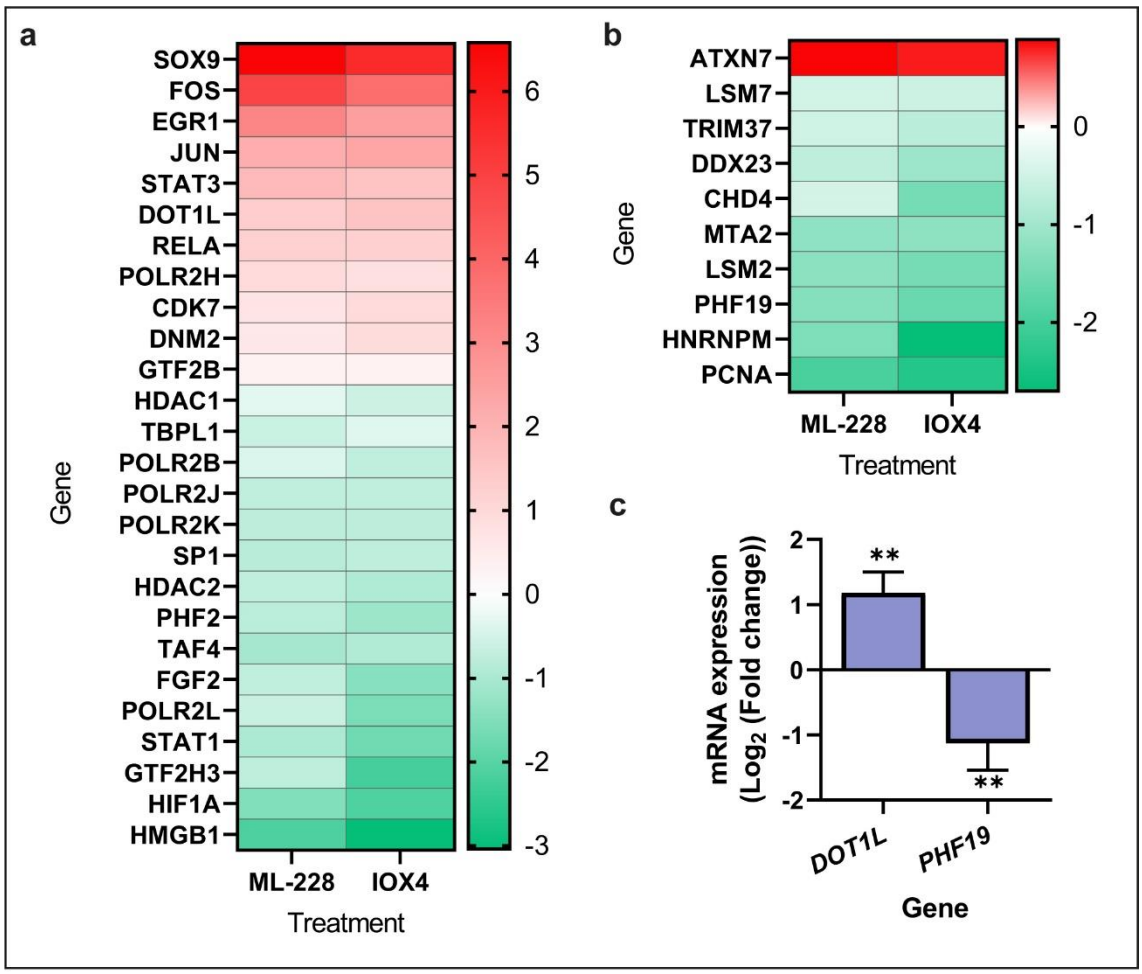

Figure 6.11. Common DEGs involved in transcription in ML228 and IOX4 treated fdSH-SY5Y. The heatmaps show the fold change in the expression of genes compared to control. **a.** Heatmap that includes DEGs in GO terms related to transcription. **b.** Heatmap that includes DEGs in Nanostring gene sets related to transcription. **c.** Graph that shows mRNA expression levels, as a fold change against control, of *DOT1L* and *PHF19* assessed by qRT-PCR in samples from fdSH-SY5Y treated with ML-228 for 24h (n=3). Statistical analysis was performed using an unpaired two-tailed Student's t test where $p<0.05$ was recorded as "*".

6.4.DISCUSSION

Our investigation employed differentiated SH-SY5Y cells treated with various HIF-1α stabilizers to analyse the HIF-1α transcriptome, identifying potentially novel neuronal pathways regulated by HIF-1α. The following section delves into these findings, particularly focusing on genes and pathways with uncharacterized links to HIF-1α and their potential relevance to PD.

6.4.1. Widespread alterations in gene expression induced by ML228 and IOX4

This study shows that ML228 and IOX4 treatments caused extensive changes in gene expression patterns, while hypoxia only deregulated a small number of genes and treatment with VH298 had no detectable impact on gene expression (Fig 6.2). In contrast, multiple studies demonstrate that hypoxia causes genome-wide changes in gene expression (Cimmino et al., 2019; Zhang at al., 2023). To date, only one study has utilized RNA-Seq to examine the distinct effects of various PHD and VHL inhibitors. This study investigates the effect of hypoxia (1% O_2) and the earlier-generation PHD inhibitor IOX2 and VHL inhibitor VH032, precursors to IOX4 and VH298 respectively, in HeLa cells. Interestingly, this study found that while hypoxia induced the most extensive transcriptional changes, IOX2 and VH032 elicited comparable transcriptional responses, although these do not completely overlap. This limited research underscores the potential variability in how distinct HIF-1α stabilization methods induce the transcriptional response, which has been shown by the present study as well. Furthermore, it highlights the possibility of off-target effects, as reported in the literature, due to altered activity of other proteins following PHD or VHL inhibition (Frost et al., 2016; Yeh et al., 2017). The limited response observed in VH298-treated cells could be attributed to several factors, including a potentially insufficient concentration of the drug. Similarly, inconsistencies in the hypoxic environment due to equipment malfunctioning or suboptimal sample processing might explain the muted response to hypoxia. To address these possibilities, future studies could benefit from incorporating parallel protein analysis alongside RNA-Seq. This would allow verification of consistent HIF-1α stabilization across all samples.

6.4.2. The links between HIF-1α signalling and genes involved in apoptosis

HIF-1α appears to have a dual role in brain diseases such as TBI and evidence of this fact is found in the Nanostring analysis where both pro-survival and apoptotic genes are deregulated. While most of these genes are already known targets of HIF-1α, including

some non-typical targets such as *NOL3* (Razorenova et al., 2014) their investigation in neuronal cells remains useful in order to verify that these pathways can be active and play a role in neuronal function and pathology. Some of these genes, such as several apoptosis-inducing members of the tumour necrosis factor receptor superfamily, are likely regulated by cell energy levels and do not constitute direct targets of HIF-1α. Of interest is the influence of HIF-1α stabilizing drugs on the downregulation of *CDK5* and its activation partner *CDK5R1* and the regulatory subunit *CDK5RAP3,* all found to be differentially expressed in this study (Fig.6.4). CDK5 is a cyclin-dependent kinase that is mainly expressed in neurons, where it plays vital roles in survival and homeostasis. It is activated by binding to p35 (*CDK5R1*) but when bound to the proteolytic fragment p25, CDK5 becomes hyperactive, causing indiscriminate phosphorylation of substrates leading to cell death (Roufayel and Murshid, 2019). Although neither CDK5 nor its cited partners have been investigated as HIF-1α targets, it has been established that CDK5 can in turn stabilize HIF-1α by phosphorylation (Antoniou et al., 2011). The CDK5 system is of special interest in PD, as CDK5 inhibition alleviates neuronal apoptosis in a PD animal model (He, R. et al., 2018). Thus, it would certainly be relevant to investigate if the effect observed on *CDK5*, or any of its partners, translates to changes in their protein levels and activity and whether it is linked to HIF-1α.

6.4.3. The links between HIF-1α signalling and genes involved in autophagy

The widely studied effect of HIF-1α in autophagy induction is observed in the Nanostring analysis, which shows expected changes in core HIF-1α targets involved in autophagy activation. The differential expression of several genes involved in lysosomal function not previously related to HIF-1α is noteworthy (Fig.6.5). Indeed, the lysosomal enzyme N-acetylglucosaminidase α gene (*NAGLU)* is downregulated under ML-228, IOX4 and hypoxia treatments, showing a potential link between these factors. Conversely, the lysosomal gene Niemann-Pick disease, type C1 (*NPC1*), which controls cholesterol trafficking, is upregulated. Mutations in both these genes and others also deregulated by the HIF-1α-stabilising treatments, including PD-linked *GBA*, cause Lysosomal storage diseases, where exaggerated accumulation of products in the lysosomes disrupts the autophagic pathway (Myerowitz et al., 2021). Taking into consideration that this transcriptomic data shows deregulation of several lysosomal genes and that HIF-1α is already known to be involved in autophagy, it would be interesting to further investigate the role of HIF-1α in lysosomal homeostasis and Lysosomal storage diseases. Remarkably, this might have an impact on other neurodegenerative conditions like PD,

where there seems to be a high occurrence of polymorphisms of Lysosomal storage disorder-associated genes (Robak et al., 2017).

6.4.4. The links between HIF-1α signalling and genes involved in cell signalling

HIF-1α is clearly intertwined with cellular signalling, influencing important membrane receptors, intracellular signalling molecules and other TFs, as shown in the transcriptomic analysis (Fig.6.6). Certainly, many of the genes in these pathways are not direct targets of HIF-1α, but a consequence of downstream signalling cascades. The information obtained shows that several pairs of genes involved in similar pathways (*NOTCH1* and *NOTCH4*, *STAT1* and *STAT3*, etc) are regulated differently pointing to a very specific regulation of these signalling cascades that might be relevant in neuronal cells. Interestingly, several known HIF-1α target genes identified by the analysis are involved in NS functions, such as the receptor *NOTCH1*, which controls neurogenesis (Li et al., 2018) and the TF *EGR1*, which seems to have a role in neuronal plasticity (Duclot and Kabbaj, 2017; Yan et al., 1999), show increased levels after the treatments. This study provides evidence that HIF-1α also controls these signal transduction genes in neuronal cells. In addition, the multifunctional cytokine gene *LIF*, with a role in neuronal differentiation, is also upregulated (He et al., 2006). However, the expression of this gene is controlled by HIF-2α in cancer (Wu et al., 2015). The drugs used in this study might also induce stabilization of HIF-2α and thus it would be necessary to investigate the possibility that some of the DEGs are controlled by this TF instead of HIF-1α.

6.4.5. The links between HIF-1α signalling and genes involved in cation channel function

The transcriptomics data acquired in this study shows several changes in genes particularly involved in Ca^{2+} signalling, including Ca^{2+} channels and Ca^{2+} binding proteins (Fig.6.7). It is interesting to note that hypoxia-mediated calcium upregulation has been closely associated with the stimulation of *HIF1A* gene transcription, HIF-1α translation, and HIF-1α stabilization, so control of Ca^{2+}-related proteins by HIF-1α could potentially act as a feedback mechanism (Lee et al., 2019). The impact of HIF-1α/hypoxia on Ca^{2+} trafficking has been explored by many research articles. However, these investigations have been performed under very specific physiological or pathological settings and a recent review unifying this knowledge and mentioning this link in the NS is not available.

Ca^{2+} is a crucial factor in synaptic transmission, where Ca^{2+} influx via voltage-gated channels opened in response to a presynaptic action potential serves as a signal for

neurotransmitter release (Sudhof, 2012). L-type calcium channels are voltage-dependent Ca^{2+} channels found in the plasma membrane of neurons and composed of five different subunits, including an α and a β subunit, that have four different isoforms (Striessnig et al., 2014). In this study, marked downregulation of L-type calcium channel α 1D subunit (*CACNA1D*), as well as two regulatory β subunits (*CACNB2*, *CACNB4*) is reported. Interestingly, the channels that contain this α 1D subunit, named $Ca_v1.3$, have been of interest in PD pathology after several studies linked these channels to SNpc vulnerability in PD (Verma and Ravindranath, 2020). Although a clinical trial investigating the effectiveness of $Ca_v1.3$ blocker isradipine against stopping or delaying PD progression showed no benefit, later studies proved limited $Ca_v1.3$ inhibition by this drug in SN DAergic-like neurons (Ortner et al., 2017). Thus, this therapeutic avenue remains open and determining the connection, hinted by this study, between hypoxia/HIF-1α-mediated signalling and $Ca_v1.3$ in neurons holds promise for discovery of novel therapeutic approaches. Ca^{2+} channels are not only located in the plasma membrane, but also in subcellular organelles that act as Ca^{2+} reservoirs, such as the sarcoplasmic reticulum. One of these channels is the ryanodine receptor family (Abu-Omar et al., 2018), whose three members are included in the Nanostring panel utilised. The results from this study indicate increased gene expression of *RYR2*, which has also been reported in HIF-1α-transduced ESC-derived cardiomyocytes (Ng et al., 2010). RNA levels of *HOMER1*, which encodes a protein regulating Ca^{2+} efflux through RYR2 channels, are also elevated (Westhoff et al., 2003). This evidence might indicate increased activity of RYR2 channels, shown to be beneficial in PD models (Vervliet, 2018). Besides Ca^{2+} trafficking via channels, intracellular Ca^{2+} levels are also controlled by a set of Ca^{2+} binding proteins, such as the ones encoded by the *CALB1* and *S100B* genes, which are severely downregulated by the treatments tested in this study. Interestingly, both increasing *CALB1* levels and reducing *S100B* expression proves to be neuroprotective in PD animal models (Angelopoulou et al., 2021; Inoue et al., 2018). Thus, in this specific research context, downregulation of Ca^{2+} channels on the cell membrane probably reduced Ca^{2+} entry while less Ca^{2+} sequestration and increased Ca^{2+} release from the sarcoplasmic reticulum might have caused increased intracellular levels of free Ca^{2+}, rendering total Ca^{2+} levels unchanged as seen in the fluorescence based Ca^{2+} detection assay performed. Ca^{2+} currents also regulate several other key processes in neurons, including synaptic plasticity and memory consolidation, activating a subset of kinases such as Calcium/calmodulin-dependent protein kinase type II (CAMKII) that subsequently induce the expression of an array of TFs and proteins involved in these pathways (Yasuda et al., 2022). *CAMKIIB*,

which encodes for the NS-targeted CAMKII β isoform is upregulated, while ubiquitous δ and γ isoforms (*CAMKIID* and *CAMKIIG*) are slightly downregulated. These subunits seem to have different roles in neuroplasticity and memory (Zalcman et al., 2018). The finding that HIF-1α controls CAMKII isoform expression levels suggests that this transcription factor may play a role in neuroplasticity, as proposed by recent investigations (Javed Butt et al., 2021). Remarkably, the previously mentioned RYR2 and HOMER1 proteins have also been identified as important players in synaptic plasticity (Clifton et al., 2017).

In conclusion, the numerous changes in specific Ca^{2+}-related genes seen in this study indicate an involvement of the HIF-1α response in this pathway that merits further investigation. Evidently, the RNA panel used does not capture the full range of genes involved in Ca^{2+} signalling, so it would be advantageous to broaden the scope of the analysis to include more genes involved in this process in order to obtain a more complete picture.

6.4.6. The links between HIF-1α signalling and genes involved in neuronal development and activity

This investigation has highlighted the role of HIF-1α in synaptic transmission and axonal homeostasis, two pathways that are impaired in PD (Gcwensa et al., 2021) .

Although several neurotransmitter receptor types are present in the panel, the treatments selectively modify specific members of these protein families, including receptors for the main excitatory neurotransmitter, glutamate, as well as the principal inhibitory neurotransmitter, Gamma-Aminobutyric Acid (GABA) (Fig.6.8). Indeed, the different subunits of the ionotropic Glutamate AMPA receptor (*GRIA2*, *GRIA3*, *GRIA4*) are specifically deregulated by the treatments, which has been described by a previous study in cancer cell lines (Hu et al., 2014). The cited study also describes increased expression of Excitatory amino acid transporter 3 (*SLC1A1*), which is also detected in this investigation. Several additional components of AMPA glutamatergic synapses, such as *DLG4* and *ARC*, are markedly upregulated and have not been previously linked to HIF-1α. Thus, this study supports a role of HIF-1α in glutamate signalling via these specific proteins in neuronal cells. Glutamate receptors, along with their mentioned interacting partners, have a prominent role in synaptic plasticity and memory consolidation (Nikolaienko et al., 2018; Torquatto et al., 2019). The finding that stabilization of HIF-1α is associated with changes in the genes that encode these proteins corroborates the

emerging evidence for the role of HIF-1α in these processes (Javed Butt et al., 2021) and provides candidate genes for future investigation. Glutamate can be transformed into GABA by glutamic acid decarboxylase 1 (*GAD1*), whose mRNA is elevated in this study. Interestingly, advanced PD patients who received cerebral delivery of GAD1 by an adeno-associated viral vector showed significant improvement in motor symptoms over baseline (Niethammer et al., 2017). While GABA-synthesising GAD1 is upregulated, the ionotropic GABA receptor pi subunit gene (*GABRP*) is severely decreased. The gene encoding the glycine receptor β subunit (*GLRB*), which can colocalise with GABA receptors, is also downregulated. Both Ionotropic GABA and Glycine receptors are essential for neurodevelopment (Peerboom and Wierenga, 2021; Salceda, 2022), as are some HIF-1α induced genes identified in this investigation, including *SOX9, VEGFA* and *NOTCH1*. Thus, the findings of this study add to the mounting evidence that HIF-1α plays a role in NS development (Bohuslavova et al., 2019). Another known HIF-1α target, the gene coding for the adenosine receptor 2A, *ADORA2A*, which also plays a role in glutamate and DA release, is increased. The role of ADORA2A as an inhibitor of DA release has led to the development of ADORA2A inhibitors to administer in conjunction with levodopa for PD treatment (Chen et al., 2020).

HIF-1α-stabilizing treatments not only affect neurotransmitter receptors, but also appear to have an impact on synaptic vesicle trafficking (Fig.6.8). This is supported by the altered levels of several genes linked to this activity, including *RAB3A*, *RAB3C*, and *SYT4*. The key finding of this study is the identification of two deregulated proteins involved in this process, β-Syn (*SNCB*) and Sph-1 (*SNCAIP*), which constitute interacting partners of α-Syn (Fig.6.9). Although they have not been previously linked to HIF-1α, this study showed upregulation of *SNCB* and downregulation of *SNCAIP*, which was replicated when analysing respective protein levels. β-Syn modulates synaptic transmission via its lipid-binding activity, regulates cell death, acts as a molecular chaperone and controls autophagic and proteasomal protein degradation (Hayashi et al., 2022). β-Syn can form heterodimeric complexes with α-Syn and reduce its expression, thereby decreasing the formation of α-Syn oligomers and protecting against α-Syn-mediated neurotoxicity (Janowska et al., 2015; Angelova et al.,2018). Subsequently, recent evidence suggests that β-Syn binds synaptic vesicles with lower affinity than α-Syn and that, likely as a consequence, the presence of β-Syn lowered α-Syn attachment to synaptic vesicles (Carnazza et al., 2022). The role of β-Syn in regulating α-Syn levels, assembly and affinity towards synaptic vesicles might be a potential target in the development of

therapeutic strategies focused on α-Syn aggregation. Indeed, β-Syn-based therapies have shown potential in reversing PD phenotypes in animal models (Windisch et al.,2002; Hashimoto et al., 2004; Shaltiel-Karyo et al., 2010). In turn, Sph-1 is localised at synapses and abundant at Lewy body lesions in PD patients, although its role is unclear (Eyal et al., 2006). While Sph-1 overexpression was reported to be protective against MPP+-mediated apoptosis in SH-SY5Y cells (Shishido et al., 2019), multiple studies described that Sph-1 caused α-syn aggregation and neurotoxicity in primary neurons and animal models (Eyal et al., 2006; Nuber et al., 2010; Carvajal-Oliveros et al., 2023). The findings of this study, which show that HIF-1α stabilization leads to the upregulation of β-Syn and downregulation of Sph-1 could be of interest in the development of new PD therapeutic approaches.

As aforementioned, several deregulated genes revealed by this study are involved in neurite dynamics (Fig.6.8). The *EPHA2* gene is a member of the ephrin family that controls axonal growth and guidance that has been identified as a hypoxia-sensitive gene in cancer (Husain et al., 2022), but the existence of a HIF-1α-EphA2 axis in neurons has not been explored to date. This gene, alongside others also implicated in axon growth, such as *DNM2* and *LRP1*, are upregulated in this investigation. Conversely, several other genes encoding proteins that also participate in axon dynamics are reduced, including βII Spectrin (*SPTBN2*), Plexin C1 (*PLXNC1*) and CD90 (*THY1*). Although HIF-1α has been shown to be involved in axonal regeneration following injury, the full complement of HIF-1α target genes involved in this process is not yet known (Cho et al., 2015). This study provides evidence that additional genes may be involved, and further research is needed to identify these genes and understand their link to HIF-1α.

In addition to synaptic and axonal growth dysfunction, alterations to myelination have also been identified in sporadic PD patients (Boshkovski et al., 2022). Intriguingly, although HIF-1α has only been superficially linked to myelination previously, several genes participating in this process are upregulated by the HIF-1α-stabilizing treatments. These include novel potential HIF-1α targets myelin regulatory factor (*MYRF* gene), Hyccin (*FAM126A* gene) and Attractin (*ATRN* gene). *FAM126A* was reported as hypoxia-responsive gene by two different meta-analyses but was not validated (Benita et al., 2009; Bono, 2020). These findings provide further evidence for the recently described role of HIF-1α in developmental myelination (Zhang et al., 2021) and reveal a new set of genes that may be important for this process. Of note, these results provide further evidence that the *MYRF* gene is not only expressed in oligodendrocytes, as previously thought

(Nakayama et al., 2018) and it is also expressed in SH-SY5Y cells, representing neurons. This is important as although oligodendrocytes carry out myelination, neurons actively support this process. To summarize, while the role of HIF-1α in the development and preservation of myelin sheaths remains poorly understood, the discovery of potential HIF-1α transcriptional targets involved in myelination opens a new and promising area of research.

The results obtained in this study establish HIF-1α as a multifaceted gene in neuronal function. This study supports the involvement of HIF-1α in well-researched processes, such as neuronal development, while indicating its participation in novel functions only superficially associated to HIF-1α previously, such as memory consolidation, axonal growth and myelination. As mentioned, many of these processes are impacted in PD development and could constitute promising therapeutic targets.

6.4.7. The links between HIF-1α signalling and genes involved in the immune response

The genes that are targeted by HIF-1α in immunity have been the subject of intense study, and several of them have been shown to be upregulated in this investigation (Fig.6.10), including pro- inflammatory chemokine receptor *CXCR4* and pro-proliferation chemokine *CXCL16* (Korbecki et al., 2021). Intriguingly, HIF-1α-stabilizing treatments also induce the mRNA expression of a previously unknown HIF-1α potential target, the anti-inflammatory Interleukin-10 receptor gene *IL10RA*. With neuroinflammation now being recognised as a hallmark of PD pathogenesis, unravelling the relationship between HIF-1α stabilization and the immune response in the NS could yield new insights into PD development (Tansey et al., 2022).

Interestingly HIF-1α can mediate a switch to glycolysis to provide energy for immune cells in low O_2 environments, which is essential for the proper functioning of the immune system (McGettrick et al., 2020). The results obtained provide new insights into the precise mechanisms by which HIF-1α regulates glucose metabolism in neuronal cells (Fig.6.10). Firstly, upregulation of glucose transporter GLUT1 (*SLC1A1*) and downregulation of Insulin degrading enzyme (*IDE*) boosts glucose entry in the cell, which is converted in pyruvate by highly expressed Phosphoglycerate Mutase 1 (*PGAM1*). The rate of conversion of pyruvate to Acetyl-CoA and its progression through the TCA is hampered by reduced levels of Pyruvate dehydrogenase (*DLAT*) and Dihydrolipoamide dehydrogenase (*DLD*) respectively. This allows a higher flux of pyruvate to be directed

towards glycolysis, which is enhanced by increased levels of Phosphoglycerate kinase 1 (*PGK1*). In addition, downregulation of carnitine O-palmitoyltransferase 1b (*CPT1B*), which facilitates mitochondrial uptake of long chain fatty acids, reduces substrate availability for the O_2-consuming β-oxidation (Angelini et al., 2021). As explored in the previous chapter, enhanced glycolytic flux via induction of PGK1 can slow down PD progression (Cai et al., 2019), so knowledge regarding HIF-1α as a critical regulator of this pathway could lead to the development of new drugs or other interventions that target glycolysis.

6.4.8. The links between HIF-1α signalling and genes involved in transcription

In addition to its function as a TF, HIF-1α controls epigenetic mechanisms, which are recently being uncovered and hold important functions in health and disease. HIF-1α mediated induction of epigenetic regulators which can contribute to the induction of HIF-1α target genes while also acting as a feedback mechanism by controlling HIF-1α levels (Chen et al., 2020). In fact, HIF-1α changes the levels of genes that encode proteins involved in several aspects of chromatin reprogramming (Fig.6.11). Indeed, the analysis shows increased expression of the Histone methyltransferase *DOT1L*, which is linked to transcriptional activation, and had only previously discovered as HIF-1a target in articular cartilage (De Roover et al., 2021). The demethylase *PHF2* and methylation regulator *PHF19* are in turn reduced by the treatments. HIF-1α is also known to regulate histone acetylation levels, which is reflected in the analysis by the inhibition of several genes on the NurD deacetylase complex, which leads to chromatin condensation, including *HDAC1*, *HDAC2*, *MTA2* and *CDH4*. Importantly, dramatic upregulation of *ATXN7*, component of several acetyltransferase complexes, has not been previously linked to HIF-1α to date and might constitute a novel target. The decrease in *TRIM37* levels, a histone ubiquitin ligase that is associated with transcriptional inhibition, suggests that HIF-1α may also regulate histone degradation. General regulator of transcription *HMGB1*, which controls the binding to DNA of several TFs, is also markedly downregulated. Some TFs have also been known to be influenced by HIF-1α, including STAT3, SOX9, EGR1 and AP-1, a heterodimer of c-fos and c-jun (*FOS* and *JUN*). Interestingly, HIF-1α and some of its targets like SOX9 and EGR1, have been implicated in the control of miRNA synthesis, as identified in the pathway enrichment analysis and described in literature (Peng et al., 2020). Certain TFs, like STAT3 and AP-1, can be involved in the recruitment of the transcription machinery to HREs (Pawlus et al., 2014; Michiels et al., 2001). In

addition, this transcriptomic analysis shows reduced expression of *GTF2H3*, member of the Transcription factor II H complex, *TAF4*, subunit of the transcription factor II D and *GTF2B,* the transcription factor II B. These TFs take part on the assembly of the RNA polymerase II preinitiation complex. The genes coding for the subunits of RNA polymerase II, which transcribes DNA, are also modified by the HIF-1α stabilizing treatments, with a moderate increase in subunit 8 levels (*POLR2H*) and lowered expression of subunits 2,11,12 and 10 (*POLR2B*, *POLR2J*, *POLR2K*, *POLR2L*). Besides controlling chromatin accessibility, HIF-1α also plays a role in the regulation of pre-mRNA splicing (Farina et al., 2020). In fact, genes encoding for proteins involved in this process such as U6 snRNA-associated Sm-like proteins *LSM2* and *LSM7*, RNA helicase *DDX23* and RNA binding protein *HNRNPM* are downregulated. Some of these epigenetic systems may contribute to a HIF-1α feedback mechanism by reducing *HIF1A* transcription, as seen in this experiment.

Gene transcription is a very complex process regulated at multiple levels, so it is difficult to determine a specific role of HIF-1α. However, from the data obtained, it seems HIF-1α can increase chromatin accessibility in neuronal cells by reducing the expression of histone deacetylases, demethylases and ubiquitinases, while inducing the expression of histone acetylases and methylases. The role of HIF-1α in neurons might be intertwined with its ability to regulate epigenetic mechanisms, which are in turn implicated in neuronal development and differentiation, as well as neuropathologies. Indeed, several histone-modificating proteins, such as DOT1L and HDACs, support neurogenesis while in neurodegenerative diseases such as PD, HDAC inhibitors are being developed due to their promising neuroprotective potential (Park et al., 2022).

This data supports the role of HIF-1α as an important regulator of mRNA dynamics, from pre-mRNA translation to its splicing. The discussed findings agree with the recent notion that regulation of gene expression by HIF-1α is substantially more complex than previously considered, including HIF-1α-mediated recruitment of additional TFs and chromatin restructuration. The study of HIF-1α-mediated changes in epigenetic and splicing mechanisms specifically in neurons and other cell types in the NS can shine a light on new therapeutic pathways in neurodegeneration.

6.5. CONCLUSION

The Nanostring nCounter RNA profiling platform was successfully utilised to identify a novel set of genes in neuronal cells that constitute potential HIF-1α targets (Fig.6.12). To confirm that the genes identified are indeed HIF-1α targets, their promoter should be scanned with bioinformatic tools in order to identify candidate HREs. Subsequently, the capacity of HIF-1α to bind these specific sequences and activate gene transcription can be investigated by ChIP, which can be used to identify the specific HREs bound by HIF-1α, and luciferase reporter assays, which can be employed to measure the transcriptional activity of these HREs under the influence of the HIF-1α stabilising drugs utilized in this study.

Further validation of the HIF-1α targets can be achieved with additional experiments. The utilization of different HIF-1α stabilization paradigms allowed this study to detect the differences in the response elicited by hypoxia and different drugs. However, due to experimental issues, it was not possible to include samples with silenced HIF-1α. Therefore, to ratify the findings of this study, it is necessary to confirm that the effects seen are specifically due to HIF-1α and not HIF-2α, which is also potentially stabilized by the treatments. To discriminate between the two TFs, it would be ideal to KO both genes separately and evaluate the effect of this silencing on the candidate target genes. To further confirm the findings of this research, the expression of these genes should be examined in other cell models. The differentiated SH-SY5Y neuroblastoma cell line was used due to lower cost and suitability for a high throughput analysis. This also contributed to the knowledge on the genes specifically expressed by differentiated SH-SY5Y cells, representing neurons. Nevertheless, it is necessary to replicate the results of this investigation in other neuronal models, including iPSCs and different subsets of primary neurons. Although this study focused on investigating neuronal cells, the rest of the cellular players in the NS should also be taken into consideration. Thus, it would be of great interest to probe the responsiveness to HIF-1α of the selected genes in different cell types in the NS, such as astrocytes. In order to gain a more complete understanding of the real consequences of HIF-1α stabilization at the cellular level in the NS, other factors should be considered. Indeed, this technique measures mRNA expression, but it does not account for splicing variants, protein levels, post-translational modifications, or protein activity. Non-coding RNAs are also not represented in the panel, so investigating these should be considered as well. Investigating the impact of HIF-1α stabilization on these factors would complement the analysis performed in this project.

This study provides evidence that supports the existence of novel HIF-1α targets in neuronal cells, which could be confirmed in upcoming studies. These candidate targets include genes not previously linked to HIF-1α, genes linked to HIF-1α outside the NS, and known HIF-1α targets. Pathway enrichment analysis suggests that HIF-1α may be involved in important NS functions such as myelination, which has not been previously described, as well as other pathways where only limited evidence is present, such as axonal dynamics and memory formation. As described in the discussion, several of these genes and pathways are linked to PD pathogenesis and constitute potential therapeutic targets. Therefore, future validation of this study is likely to increase our understanding of the HIF-1α neuronal targetome and the NS pathways in which HIF-1α plays a role, while also contributing to our understanding of neurodegenerative diseases such as PD.

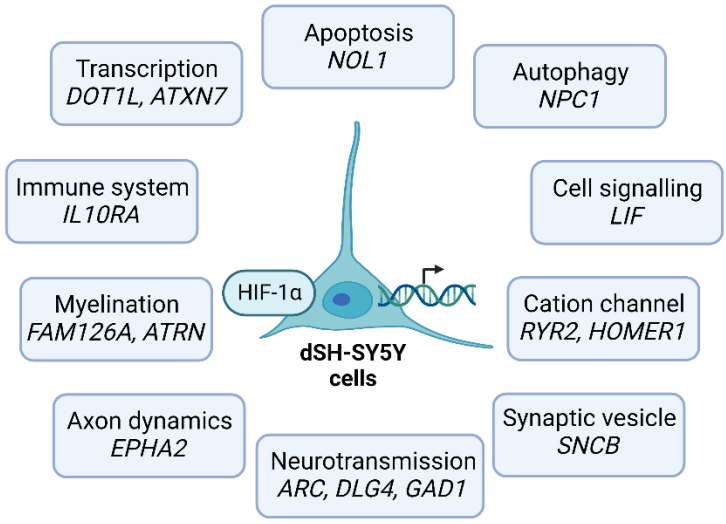

Figure 6.12. Novel HIF-1α potential target genes in neuronal cells. The illustration shows a selection of genes described in this study grouped in different pathways. These genes are significantly upregulated upon HIF-1α stabilizing treatments and have not been described as HIF-1α responsive in neuronal cells by previous research.

CHAPTER VII

CONCLUSIONS AND FUTURE DIRECTIONS

7.1. CONCLUSIONS

Despite decades of research, the underlying causes of DAergic neuronal loss in PD remain elusive. This makes the development of effective therapeutic solutions challenging, as evidenced by the lack of disease-modifying drugs currently available to PD patients (Emamzadeh and Surguchov, 2018). Deficits in HIF-1α stabilization, alongside HIF-1α polymorphisms have been implicated in PD (Qin et al., 2019). Furthermore, risk factors associated with hypoxic episodes have been linked to PD development (Gardner et al., 2018) . In addition, multiple HIF-1α stabilizers have shown neuroprotective potential in animal and cellular PD models (Lestón Pinilla et al., 2021). Thus, this research investigates the complex interplay between the hypoxia response via HIF-1α and the biochemical events that are associated with PD. The research identifies several key factors involved in linking these parameters some of which are novel and have not been previously described. HIF-1α and hypoxia signalling have also been implicated in other neurodegenerative diseases, such as AD (Sun et al., 2006), which suggests that this investigation could have far-reaching implications. The main findings of this study are outlined below.

7.1.1. Hypoxia and HIF-α stabilisation can modify the levels of proteins associated with PD

This study is the first systematic investigation of the responsiveness of a set of PD-related genes to HIF-α stabilization. Several genes, including ATP13A2, DJ1, PINK1, PRKN, and VPS35, produced high prediction scores for the presence of hypoxia response elements (HREs) in their promoters. However, treatment of SH-SY5Y cells with $CoCl_2$ to stabilise HIF-1α did not increase the levels of any of the proteins encoded by these genes. Instead, $CoCl_2$ treatment decreased the levels of ATPase 13A2 and PINK1. These results were replicated when SH-SY5Y cells were cultured in a hypoxic environment, suggesting that the observed effect was likely HIF-dependent. Interestingly, the mRNA expression of ATP13A2 and PINK1 remained unchanged, indicating that HIF does not regulate protein levels by reducing gene expression. The reduction in PINK1 was also observed in another neuronal cell population, dLUHMES cells, but not in cells of astroglial origin, U-87MG, whilst the decrease in ATP13A2 was not replicated in either dLUHMES or U-87MG cells. These findings highlight the fact that HIF-1α can have different effects depending on cell type, which is consistent with recent literature (Xia and Kung, 2009). The reduction in PINK1 levels under conditions that stabilize HIF-1α appears to be restricted to neuronal cells. Although more research is needed, this finding

suggests a potential mechanism by which hypoxic events, often a consequence of TBI or stroke could increase the risk of PD (Gardner et al., 2018).

7.1.2. Deregulation of pathways involved in PD pathogenesis can impair HIF-1α stabilisation

This study investigated how alterations in PD-related pathways affected HIF-1α stabilisation during PHD inhibition. Mitochondrial dysfunction caused by MPP+ reduced HIF-1α levels independently of PHD inhibition, in both SH-SY5Y and U-87MG cells. Antioxidants did not reverse this effect, but cotreatment with the autophagy blocker CQ did. Additionally, MPP+ reduced *HIF1A* mRNA expression. An increased production of ROS by AAPH also reduced HIF-1α levels, but only in neuronal cell populations, SH-SY5Y and dLUHMES cells. This effect was ameliorated by the addition of the antioxidants, NAC and GSH, irrespectively of the PHD inhibitor used. Similar to the response seen with MPP+, cotreatment with CQ rescued HIF-1α levels in neuronal cells, although HIF1A mRNA levels remained unaltered. Both treatments induced a significant reduction in proteasome activity. Therefore, we hypothesize that neuronal cells can divert HIF-1α for degradation through autophagy to prevent its accumulation due to proteasome impairment during events when PHDs are inactive. When directly investigating the effects of proteasome and autophagy inhibitors on HIF-1α levels in the presence of PHD blockers, we revealed that the use of the proteasome inhibitor Lactacystin significantly decreased HIF-1α levels exclusively in $CoCl_2$-treated SH-SY5Y cells, while CQ treatment had no effect. This indicates that HIF-1α is not normally degraded by autophagy in basal conditions. However, a combination of autophagy and proteasome inhibition caused a substantial accumulation of HIF-1α levels. These results provide further evidence that HIF-1α degradation can be diverted to autophagy for degradation when proteasomal activity is hindered. The mechanism underlying this process remains to be elucidated, although previous research has identified some proteins involved in targeting HIF-1α for autophagic degradation (Ferreira et al., 2015; Hubbi et al., 2014). Notably, the discrepancies in the effects of PD-related pathway disruption between astrocytes and neurons may be linked to differences in antioxidant defences and their reliance on degradation systems. Overall, the findings in this study suggest a potential mechanism by which dysregulation of biochemical pathways involved in the progression of PD impair HIF-1α stabilisation in neuronal cells, which could lead to defective responses to hypoxia in PD patients. Since HIF-1α has been implicated in several physiological functions and neurological disorders, more knowledge about its regulation could benefit other fields.

7.1.3. HIF-1α stabiliser ML228 is protective against rotenone-mediated damage in a PD cellular model

This study investigates the neuroprotective qualities of two novel PHD inhibitors, IOX4 and ML228, against rotenone induced toxicity in SH-SY5Y and U-87MG cells. IOX4 and ML228 significantly improved cell viability in the presence of rotenone, blocking apoptotic mechanisms such as caspase-3/7 activation. Additionally, both compounds reversed the increase in mitochondrial membrane depolarization and ROS production elicited by rotenone, despite their ability to reduce ATP levels. Indeed, studies have consistently shown that HIF-1α can slow down ATP production through the mitochondrial ETC to reduce O_2 consumption and ROS production (Fukuda et al., 2007). Although cotreatment with IOX4 could mitigate the effects of rotenone, we found that IOX4 treatment alone reduced cell viability with a moderate increase in caspase activation. IOX4 also reduced mitochondrial membrane potential and the levels of proteins involved in mitochondrial dynamics, suggesting that it could cause mitochondrial toxicity. Therefore, we discontinued our investigation of IOX4. Since ML228 also caused potent HIF-1α stabilization without affecting cell viability, it is likely that these adverse effects observed were specific to IOX4 and unrelated to HIF-1α. Remarkably, the protective effects observed with these compounds that stabilised HIF-1α were limited to neuronal cells, represented by SH-SY5Y cells, and not observed in astrocytic cells, represented by U-87MG cells. This suggested that HIF-1α has the potential to activate different transcriptional responses in neurons and astrocytes. Our results indicate that ML228 may protect against apoptosis by reducing cytochrome c loss from mitochondria and activating the pro-survival ERK1/2 pathway in rotenone-treated SH-SY5Y cells. Further investigation revealed that the beneficial effect of ML228 against rotenone toxicity in SH-SY5Y cells was dependent on the interplay between HIF-1α and glycolytic energy production. This effect persisted in differentiated SH-SY5Y cells, though for a shorter period. Additionally, ML228 reversed the damage to mitochondrial networks caused by rotenone alongside other pathways in SH-SY5Y cells. Specifically, ML228 increased autophagy, maintained cell cycle regulation, and reduced intracellular Ca^{2+} levels. These effects of ML228 were likely due to its activation of HIF-1α, whose expression is known to regulate autophagy, cell cycle regulators p21 and p27, and Ca^{2+} trafficking (Azimi, 2018; Goda et al., 2003; Lu et al., 2018). Analysis of gene expression patterns suggested that the genes involved in vesicle trafficking, glycolysis, and myelination were all altered

in response to ML228 and therefore may play a role in ML228-mediated neuroprotection against rotenone.

This study shows that HIF-1α stabilizing drugs, such as ML228, can protect neuronal cells from rotenone-induced damage. The fact that several PHD inhibitors are already approved for human use suggests that these drugs are well tolerated and effective at inducing the HIF-1α response. Therefore, these findings provide additional support that promotes ML228 as a promising candidate for further evaluation in preclinical models of PD.

7.1.4. Stabilisation of HIF-1α modifies the expression of an array of genes linked to PD

The transcriptomic analysis of the consequence of HIF stabilisation in fully differentiated SH-SY5Y cells showed the expression of more than 150 genes were significantly altered after treatment with the HIF-1α stabilizers, IOX4 and ML228. Gene ontology analysis revealed that these genes are clustered in pathways related to apoptosis, autophagy, cell signalling, cation channel function, neuronal development and function, immunity and transcription. Some of these genes were already known to be regulated by HIF-1α, which provided confidence in the data and indirectly validated the approach. Interestingly, we also uncovered genes that had not been previously associated with HIF-1α. Of particular interest to PD research was the discovery of increased β-Syn gene expression and the concomitant decreased Sph-1 expression, which was replicated at the protein level. These proteins are known to interact with α-synuclein to decrease or increase its aggregation, respectively, although their exact function and regulation remain to be determined (Angelova et al., 2018; Eyal et al., 2006b). These findings suggest that β-Syn and Sph-1 can be regulated by HIF-1α. We also identified other potential HIF-1α target genes involved in pathways where the role of HIF-1α is only beginning to emerge, such as FAM126A in myelination and ARC or HOMER1 in synaptic plasticity.

Importantly, this investigation adds to the growing body of evidence that HIF-1α is not just a TF involved in the response to hypoxia, but rather an important regulator of physiological functions, especially in the NS.

7.1.5. General conclusion

This study, building upon previous literature, offers original evidence implicating the HIF-1α pathway in PD pathophysiology. Notably, key stresses associated with PD development, including mitochondrial dysfunction, oxidative stress, and impaired protein degradation, all hinder HIF-1α stabilization under hypoxia-like conditions. This finding may explain why hypoxic episodes and exposure to pesticides that disrupt mitochondrial function are risk factors for PD. Further strengthening this link, our results demonstrate that stabilizing HIF-1α using novel PHD inhibitors offers neuroprotective effects in a cellular PD model. While the precise role of HIF-1α in the nervous system remains elusive, the pathways identified through our transcriptomic analysis provide valuable clues about where HIF-1α may play a critical role and why its dysregulation could contribute to PD. In conclusion, this research sheds light on the potential protective function of HIF-1α in PD, highlighting the need for further investigation to fully elucidate its specific mechanisms.

7.2. FUTURE WORK

Key areas for future work have been selected and are discussed below.

7.2.1. Characterising the interactions between PD-related genes and the activation of the hypoxia response

This study was limited in scope, as it only investigated the effect of hypoxia and HIF-1α stabilization on protein levels of a small set of PD-associated genes, and gene expression was not investigated for all genes. Thus, a comprehensive study of the genetic landscape of PD and related gene expression under HIF-1α stabilising conditions should be considered.

The interplay between the response to hypoxia and genes associated with PD can involve other factors, such as the location and PTMs of PD-related proteins. For example, while this study investigated the levels of Parkin, the most important function of Parkin is its phosphorylation and recruitment to mitochondria, which was not evaluated. Similarly, DJ-1 needs to be oxidized to carry out its function, and as oxidation is dependent on oxygen levels, hypoxia might affect this process. The state of PTMs and protein location could easily be studied by cell fractionation and Western blot. Research has shown that knockout of DJ1, PRKN, and PINK1 genes can lower HIF-1α levels in hypoxia (Lestón Pinilla et al., 2021). Thus, it would be of value to knockdown or mutate other genes

involved in similar pathways, using the CRISPR system, to investigate HIF-1α protein levels and *HIF1A* gene expression. This could signal a trend of PD mutations affecting the hypoxia response, which could directly affect neuronal homeostasis even in normoxia, as HIF-1α has been shown to also be activated and support neuronal function under basal conditions (Javed Butt et al., 2021).

Investigating these factors could provide valuable insights into the role of the hypoxia response in regulating PD-associated genes, as well as the effect of PD gene mutations or knockouts on HIF-1α stabilization and target gene induction.

7.2.2. Identifying factors involved in non-canonical HIF-1α degradation triggered by PD-linked pathway deregulation

The factors involved in HIF-1α destabilization and its targeting for autophagic degradation under PD-related conditions have not yet been identified. These factors could be investigated by examining the interaction partners of HIF-1α under these conditions, namely increased oxidative stress, mitochondrial dysfunction, and protein degradation impairment. The interaction partners of HIF-1α could be investigated using both *in silico* approaches, such as sequence matching and phytogenic profiling, and *in vitro* methods, such as tandem affinity purification-mass spectrometry (Rao et al., 2014). The results obtained could be confirmed by coimmunoprecipitation. As both CMA and macroautophagy have been reported to degrade HIF-1α, it would be important to determine which of the two is specifically involved. This could be investigated by studying the interaction and colocalization of HIF-1α with proteins involved in both autophagy pathways. The use of specific inhibitors of macroautophagy could also be exploited for this purpose. Additionally, differences between cell lines could be further assessed. It would be worthwhile to investigate whether stress-mediated autophagic degradation of HIF-1α can be triggered in astrocytic U-87MG cells by enhancing ROS production and/or increasing the flux through degradation systems, as the threshold for activation of this system may be different between cell types.

These experiments could shed light on the regulation of HIF-1α in a wider range of conditions including other neurodegenerative disorders and embryonic neuronal development.

7.2.3. Confirming the protective effect of ML228 against rotenone in iPSC-derived neurons and animal models

While our comprehensive study of a variety of parameters provided valuable insights into the molecular pathways involved in ML228-mediated neuroprotection against rotenone, further investigation could provide a clearer understanding of how ML228 exerts its beneficial effects. In particular, it would be important to verify the mechanism of PHD inhibition, which is believed to be through iron chelation (Theriault et al., 2012). Since HIF-1α inhibition does not completely abolish the effect of ML228, it would be of interest to evaluate the contribution of iron chelation to this process, as iron accumulates in the brains of PD patients (Alvarez Jerez et al., 2023). Similarly, because ML228 is a general PHD inhibitor, it is likely that it also stabilizes HIF-2α, so its contribution to the effect of ML228 should also be assessed. The neuroprotective effects of ML228 should be investigated in iPSCs and animal models treated with rotenone in order to assess improvements in the parameters investigated in this study, as well as other pathological features of PD that are replicated in animal models, such as α-Syn accumulation and motor deficits. In addition, it would be of interest to assess the efficacy of ML228 in iPSC and animal models carrying mutations in genes involved in mitochondrial function such as *PRKN* and *PINK1*.

This supplementary research will assess the feasibility of using ML228, or similar drugs with the same formulation and mode of action, as a potential lead optimisation compound for PD treatment.

7.2.4. Validating potential HIF-1α targets in neuronal homeostasis and degeneration

Given that β-Syn, which is upregulated at the mRNA and protein levels by HIF-1α, has been shown to reduce α-Syn aggregation (Janowska et al., 2015), it would be intriguing to investigate whether HIF-1α stabilizers can block this process *in vitro* through β-Syn induction. Verification that β-Syn is a HIF-1α target is of paramount importance. This could be achieved using CHIP and luciferase reporter assays. Additional genes of interest, including those involved in less-studied HIF-1α functions such as axonal guidance or synaptic plasticity, could also be validated using these methods. It is also of interest to investigate whether these changes in gene expression can be observed in other cell lines, such as astrocytes, and other neuronal cells, such as iPSCs and primary neurons.

Further exploration of the transcriptomic data could reveal novel HIF-1α targets involved in neuronal degeneration and homeostasis.

CHAPTER VIII

SUPPLEMENTARY INFORMATION

SI Table 8.1. List of compounds utilised for cell treatments in this project.

Compound	Product code	Company
2,2'-Azobis(2-amidinopropane) dihydrochloride (AAPH)	440914	Merck
2-Deoxyglucose (2-DG)	D8375	Merck
3-Methyladenine (3-MA)	M9281	Merck
Bafilomycin	B0025	Cambridge Biosciences
Carbonyl cyanide 3-chlorophenylhydrazone (CCCP)	C2759	Merck
Chloroquine diphosphate salt (CQ)	C6628	Merck
Cobalt (II) chloride hexahydrate ($CoCl_2$)	C8661	Merck
Dopamine hydrochloride	H8502	Merck
FG-2216	CAY18382	Cayman Chemical
GSK1278863 (Daprodustat)	CAY19915	Cayman Chemical
HIF inhibitor	Sc205346A	Insight Biotechnology
IOX4	CAY18181	Cayman Chemical
L -Buthionine-sulfoximine (BSO)	B2515	Merck
Lactacystin	BML-PI104-0200	Enzo Life Sciences
L-Ascorbic acid	A4403	Merck
L-Glutathione reduced (GSH)	G6013	Merck
MG132	474790	Merck
ML228	CAY14568	Cayman Chemical
MPP+ iodide	D048	Merck
N-Acetylcysteine (NAC)	A9165	Merck
Oligomycin	CAY11342	Cayman Chemical
Rotenone	R8875	Merck
VH298	SML1896	Merck

SI Table 8.2. Percentage of SDS-PAGE gel according to protein size.

Gel percentage	8%	10%	12%	14%	15%
Protein size (kDa)	30-200	25-100	15-70	10-55	5-45

SI Table 8.3. Composition of SDS-PAGE gels prepared in this project.

	Resolving gel				
Reagents (10 ml gel solution)	8%	10%	12%	14%	15%
40% (w/v) Acrylamide (10001313, Fisher)	2 ml	2.5 ml	3 ml	3.5 ml	3.75 ml
1.5M Tris pH 8.8	2.5 ml	2.5 ml	2.5 ml	2.5 ml	2.5 ml
10% (w/v) Sodium dodecyl sulfate (SDS)	100 µl	100 µl	100 µl	100 µl	100 µl
Distilled Water	5.4 ml	4.9 ml	4.4 ml	3.9 ml	3.65 ml
Reagents for gel polymerisation					
Tetramethylethylenediamine (TEMED) (T9281, Merck)	10 µl	10 µl	10 µl	10 µl	10 µl
Ammonium persulphate (APS) 10 % (w/v) (A3678, Merck)	50 µl	50 µl	50 µl	50 µl	50 µl

	Stacking gel
Reagents (10 ml gel solution)	4%
40% (w/v) Acrylamide	1 ml
0.5M Tris pH 6.8	2.5 ml
10% (w/v) SDS	100 µl
Distilled Water	6.4 ml
Reagents for gel polymerisation	
TEMED	20 µl
APS 10 % (w/v)	50 µl

SI Table 8.4. List of primary antibodies utilised in this project.

Antibody	Source and type	Product code	Company	Dilution
ATP13A2	Rabbit Polyclonal	5879	CST	1:1000
Cleaved Caspase 3	Mouse monoclonal	9664	CST	1:500
Cytochrome c	Rabbit monoclonal	11940	CST	1:1000
DJ-1	Rabbit polyclonal	GTX132552	Genentech	1:1000
Drp1	Rabbit polyclonal	12957-1-AP	Proteintech	1:1000
ERK1/2	Rabbit polyclonal	11257	Proteintech	1:1000
HIF-1α	Rabbit Polyclonal	ab82832	Abcam	1:500
HIF-1α	Rabbit Monoclonal	ab255733	Abcam	1:100 (IF)
HUMMR	Rabbit polyclonal	22569-1-AP	Proteintech	1:1000
LC3B	Rabbit Polyclonal	2775	CST	1:1000
Mitofusin 1	Rabbit polyclonal	13798-1-AP	Proteintech	1:1000
Mitofusin 2	Rabbit polyclonal	12186-1-AP	Proteintech	1:1000
OPA1	Mouse monoclonal	612607	BD Biosciences	1:1000
Parkin	Rabbit polyclonal	14060-1-AP	Proteintech	1:1000
p-Drp1 (S616)	Rabbit polyclonal	3455	CST	1:1000
p-ERK1/2 (T183/Y185)	Mouse monoclonal	M-9692	Sigma	1:1000
PINK1	Rabbit polyclonal	BC-100-494	Novus Biologicals	1:1000
Synaptophysin	Rabbit monoclonal	Ab32127	Abcam	1:1000
Synphilin	Rabbit polyclonal	17818-1-AP	Proteintech	1:1000
VDAC2	Goat polyclonal	Ab37985	Abcam	1:1000
VPS35	Goat polyclonal	NB100-1397	Novus Biologicals	1:1000
α-Synuclein	Rabbit polyclonal	10842	Proteintech	1:1000
α-Tubulin	Mouse monoclonal	T-4026	Sigma	1:4000
β-Actin	Mouse monoclonal	60008	Proteintech	1:2000
βIII-Tubulin	Mouse monoclonal	ab78078	Abcam	1:1000
β-Synuclein	Mouse monoclonal	68046-1-Ig	Proteintech	1:2000

SI Table 8.5. List of secondary antibodies utilised in this project.

Name	Product code	Company	Dilution
Donkey anti-Rabbit IgG (H+L) Highly Cross-Adsorbed Secondary Antibody, Alexa Fluor™ 488	ab32127	Abcam	1:250 (IF)
Anti-rabbit IgG, HRP-linked Antibody	7074	CST	1:2000
Anti-mouse IgG, HRP-linked Antibody	7076	CST	1:4000

SI Table 8.6. List of RT-qPCR primers utilised in this project.

Gene	Forward primer 5'-3'	Reverse primer 5'-3'	Tm (ºC)
ADORA2A	TGGTCTCTTCTCCCCAGGTA	AGTGGTTCTTGCCCTCCTTT	60
ATP13A2	GGCCCTCTACAGCCTGACT	CCAGGTT GGTGTTGATTGTG	58
BACT	CCTGACTGACTACCTCATGAAG	GACGTAGCACAGCTTCTCCTTA	62
CACNA1D	CGCGAACGAGGCAAACTATG	TTGGAGCTATTCGGCTGAGAA	63
CALB1	GGCTCCATTTCGACGCTGA	GCCCATACTGATCCACAAAAGTT	63
CAMK2B	CTCTACGAGGATATTGGCAAGGG	GCTTCTGGTGATCTCTGGCTG	64
CDK5	GGAAGGCACCTACGGAACTG	GGCACACCCTCATCATCGT	65
CXCR4	ACTACACCGAGGAAATGGGCT	CCCACAATGCCAGTTAAGAAGA	64
DOT1L	GAGACCTCCTTCGACCTGGT	CGACGCCATAGTGATGTTTGC	62
EGR1	GGTCAGTGGCCTAGTGAGC	GTGCCGCTGAGTAAATGGGA	65
FAM126A	GTTGTGGAGGAATGGTTGTCA	GACAGGTTCTAGCAACTCACTTT	62
GABRP	CTTGGCCTTCGTGTGTCTGAG	CCGACCTCGACGTTGAACT	65
GAD1	GCGGACCCCAATACCACTAAC	CACAAGGCGACTCTTCTCTTC	62
GRIA2	CACCCCACATCGACAATTTGG	GACGTGGAGTGTTCCGCAA	65
GRIA3	TCCGGGCGGTCTTCTTTTTAG	TCCACCTATGCTGATGGTGTT	64
HIF1A	GCGCGAACGACAAGAAA	GAAGTGGCAACTGATGAGCA	60
IL10RA	CCTCCGTCTGTGTGGTTTGAA	CACTGCGGTAAGGTCATAGGA	64
LIF	CCTTCTGCCCCTCAGTACAC	GGGGTTGAGGATCTTCTGGT	60
NAGLU	CAGGGTGTTCCCTCAGGTCA	AGGAAGAGGCTCCCGATGAT	61
NOL3	GACCGCAGCTATGACCCTC	CTCCGGTTCAGCCTCTTTAGA	61
NPC1	GTCTCCGAGTACACTCCCATC	CGCAGTAATGAAGACCAGCGA	62
PGAM1	GTGCAGAAGAGAGCGATCCG	CGGTTAGACCCCCATAGTGC	65
PHF19	ACTCGGGACTCCTATGGTGC	CCTCCGTCAGTTTGGACATCA	62
PINK1	GGACGCTGTTCCTCGTTA	ATCTGCGATCACCAGCCA	58
SLC1A1	GCGAGGAAAGGATGCGAGT	GCTGTGTTCTCGAACCAAGACT	65
SNCAIP	GTTGCTATGGCCAGGAAAAG	TGCTGTGAGGCTACGTGAAC	62
SNCB	AAGCAAGACCCGAGAAGGTGTG	ATTCCTCCCTCTTCACCAGTCC	62
SOX9	AGCGAACGCACATCAAGAC	CTGTAGGCGATCTGTTGGGG	61

SI Table 8.7. List of GO Biological process grouping after curation with Revigo.

Main GO Biological Process	GO Biological Processes Included	Genes comprised in all GO Biological Processes	Average adjusted p-value
Negative regulation of apoptotic process (GO:0043066)	Negative regulation of programmed cell death (GO:0043069)	NTRK1; HDAC2; NOTCH1; PRKAA2; HDAC1; SRC; GSTP1; BNIP3; PARK7; PSEN1; NOL3; SOD2; RELA; TNFRSF10D; VEGFA; NFKBIA; OPA1; PIK3CA; PPT1; MAPK1; FAS; SOX9; SQSTM1; MYD88	2.17E-08
Regulation of autophagy (GO:0010506)	Regulation of macroautophagy (GO:0016241)	ATP6V1A; ATP6V1G2; PRKAA2; BAD; IL10RA; BNIP3; GBA; STAT3; HTRA2; PIK3CB; HMGB1; MTOR; CDK5; DDIT3; ATM; PRKACA; ATP6V0E2; OPTN; CDK5R1; PIK3CA	2.92E-07
Protein phosphorylation (GO:0006468)	Phosphorylation (GO:0016310) Peptidyl-serine modification (GO:0018209) Peptidyl-serine phosphorylation (GO:0018105)	ACVRL1; CAMK2B; NTRK1; MAP2K1; CAMK2D; PRKAA2; SRC; GTF2H3; MTOR; TGFBR2; MAPK10; MAPK9; CDK7; CDK5; CDK2; MAPK1; PRKCQ; ATM; PRKACA; CDK5R1; PARP1; PGK1; PIK3CA; PIK3CB; STAT3	6.83E-07
Regulation of cation channel activity (GO:2001257)		CAMK2B; CACNB2; GRIA2; CAMK2D; CACNB4; FGF14; HOMER1; DLG4; PRKACA; GRIA4	6.88E-07
Regulation of intracellular signal transduction (GO:1902531)	Transmembrane receptor protein tyrosine kinase signaling pathway (GO:0007169) Regulation of signal transduction by p53 class mediator (GO:1901796)	NTRK1; HDAC2; PRKAA2; HDAC1; GBA; CHD4; RELA; MTOR; VEGFA; NFKBIA; CDK5; CDK2; MAPK1; ATM; MTA2; TAF4; SQSTM1; OPTN; CDK5R1; AP2A2; AP2B1; AP3S1; ATP6V0E2; ATP6V1A; ATP6V1G2; EPHA2; FGF2; HNRNPM; IDE; PIK3CA; PIK3CB; POLR2B; POLR2H; POLR2J; POLR2K; POLR2L; PSEN1; SRC; STAT3; CDK5RAP3	7.61E-07
Regulation of pri-miRNA transcription by RNA polymerase II (GO:1902893)	Positive regulation of pri-miRNAtranscription by RNA polymerase II (GO:1902895)	EGR1; JUN; STAT3; SOX9; FOS; FGF2; HIF1A; RELA	9.80E-07
Central nervous system development (GO:0007417)		MYRF; GSTP1; STAT3; SLC2A1; CXCR4; S100B; TGFBR2; CDK5; ADORA2A; NF1; PPT1; DCX; SOX9; CDK5RAP3; CDK5R1	1.24E-06
Regulation of apoptotic process (GO:0042981)	Apoptotic process (GO:0006915)	HDAC2; PRKAA2; HDAC1; SRC; GSTP1; HTRA2; PARK7; PSEN1; HMGB1; NOL3; RTN4; RELA;	1.25E-06

	Regulation of extrinsic apoptotic signaling pathway (GO:2001236) Regulation of programmed cell death (GO:0043067) Intrinsic apoptotic signaling pathway (GO:0097193) Regulation of neuron death (GO:1901214)	CASP9; OPA1; CASP6; SOX9; NTRK1; JUN; TNFRSF12A; APAF1; BAD; STAT1; BNIP3; TNFRSF10B; TNFRSF10A; TNFRSF10D; DNM2; VEGFA; NFKBIA; CDK5; NF1; PPT1; FAS; ATM; SQSTM1; MYD88; GSTP1; NOL3; PARK7; SRC; TNFRSF12A; ATM; CCL5; EGR1; FOS; GBA; HTRA2; PARK7; PRNP; SNCB; CDKN1A; DDIT3; EPHA2	
Axonogenesis (GO:0007409)	Axon guidance (GO:0007411)	RAB3A; NOTCH1; SRC; CXCR4; PIK3CB; S100B; CDK5; PIK3CA; MAPK1; PRKCQ; NCAM1; B4GALT6; EPHA2; SPTBN2; CDK5R1; PLXNC1; VEGFA	1.26E-06
Cytokine-mediated signaling pathway (GO:0019221)	Cellular response to cytokine stimulus (GO:0071345)	CAMK2B; CDKN1A; CAMK2D; SRC; PIK3CB; FGF2; HIF1A; RELA; UGCG; CCL5; NCAM1; PRKACA; CAMK2G; EGR1; TNFRSF12A; STAT1; IL10RA; STAT3; LIF; FOS; SOD2; VEGFA; NFKBIA; PIK3CA; SQSTM1; MYD88; CXCR4; GBA; HTRA2; SOX9	1.42E-06
Regulation of blood vessel endothelial cell migration (GO:0043535)		ACVRL1; SP1; NF1; HMGB1; FGF2; HIF1A; EPHA2; VEGFA	1.90E-06
Nucleotide-excision repair (GO:0006289)		CDK7; PCNA; PARP1; POLR2B; POLR2H; GTF2H3; RAD23B; POLR2J; POLR2K; POLR2L	2.00E-06
Positive regulation of gene expression (GO:0010628)	DNA-templated transcription, initiation (GO:0006352) Transcription initiation from RNA polymerase II promoter (GO:0006367) Positive regulation of nucleic acid-templated transcription (GO:1903508) 7-methylguanosine mRNA capping (GO:0006370) 7-methylguanosine RNA capping (GO:0009452) Positive regulation of transcription, DNA-templated (GO:0045893) Positive regulation of transcription by RNA	EGR1; PHF2; MAP2K1; NOTCH1; STAT3; PARK7; PSEN1; PIK3CB; FGF2; HIF1A; MTOR; VEGFA; MAPK9; SP1; TMEM119; MAPK1; ATM; SOX9; POLR2H; MYD88; POLR2K; POLR2L; CDK7; GTF2B; GTF2H3; HDAC1; NOTCH4, POLR2B; POLR2J; TAF4; TBPL1; ACVRL1; DDIT3; DNM2; FOS; HDAC2; JUN; MYRF; RELA; STAT1; DOT1L; HMGB1; LIF, NFKBIA; PARP1; SQSTM1	2.16E-06

	polymerase II (GO:0045944) Transcription by RNA polymerase II (GO:0006366)		
Positive regulation of apoptotic process (GO:0043065)	Positive regulation of programmed cell death (GO:0043068) Positive regulation of neuron death (GO:1901216)	PRNP; JUN; TNFRSF12A; APAF1; BAD; BNIP3; HTRA2; TNFRSF10B; TNFRSF10A; PSEN1; HMGB1; DNM2; CASP9; CDK5; DDIT3; NF1; FAS; ATM; SQSTM1; CDK5R1; NTRK1; EGR1; FOS	2.78E-06
Chemical synaptic transmission (GO:0007268)	Anterograde trans-synaptic signaling (GO:0098916)	GRIA2; GABRP; RAB3A; HOMER1; GAD1; SLC1A1; CACNB2; CACNB4; CDK5; GLRB; DLG4; MAPK1; PRKACA; SNCB; GRIA4	3.42E-06
Positive regulation of macromolecule metabolic process (GO:0010604)	Positive regulation of cellular process (GO:0048522)	NSF; EGR1; MAP2K1; NOTCH1; GBA; STAT3; PARK7; PSEN1; PIK3CB; FGF2; HIF1A; MTOR; VEGFA; MAPK9; SP1; TMEM119; MAPK1; ATM; SOX9; MYD88; EGR1; GBA; HIF1A; MAP2K1; MAPK1; MAPK9; MTOR; MYD88; NSF; PARK7; PIK3CB, PSEN1, SP1; STAT3; TMEM119	3.48E-06
Cellular response to oxidative stress (GO:0034599)	Cellular response to oxygen-containing compound (GO:1901701)	MAPK9; JUN; PRKAA2; PARP1; GSTP1; HTRA2; MAPK1; PARK7; FOS; SOD2; HIF1A; ATM; CDK2; EGR1; GNG2; HMGB1; MTOR; MYD88; RELA; SOX9	4.72E-06
Negative regulation of macromolecule metabolic process (GO:0010605)		ACVRL1; MAP2K1; NOTCH1; PRKAA2; DLG4; HDAC1; PARK7; PSEN1; FGF2; HIF1A; OPTN; VEGFA	7.43E-06
Positive regulation of cell population proliferation (GO:0008284)	Cellular response to fibroblast growth factor stimulus (GO:0044344)	CDKN1A; HDAC2; NOTCH1; HDAC1; BAD; STAT1; DOT1L; LIF; EMP2; S100B; FGF2; RELA; TGFBR2; VEGFA; CCL5; CDK2; TMEM119; SOX9; HNRNPM; MAPK1; POLR2B; POLR2H; POLR2J, POLR2K; POLR2L	7.57E-06
SnRNA transcription by RNA polymerase II (GO:0042795)	SnRNA transcription (GO:0009301)	CDK7; POLR2B; SP1; GTF2B; POLR2H; POLR2J; POLR2K; POLR2L	8.68E-06

SI Table 8.8. List of GO Biological process terms and Nanostring gene sets included on each main pathway.

Main pathway	Main GO terms included	Nanostring gene sets included
Apoptosis	Negative regulation of apoptotic process (GO:0043066) Regulation of apoptotic process (GO:0042981) Positive regulation of apoptotic process (GO:0043065)	Apoptosis Unfolded protein response
Autophagy	Regulation of autophagy (GO:0010506)	Autophagy
Cell signalling	Protein phosphorylation (GO:0006468) Regulation of intracellular signal transduction (GO:1902531)	Growth Factor Signalling
Cation channel function	Regulation of cation channel activity (GO:2001257)	Ca^{2+} regulation genes (Not present specifically on Nanostring gene sets)
Neuronal development and activity	Central nervous system development (GO:0007417) Axonogenesis (GO:0007409) Chemical synaptic transmission (GO:0007268)	Axon and Dendrite Structure Myelination Neural Connectivity Neuronal Cytoskeleton Transmitter Release Transmitter Response and Reuptake Transmitter Synthesis and Storage Vesicle Trafficking
Immune Response	Cytokine-mediated signaling pathway (GO:0019221)	Activated Microglia Cytokines Carbohydrate metabolism
Transcription	Regulation of pri-miRNA transcription by RNA polymerase II (GO:1902893) Positive regulation of gene expression (GO:0010628) SnRNA transcription by RNA polymerase II (GO:0042795)	Chromatin Modification Transcription and Splicing

REFERENCES

Abbastabar, M.; Kheyrollah, M.; Azizian, K.; Bagherlou, N.; Tehrani, S. S.; Maniati, M.; Karimian, A. Multiple functions of p27 in cell cycle, apoptosis, epigenetic modification and transcriptional regulation for the control of cell growth: A double-edged sword protein. DNA repair 2018, 69, 63-72 DOI:10.1016/j.dnarep.2018.07.008.

Abu-Omar, N.; Das, J.; Szeto, V.; Feng, Z. Neuronal Ryanodine Receptors in Development and Aging. Mol Neurobiol 2018, 55, 1183-1192 DOI:10.1007/s12035-016-0375-4.

Ahluwalia, A.; Narula, J.; Jones, M. K.; Deng, X.; Tarnawski, A. S. Impaired angiogenesis in aging myocardial microvascular endothelial cells is associated with reduced importin alpha and decreased nuclear transport of HIF1 alpha: mechanistic implications. Journal of physiology and pharmacology : an official journal of the Polish Physiological Society 2010, 61, 133.

Albanese, A.; Daly, L. A.; Mennerich, D.; Kietzmann, T.; Sée, V. The Role of Hypoxia-Inducible Factor Post-Translational Modifications in Regulating Its Localisation, Stability, and Activity. International journal of molecular sciences 2020, 22, 268 DOI:10.3390/ijms22010268.

Alberts, B.; Johnson, A.; Lewis, J.; Raff, M.; Roberts, K.; Walter, P. How Cells Obtain Energy from Food. Molecular Biology of the Cell. 4th edition 2002.

Allen, S. P.; Seehra, R. S.; Heath, P. R.; Hall, B. P. C.; Bates, J.; Garwood, C. J.; Matuszyk, M. M.; Wharton, S. B.; Simpson, J. E. Transcriptomic Analysis of Human Astrocytes In Vitro Reveals Hypoxia-Induced Mitochondrial Dysfunction, Modulation of Metabolism, and Dysregulation of the Immune Response. IJMS 2020, 21.

Altman, T.; Travers, M.; Kothari, A.; Caspi, R.; Karp, P. D. A systematic comparison of the MetaCyc and KEGG pathway databases. BMC Bioinformatics 2013, 14, 112 DOI:10.1186/1471-2105-14-112.

Alvarez Jerez, P.; Alcantud, J. L.; De Los Reyes-Ramírez, L.; Moore, A.; Ruz, C.; Vives Montero, F.; Rodriguez-Losada, N.; Saini, P.; Gan-Or, Z.; Alvarado, C. X.; Makarious, M. B.; Billingsley, K. J.; Blauwendraat, C.; Noyce, A. J.; Singleton, A. B.; Duran, R.; Bandres-Ciga, S. Exploring the genetic and genomic connection underlying neurodegeneration with brain iron accumulation and the risk for Parkinson’s disease. npj Parkinsons Dis. 2023, 9.

Andrysik, Z.; Bender, H.; Galbraith, M. D.; Espinosa, J. M. Multi-omics analysis reveals contextual tumor suppressive and oncogenic gene modules within the acute hypoxic response. Nat Commun 2021, 12.

Angelini, A.; Saha, P. K.; Jain, A.; Jung, S. Y.; Mynatt, R. L.; Pi, X.; Xie, L. PHDs/CPT1B/VDAC1 axis regulates long-chain fatty acid oxidation in cardiomyocytes. Cell reports (Cambridge) 2021, 37, 109767 DOI:10.1016/j.celrep.2021.109767.

Angelopoulou, E.; Paudel, Y. N.; Piperi, C. Emerging role of S100B protein implication in Parkinson's disease pathogenesis. Cell. Mol. Life Sci 2021, 78, 1445-1453 DOI:10.1007/s00018-020-03673-x.

Angelova, D. M.; Jones, H. B. L.; Brown, D. R. Levels of α- and β-synuclein regulate cellular susceptibility to toxicity from α-synuclein oligomers. The FASEB journal 2018, 32, 995-1006 DOI:10.1096/fj.201700675R.

Antoniou, X.; Gassmann, M.; Ogunshola, O. O. Cdk5 interacts with Hif-1α in neurons: A new hypoxic signalling mechanism? Brain research 2011, 1381, 1-10 DOI:10.1016/j.brainres.2010.10.071.

Armstrong, M. J.; Okun, M. S. Diagnosis and Treatment of Parkinson Disease: A Review. JAMA : the journal of the American Medical Association 2020, 323, 548-560 DOI:10.1001/jama.2019.22360.

Avazzadeh, S.; Baena, J. M.; Keighron, C.; Feller-Sanchez, Y.; Quinlan, L. R. Modelling Parkinson's Disease: iPSCs towards Better Understanding of Human Pathology. Brain Sciences 2021, 11.

Badawi, Y.; Ramamoorthy, P.; Shi, H. Hypoxia-Inducible Factor 1 Protects Hypoxic Astrocytes against Glutamate Toxicity. ASN NEURO 2012, 4, 231-241 DOI:10.1042/AN20120006.

Bae, Y.; Joo, H.; Bae, J.; Hyeon, S. J.; Her, S.; Ko, E.; Choi, H. G.; Ryu, H.; Hur, E.; Bu, Y.; Lee, B. D. Brain injury induces HIF-1α-dependent transcriptional activation of LRRK2 that exacerbates brain damage. Cell Death Dis 2018, 9.

Baek, J. H.; Mahon, P. C.; Oh, J.; Kelly, B.; Krishnamachary, B.; Pearson, M.; Chan, D. A.; Giaccia, A. J.; Semenza, G. L. OS-9 Interacts with Hypoxia-Inducible Factor 1α and Prolyl Hydroxylases to Promote Oxygen-Dependent Degradation of HIF-1α. Molecular Cell 2005, 17, 503-512 DOI:10.1016/j.molcel.2005.01.011.

Balakrishnan, R.; Harris, M. A.; Huntley, R.; Van Auken, K.; Cherry, J. M. A guide to best practices for Gene Ontology (GO) manual annotation. Database : the journal of biological databases and curation 2013, 2013, bat054 DOI:10.1093/database/bat054.

Bao, Q.; Shi, Y. Apoptosome: a platform for the activation of initiator caspases. Cell death and differentiation 2007, 14, 56-65 DOI:10.1038/sj.cdd.4402028.

Barreca, D.; Currò, M.; Bellocco, E.; Ficarra, S.; Laganà, G.; Tellone, E.; Laura Giunta, M.; Visalli, G.; Caccamo, D.; Galtieri, A.; Ientile, R. Neuroprotective effects of phloretin and its glycosylated derivative on rotenone-induced toxicity in human SH-SY5Y neuronal-like cells. BioFactors (Oxford) 2017, 43, 549-557 DOI:10.1002/biof.1358.

Bastian, A.; Matsuzaki, S.; Humphries, K. M.; Pharaoh, G. A.; Doshi, A.; Zaware, N.; Gangjee, A.; Ihnat, M. A. AG311, a small molecule inhibitor of complex I and hypoxia-induced HIF-1α stabilization. Cancer letters 2017, 388, 149-157 DOI:10.1016/j.canlet.2016.11.040.

Batie, M.; Frost, J.; Frost, M.; Wilson, J. W.; Schofield, P.; Rocha, S. Hypoxia induces rapid changes to histone methylation and reprograms chromatin. Science 2019, 363, 1222.

Bayati, A.; Banks, E.; Han, C.; Luo, W.; Reintsch, W. E.; Zorca, C. E.; Shlaifer, I.; Del Cid Pellitero, E.; Vanderperre, B.; McBride, H. M.; Fon, E. A.; Durcan, T. M.; McPherson, P. S. Rapid macropinocytic transfer of α-synuclein to lysosomes. Cell reports (Cambridge) 2022, 40, 111102 DOI:10.1016/j.celrep.2022.111102.

Bélanger, M.; Allaman, I.; Magistretti, P. Brain Energy Metabolism: Focus on Astrocyte-Neuron Metabolic Cooperation. Cell Metabolism 2011, 14, 724-738 DOI:10.1016/j.cmet.2011.08.016.

Beliakov, S. V.; Blokhin, V.; Surkov, S. A.; Ugrumov, M. V. LUHMES Cells: Phenotype Refinement and Development of an MPP + -Based Test System for Screening Antiparkinsonian Drugs. International journal of molecular sciences 2023, 24, 733 DOI:10.3390/ijms24010733.

Benita, Y.; Kikuchi, H.; Smith, A. D.; Zhang, M. Q.; Chung, D. C.; Xavier, R. J. integrative genomics approach identifies Hypoxia Inducible Factor-1 (HIF-1)-target genes that form the core response to hypoxia. Nucleic Acids Research 2009, 37, 4587-4602 DOI:10.1093/nar/gkp425.

Bento, C. F.; Fernandes, R.; Ramalho, J.; Marques, C.; Shang, F.; Taylor, A.; Pereira, P.; Ko, B. C. B. Chaperone-Dependent Ubiquitin Ligase CHIP Targets HIF-1α for Degradation in the Presence of Methylglyoxal. PLoS ONE 2010, 5, e15062 DOI:10.1371/journal.pone.0015062.

Berchner-Pfannschmidt, U.; Yamac, H.; Trinidad, B.; Fandrey, J. Nitric Oxide Modulates Oxygen Sensing by Hypoxia-inducible Factor 1-dependent Induction of Prolyl Hydroxylase 2. The Journal of biological chemistry 2007, 282, 1788-1796 DOI:10.1074/jbc.M607065200.

Berra, E.; Benizri, E.; Ginouve, A.; Ronique Volmat ², V. Â; Le Roux, D. Á; Pouysse, J.; Gur, Â HIF prolyl-hydroxylase 2 is the key oxygen sensor setting low steady-state levels of HIF-1α in normoxia (Berra, 2003).

Blagosklonny, M. V.; An, W. G.; Romanova, L. Y.; Trepel, J.; Fojo, T.; Neckers, L. p53 Inhibits Hypoxia-inducible Factor-stimulated Transcription. The Journal of biological chemistry 1998, 273, 11995-11998 DOI:10.1074/jbc.273.20.11995.

Bloem, B. R.; Okun, M. S.; Klein, C. Parkinson's disease. Seminar 2284 www.thelancet.com 2021, 397.

Bohush, A.; Niewiadomska, G.; Filipek, A. Role of Mitogen Activated Protein Kinase Signaling in Parkinson’s Disease. International Journal of Molecular Sciences 2018, 19, 2973 DOI:10.3390/ijms19102973.

Bohuslavova, R.; Cerychova, R.; Papousek, F.; Olejnickova, V.; Bartos, M.; Görlach, A.; Kolar, F.; Sedmera, D.; Semenza, G. L.; Pavlinkova, G. HIF-1α is required for

development of the sympathetic nervous system. Proceedings of the National Academy of Sciences - PNAS 2019, 116, 13414-13423 DOI:10.1073/pnas.1903510116.

Bonello, S.; Zähringer, C.; BelAiba, R.; Djordjevic, T.; Hess, J.; Michiels, C.; Kietzmann, T.; Görlach, A. Reactive Oxygen Species Activate the HIF-1α Promoter Via a Functional NFκB Site. Arteriosclerosis, thrombosis, and vascular biology 2007, 27, 755-761 DOI:10.1161/01.ATV.0000258979.92828.bc.

Bono, H.; Hirota, K. Meta-Analysis of Hypoxic Transcriptomes from Public Databases. Biomedicines 2020, 8, 10 DOI:10.3390/biomedicines8010010.

Booth, H. D. E.; Hirst, W. D.; Wade-Martins, R. The Role of Astrocyte Dysfunction in Parkinson's Disease Pathogenesis. Trends in Neurosciences 2017, 40, 358.

Booth, H. D. E.; Wessely, F.; Connor-Robson, N.; Rinaldi, F.; Vowles, J.; Browne, C.; Evetts, S. G.; Hu, M. T.; Cowley, S. A.; Webber, C.; Wade-Martins, R. RNA sequencing reveals MMP2 and TGFB1 downregulation in LRRK2 G2019S Parkinson's iPSC-derived astrocytes. Neurobiology of Disease 2019, 129, 56.

Boshkovski, T.; Cohen-adad, J.; Misic, B.; Arnulf, I.; Corvol, J.; Vidailhet, M.; Lehéricy, S.; Stikov, N.; Mancini, M. The Myelin-Weighted Connectome in Parkinson's Disease. Movement Disorders 2021, 37, 724.

Brichta, L.; Greengard, P. Molecular determinants of selective dopaminergic vulnerability in Parkinsonâ€™s disease: an update. Front. Neuroanat. 2014, 8.

Brix, B.; Mesters, J. R.; Pellerin, L.; Johren, O. Endothelial Cell-Derived Nitric Oxide Enhances Aerobic Glycolysis in Astrocytes via HIF-1 -Mediated Target Gene Activation. Journal of Neuroscience 2012, 32, 9727.

Brown, J. W. P.; Buell, A. K.; Michaels, T. C. T.; Meisl, G.; Carozza, J.; Flagmeier, P.; Vendruscolo, M.; Knowles, T. P. J.; Dobson, C. M.; Galvagnion, C. β-Synuclein suppresses both the initiation and amplification steps of α-synuclein aggregation via competitive binding to surfaces. Scientific Reports 2016, 6, 36010 DOI:10.1038/srep36010.

Bruning, U.; Cerone, L.; Neufeld, Z.; Fitzpatrick, S. F.; Cheong, A.; Scholz, C. C.; Simpson, D. A.; Leonard, M. O.; Tambuwala, M. M.; Cummins, E. P.; Taylor, C. T. MicroRNA-155 Promotes Resolution of Hypoxia-Inducible Factor 1α Activity during Prolonged Hypoxia. Molecular and Cellular Biology 2011, 31, 4087-4096 DOI:10.1128/MCB.01276-10.

Burtscher, J.; Syed, M. M. K.; Keller, M. A.; Lashuel, H. A.; Millet, G. P. Fatal attraction – The role of hypoxia when alpha-synuclein gets intimate with mitochondria. Neurobiology of aging 2021, 107, 128-141 DOI:10.1016/j.neurobiolaging.2021.07.017.

Cabeza-Arvelaiz, Y.; Schiestl, R. H. Transcriptome Analysis of a Rotenone Model of Parkinsonism Reveals Complex I-Tied and -Untied Toxicity Mechanisms Common to Neurodegenerative Diseases. PLoS ONE 2012, 7, e44700 DOI:10.1371/journal.pone.0044700.

Cai, R.; Zhang, Y.; Simmering, J. E.; Schultz, J. L.; Li, Y.; Fernandez-Carasa, I.; Consiglio, A.; Raya, A.; Polgreen, P. M.; Narayanan, N. S.; Yuan, Y.; Chen, Z.; Su, W.; Han, Y.; Zhao, C.; Gao, L.; Ji, X.; Welsh, M. J.; Liu, L. Enhancing glycolysis attenuates Parkinson's disease progression in models and clinical databases. Journal of Clinical Investigation 2019, 129, 4539.

Callapina, M.; Zhou, J.; Schmid, T.; Köhl, R.; Brüne, B. NO restores HIF-1α hydroxylation during hypoxia: Role of reactive oxygen species. Free radical biology & medicine 2005, 39, 925-936 DOI:10.1016/j.freeradbiomed.2005.05.009.

Carocho, M.; Ferreira, I. C. F. R. A review on antioxidants, prooxidants and related controversy: Natural and synthetic compounds, screening and analysis methodologies and future perspectives. Food and chemical toxicology 2013, 51, 15-25 DOI:10.1016/j.fct.2012.09.021.

Carrica, L.; Li, L.; Newville, J.; Kenton, J.; Gustus, K.; Brigman, J.; Cunningham, L. A. Genetic inactivation of hypoxia inducible factor 1-alpha (HIF-1α) in adult hippocampal progenitors impairs neurogenesis and pattern discrimination learning. Neurobiology of learning and memory 2019, 157, 79-85 DOI:10.1016/j.nlm.2018.12.002.

Castro-Mondragon, J. A.; Riudavets-Puig, R.; Rauluseviciute, I.; Berhanu Lemma, R.; Turchi, L.; Blanc-Mathieu, R.; Lucas, J.; Boddie, P.; Khan, A.; Manosalva Pérez, N.; Fornes, O.; Leung, T.; Aguirre, A.; Hammal, F.; Schmelter, D.; Baranasic, D.; Ballester, B.; Sandelin, A.; Lenhard, B.; Vandepoele, K.; Wasserman, W. W.; Parcy, F.; Mathelier, A. JASPAR 2022: the 9th release of the open-access database of transcription factor binding profiles. Nucleic acids research 2022, 50, D165-D173 DOI:10.1093/nar/gkab1113.

Cattaneo, M. G.; Cappellini, E.; Benfante, R.; Ragni, M.; Omodeo-Salè, F.; Nisoli, E.; Borgese, N.; Vicentini, L. M. Chronic Deficiency of Nitric Oxide Affects Hypoxia Inducible Factor-1α (HIF-1α) Stability and Migration in Human Endothelial Cells. PloS one 2011, 6, e29680 DOI:10.1371/journal.pone.0029680.

Cavadas, M. A. S.; Mesnieres, M.; Crifo, B.; Manresa, M. C.; Selfridge, A. C.; Scholz, C. C.; Cummins, E. P.; Cheong, A.; Taylor, C. T. REST mediates resolution of HIF-dependent gene expression in prolonged hypoxia. Sci Rep 2015, 5.

Chamboredon, S.; Ciais, D.; Desroches-Castan, A.; Savi, P.; Bono, F.; Feige, J.; Cherradi, N. Hypoxia-inducible factor-1α mRNA: a new target for destabilization by tristetraprolin in endothelial cells. Molecular Biology of the Cell 2011, 22, 3366-3378 DOI:10.1091/mbc.E10-07-0617.

Chan, M. C.; Atasoylu, O.; Hodson, E.; Tumber, A.; Leung, I. K. H.; Chowdhury, R.; Gómez-Pérez, V.; Demetriades, M.; Rydzik, A. M.; Holt-Martyn, J.; Tian, Y.; Bishop, T.; Claridge, T. D. W.; Kawamura, A.; Pugh, C. W.; Ratcliffe, P. J.; Schofield, C. J. Potent and Selective Triazole-Based Inhibitors of the Hypoxia-Inducible Factor Prolyl-Hydroxylases with Activity in the Murine Brain. PloS one 2015, 10, e0132004 DOI:10.1371/journal.pone.0132004.

Chandrasekaran, S.; Bonchev, D. A network view on Parkinson's disease. Computational and Structural Biotechnology Journal 2013, 7, e201304004 DOI:10.5936/csbj.201304004.

Chemmarappally, J. M.; Pegram, H. C. N.; Abeywickrama, N.; Fornari, E.; Hargreaves, A. J.; De Girolamo, L. A.; Stevens, B. A co-culture nanofibre scaffold model of neural cell degeneration in relevance to Parkinson’s disease. Sci Rep 2020, 10.

Chen, H.; Li, J.; Liang, S.; Lin, B.; Peng, Q.; Zhao, P.; Cui, J.; Rao, Y. Effect of hypoxia-inducible factor-1/vascular endothelial growth factor signaling pathway on spinal cord injury in rats. Experimental and Therapeutic Medicine 2017, 13, 861-866 DOI:10.3892/etm.2017.4049.

Chen, S.; Luo, S.; Zhang, Z.; Ma, D. K. VHL-1 inactivation and mitochondrial antioxidants rescue C. elegans dopaminergic neurodegeneration. Protein Cell 2019, 10, 610.

Chen, S.; Zhang, M.; Xing, L.; Wang, Y.; Xiao, Y.; Wu, Y. HIF-1α Contributes to Proliferation and Invasiveness of Neuroblastoma Cells via SHH Signaling. PLoS ONE 2015, 10, e0121115 DOI:10.1371/journal.pone.0121115.

Chen, T.; Wang, Q.; Chao, D.; Xia, T. C.; Sheng, S.; Li, Z.; Zhao, J.; Wen, G.; Ding, G.; Xia, Y. δ-Opioid Receptor Activation Attenuates the Oligomer Formation Induced by Hypoxia and/or α-Synuclein Overexpression/Mutation Through Dual Signaling Pathways. Mol Neurobiol 2019, 56, 3463-3475 DOI:10.1007/s12035-018-1316-1.

Chen, W.; Ostrowski, R. P.; Obenaus, A.; Zhang, J. H. Prodeath or prosurvival: Two facets of hypoxia inducible factor-1 in perinatal brain injury. Experimental neurology 2009, 216, 7-15 DOI:10.1016/j.expneurol.2008.10.016.

Chen, Y.; Liu, M.; Niu, Y.; Wang, Y. Romance of the three kingdoms in hypoxia: HIFs, epigenetic regulators, and chromatin reprogramming. Cancer letters 2020, 495, 211-223 DOI:10.1016/j.canlet.2020.09.009.

Chen, Y.; Qin, C.; Huang, J.; Tang, X.; Liu, C.; Huang, K.; Xu, J.; Guo, G.; Tong, A.; Zhou, L. The role of astrocytes in oxidative stress of central nervous system: A mixed blessing. Cell Proliferation 2020, 53, e12781-n/a DOI:10.1111/cpr.12781.

Chertok, V. M.; Nevzorova, V. A.; Zakharchuk, N. V. Comparative Study of HIF-1α- and HIF-2α-Immunopositive Neurons and Capillaries in Rat Cortex under Conditions of Tissue Hypoxia. Bull Exp Biol Med 2018, 165, 516-520 DOI:10.1007/s10517-018-4207-6.

Chicco, D.; Agapito, G. Nine quick tips for pathway enrichment analysis. PLoS computational biology 2022, 18, e1010348 DOI:10.1371/journal.pcbi.1010348.

Cho, Y.; Shin, J.; Ewan, E.; Oh, Y.; Pita-Thomas, W.; Cavalli, V. Activating Injury-Responsive Genes with Hypoxia Enhances Axon Regeneration through Neuronal HIF-1α. Neuron 2015, 88, 720-734 DOI:10.1016/j.neuron.2015.09.050.

Christie, I. N.; Theparambil, S. M.; Braga, A.; Doronin, M.; Hosford, P. S.; Brazhe, A.; Mascarenhas, A.; Nizari, S.; Hadjihambi, A.; Wells, J. A.; Hobbs, A.; Semyanov, A.;

Abramov, A. Y.; Angelova, P. R.; Gourine, A. V. Astrocytes produce nitric oxide via nitrite reduction in mitochondria to regulate cerebral blood flow during brain hypoxia. Cell Reports 2023, 42.

Chuaqui, R. F.; Bonner, R. F.; Best, C. J. M.; Gillespie, J. W.; Flaig, M. J.; Hewitt, S. M.; Phillips, J. L.; Krizman, D. B.; Tangrea, M. A.; Ahram, M.; Linehan, W. M.; Knezevic, V.; Emmert-Buck, M. R. Post-analysis follow-up and validation of microarray experiments. Nature genetics 2002, 32 Suppl, 509-514 DOI:10.1038/ng1034.

Cimmino, F.; Avitabile, M.; Lasorsa, V. A.; Montella, A.; Pezone, L.; Cantalupo, S.; Visconte, F.; Corrias, M. V.; Iolascon, A.; Capasso, M. HIF-1 transcription activity: HIF1A driven response in normoxia and in hypoxia. BMC Med Genet 2019, 20.

Clark, M. J.; Homer, N.; O'Connor, B. D.; Chen, Z.; Eskin, A.; Lee, H.; Merriman, B.; Nelson, S. F. U87MG Decoded: The Genomic Sequence of a Cytogenetically Aberrant Human Cancer Cell Line. PLoS Genetics 2010, 6, e1000832 DOI:10.1371/journal.pgen.1000832.

Clifton, N. E.; Cameron, D.; Trent, S.; Sykes, L. H.; Thomas, K. L.; Hall, J. Hippocampal Regulation of Postsynaptic Density Homer1 by Associative Learning. Journal of neural transplantation & plasticity 2017, 2017, 5959182-11 DOI:10.1155/2017/5959182.

Connolly, N. M. C.; Theurey, P.; Adam-Vizi, V.; Bazan, N. G.; Bernardi, P.; Bolaños, J. P.; Culmsee, C.; Dawson, V. L.; Deshmukh, M.; Duchen, M. R.; Düssmann, H. H.; Fiskum, G. G.; Galindo, M. F.; Hardingham, G. E.; Hardwick, J. M.; Jekabsons, M. B.; Jonas, E. A.; Jordán, J.; Lipton, S. A.; Manfredi, G.; Mattson, M. P.; Mclaughlin, B.; Methner, A.; Murphy, A. N.; Murphy, M. P.; Nicholls, D. G.; Polster, B. M.; Pozzan, T.; Rizzuto, R.; Satrústegui, J.; Slack, R. S.; Swanson, R. A.; Swerdlow, R. H.; Will, Y.; Ying, Z.; Joselin, A.; Gioran, A.; Moreira Pinho, C.; Watters, O. O.; Salvucci, M.; Llorente-Folch, I.; Park, D. S.; Bano, D.; Ankarcrona, M.; Pizzo, P.; Prehn, J. H. M. Guidelines on experimental methods to assess mitochondrial dysfunction in cellular models of neurodegenerative diseases. Cell Death Differ 2017, 25, 542.

Cornpemolle, V.; Brusselrnans, K.; Franco, D.; Moorman, A.; Dewerchin, M.; Collen, D.; Carmeliet, P. Cardia bifida, defective heart development and abnormal neural crest migration in embryos lacking hypoxia-inducible factor-1α. Cardiovascular research 2003, 60, 569-579 DOI:10.1016/j.cardiores.2003.07.003.

Cosentino, K.; García-Sáez, A. J. Bax and Bak Pores: Are We Closing the Circle? Trends in cell biology 2017, 27, 266-275 DOI:10.1016/j.tcb.2016.11.004.

Cutz, E.; Pan, J.; Yeger, H.; Domnik, N. J.; Fisher, J. T. Recent advances and contraversies on the role of pulmonary neuroepithelial bodies as airway sensors. Seminars in cell & developmental biology 2013, 24, 40-50 DOI:10.1016/j.semcdb.2012.09.003.

Davis, C. K.; Jain, S. A.; Bae, O. -.; Majid, A.; Rajanikant, G. K. Hypoxia mimetic agents for ischemic stroke. Front. Cell Dev. Biol. 2019, 6 DOI:10.3389/fcell.2018.00175.

De Almeida, A. J. P. O.; de Oliveira, J. C. P. L.; da Silva Pontes, L. V.; de Souza Júnior, J. F.; Gonçalves, T. A. F.; Dantas, S. H.; de Almeida Feitosa, M. S.; Silva, A. O.; de Medeiros, I. A. ROS: Basic Concepts, Sources, Cellular Signaling, and its Implications in

Aging Pathways. Oxidative medicine and cellular longevity 2022, 2022, 1-23 DOI:10.1155/2022/1225578.

De Conto, V.; Cheung, V.; Maubon, G.; Souguir, Z.; Maubon, N.; Vandenhaute, E.; Bérézowski, V. In vitro differentiation modifies the neurotoxic response of SH-SY5Y cells. Toxicology in vitro 2021, 77, 105235 DOI:10.1016/j.tiv.2021.105235.

De Gasperi, R.; Sosa, M. A. G.; Dracheva, S.; Elder, G. A. Presenilin-1 regulates induction of hypoxia inducible factor-1α: altered activation by a mutation associated with familial Alzheimer's disease.

De Roover, A.; Núñez, A. E.; Cornelis, F. M. F.; Cherifi, C.; Casas-Fraile, L.; Sermon, A.; Cailotto, F.; Lories, R. J.; Monteagudo, S. Hypoxia induces DOT1L in articular cartilage to protect against osteoarthritis. JCI Insight 2021, 6.

Dengler, V. L.; Galbraith, M. D.; Espinosa, J. M. Transcriptional regulation by hypoxia inducible factors. Critical reviews in biochemistry and molecular biology 2014, 49, 1-15 DOI:10.3109/10409238.2013.838205.

Depping, R.; Steinhoff, A.; Schindler, S. G.; Friedrich, B.; Fagerlund, R.; Metzen, E.; Hartmann, E.; Köhler, M. Nuclear translocation of hypoxia-inducible factors (HIFs): Involvement of the classical importin α/β pathway. Biochimica et Biophysica Acta (BBA) - Molecular Cell Research 2008, 1783, 394-404 DOI:10.1016/j.bbamcr.2007.12.006.

Desideri, E.; Ciccarone, F.; Ciriolo, M. R. Targeting Glutathione Metabolism: Partner in Crime in Anticancer Therapy. Nutrients 2019, 11.

Dexter, D. T.; Statton, S. A.; Whitmore, C.; Freinbichler, W.; Weinberger, P.; Tipton, K. F.; Della Corte, L.; Ward, R. J.; Crichton, R. R. Clinically available iron chelators induce neuroprotection in the 6-OHDA model of Parkinson's disease after peripheral administration. J Neural Transm 2011, 118, 223-231 DOI:10.1007/s00702-010-0531-3.

Di Domenico, A.; Carola, G.; Calatayud, C.; Pons-Espinal, M.; Muñoz, J. P.; Richaud-Patin, Y.; Fernandez-Carasa, I.; Gut, M.; Faella, A.; Parameswaran, J.; Soriano, J.; Ferrer, I.; Tolosa, E.; Zorzano, A.; Cuervo, A. M.; Raya, A.; Consiglio, A. Patient-Specific iPSC-Derived Astrocytes Contribute to Non-Cell-Autonomous Neurodegeneration in Parkinson's Disease. Stem Cell Reports 2019, 12, 213.

Dionísio, P. A.; Amaral, J. D.; Rodrigues, C. M. P. Oxidative stress and regulated cell death in Parkinson's disease. Ageing research reviews 2021, 67, 101263 DOI:10.1016/j.arr.2021.101263.

Dovonou, A.; Bolduc, C.; Soto Linan, V.; Gora, C.; Peralta Iii, M. R.; Lévesque, M. Animal models of Parkinson's disease: bridging the gap between disease hallmarks and research questions. Transl Neurodegener 2023, 12.

Duclot, F.; Kabbaj, M. The Role of Early Growth Response 1 (EGR1) in Brain Plasticity and Neuropsychiatric Disorders. Frontiers in Behavioral Neuroscience 2017, 11, 35 DOI:10.3389/fnbeh.2017.00035.

Ebert, B. L.; Gleadle, J. M.; O'Rourke, J. F.; Bartlett, S. M.; Poulton, J.; Ratcliffe, P. J. Isoenzyme-specific regulation of genes involved in energy metabolism by hypoxia: similarities with the regulation of erythropoietin. Biochemical journal 1996, 313 (Pt 3), 809-814 DOI:10.1042/bj3130809.

Elmore, S. Apoptosis: A Review of Programmed Cell Death. Toxicologic Pathology 2007, 35, 495-516.

Emamzadeh, F. N.; Surguchov, A. Parkinson's Disease: Biomarkers, Treatment, and Risk Factors. Frontiers in Neuroscience 2018, 12, 612 DOI:10.3389/fnins.2018.00612.

Encinas, M.; Iglesias, M.; Liu, Y.; Wang, H.; Muhaisen, A.; Ceña, V.; Gallego, C.; Comella, J. X. Sequential Treatment of SH-SY5Y Cells with Retinoic Acid and Brain-Derived Neurotrophic Factor Gives Rise to Fully Differentiated, Neurotrophic Factor-Dependent, Human Neuron-Like Cells. Journal of neurochemistry 2000, 75, 991-1003 DOI:10.1046/j.1471-4159.2000.0750991.x.

Erecińska, M.; Silver, I. A. Tissue oxygen tension and brain sensitivity to hypoxia. Respiration physiology 2001, 128, 263-276 DOI:10.1016/S0034-5687(01)00306-1.

Eyal, A.; Szargel, R.; Avraham, E.; Liani, E.; Haskin, J.; Rott, R.; Engelender, S. Synphilin-1A: An Aggregation-Prone Isoform of Synphilin-1 That Causes Neuronal Death and Is Present in Aggregates from α-Synucleinopathy Patients. Proceedings of the National Academy of Sciences - PNAS 2006, 103, 5917-5922 DOI:10.1073/pnas.0509707103.

Eyrich, N. W.; Potts, C. R.; Robinson, M. H.; Maximov, V.; Kenney, A. M. Reactive Oxygen Species Signaling Promotes Hypoxia-Inducible Factor 1α Stabilization in Sonic Hedgehog-Driven Cerebellar Progenitor Cell Proliferation. Molecular and Cellular Biology 2019, 39.

Falkenburger, B. H.; Saridaki, T.; Dinter, E. Cellular models for Parkinson's disease. Journal of Neurochemistry 2016, 139, 121.

Fang, Y.; Lu, J.; Wang, X.; Wu, H.; Mei, S.; Zheng, J.; Xu, S.; Lenahan, C.; Chen, S.; Zhang, J.; Hong, Y. HIF-1α Mediates TRAIL-Induced Neuronal Apoptosis via Regulating DcR1 Expression Following Traumatic Brain Injury. Frontiers in cellular neuroscience 2020, 14, 192 DOI:10.3389/fncel.2020.00192.

Farina, A. R.; Cappabianca, L.; Sebastiano, M.; Zelli, V.; Guadagni, S.; Mackay, A. R. Hypoxia-induced alternative splicing: the 11th Hallmark of Cancer. Journal of experimental & clinical cancer research 2020, 39, 110 DOI:10.1186/s13046-020-01616-9.

Feldser, D.; Agani, F.; Iyer, N. V.; Pak, B.; Ferreira, G.; Semenza, G. L. Reciprocal positive regulation of hypoxia-inducible factor 1α and insulin-like growth factor 2. Cancer research (Chicago, Ill.) 1999, 59, 3915-3918.

Feng, Y.; Liu, T.; Li, X.; Liu, Y.; Zhu, X.; Jankovic, J.; Pan, T.; Wu, Y. Neuroprotection by Orexin-A via HIF-1α induction in a cellular model of Parkinson's disease. Neuroscience letters 2014, 579, 35-40 DOI:10.1016/j.neulet.2014.07.014.

Fernández-Martínez, A. B.; Arenas Jiménez, M. I.; Lucio Cazaña, F. J. Retinoic acid increases hypoxia-inducible factor-1α through intracrine prostaglandin E2 signaling in human renal proximal tubular cells HK-2. Biochimica et biophysica acta. Molecular and cell biology of lipids 2012, 1821, 672-683 DOI:10.1016/j.bbalip.2012.01.010.

Ferreira, J. V.; Soares, A. R.; Ramalho, J. S.; Pereira, P.; Girao, H. K63 linked ubiquitin chain formation is a signal for HIF1A degradation by Chaperone-Mediated Autophagy. Scientific Reports 2015, 5, 10210 DOI:10.1038/srep10210.

Finkel, T. Signal Transduction by Mitochondrial Oxidants. The Journal of biological chemistry 2012, 287, 4434-4440 DOI:10.1074/jbc.R111.271999.

Flügel, D.; Görlach, A.; Michiels, C.; Kietzmann, T. Glycogen Synthase Kinase 3 Phosphorylates Hypoxia-Inducible Factor 1α and Mediates Its Destabilization in a VHL-Independent Manner. Molecular and Cellular Biology 2007, 27, 3253-3265 DOI:10.1128/MCB.00015-07.

Fong, G.; Takeda, K. Role and regulation of prolyl hydroxylase domain proteins. Cell death and differentiation 2008, 15, 635-641 DOI:10.1038/cdd.2008.10.

Forsythe, J. A.; Jiang, B.; Iyer, N. V.; Agani, F.; Leung, S. W.; Koos, R. D.; Semenza, G. L. Activation of vascular endothelial growth factor gene transcription by hypoxia-inducible factor 1. Molecular and Cellular Biology 1996, 16, 4604-4613 DOI:10.1128/MCB.16.9.4604.

Frenkel-Denkberg, G.; Gershon, D.; Levy, A. P. The function of hypoxia-inducible factor 1 (HIF-1) is impaired in senescent mice. FEBS Letters 1999, 462, 341.

Frost, J.; Ciulli, A.; Rocha, S. RNA-seq analysis of PHD and VHL inhibitors reveals differences and similarities to the hypoxia response. Wellcome Open Res 2019, 4.

Frost, J.; Galdeano, C.; Soares, P.; Gadd, M. S.; Grzes, K. M.; Ellis, L.; Epemolu, O.; Shimamura, S.; Bantscheff, M.; Grandi, P.; Read, K. D.; Cantrell, D. A.; Rocha, S.; Ciulli, A. Potent and selective chemical probe of hypoxic signalling downstream of HIF-α hydroxylation via VHL inhibition. Nature Communications 2016, 7, 13312 DOI:10.1038/ncomms13312.

Fukuda, R.; Zhang, H.; Kim, J.; Shimoda, L.; Dang, C. V.; Semenza, G. HIF-1 Regulates Cytochrome Oxidase Subunits to Optimize Efficiency of Respiration in Hypoxic Cells. Cell 2007, 129, 111-122 DOI:10.1016/j.cell.2007.01.047.

Gal, S.; Zheng, H.; Fridkin, M.; Youdim, M. B. H. Restoration of Nigrostriatal Dopamine Neurons in Post-MPTP Treatment by the Novel Multifunctional Brain-Permeable Iron Chelator-Monoamine Oxidase Inhibitor Drug, M30. Neurotox Res 2010, 17, 15-27 DOI:10.1007/s12640-009-9070-9.

Galban, S.; Gorospe, M. Factors Interacting with HIF-1α mRNA: Novel Therapeutic Targets. Current pharmaceutical design 2009, 15, 3853-3860 DOI:10.2174/138161209789649376.

Gallastegui, E.; Domuro, C.; Serratosa, J.; Larrieux, A.; Sin, L.; Martinez, J.; Besson, A.; Morante-Redolat, J. M.; Orlando, S.; Aligue, R.; Fariñas, I.; Pujol, M. J.; Bachs, O.

p27Kip1 regulates alpha-synuclein expression. Oncotarget 2018, 9, 16368-16379 DOI:10.18632/oncotarget.24687.

Gan, J.; Leestemaker, Y.; Sapmaz, A.; Ovaa, H. Highlighting the Proteasome: Using Fluorescence to Visualize Proteasome Activity and Distribution. Frontiers in Molecular Biosciences 2019, 6, 14 DOI:10.3389/fmolb.2019.00014.

Ganeshan, K.; Chawla, A. Metabolic Regulation of Immune Responses. Annual review of immunology 2014, 32, 609-634 DOI:10.1146/annurev-immunol-032713-120236.

Gao, P.; Zhang, H.; Dinavahi, R.; Li, F.; Xiang, Y.; Raman, V.; Bhujwalla, Z. M.; Felsher, D. W.; Cheng, L.; Pevsner, J.; Lee, L. A.; Semenza, G. L.; Dang, C. V. HIF-Dependent Antitumorigenic Effect of Antioxidants In Vivo. Cancer Cell 2007, 12, 230-238 DOI:10.1016/j.ccr.2007.08.004.

Gcwensa, N. Z.; Russell, D. L.; Cowell, R. M.; Volpicelli-Daley, L. A. Molecular Mechanisms Underlying Synaptic and Axon Degeneration in Parkinson's Disease. Frontiers in cellular neuroscience 2021, 15, 626128 DOI:10.3389/fncel.2021.626128.

Geiss, G. K.; Bumgarner, R. E.; Birditt, B.; Dahl, T.; Dowidar, N.; Dunaway, D. L.; Fell, H. P.; Ferree, S.; George, R. D.; Grogan, T.; James, J. J.; Maysuria, M.; Mitton, J. D.; Oliveri, P.; Osborn, J. L.; Peng, T.; Ratcliffe, A. L.; Webster, P. J.; Davidson, E. H.; Hood, L.; Dimitrov, K. Direct multiplexed measurement of gene expression with color-coded probe pairs. Nature biotechnology 2008, 26, 317-325 DOI:10.1038/nbt1385.

Golan, M.; Mabjeesh, N. J. SEPT9_i1 is required for the association between HIF-1α and importin-α to promote efficient nuclear translocation. Cell cycle (Georgetown, Tex.) 2013, 12, 2297-2308 DOI:10.4161/cc.25379.

Greijer, A. E. The role of hypoxia inducible factor 1 (HIF-1) in hypoxia induced apoptosis. Journal of Clinical Pathology 2004, 57, 1009.

Gross, A.; Jockel, J.; Wei, M. C.; Korsmeyer, S. J. Enforced dimerization of BAX results in its translocation, mitochondrial dysfunction and apoptosis. The EMBO journal 1998, 17, 3878-3885 DOI:10.1093/emboj/17.14.3878.

Guo, M.; Ji, X.; Liu, J. Hypoxia and Alpha-Synuclein: Inextricable Link Underlying the Pathologic Progression of Parkinson's Disease. Frontiers in aging neuroscience 2022, 14, 919343 DOI:10.3389/fnagi.2022.919343.

Guo, M.; Ma, X.; Feng, Y.; Han, S.; Dong, Q.; Cui, M.; Zhao, Y. In chronic hypoxia, glucose availability and hypoxic severity dictate the balance between HIF-1 and HIF-2 in astrocytes. FASEB j. 2019, 33, 11123.

Guzy, R. D.; Hoyos, B.; Robin, E.; Chen, H.; Liu, L.; Mansfield, K. D.; Simon, M. C.; Hammerling, U.; Schumacker, P. T. Mitochondrial complex III is required for hypoxia-induced ROS production and cellular oxygen sensing. Cell Metabolism 2005, 1, 401-408 DOI:10.1016/j.cmet.2005.05.001.

Hall, C. N.; Klein-Flügge, M. C.; Howarth, C.; Attwell, D. Oxidative Phosphorylation, Not Glycolysis, Powers Presynaptic and Postsynaptic Mechanisms Underlying Brain

Information Processing. Journal of neuroscience 2012, 32, 8940-8951 DOI:10.1523/jneurosci.0026-12.2012.

Hamrick, S. E. G.; McQuillen, P. S.; Jiang, X.; Mu, D.; Madan, A.; Ferriero, D. M. A role for hypoxia-inducible factor-1α in desferoxamine neuroprotection. Neuroscience letters 2005, 379, 96-100 DOI:10.1016/j.neulet.2004.12.080.

Han, X.; Han, B.; Zhao, Y.; Li, G.; Wang, T.; He, J.; Du, W.; Cao, X.; Gan, J.; Wang, Z.; Zheng, W. Rosmarinic Acid Attenuates Rotenone-Induced Neurotoxicity in SH-SY5Y Parkinson's Disease Cell Model through Abl Inhibition. Nutrients 2022, 14, 3508 DOI:10.3390/nu14173508.

Hartmann, A. Postmortem studies in Parkinson's disease. Dialogues in Clinical Neuroscience 2004, 6, 281-293 DOI:10.31887/DCNS.2004.6.3/ahartmann.

Hartmann, A.; Hunot, S.; Michel, P. P.; Muriel, M. P.; Vyas, S.; Faucheux, B. A.; Mouatt-Prigent, A.; Turmel, H.; Srinivasan, A.; Ruberg, M.; Evan, G. I.; Agid, Y.; Hirsch, E. C. Caspase-3: A Vulnerability Factor and Final Effector in Apoptotic Death of Dopaminergic Neurons in Parkinson's Disease. Proceedings of the National Academy of Sciences - PNAS 2000, 97, 2875-2880 DOI:10.1073/pnas.040556597.

Hartmann, A.; Troadec, J.; Hunot, S.; Kikly, K.; Faucheux, B. A.; Mouatt-Prigent, A.; Ruberg, M.; Agid, Y.; Hirsch, E. C. Caspase-8 Is an Effector in Apoptotic Death of Dopaminergic Neurons in Parkinson's Disease, But Pathway Inhibition Results in Neuronal Necrosis. The Journal of neuroscience 2001, 21, 2247-2255 DOI:10.1523/JNEUROSCI.21-07-02247.2001.

Hatcher, J. M.; Pennell, K. D.; Miller, G. W. Parkinson's disease and pesticides: a toxicological perspective. Trends in pharmacological sciences (Regular ed.) 2008, 29, 322-329 DOI:10.1016/j.tips.2008.03.007.

He, R.; Huang, W. W.; Huang, Y. W.; Xu, M.; Song, P.; Huang, Y. W.; Xie, H.; Hu, Y. Cdk5 Inhibitory Peptide Prevents Loss of Dopaminergic Neurons and Alleviates Behavioral Changes in an MPTP Induced Parkinson's Disease Mouse Model. Front. Aging Neurosci. 2018, 10.

He, Z.; LI, J.; Zhen, C.; Feng, L.; Ding, X. Effect of leukemia inhibitory factor on embryonic stem cell differentiation： implications for supporting neuronal differentiation. Acta pharmacologica Sinica 2006, 27, 80-90 DOI:10.1111/j.1745-7254.2006.00254.x.

Hetz, C. The unfolded protein response: controlling cell fate decisions under ER stress and beyond. Nature reviews. Molecular cell biology 2012, 13, 89-102 DOI:10.1038/nrm3270.

Ho, D. H.; Nam, D.; Seo, M. K.; Park, S. W.; Seol, W.; Son, I. LRRK2 Kinase Inhibitor Rejuvenates Oxidative Stress-Induced Cellular Senescence in Neuronal Cells. Oxidative medicine and cellular longevity 2021, 2021, 9969842-16 DOI:10.1155/2021/9969842.

Höglinger, G. U.; Carrard, G.; Michel, P. P.; Medja, F.; Lombès, A.; Ruberg, M.; Friguet, B.; Hirsch, E. C. Dysfunction of mitochondrial complex I and the proteasome: interactions between two biochemical deficits in a cellular model of Parkinson's

disease. Journal of neurochemistry 2003, 86, 1297-1307 DOI:10.1046/j.1471-4159.2003.01952.x.

Höllerhage, M.; Stepath, M.; Kohl, M. M.; Pfeiffer, K.; Chua, O. W. H.; Duan, L.; Hopfner, F.; Eisenacher, M.; Marcus, K.; Höglinger, G. U. Transcriptome and Proteome Analysis in LUHMES Cells Overexpressing Alpha-Synuclein. Front. Neurol. 2022, 13.

Hollville, E.; Romero, S. E.; Deshmukh, M. Apoptotic cell death regulation in neurons. The FEBS Journal 2019, 286, 3276.

Holmquist-Mengelbier, L.; Fredlund, E.; Löfstedt, T.; Noguera, R.; Navarro, S.; Nilsson, H.; Pietras, A.; Vallon-Christersson, J.; Borg, Å; Gradin, K.; Poellinger, L.; Påhlman, S. Recruitment of HIF-1α and HIF-2α to common target genes is differentially regulated in neuroblastoma: HIF-2α promotes an aggressive phenotype. Cancer Cell 2006, 10, 413-423 DOI:10.1016/j.ccr.2006.08.026.

Horrée, N.; Gort, E.; van der Groep, P.; Heintz, A.; Vooijs, M.; van Diest, P. Hypoxia-inducible factor 1α is essential for hypoxic p27 induction in endometrioid endometrial carcinoma. The Journal of pathology 2008, 214, 38-45 DOI:10.1002/path.2244.

Hota, S. K.; Hota, K. B.; Prasad, D.; Ilavazhagan, G.; Singh, S. B. Oxidative-stress-induced alterations in Sp factors mediate transcriptional regulation of the NR1 subunit in hippocampus during hypoxia. Free radical biology & medicine 2010, 49, 178-191 DOI:10.1016/j.freeradbiomed.2010.03.027.

Hromadkova, L.; Bezdekova, D.; Pala, J.; Schedin-Weiss, S.; Tjernberg, L. O.; Hoschl, C.; Ovsepian, S. V. Brain-derived neurotrophic factor (BDNF) promotes molecular polarization and differentiation of immature neuroblastoma cells into definitive neurons. Biochimica et biophysica acta. Molecular cell research 2020, 1867, 118737 DOI:10.1016/j.bbamcr.2020.118737.

Hu, H.; Takano, N.; Xiang, L.; Gilkes, D. M.; Luo, W.; Semenza, G. L. Hypoxia-inducible factors enhance glutamate signaling in cancer cells. Oncotarget 2014, 5, 8853-8868 DOI:10.18632/oncotarget.2593.

Huang, L. E.; Gu, J.; Schau, M.; Bunn, H. F. Regulation of Hypoxia-Inducible Factor 1α is Mediated by an O2-dependent Degradation Domain via the Ubiquitin-Proteasome Pathway. Proceedings of the National Academy of Sciences - PNAS 1998, 95, 7987-7992 DOI:10.1073/pnas.95.14.7987.

Hubbi, M. E.; Gilkes, D. M.; Hu, H.; Kshitiz; Ahmed, I.; Semenza, G. L. Cyclin-dependent kinases regulate lysosomal degradation of hypoxia-inducible factor 1α to promote cell-cycle progression. Proceedings of the National Academy of Sciences - PNAS 2014, 111, E3325-E3334 DOI:10.1073/pnas.1412840111.

Hubbi, M. E.; Hu, H.; Kshitiz; Ahmed, I.; Levchenko, A.; Semenza, G. L. Chaperone-mediated Autophagy Targets Hypoxia-inducible Factor-1α (HIF-1α) for Lysosomal Degradation. The Journal of biological chemistry 2013, 288, 10703-10714 DOI:10.1074/jbc.M112.414771.

Hubert, V.; Weiss, S.; Rees, A. J.; Kain, R. Modulating Chaperone-Mediated Autophagy and Its Clinical Applications in Cancer. Cells (Basel, Switzerland) 2022, 11, 2562 DOI:10.3390/cells11162562.

Husain, A.; Chiu, Y.; Sze, K. M.; Ho, D. W.; Tsui, Y.; Suarez, E. M. S.; Zhang, V. X.; Chan, L.; Lee, E.; Lee, J. M.; Cheung, T.; Wong, C. C.; Chung, C. Y.; Ng, I. O. Ephrin-A3/EphA2 axis regulates cellular metabolic plasticity to enhance cancer stemness in hypoxic hepatocellular carcinoma. Journal of hepatology 2022, 77, 383-396 DOI:10.1016/j.jhep.2022.02.018.

Ilaria M.C. Orlando; Véronique N. Lafleur; Federica Storti; Patrick Spielmann; Lisa Crowther; Sara Santambrogio; Johannes Schödel; David Hoogewijs; David R. Mole; Roland H. Wenger Distal and proximal hypoxia response elements cooperate to regulate organ-specific erythropoietin gene expression. haematol 2019, 105, 2774.

Ilias Mylonis; Georgia Chachami; Martina Samiotaki; George Panayotou; Efrosini Paraskeva; Alkmini Kalousi; Eleni Georgatsou; Sofia Bonanou; George Simos Identification of MAPK Phosphorylation Sites and Their Role in the Localization and Activity of Hypoxia-inducible Factor-1Î. The Journal of biological chemistry 2006, 281, 33095 DOI:10.1074/jbc.M605058200.

Inoue, K.; Miyachi, S.; Nishi, K.; Okado, H.; Nagai, Y.; Minamimoto, T.; Nambu, A.; Takada, M. Recruitment of calbindin into nigral dopamine neurons protects against MPTP-Induced parkinsonism. Movement Disorders 2018, 34, 200.

Ioghen, O. C.; Ceafalan, L. C.; Popescu, B. O. SH-SY5Y Cell Line In Vitro Models for Parkinson Disease Research—Old Practice for New Trends. J. Integr. Neurosci. 2023, 22.

Jang, W.; Kim, H. J.; Li, H.; Jo, K. D.; Lee, M. K.; Song, S. H.; Yang, H. O. 1,25-Dyhydroxyvitamin D.sub.3 attenuates rotenone-induced neurotoxicity in SH-SY5Y cells through induction of autophagy. Biochemical and biophysical research communications 2014, 451, 142 DOI:10.1016/j.bbrc.2014.07.081.

Jang, W.; Kim, H. J.; Li, H.; Jo, K. D.; Lee, M. K.; Yang, H. O. The Neuroprotective Effect of Erythropoietin on Rotenone-Induced Neurotoxicity in SH-SY5Y Cells Through the Induction of Autophagy. Mol Neurobiol 2016, 53, 3812-3821 DOI:10.1007/s12035-015-9316-x.

Janke, K.; Brockmeier, U.; Kuhlmann, K.; Eisenacher, M.; Nolde, J.; Meyer, H. E.; Mairbäurl, H.; Metzen, E. Factor Inhibiting HIF-1 (FIH-1) modulates protein interactions of Apoptosis-Stimulating p53 binding Protein 2 (ASPP2). Journal of cell science 2013, 126, 2629-2640 DOI:10.1242/jcs.117564.

Janowska, M. K.; Wu, K.; Baum, J. Unveiling transient protein-protein interactions that modulate inhibition of alpha-synuclein aggregation by beta-synuclein, a pre-synaptic protein that co-localizes with alpha-synuclein. Scientific Reports 2015, 5, 15164 DOI:10.1038/srep15164.

Javed Butt, U.; Steixner-Kumar, A. A.; Depp, C.; Ting Sun ; Hassouna, I.; Wüstefeld, L.; Arinrad, S.; Zillmann, M. R.; Schopf, N.; Fernandez, L.; , G.; Mohrmann, L.; Bode, U.; Ronnenberg, A.; Hindermann, M.; Goebbels, S.; Bonn, S.; Dörthe; Katschinski, M.;

Kamilla; Miskowiak, W.; Nave, K.; Ehrenreich, H. Hippocampal neurons respond to brain activity with functional hypoxia. Molecular Psychiatry 2021b, 26, 1790.

Jiang, B. H.; Rue, E.; Wang, G. L.; Roe, R.; Semenza, G. L. Dimerization, DNA Binding, and Transactivation Properties of Hypoxia-inducible Factor 1. The Journal of biological chemistry 1996, 271, 17771-17778 DOI:10.1074/jbc.271.30.17771.

Jiang, P.; Dickson, D. W. Parkinson's disease: experimental models and reality. Acta Neuropathol 2018, 135, 13-32 DOI:10.1007/s00401-017-1788-5.

Jin Hyen Baek; Ye V. Liu; Karin R. McDonald; Jacob B. Wesley; Maimon E. Hubbi; Hweejo Byun; Gregg L. Semenza Spermidine/Spermine-N1-Acetyltransferase 2 Is an Essential Component of the Ubiquitin Ligase Complex That Regulates Hypoxia-inducible Factor 1Î. The Journal of biological chemistry 2007, 282, 23572 DOI:10.1074/jbc.M703504200.

Jin, W.; Kong, Z.; Shen, Z.; Jin, Y.; Zhang, W.; Chen, G. Regulation of hypoxia inducible factor-1α expression by the alteration of redox status in HepG2 cells. Journal of Experimental & Clinical Cancer Research 2011, 30, 61 DOI:10.1186/1756-9966-30-61.

Johnson, M. E.; Bobrovskaya, L. An update on the rotenone models of Parkinson's disease: Their ability to reproduce the features of clinical disease and model gene–environment interactions. Neurotoxicology 2015, 46, 101-116 DOI:10.1016/j.neuro.2014.12.002.

Joseph, C.; Mangani, A. S.; Gupta, V.; Chitranshi, N.; Shen, T.; Dheer, Y.; KB, D.; Mirzaei, M.; You, Y.; Graham, S. L.; Gupta, V. Cell Cycle Deficits in Neurodegenerative Disorders: Uncovering Molecular Mechanisms to Drive Innovative Therapeutic Development. Aging and disease 2020, 11, 946-966 DOI:10.14336/AD.2019.0923.

Joshi, S.; Singh, A. R.; Durden, D. L. MDM2 Regulates Hypoxic Hypoxia-inducible Factor 1α Stability in an E3 Ligase, Proteasome, and PTEN-Phosphatidylinositol 3-Kinase-AKT-dependent Manner. The Journal of biological chemistry 2014, 289, 22785-22797 DOI:10.1074/jbc.M114.587493.

Juaristi, I.; Contreras, L.; González-Sánchez, P.; Pérez-Liébana, I.; González-Moreno, L.; Pardo, B.; Del Arco, A.; Satrústegui, J. The Response to Stimulation in Neurons and Astrocytes. Neurochem Res 2019, 44, 2385.

Jung, C.; Hwang, K.; Yoo, J.; Cho, W.; Kim, J.; Kim, W. H.; Im, D. E2-EPF UCP targets pVHL for degradation and associates with tumor growth and metastasis. Nature medicine 2006, 12, 809-816 DOI:10.1038/nm1440.

Kale, J.; Osterlund, E. J.; Andrews, D. W. BCL-2 family proteins: changing partners in the dance towards death. Cell Death Differ 2018, 25, 65.

Kane, A. D.; Kothmann, E.; Giussani, D. A. Detection and response to acute systemic hypoxia. BJA education 2020, 20, 58-64 DOI:10.1016/j.bjae.2019.10.004.

Karimi-Moghadam, A.; Charsouei, S.; Bell, B.; Jabalameli, M. R. Parkinson Disease from Mendelian Forms to Genetic Susceptibility: New Molecular Insights into the

Neurodegeneration Process. Cell Mol Neurobiol 2018, 38, 1153-1178 DOI:10.1007/s10571-018-0587-4.

Katerji, M.; Filippova, M.; Duerksen-Hughes, P. Approaches and Methods to Measure Oxidative Stress in Clinical Samples: Research Applications in the Cancer Field. Oxidative Medicine and Cellular Longevity 2019, 2019, 1279250-29 DOI:10.1155/2019/1279250.

Kawamoto, Y.; Ito, H.; Ayaki, T.; Takahashi, R. Immunohistochemical localization of apoptosome-related proteins in Lewy bodies in Parkinson′s disease and dementia with Lewy bodies. Brain research 2014, 1571, 39-48 DOI:10.1016/j.brainres.2014.05.007.

Kedishvili, N. Y. Retinoic Acid Synthesis and Degradation; In Sub-cellular biochemistry; Springer Netherlands: The Netherlands, 2016; Vol. 81, pp 127-161.

Kelts, J. L.; Cali, J. J.; Duellman, S. J.; Shultz, J. Altered cytotoxicity of ROS-inducing compounds by sodium pyruvate in cell culture medium depends on the location of ROS generation. SpringerPlus 2015, 4, 269 DOI:10.1186/s40064-015-1063-y.

Kenneth, N. S.; Rocha, S. Regulation of gene expression by hypoxia. Biochemical journal 2008, 414, 19-29 DOI:10.1042/BJ20081055.

Khatib, T.; Marini, P.; Nunna, S.; Chisholm, D. R.; Whiting, A.; Redfern, C.; Greig, I. R.; McCaffery, P. Genomic and non-genomic pathways are both crucial for peak induction of neurite outgrowth by retinoids. Cell Communication and Signaling 2019, 17, 40 DOI:10.1186/s12964-019-0352-4.

Kim, J.; Cunningham, R.; James, B.; Wyder, S.; Gibson, J. D.; Niehuis, O.; Zdobnov, E. M.; Robertson, H. M.; Robinson, G. E.; Werren, J. H.; Sinha, S. Functional Characterization of Transcription Factor Motifs Using Cross-species Comparison across Large Evolutionary Distances. PLoS Computational Biology 2010, 6, e1000652 DOI:10.1371/journal.pcbi.1000652.

Kim, S.; Kim, H.; Lee, J.; Park, K. S.; Jeon, G. S.; Shon, J.; Ahn, S.; Kim, S. H.; Lee, K. M.; Sung, J.; Lee, K. Intermittent Hypoxia Can Aggravate Motor Neuronal Loss and Cognitive Dysfunction in ALS Mice. PLoS ONE 2013, 8, e81808 DOI:10.1371/journal.pone.0081808.

Kim, T.; Mehta, S. L.; Kaimal, B.; Lyons, K.; Dempsey, R. J.; Vemuganti, R. Poststroke Induction of α-Synuclein Mediates Ischemic Brain Damage. The Journal of neuroscience 2016, 36, 7055-7065 DOI:10.1523/JNEUROSCI.1241-16.2016.

Kimura, H.; Weisz, A.; Ogura, T.; Hitomi, Y.; Kurashima, Y.; Hashimoto, K.; D'Acquisto, F.; Makuuchi, M.; Esumi, H. Identification of Hypoxia-inducible Factor 1 Ancillary Sequence and Its Function in Vascular Endothelial Growth Factor Gene Induction by Hypoxia and Nitric Oxide. The Journal of biological chemistry 2001, 276, 2292-2298 DOI:10.1074/jbc.m008398200.

Klucken, J.; Poehler, A.; Ebrahimi-Fakhari, D.; Schneider, J.; Nuber, S.; Rockenstein, E.; Schlötzer-Schrehardt, U.; Hyman, B. T.; McLean, P. J.; Masliah, E.; Winkler, J. Alpha-

synuclein aggregation involves a bafilomycin A1-sensitive autophagy pathway. Autophagy 2012, 8, 754-766 DOI:10.4161/auto.19371.

Knaup, K. X.; Jozefowski, K.; Schmidt, R.; Bernhardt, W. M.; Weidemann, A.; Juergensen, J. S.; Warnecke, C.; Eckardt, K.; Wiesener, M. S. Mutual Regulation of Hypoxia-Inducible Factor and Mammalian Target of Rapamycin as a Function of Oxygen Availability. Molecular cancer research 2009, 7, 88-98 DOI:10.1158/1541-7786.MCR-08-0288.

Kobayashi, Y.; Oguro, A.; Hirata, Y.; Imaoka, S. The regulation of Hypoxia-Inducible Factor-1 (HIF-1alpha) expression by Protein Disulfide Isomerase (PDI). PLoS ONE 2021, 16.

Koh, M. Y.; Darnay, B. G.; Powis, G. Hypoxia-Associated Factor, a Novel E3-Ubiquitin Ligase, Binds and Ubiquitinates Hypoxia-Inducible Factor 1α, Leading to Its Oxygen-Independent Degradation. Molecular and Cellular Biology 2008, 28, 7081-7095 DOI:10.1128/MCB.00773-08.

Koh, M. Y.; Spivak-Kroizman, T. R.; Powis, G. HIF-1 regulation: not so easy come, easy go. Trends in biochemical sciences (Amsterdam. Regular ed.) 2008, 33, 526-534 DOI:10.1016/j.tibs.2008.08.002.

Korbecki, J.; Kojder, K.; Kapczuk, P.; Kupnicka, P.; Gawrońska-Szklarz, B.; Gutowska, I.; Chlubek, D.; Baranowska-Bosiacka, I. The Effect of Hypoxia on the Expression of CXC Chemokines and CXC Chemokine Receptors—A Review of Literature. International journal of molecular sciences 2021, 22, 843 DOI:10.3390/ijms22020843.

Korchounov, A.; Meyer, M. F.; Krasnianski, M. Postsynaptic nigrostriatal dopamine receptors and their role in movement regulation. J Neural Transm 2010, 117, 1359-1369 DOI:10.1007/s00702-010-0454-z.

Korsmeyer, S. J.; Wei, M. C.; Saito, M.; Weiler, S.; Oh, K. J.; Schlesinger, P. H. Pro-apoptotic cascade activates BID, which oligomerizes BAK or BAX into pores that result in the release of cytochrome c. Cell death and differentiation 2000, 7, 1166-1173 DOI:10.1038/sj.cdd.4400783.

Koshiji, M.; Kageyama, Y.; Pete, E. A.; Horikawa, I.; Barrett, J. C.; Huang, L. E. HIF-1α induces cell cycle arrest by functionally counteracting Myc. The EMBO journal 2004, 23, 1949-1956 DOI:10.1038/sj.emboj.7600196.

Kovalevich, J.; Langford, D. Considerations for the Use of SH-SY5Y Neuroblastoma Cells in Neurobiology. Neuronal Cell Culture 2013, 9.

Krishna, A.; Biryukov, M.; Trefois, C.; Antony, P. M. A.; Hussong, R.; Lin, J.; Heinäniemi, M.; Glusman, G.; Köglsberger, S.; Boyd, O.; van den Berg, B. H. J.; Linke, D.; Huang, D.; Wang, K.; Hood, L.; Tholey, A.; Schneider, R.; Galas, D. J.; Balling, R.; May, P. Systems genomics evaluation of the SH-SY5Y neuroblastoma cell line as a model for Parkinson's disease. BMC Genomics 2014, 15, 1154 DOI:10.1186/1471-2164-15-1154.

Kulkarni, A.; Dong, A.; Kulkarni, V. V.; Chen, J.; Laxton, O.; Anand, A.; Maday, S. Differential regulation of autophagy during metabolic stress in astrocytes and neurons. Autophagy 2020, 16, 1651-1667 DOI:10.1080/15548627.2019.1703354.

Kumar, A.; Vaish, M.; Karuppagounder, S. S.; Gazaryan, I.; Cave, J. W.; Starkov, A. A.; Anderson, E. T.; Zhang, S.; Pinto, J. T.; Rountree, A. M.; Wang, W.; Sweet, I. R.; Ratan, R. R. HIF1α stabilization in hypoxia is not oxidant-initiated. eLife 2021, 10.

Kunej, T. Integrative Map of HIF1A Regulatory Elements and Variations. Genes 2021, 12, 1526 DOI:10.3390/genes12101526.

Kung-Chun Chiu, D.; Pui-Wah Tse, A.; Law, C.; Ming-Jing Xu, I.; Lee, D.; Chen, M.; Kit-Ho Lai, R.; Wai-Hin Yuen, V.; Wing-Sum Cheu, J.; Wai-Hung Ho, D.; Wong, C.; Zhang, H.; Oi-Lin Ng, I.; Chak-Lui Wong, C. Hypoxia regulates the mitochondrial activity of hepatocellular carcinoma cells through HIF/HEY1/PINK1 pathway. Cell Death Dis 2019, 10.

Lacher, S. E.; Levings, D. C.; Freeman, S.; Slattery, M. Identification of a functional antioxidant response element at the HIF1A locus. Redox Biology 2018, 19, 401-411 DOI:10.1016/j.redox.2018.08.014.

Lando, D.; Peet, D. J.; Whelan, D. A.; Gorman, J. J.; Whitelaw, M. L. Asparagine Hydroxylation of the HIF Transactivation Domain: A Hypoxic Switch. Science 2002, 295, 858-861 DOI:10.1126/science.1068592.

Lee, H. J.; Jung, Y. H.; Choi, G. E.; Kim, J. S.; Chae, C. W.; Han, H. J. Role of HIF1 α Regulatory Factors in Stem Cells. International Journal of Stem Cells 2019, 12, 8-20 DOI:10.15283/ijsc18109.

Lee, H. J.; Jung, Y. H.; Oh, J. Y.; Choi, G. E.; Chae, C. W.; Kim, J. S.; Lim, J. R.; Kim, S. Y.; Lee, S.; Seong, J. K.; Han, H. J. BICD1 mediates HIF1α nuclear translocation in mesenchymal stem cells during hypoxia adaptation. Cell Death and Differentiation 2019, 26, 1716-1734 DOI:10.1038/s41418-018-0241-1.

Lee, H.; Jeong, G. Protective Effects of 6,7,4′-Trihydroxyflavanone on Hypoxia-Induced Neurotoxicity by Enhancement of HO-1 through Nrf2 Signaling Pathway. Antioxidants 2021, 10, 341 DOI:10.3390/antiox10030341.

Lee, J. W.; Ko, J.; Ju, C.; Eltzschig, H. K. Hypoxia signaling in human diseases and therapeutic targets. Experimental & Molecular Medicine 2019, 51, 1-13 DOI:10.1038/s12276-019-0235-1.

Lee, J.; Escher, B. I.; Scholz, S.; Schlichting, R. Inhibition of neurite outgrowth and enhanced effects compared to baseline toxicity in SH-SY5Y cells. Arch Toxicol 2022, 96, 1039-1053 DOI:10.1007/s00204-022-03237-x.

Lehtonen, Š; Sonninen, T.; Wojciechowski, S.; Goldsteins, G.; Koistinaho, J. Dysfunction of Cellular Proteostasis in Parkinson's Disease. Front. Neurosci. 2019, 13.

Lestón Pinilla, L.; Ugun-Klusek, A.; Rutella, S.; De Girolamo, L. A. Hypoxia Signaling in Parkinson's Disease: There Is Use in Asking "What HIF?". Biology (Basel, Switzerland) 2021, 10, 723 DOI:10.3390/biology10080723.

Li, J.; Yuan, J. Caspases in apoptosis and beyond. Oncogene 2008, 27, 6194-6206 DOI:10.1038/onc.2008.297.

Li, M.; Hu, J.; Yuan, X.; Shen, L.; Zhu, L.; Luo, Q. Hepcidin Decreases Rotenone-Induced α-Synuclein Accumulation via Autophagy in SH-SY5Y Cells. Frontiers in molecular neuroscience 2020, 13, 560891 DOI:10.3389/fnmol.2020.560891.

Li, P.; Lv, H.; Zhang, B.; Duan, R.; Zhang, X.; Lin, P.; Song, C.; Liu, Y. Growth Differentiation Factor 15 Protects SH-SY5Y Cells From Rotenone-Induced Toxicity by Suppressing Mitochondrial Apoptosis. Frontiers in aging neuroscience 2022, 14, 869558 DOI:10.3389/fnagi.2022.869558.

Li, X.; Cui, X. X.; Chen, Y.; Wu, T.; Xu, H.; Yin, H.; Wu, Y. Therapeutic Potential of a Prolyl Hydroxylase Inhibitor FG-4592 for Parkinson's Diseases in Vitro and in Vivo: Regulation of Redox Biology and Mitochondrial Function. Front. Aging Neurosci. 2018, 10.

Li, Y.; Wu, L.; Yu, M.; Yang, F.; Wu, B.; Lu, S.; Tu, M.; Xu, H. HIF-1α is Critical for the Activation of Notch Signaling in Neurogenesis During Acute Epilepsy. Neuroscience 2018, 394, 206-219 DOI:10.1016/j.neuroscience.2018.10.037.

Lin, A.; Li, C.; Xing, Z.; Hu, Q.; Liang, K.; Han, L.; Wang, C.; Hawke, D. H.; Wang, S.; Zhang, Y.; Wei, Y.; Ma, G.; Park, P. K.; Zhou, J.; Zhou, Y.; Hu, Z.; Zhou, Y.; Marks, J. R.; Liang, H.; Hung, M.; Lin, C.; Yang, L. The LINK-A lncRNA activates normoxic HIF1α signalling in triple-negative breast cancer. Nat Cell Biol 2016, 18, 213.

Liu, X.; Cai, T.; Zhu, H.; Cao, J.; Su, Y.; Hu, Y.; He, Q.; Yang, B. Q6, a novel hypoxia-targeted drug, regulates hypoxia-inducible factor signaling via an autophagy-dependent mechanism in hepatocellular carcinoma. Autophagy 2014, 10, 111-122 DOI:10.4161/auto.26838.

Liu, X.; Cheng, R.; Verbitsky, M.; Kisselev, S.; Browne, A.; Mejia-Sanatana, H.; Louis, E. D.; Cote, L. J.; Andrews, H.; Waters, C.; Ford, B.; Frucht, S.; Fahn, S.; Marder, K.; Clark, L. N.; Lee, J. H. Genome-Wide association study identifies candidate genes for Parkinson's disease in an Ashkenazi Jewish population. BMC Medical Genetics 2011, 12, 104 DOI:10.1186/1471-2350-12-104.

Liu, X.; Lu, J.; Xing, J. Stabilization of HIF-1α modulates VEGF and Caspase-3 in the hippocampus of rats following transient global ischemia induced by asphyxial cardiac arrest. Life sciences (1973) 2016, 151, 243-249 DOI:10.1016/j.lfs.2016.03.005.

Liu, Y. V.; Baek, J. H.; Zhang, H.; Diez, R.; Cole, R. N.; Semenza, G. L. RACK1 Competes with HSP90 for Binding to HIF-1α and Is Required for O2-Independent and HSP90 Inhibitor-Induced Degradation of HIF-1α. Molecular Cell 2007, 25, 207-217 DOI:10.1016/j.molcel.2007.01.001.

Liu, Y.; Chen, L.; Gao, L.; Pei, X.; Tao, Z.; Xu, Y.; Li, R. LRRK2 deficiency protects the heart against myocardial infarction injury in mice via the P53/HMGB1 pathway. Free radical biology & medicine 2022, 191, 119-127 DOI:10.1016/j.freeradbiomed.2022.08.035.

Loh, X.; Sun, Q.; Ding, L.; Mayakonda, A.; Venkatachalam, N.; Yeo, M.; Silva, T. C.; Xiao, J.; Doan, N. B.; Said, J. W.; Ran, X.; Zhou, S.; Dakle, P.; Shyamsunder, P.; Koh, A. P.; Huang, R. Y.; Berman, B. P.; Tan, S.; Yang, H.; Lin, D.; Koeffler, H. P. RNA-Binding Protein ZFP36L1 Suppresses Hypoxia and Cell-Cycle Signaling. Cancer Research 2020, 80, 219.

Lopes, F. M.; Schröder, R.; Júnior, M. L. C. d. F.; Zanotto-Filho, A.; Müller, C. B.; Pires, A. S.; Meurer, R. T.; Colpo, G. D.; Gelain, D. P.; Kapczinski, F.; Moreira, J. C. F.; Fernandes, M. d. C.; Klamt, F. Comparison between proliferative and neuron-like SH-SY5Y cells as an in vitro model for Parkinson disease studies. Brain research 2010, 1337, 85-94 DOI:10.1016/j.brainres.2010.03.102.

López-Barneo, J.; Macías, D.; Platero-Luengo, A.; Ortega-Sáenz, P.; Pardal, R. Carotid body oxygen sensing and adaptation to hypoxia. Pflugers Arch - Eur J Physiol 2016, 468, 59-70 DOI:10.1007/s00424-015-1734-0.

López-Carballo, G.; Moreno, L.; Masiá, S.; Pérez, P.; Barettino, D. Activation of the Phosphatidylinositol 3-Kinase/Akt Signaling Pathway by Retinoic Acid Is Required for Neural Differentiation of SH-SY5Y Human Neuroblastoma Cells. The Journal of biological chemistry 2002, 277, 25297-25304 DOI:10.1074/jbc.M201869200.

López-Grueso, M. J.; Padilla, C. A.; Bárcena, J. A.; Requejo-Aguilar, R. Deficiency of Parkinson's Related Protein DJ-1 Alters Cdk5 Signalling and Induces Neuronal Death by Aberrant Cell Cycle Re-entry. Cell Mol Neurobiol 2023, 43, 757-769 DOI:10.1007/s10571-022-01206-7.

Lowe, R.; Shirley, N.; Bleackley, M.; Dolan, S.; Shafee, T. Transcriptomics technologies. PLoS Computational Biology 2017, 13, e1005457 DOI:10.1371/journal.pcbi.1005457.

Lu, J.; Chen, S.; Shen, M.; He, Q.; Zhang, Y.; Shi, Y.; Ding, F.; Zhang, Q. Mitochondrial regulation by pyrroloquinoline quinone prevents rotenone-induced neurotoxicity in Parkinson's disease models. Neuroscience letters 2018, 687, 104-110 DOI:10.1016/j.neulet.2018.09.031.

Lu, N.; Li, X.; Tan, R.; An, J.; Cai, Z.; Hu, X.; Wang, F.; Wang, H.; Lu, C.; Lu, H. HIF-1α/Beclin1-Mediated Autophagy Is Involved in Neuroprotection Induced by Hypoxic Preconditioning. J Mol Neurosci 2018, 66, 238-250 DOI:10.1007/s12031-018-1162-7.

Lu, Z.; Xu, S. ERK1/2 MAP kinases in cell survival and apoptosis. IUBMB life 2006, 58, 621-631 DOI:10.1080/15216540600957438.

Luo, W.; Zhong, J.; Chang, R.; Hu, H.; Pandey, A.; Semenza, G. L. Hsp70 and CHIP Selectively Mediate Ubiquitination and Degradation of Hypoxia-inducible Factor (HIF)-1α but Not HIF-2α. The Journal of biological chemistry 2010, 285, 3651-3663 DOI:10.1074/jbc.M109.068577.

Ma, J.; Gao, S.; Yang, H.; Wang, M.; Cheng, B.; Feng, Z.; Wang, L. Neuroprotective Effects of Proanthocyanidins, Natural Flavonoids Derived From Plants, on Rotenone-Induced Oxidative Stress and Apoptotic Cell Death in Human Neuroblastoma SH-SY5Y Cells. Front. Neurosci. 2018, 12.

Maher, E. R.; Neumann, H. P.; Richard, S. von Hippel-Lindau disease: A clinical and scientific review. European journal of human genetics : EJHG 2011, 19, 617-623 DOI:10.1038/ejhg.2010.175.

Malagelada, C.; Jin, Z. H.; Jackson-Lewis, V.; Przedborski, S.; Greene, L. A. Rapamycin Protects against Neuron Death in In Vitro and In Vivo Models of Parkinson's Disease. The Journal of neuroscience 2010, 30, 1166-1175 DOI:10.1523/JNEUROSCI.3944-09.2010.

Martin, E.; Gandawijaya, J.; Oguro-Ando, A. A novel method for generating glutamatergic SH-SY5Y neuron-like cells utilizing B-27 supplement. Frontiers in pharmacology 2022, 13, 943627 DOI:10.3389/fphar.2022.943627.

Martinez, C.; Jiramongkol, Y.; Bal, N.; Alwis, I.; Nedoboy, P. E.; Farnham, M. M. J.; White, M. D.; Cistulli, P. A.; Cook, K. M. Intermittent hypoxia enhances the expression of hypoxia inducible factor HIF1A through histone demethylation. The Journal of biological chemistry 2022, 298, 102536 DOI:10.1016/j.jbc.2022.102536.

Mat Taib, C. N.; Mustapha, M. MPTP-induced mouse model of Parkinson’s disease: A promising direction of therapeutic strategies. Bosnian journal of basic medical sciences 2021, 21, 422-433 DOI:10.17305/bjbms.2020.5181.

McGettrick, A. F.; O’Neill, L. A. J. The Role of HIF in Immunity and Inflammation. Cell metabolism 2020, 32, 524-536 DOI:10.1016/j.cmet.2020.08.002.

McGinnis, S.; Madden, T. L. BLAST: at the core of a powerful and diverse set of sequence analysis tools. Nucleic acids research 2004, 32, W20-W25 DOI:10.1093/nar/gkh435.

Mey, J.; Mccaffery, P. Retinoic Acid Signaling in the Nervous System of Adult Vertebrates. The Neuroscientist (Baltimore, Md.) 2004, 10, 409-421 DOI:10.1177/1073858404263520.

Miao, M.; Wu, M.; Li, Y.; Zhang, L.; Jin, Q.; Fan, J.; Xu, X.; Gu, R.; Hao, H.; Zhang, A.; Jia, Z. Clinical Potential of Hypoxia Inducible Factors Prolyl Hydroxylase Inhibitors in Treating Nonanemic Diseases. Front. Pharmacol. 2022, 13.

Michiels, C.; Minet, E.; Michel, G.; Mottet, D.; Piret, J.; Raes, M. HIF-1 and AP-1 Cooperate to Increase Gene Expression in Hypoxia: Role of MAP Kinases. IUBMB Life 2001, 52, 49-53.

Mitroshina, E. V.; Savyuk, M. O.; Ponimaskin, E.; Vedunova, M. V. Hypoxia-Inducible Factor (HIF) in Ischemic Stroke and Neurodegenerative Disease. Frontiers in cell and developmental biology 2021, 9, 703084 DOI:10.3389/fcell.2021.703084.

Mizushima, N.; Yoshimori, T.; Levine, B. Methods in Mammalian Autophagy Research. Cell 2010, 140, 313-326 DOI:10.1016/j.cell.2010.01.028.

Mogi, M.; Togari, A.; Kondo, T.; Mizuno, Y.; Komure, O.; Kuno, S.; Ichinose, H.; Nagatsu, T. Caspase activities and tumor necrosis factor receptor R1 (p55) level are elevated in the substantia nigra from Parkinsonian brain. Journal of Neural Transmission 2000, 107, 335-341 DOI:10.1007/s007020050028.

Mole, D. R.; Blancher, C.; Copley, R. R.; Pollard, P. J.; Gleadle, J. M.; Ragoussis, J.; Ratcliffe, P. J. Genome-wide Association of Hypoxia-inducible Factor (HIF)-1α and HIF-2α DNA Binding with Expression Profiling of Hypoxia-inducible Transcripts. Journal of Biological Chemistry 2009, 284, 16767.

Mole, D. R.; Blancher, C.; Copley, R. R.; Pollard, P. J.; Gleadle, J. M.; Ragoussis, J.; Ratcliffe, P. J. Genome-wide Association of Hypoxia-inducible Factor (HIF)-1α and HIF-2α DNA Binding with Expression Profiling of Hypoxia-inducible Transcripts. The Journal of Biological Chemistry 2009, 284, 16767-16775 DOI:10.1074/jbc.M901790200.

Mole, D. R.; Schlemminger, I.; Mcneill, L. A.; Hewitson, K. S.; Pugh, C. W.; Ratcliffe, P. J.; Schofield, C. J. 2-Oxoglutarate analogue inhibitors of hif prolyl hydroxylase. Bioorganic & Medicinal Chemistry Letters 2003, 13, 2677.

Monti, D. A.; Zabrecky, G.; Kremens, D.; Liang, T.; Wintering, N. A.; Bazzan, A. J.; Zhong, L.; Bowens, B. K.; Chervoneva, I.; Intenzo, C.; Newberg, A. B. N-Acetyl Cysteine Is Associated With Dopaminergic Improvement in Parkinson's Disease. Clin Pharma and Therapeutics 2019, 106, 884.

Muddapu, V. R.; Mandali, A.; Chakravarthy, V. S.; Ramaswamy, S. A computational model of loss of dopaminergic cells in Parkinson's disease due to glutamate-induced excitotoxicity. Frontiers in Neural Circuits 2019, 13, 11 DOI:10.3389/fncir.2019.00011.

Muñoz-Sánchez, J.; Chánez-Cárdenas, M. E. The use of cobalt chloride as a chemical hypoxia model. Journal of applied toxicology 2019, 39, 556-570 DOI:10.1002/jat.3749.

Myerowitz, R.; Puertollano, R.; Raben, N. Impaired autophagy: The collateral damage of lysosomal storage disorders. EBioMedicine 2021, 63, 103166 DOI:10.1016/j.ebiom.2020.103166.

Nagara, Y.; Tateishi, T.; Yamasaki, R.; Hayashi, S.; Kawamura, M.; Kikuchi, H.; Iinuma, K. M.; Tanaka, M.; Iwaki, T.; Matsushita, T.; Ohyagi, Y.; Kira, J. Impaired Cytoplasmic–Nuclear Transport of Hypoxia-Inducible Factor-1α in Amyotrophic Lateral Sclerosis. Brain Pathology 2013, 23, 534.

Nakayama, S.; Yumimoto, K.; Kawamura, A.; Nakayama, K. I. Degradation of the endoplasmic reticulum–anchored transcription factor MyRF by the ubiquitin ligase SCFFbxw7 in a manner dependent on the kinase GSK-3. The Journal of biological chemistry 2018, 293, 5705-5714 DOI:10.1074/jbc.RA117.000741.

Narrandes, S.; Xu, W. Gene Expression Detection Assay for Cancer Clinical Use. J. Cancer 2018, 9, 2249.

Newhouse, K.; Hsuan, S.; Chang, S. H.; Cai, B.; Wang, Y.; Xia, Z. Rotenone-Induced Apoptosis Is Mediated By p38 And JNK MAP Kinases In Human Dopaminergic SH-SY5Y Cells. Toxicological sciences 2004, 79, 137-146 DOI:10.1093/toxsci/kfh089.

Ng, K.; Lee, Y.; Chan, Y.; Lai, W.; Fung, M.; Li, R. A.; Siu, C.; Tse, H. Exogenous expression of HIF-1α promotes cardiac differentiation of embryonic stem cells. Journal of molecular and cellular cardiology 2010, 48, 1129-1137 DOI:10.1016/j.yjmcc.2010.01.015.

Ni, H.; Williams, J. A.; Ding, W. Mitochondrial dynamics and mitochondrial quality control. Redox Biology 2015, 4, 6-13 DOI:10.1016/j.redox.2014.11.006.

Nieber, K. Hypoxia and Neuronal Function under in Vitro Conditions. Pharmacology and Therapeutics 1999, 82, 71-86 DOI:10.1016/S0163-7258(98)00061-8.

Niecknig, H.; Tug, S.; Reyes, B. D.; Kirsch, M.; Fandrey, J.; Berchner-Pfannschmidt, U. Role of reactive oxygen species in the regulation of HIF-1 by prolyl hydroxylase 2 under mild hypoxia. Free radical research 2012, 46, 705-717 DOI:10.3109/10715762.2012.669041.

Niethammer, M.; Tang, C. C.; Lewitt, P. A.; Rezai, A. R.; Leehey, M. A.; Ojemann, S. G.; Flaherty, A. W.; Eskandar, E. N.; Kostyk, S. K.; Sarkar, A.; Siddiqui, M. S.; Tatter, S. B.; Schwalb, J. M.; Poston, K. L.; Henderson, J. M.; Kurlan, R. M.; Richard, I. H.; Sapan, C. V.; Eidelberg, D.; During, M. J.; Kaplitt, M. G.; Feigin, A. Long-term follow-up of a randomized AAV2-GAD gene therapy trial for Parkinson's disease. JCI Insight 2017, 2.

Nikolaienko, O.; Patil, S.; Eriksen, M. S.; Bramham, C. R. Arc protein: a flexible hub for synaptic plasticity and cognition. Seminars in cell & developmental biology 2018, 77, 33-42 DOI:10.1016/j.semcdb.2017.09.006.

Nishi, H.; Nakada, T.; Kyo, S.; Inoue, M.; Shay, J. W.; Isaka, K. Hypoxia-Inducible Factor 1 Mediates Upregulation of Telomerase (hTERT). Molecular and Cellular Biology 2004, 24, 6076-6083 DOI:10.1128/MCB.24.13.6076-6083.2004.

Nissen, S. B.; Magidson, T.; Gross, K.; Bergstrom, C. T. Publication bias and the canonization of false facts. 2019.

O'Flanagan, C. H.; Morais, V. A.; Wurst, W.; De Strooper, B.; O'Neill, C. The Parkinson's gene PINK1 regulates cell cycle progression and promotes cancer-associated phenotypes. Oncogene 2015, 34, 1363-1374 DOI:10.1038/onc.2014.81.

Okunoye, O.; Marston, L.; Walters, K.; Schrag, A. Change in the incidence of Parkinson's disease in a large UK primary care database. npj Parkinsons Dis. 2022, 8.

Ōmura, S.; Crump, A. Lactacystin: first-in-class proteasome inhibitor still excelling and an exemplar for future antibiotic research. Journal of antibiotics 2019, 72, 189-201 DOI:10.1038/s41429-019-0141-8.

Ortner, N. J.; Bock, G.; Dougalis, A.; Kharitonova, M.; Duda, J.; Hess, S.; Tuluc, P.; Pomberger, T.; Stefanova, N.; Pitterl, F.; Ciossek, T.; Oberacher, H.; Draheim, H. J.; Kloppenburg, P.; Liss, B.; Striessnig, J. Lower Affinity of Isradipine for L-Type Ca2+ Channels during Substantia Nigra Dopamine Neuron-Like Activity: Implications for Neuroprotection in Parkinson's Disease. The Journal of neuroscience 2017, 37, 6761-6777 DOI:10.1523/JNEUROSCI.2946-16.2017.

Ostrowski, R. P.; Zhang, J. H. The insights into molecular pathways of hypoxia-inducible factor in the brain. Journal of neuroscience research 2020, 98, 57-76 DOI:10.1002/jnr.24366.

Ou, Z.; Pan, J.; Tang, S.; Duan, D.; Yu, D.; Nong, H.; Wang, Z. Global Trends in the Incidence, Prevalence, and Years Lived With Disability of Parkinson's Disease in 204 Countries/Territories From 1990 to 2019. Front. Public Health 2021, 9.

Papandreou, I.; Cairns, R. A.; Fontana, L.; Lim, A. L.; Denko, N. C. HIF-1 mediates adaptation to hypoxia by actively downregulating mitochondrial oxygen consumption. Cell Metabolism 2006, 3, 187-197 DOI:10.1016/j.cmet.2006.01.012.

Park, H. J.; Kim, H. Inhibitory effect of nicardipine on rotenone-induced apoptosis in SH-SY5Y human neuroblastoma cells. Molecular medicine reports 2013, 7, 941-946 DOI:10.3892/mmr.2013.1260.

Park, J.; Lee, K.; Kim, K.; Yi, S. The role of histone modifications: from neurodevelopment to neurodiseases. Signal transduction and targeted therapy 2022, 7, 217 DOI:10.1038/s41392-022-01078-9.

Partch, C. L.; Gardner, K. H.; Wright, P. E. Coactivators necessary for transcriptional output of the hypoxia inducible factor, HIF, are directly recruited by ARNT PAS-B. Proceedings of the National Academy of Sciences - PNAS 2011, 108, 7739-7744 DOI:10.1073/pnas.1101357108.

Pastukh, V.; Roberts, J. T.; Clark, D. W.; Bardwell, G. C.; Patel, M.; Al-Mehdi, A.; Borchert, G. M.; Gillespie, M. N. An oxidative DNA “damage” and repair mechanism localized in the VEGF promoter is important for hypoxia-induced VEGF mRNA expression. American journal of physiology. Lung cellular and molecular physiology 2015, 309, L1367-L1375 DOI:10.1152/ajplung.00236.2015.

Patel, B.; Cuervo, A. M. Methods to study chaperone-mediated autophagy. Methods (San Diego, Calif.) 2015, 75, 133-140 DOI:10.1016/j.ymeth.2015.01.003.

Pawlus, M. R.; Wang, L.; Hu, C. STAT3 and HIF1α cooperatively activate HIF1 target genes in MDA-MB-231 and RCC4 cells. Oncogene 2014, 33, 1670-1679 DOI:10.1038/onc.2013.115.

Peerboom, C.; Wierenga, C. J. The postnatal GABA shift: A developmental perspective. Neuroscience and biobehavioral reviews 2021, 124, 179-192 DOI:10.1016/j.neubiorev.2021.01.024.

Peng, X.; Gao, H.; Xu, R.; Wang, H.; Mei, J.; Liu, C. The interplay between HIF-1α and noncoding RNAs in cancer. J Exp Clin Cancer Res 2020, 39.

Pierre, C. C.; Longo, J.; Bassey-Archibong, B. I.; Hallett, R. M.; Milosavljevic, S.; Beatty, L.; Hassell, J. A.; Daniel, J. M. Methylation-dependent regulation of hypoxia inducible factor-1 alpha gene expression by the transcription factor Kaiso. Biochimica et biophysica acta 2015, 1849, 1432-1441 DOI:10.1016/j.bbagrm.2015.10.018.

Pisoschi, A. M.; Pop, A. The role of antioxidants in the chemistry of oxidative stress: A review. European journal of medicinal chemistry 2015, 97, 55-74 DOI:10.1016/j.ejmech.2015.04.040.

Poloznikov, A. A.; Nersisyan, S. A.; Hushpulian, D. M.; Kazakov, E. H.; Tonevitsky, A. G.; Kazakov, S. V.; Vechorko, V. I.; Nikulin, S. V.; Makarova, J. A.; Gazaryan, I. G. HIF

Prolyl Hydroxylase Inhibitors for COVID-19 Treatment: Pros and Cons. Front. Pharmacol. 2021, 11.

Puspita, L.; Chung, S. Y.; Shim, J. Oxidative stress and cellular pathologies in Parkinson's disease. Molecular Brain 2017, 10, 53 DOI:10.1186/s13041-017-0340-9.

Qiao, H.; He, X.; Zhang, Q.; Zhang, N.; Li, L.; Hui, Y.; Li, W.; Wang, D.; Wu, Z. A-synuclein induces microglial cell migration through stimulating HIF-1α accumulation. Journal of neuroscience research 2017, 95, 1809-1817 DOI:10.1002/jnr.24012.

Qin, L.; Shu, L.; Zhong, J.; Pan, H.; Guo, J.; Sun, Q.; Yan, X.; Tang, B.; Xu, Q. Association of HIF1A and Parkinson's disease in a Han Chinese population demonstrated by molecular inversion probe analysis. Neurol Sci 2019, 40, 1927-1931 DOI:10.1007/s10072-019-03905-4.

Qiu, S.; Jia, Y.; Sun, Y.; Han, P.; Xu, J.; Wen, G.; Chai, Y. Von Hippel-Lindau (VHL) Protein Antagonist VH298 Improves Wound Healing in Streptozotocin-Induced Hyperglycaemic Rats by Activating Hypoxia-Inducible Factor- (HIF-) 1 Signalling. Journal of Diabetes Research 2019, 2019, 1897174-10 DOI:10.1155/2019/1897174.

Rajagopalan, S.; Rane, A.; Chinta, S. J.; Andersen, J. K. Regulation of ATP13A2 via PHD2-HIF1α Signaling Is Critical for Cellular Iron Homeostasis: Implications for Parkinson's Disease. The Journal of neuroscience 2016, 36, 1086-1095 DOI:10.1523/JNEUROSCI.3117-15.2016.

Rao, V. S.; Srinivas, K.; Sujini, G. N.; Kumar, G. N. S. Protein-Protein Interaction Detection: Methods and Analysis. International Journal of Proteomics 2014, 2014, 147648-12 DOI:10.1155/2014/147648.

Rao, X.; Lai, D.; Huang, X. A New Method for Quantitative Real-Time Polymerase Chain Reaction Data Analysis. Journal of computational biology 2013, 20, 703-711 DOI:10.1089/cmb.2012.0279.

Rashid, I.; Pathak, A. K.; Kumar, R.; Srivastava, P. R.; Singh, M.; Murali, S.; Kushwaha, B. Genome-Wide Comparative Analysis of HIF Binding Sites in Cyprinus Carpio for In Silico Identification of Functional Hypoxia Response Elements. Front. Genet. 2019a, 10.

Razorenova, O. V.; Castellini, L.; Colavitti, R.; Edgington, L. E.; Nicolau, M.; Huang, X.; Bedogni, B.; Mills, E. M.; Bogyo, M.; Giaccia, A. J. The Apoptosis Repressor with a CARD Domain (ARC) Gene Is a Direct Hypoxia-Inducible Factor 1 Target Gene and Promotes Survival and Proliferation of VHL-Deficient Renal Cancer Cells. Molecular and Cellular Biology 2014, 34, 739.

Requejo-Aguilar, R.; Lopez-Fabuel, I.; Fernandez, E.; Martins, L. M.; Almeida, A.; Bolaños, J. P. PINK1 deficiency sustains cell proliferation by reprogramming glucose metabolism through HIF1. Nature communications 2014, 5, 4514 DOI:10.1038/ncomms5514.

Robak, L. A.; Jansen, I. E.; Van Rooij, J.; Uitterlinden, A. G.; Kraaij, R.; Jankovic, J.; Heutink, P.; Shulman, J. M.; Nalls, M. A.; Plagnol, V.; Hernandez, D. G.; Sharma, M.; Sheerin, U.; Saad, M.; Simón-Sánchez, J.; Schulte, C.; Lesage, S.; Sveinbjörnsdóttir, S.; Arepalli, S.; Barker, R.; Ben-, Y.; Berendse, H. W.; Berg, D.; Bhatia, K.; De Bie, R. M.

A.; Biffi, A.; Bloem, B.; Bochdanovits, Z.; Bonin, M.; Bras, J. M.; Brockmann, K.; Brooks, J.; Burn, D. J.; Majounie, E.; Charlesworth, G.; Lungu, C.; Chen, H.; Chinnery, P. F.; Chong, S.; Clarke, C. E.; Cookson, M. R.; Mark Cooper, J.; Corvol, J. C.; Counsell, C.; Damier, P.; Dartigues, J.; Deloukas, P.; Deuschl, G.; Dexter, D. T.; Van Dijk, K. D.; Dillman, A.; Durif, F.; Dürr, A.; Edkins, S.; Evans, J. R.; Foltynie, T.; Dong, J.; Gardner, M.; Raphael Gibbs, J.; Goate, A.; Gray, E.; Guerreiro, R.; Harris, C.; Van Hilten, J. J.; Hofman, A.; Hollenbeck, A.; Holton, J.; Hu, M.; Huang, X.; Wurster, I.; Mätzler, W.; Hudson, G.; Hunt, S. E.; Huttenlocher, J.; Illig, T.; Jónsson, P. V.; Lambert, J.; Langford, C.; Lees, A.; Lichtner, P.; Limousin, P.; Lopez, G.; Lorenz, D.; Lungu, C.; Mcneill, A.; Moorby, C.; Moore, M.; Morris, H. R.; Morrison, K. E.; Escott-Price, V.; Mudanohwo, E.; O'sullivan, S. S.; Pearson, J.; Perlmutter, J. S.; Pétursson, H.; Pollak, P.; Post, B.; Potter, S.; Ravina, B.; Revesz, T.; Riess, O.; Rivadeneira, F.; Rizzu, P.; Ryten, M.; Sawcer, S.; Schapira, A.; Scheffer, H.; Shaw, K.; Shoulson, I.; Shulman, J. M.; Sidransky, E.; Smith, C.; Spencer, C. C. A.; Stefánsson, H.; Bettella, F.; Stockton, J. D.; Strange, A.; Talbot, K.; Tanner, C. M.; Tashakkori-Ghanbaria, A.; Tison, F.; Trabzuni, D.; Traynor, B. J.; Uitterlinden, A. G.; Velseboer, D.; Vidailhet, M.; Walker, R.; Van De Warrenburg, B.; Wickremaratchi, M.; Williams, N.; Williams-Gray, C. H.; Winder-Rhodes, S.; Stefánsson, K.; Martinez, M.; Wood, N. W.; Hardy, J.; Heutink, P.; Brice, A.; Gasser, T.; Singleton, A. B. Excessive burden of lysosomal storage disorder gene variants in Parkinson's disease. Brain 2017, 140, 3191.

Rocha, S. Gene regulation under low oxygen: holding your breath for transcription. Trends in biochemical sciences (Amsterdam. Regular ed.) 2007, 32, 389-397 DOI:10.1016/j.tibs.2007.06.005.

Rodchenkov, I.; Babur, O.; Luna, A.; Aksoy, B. A.; Wong, J. V.; Fong, D.; Franz, M.; Siper, M. C.; Cheung, M.; Wrana, M.; Mistry, H.; Mosier, L.; Dlin, J.; Wen, Q.; O'Callaghan, C.; Li, W.; Elder, G.; Smith, P. T.; Dallago, C.; Cerami, E.; Gross, B.; Dogrusoz, U.; Demir, E.; Bader, G. D.; Sander, C. Pathway Commons 2019 Update: integration, analysis and exploration of pathway data. Nucleic Acids Research 2020, 48, D489-D497 DOI:10.1093/nar/gkz946.

Roitbak, T.; Surviladze, Z.; Cunningham, L. A. Continuous Expression of HIF-1α in Neural Stem/Progenitor Cells. Cell Mol Neurobiol 2011, 31, 119-133 DOI:10.1007/s10571-010-9561-5.

Rolfs, A.; Kvietikova, I.; Gassmann, M.; Wenger, R. H. Oxygen-regulated Transferrin Expression Is Mediated by Hypoxia-inducible Factor-1. The Journal of biological chemistry 1997, 272, 20055-20062 DOI:10.1074/jbc.272.32.20055.

Roufayel, R.; Murshid, N. CDK5: Key Regulator of Apoptosis and Cell Survival. Biomedicines 2019, 7, 88 DOI:10.3390/biomedicines7040088.

Sahin, M.; Oncu, G.; Yilmaz, M. A.; Ozkan, D.; Saybasili, H. Transformation of SH-SY5Y cell line into neuron-like cells: Investigation of electrophysiological and biomechanical changes. Neuroscience letters 2021, 745, 135628 DOI:10.1016/j.neulet.2021.135628.

Salceda, R. Glycine neurotransmission: Its role in development. Frontiers in neuroscience 2022, 16, 947563 DOI:10.3389/fnins.2022.947563.

Salnikow, K.; Costa, M.; Figg, W. D.; Blagosklonny, M. V.; , [. W. D. F.; , M. V. B.]. Hyperinducibility of Hypoxia-responsive Genes without p53/p21-dependent Checkpoint in Aggressive Prostate Cancer 1. Cancer research 2000, 60, 5630.

Samet, J. M.; Wages, P. A. Oxidative stress from environmental exposures. Current opinion in toxicology 2018, 7, 60-66 DOI:10.1016/j.cotox.2017.10.008.

Schapira, A. H. V.; Chaudhuri, K. R.; Jenner, P. Non-motor features of Parkinson disease Nature Reviews Neuroscience 2017;18(7):435-50.

Schödel, J.; Oikonomopoulos, S.; Ragoussis, J.; Pugh, C. W.; Ratcliffe, P. J.; Mole, D. R. High-resolution genome-wide mapping of HIF-binding sites by ChIP-seq. Blood 2011, 117, e207-e217 DOI:10.1182/blood-2010-10-314427.

Scholz, D.; Pöltl, D.; Genewsky, A.; Weng, M.; Waldmann, T.; Schildknecht, S.; Leist, M. Rapid, complete and large-scale generation of post-mitotic neurons from the human LUHMES cell line. Journal of neurochemistry 2011, 119, 957-971 DOI:10.1111/j.1471-4159.2011.07255.x.

Semenza, G. L. A compendium of proteins that interact with HIF-1α. Experimental Cell Research 2017, 356, 128.

Semenza, G. L. Life with Oxygen. Science 2007, 318, 62-64 DOI:10.1126/science.1147949.

Semenzas, G. L.; Roth, P. H.; Fang, H.; Wang, G. L. Transcriptional Regulation of Genes Encoding Glycolytic Enzymes by Hypoxia-inducible Factor l*. The journal of biological chemistry 1994, 269, 23757.

Sen, T.; Sen, N. Treatment with an activator of hypoxia-inducible factor 1, DMOG provides neuroprotection after traumatic brain injury. Neuropharmacology 2016, 107, 79-88 DOI:10.1016/j.neuropharm.2016.03.009.

Shamoto-Nagai, M.; Maruyama, W.; Kato, Y.; Isobe, K.; Tanaka, M.; Naoi, M.; Osawa, T. An inhibitor of mitochondrial complex I, rotenone, inactivates proteasome by oxidative modification and induces aggregation of oxidized proteins in SH-SY5Y cells. Journal of neuroscience research 2003, 74, 589-597 DOI:10.1002/jnr.10777.

Sheflin, L. G.; Zou, A.; Spaulding, S. W. Androgens regulate the binding of endogenous HuR to the AU-rich 3′UTRs of HIF-1α and EGF mRNA. Biochemical and biophysical research communications 2004, 322, 644-651 DOI:10.1016/j.bbrc.2004.07.173.

Sherman, D. J.; Li, J. Proteasome Inhibitors: Harnessing Proteostasis to Combat Disease. Molecules 2020, 25, 671 DOI:10.3390/molecules25030671.

Shishido, T.; Nagano, Y.; Araki, M.; Kurashige, T.; Obayashi, H.; Nakamura, T.; Takahashi, T.; Matsumoto, M.; Maruyama, H. Synphilin-1 has neuroprotective effects on MPP+-induced Parkinson's disease model cells by inhibiting ROS production and apoptosis. Neuroscience letters 2019, 690, 145-150 DOI:10.1016/j.neulet.2018.10.020.

Sies, H.; Jones, D. P. Reactive oxygen species (ROS) as pleiotropic physiological signalling agents. Nat Rev Mol Cell Biol 2020, 21, 363.

Simon, D. K., MD PhD; Tanner, Caroline M., MD, PhD; Brundin, Patrik, MD, PhD Parkinson Disease Epidemiology, Pathology, Genetics and Pathophysiology. Clinics in geriatric medicine 2020, 36, 1-12 DOI:10.1016/j.cger.2019.08.002.

Singh, A.; Wilson, J. W.; Schofield, C. J.; Chen, R. Hypoxia-inducible factor (HIF) prolyl hydroxylase inhibitors induce autophagy and have a protective effect in an in-vitro ischaemia model. Scientific Reports 2020, 10, 1597 DOI:10.1038/s41598-020-58482-w.

Sofroniew, M. V.; Vinters, H. V. Astrocytes: biology and pathology. Acta Neuropathol 2009, 119, 7.

Sonninen, T.; Hämäläinen, R. H.; Koskuvi, M.; Oksanen, M.; Shakirzyanova, A.; Wojciechowski, S.; Puttonen, K.; Naumenko, N.; Goldsteins, G.; Laham-Karam, N.; Lehtonen, M.; Tavi, P.; Koistinaho, J.; Lehtonen, Š Metabolic alterations in Parkinson's disease astrocytes. Sci Rep 2020, 10.

Stiehl, D. P.; Wirthner, R.; Köditz, J.; Spielmann, P.; Camenisch, G.; Wenger, R. H. Increased Prolyl 4-Hydroxylase Domain Proteins Compensate for Decreased Oxygen Levels. The Journal of biological chemistry 2006, 281, 23482-23491 DOI:10.1074/jbc.M601719200.

Striessnig, J.; Pinggera, A.; Kaur, G.; Bock, G.; Tuluc, P. L-type Ca 2+ channels in heart and brain. Wiley interdisciplinary reviews. Membrane transport and signaling 2014, 3, 15-38 DOI:10.1002/wmts.102.

Stroka, D. M.; Burkhardt, T.; Desbaillets, I.; Wenger, R. H.; Neil, D. A. H.; Bauer, C.; Gassmann, M.; Candinas, D. HIF-1 is expressed in normoxic tissue and displays an organ-specific regulation under systemic hypoxia. The FASEB Journal 2001, 15, 2445-2453 DOI:10.1096/fj.01-0125com.

Sudhof, T. C. Calcium Control of Neurotransmitter Release. Cold Spring Harbor perspectives in biology 2012, 4, a011353 DOI:10.1101/cshperspect.a011353.

Sun, X.; He, G.; Qing, H.; Zhou, W.; Dobie, F.; Cai, F.; Staufenbiel, M.; Huang, L. E.; Song, W. Hypoxia Facilitates Alzheimer's Disease Pathogenesis by Up-Regulating BACE1 Gene Expression. Proceedings of the National Academy of Sciences - PNAS 2006, 103, 18727-18732 DOI:10.1073/pnas.0606298103.

Supek, F.; Bošnjak, M.; Škunca, N.; Šmuc, T. REVIGO Summarizes and Visualizes Long Lists of Gene Ontology Terms. PloS one 2011, 6, e21800 DOI:10.1371/journal.pone.0021800.

Szklarczyk, D.; Kirsch, R.; Koutrouli, M.; Nastou, K.; Mehryary, F.; Hachilif, R.; Gable, A. L.; Fang, T.; Doncheva, N. T.; Pyysalo, S.; Bork, P.; Jensen, L. J.; Von mering, C. The STRING database in 2023: protein–protein association networks and functional enrichment analyses for any sequenced genome of interest. Nucleic Acids Research 2023, 51, D638.

Tagliaferro, P.; Burke, R. E. Retrograde Axonal Degeneration in Parkinson Disease. JPD 2016, 6, 1.

Tait, S. W. G.; Green, D. R. Mitochondrial Regulation of Cell Death. Cold Spring Harbor perspectives in biology 2013, 5, a008706 DOI:10.1101/cshperspect.a008706.

Tanida, I.; Minematsu-Ikeguchi, N.; Ueno, T.; Kominami, E. Lysosomal Turnover, but Not a Cellular Level, of Endogenous LC3 is a Marker for Autophagy. Autophagy 2005, 1, 84-91 DOI:10.4161/auto.1.2.1697.

Tatton, N. A. Increased Caspase 3 and Bax Immunoreactivity Accompany Nuclear GAPDH Translocation and Neuronal Apoptosis in Parkinson's Disease. Experimental neurology 2000, 166, 29-43 DOI:10.1006/exnr.2000.7489.

Tello, D.; Balsa, E.; Acosta-Iborra, B.; Fuertes-Yebra, E.; Elorza, A.; Ordóñez, Á; Corral-Escariz, M.; Soro, I.; López-Bernardo, E.; Perales-Clemente, E.; Martínez-Ruiz, A.; Enríquez, J.; Aragonés, J.; Cadenas, S.; Landázuri, M. Induction of the Mitochondrial NDUFA4L2 Protein by HIF-1α Decreases Oxygen Consumption by Inhibiting Complex I Activity. Cell metabolism 2011, 14, 768-779 DOI:10.1016/j.cmet.2011.10.008.

Theriault, J. R.; Felts, A. S.; Bates, B. S.; Perez, J. R.; Palmer, M.; Gilbert, S. R.; Dawson, E. S.; Engers, J. L.; Lindsley, C. W.; Emmitte, K. A. Discovery of a new molecular probe ML228: An activator of the hypoxia inducible factor (HIF) pathway. Bioorganic & medicinal chemistry letters 2012, 22, 76-81 DOI:10.1016/j.bmcl.2011.11.077.

Thomas, L. W.; Ashcroft, M. Exploring the molecular interface between hypoxia-inducible factor signalling and mitochondria. Cell. Mol. Life Sci 2019, 76, 1759-1777 DOI:10.1007/s00018-019-03039-y.

Tokujiro Uchida; Fabrice Rossignol; Michael A. Matthay; Rami Mounier; Sylvianne Couette; Eric Clottes; Christine Clerici Prolonged Hypoxia Differentially Regulates Hypoxia-inducible Factor (HIF)-1Î± and HIF-2Î± Expression in Lung Epithelial Cells. The Journal of biological chemistry 2004, 279, 14871 DOI:10.1074/jbc.M400461200.

Tolonen, J.; Heikkilä, M.; Malinen, M.; Lee, H.; Palvimo, J. J.; Wei, G.; Myllyharju, J. A long hypoxia-inducible factor 3 isoform 2 is a transcription activator that regulates erythropoietin. Cell. Mol. Life Sci 2020, 77, 3627-3642 DOI:10.1007/s00018-019-03387-9.

Tomita, S.; Ueno, M.; Sakamoto, M.; Kitahama, Y.; Ueki, M.; Maekawa, N.; Sakamoto, H.; Gassmann, M.; Kageyama, R.; Ueda, N.; Gonzalez, F. J.; Takahama, Y. Defective Brain Development in Mice Lacking the Hif-1α Gene in Neural Cells. Molecular and Cellular Biology 2003, 23, 6739.

Tong, M.; Ma, S. Protocols to culture and harvest hepatic tumor organoids for metabolic assays. STAR protocols 2022, 3, 101597 DOI:10.1016/j.xpro.2022.101597.

Torquatto, K. I.; Menegolla, A. P.; Popik, B.; Casagrande, M. A.; de Oliveira Alvares, L. Role of calcium-permeable AMPA receptors in memory consolidation, retrieval and updating. Neuropharmacology 2019, 144, 312-318 DOI:10.1016/j.neuropharm.2018.10.030.

Tsang, A. H. K.; Lee, Y.; Ko, H. S.; Savitt, J. M.; Pletnikova, O.; Troncoso, J. C.; Dawson, V. L.; Dawson, T. M.; Chung, K. K. K. S-nitrosylation of XIAP compromises

neuronal survival in Parkinson's disease. Proceedings of the National Academy of Sciences - PNAS 2009, 106, 4900-4905 DOI:10.1073/pnas.0810595106.

Tüshaus, J.; Kataka, E. S.; Zaucha, J.; Frishman, D.; Müller, S. A.; Lichtenthaler, S. F. Neuronal Differentiation of LUHMES Cells Induces Substantial Changes of the Proteome. Proteomics 2020, 21.

Tydlacka, S.; Wang, C.; Wang, X.; Li, S.; Li, X. Differential Activities of the Ubiquitin-Proteasome System in Neurons versus Glia May Account for the Preferential Accumulation of Misfolded Proteins in Neurons. The Journal of neuroscience 2008, 28, 13285-13295 DOI:10.1523/JNEUROSCI.4393-08.2008.

Unal-Cevik, I.; Gursoy-Ozdemir, Y.; Yemisci, M.; Lule, S.; Gurer, G.; Can, A.; Müller, V.; Kahle, P. J.; Dalkara, T. Alpha-Synuclein Aggregation Induced by Brief Ischemia Negatively Impacts Neuronal Survival in vivo: A Study in [A30P]alpha-Synuclein Transgenic Mouse. Journal of cerebral blood flow and metabolism 2011, 31, 913-923 DOI:10.1038/jcbfm.2010.170.

Vangeison, G.; Carr, D.; Federoff, H. J.; Rempe, D. A. The Good, the Bad, and the Cell Type-Specific Roles of Hypoxia Inducible Factor-1α in Neurons and Astrocytes. The Journal of neuroscience 2008, 28, 1988-1993 DOI:10.1523/JNEUROSCI.5323-07.2008.

Verhagen, A. M.; Ekert, P. G.; Pakusch, M.; Silke, J.; Connolly, L. M.; Reid, G. E.; Moritz, R. L.; Simpson, R. J.; Vaux, D. L. Identification of DIABLO, a Mammalian Protein that Promotes Apoptosis by Binding to and Antagonizing IAP Proteins. Cell 2000, 102, 43.

Verma, A.; Ravindranath, V. CaV1.3 L-Type Calcium Channels Increase the Vulnerability of Substantia Nigra Dopaminergic Neurons in MPTP Mouse Model of Parkinson’s Disease. Frontiers in Aging Neuroscience 2020, 11, 382 DOI:10.3389/fnagi.2019.00382.

Vernon, A. C.; Johansson, S. M.; Modo, M. M. Non-invasive evaluation of nigrostriatal neuropathology in a proteasome inhibitor rodent model of Parkinson's disease. BMC Neuroscience 2010, 11, 1 DOI:10.1186/1471-2202-11-1.

Vervliet, T. Ryanodine Receptors in Autophagy: Implications for Neurodegenerative Diseases? Frontiers in cellular neuroscience 2018, 12, 89 DOI:10.3389/fncel.2018.00089.

Wang, G. L.; Jiang, B. H.; Rue, E. A.; Semenza, G. L. Hypoxia-inducible factor 1 is a basic-helix-loop-helix-PAS heterodimer regulated by cellular O2 tension. Proceedings of the National Academy of Sciences - PNAS 1995, 92, 5510-5514 DOI:10.1073/pnas.92.12.5510.

Wang, H.; Chen, Y.; Chen, J.; Zhang, Z.; Lao, W.; Li, X.; Huang, J.; Wang, T. Cell Cycle Regulation of DNA Polymerase Beta in Rotenone-Based Parkinson's Disease Models. PLoS ONE 2014, 9, e109697 DOI:10.1371/journal.pone.0109697.

Wang, X.; Xu, J. Possible involvement of Ca 2+ signaling in rotenone-induced apoptosis in human neuroblastoma SH-SY5Y cells. Neuroscience letters 2005, 376, 127-132 DOI:10.1016/j.neulet.2004.11.041.

Weidemann, A.; Johnson, R. Biology of HIF-1. Cell death and differentiation 2008, 15, 621-627 DOI:10.1038/cdd.2008.12.

Weiszenstein, M.; Musutova, M.; Plihalova, A.; Westlake, K.; Elkalaf, M.; Koc, M.; Prochazka, A.; Pala, J.; Gulati, S.; Trnka, J.; Polak, J. Adipogenesis, lipogenesis and lipolysis is stimulated by mild but not severe hypoxia in 3T3-L1 cells. Biochemical and biophysical research communications 2016, 478, 727-732 DOI:10.1016/j.bbrc.2016.08.015.

Westhoff, J. H.; Hwang, S.; Scott Duncan, R.; Ozawa, F.; Volpe, P.; Inokuchi, K.; Koulen, P. Vesl/Homer proteins regulate ryanodine receptor type 2 function and intracellular calcium signaling. Cell Calcium 2003, 34, 261.

Wiesener, M. S.; Jürgensen, J. S.; Rosenberger, C.; Scholze, C.; Hörstrup, J. H.; Warnecke, C.; Mandriota, S.; Bechmann, I.; Frei, U. A.; Pugh, C. W.; Ratcliffe, P. J.; Bachmann, S.; Maxwell, P. H.; Eckardt, K. Widespread, hypoxia-inducible expression of HIF-2α in distinct cell populations of different organs. FASEB j. 2002, 17, 271.

Wilson, M. R. Apoptosis: unmasking the executioner. Cell death and differentiation 1998a, 5, 646-652 DOI:10.1038/sj.cdd.4400394.

Wu, L.; Luo, N.; Zhao, H.; Gao, Q.; Lu, J.; Pan, Y.; Shi, J.; Tian, Y.; Zhang, Y. Salubrinal protects against rotenone-induced SH-SY5Y cell death via ATF4-parkin pathway. Brain research 2014, 1549, 52-62 DOI:10.1016/j.brainres.2014.01.003.

Wu, L.; Yu, H.; Zhao, Y.; Zhang, C.; Wang, J.; Yue, X.; Yang, Q.; Hu, W. HIF-2α mediates hypoxia-induced LIF expression in human colorectal cancer cells. Oncotarget 2015, 6, 4406.

Xia, X.; Kung, A. L. Preferential binding of HIF-1 to transcriptionally active loci determines cell-type specific response to hypoxia. Genome Biology 2009, 10, R113 DOI:10.1186/gb-2009-10-10-r113.

Xicoy, H.; Wieringa, B.; Martens, G. J. M. The SH-SY5Y cell line in Parkinson's disease research: a systematic review. Mol Neurodegeneration 2017, 12.

Xie, Z.; Bailey, A.; Kuleshov, M. V.; Clarke, D. J. B.; Evangelista, J. E.; Jenkins, S. L.; Lachmann, A.; Wojciechowicz, M. L.; Kropiwnicki, E.; Jagodnik, K. M.; Jeon, M.; Ma'ayan, A. Gene Set Knowledge Discovery with Enrichr. Current protocols 2021, 1, e90-n/a DOI:10.1002/cpz1.90.

Xiong, N.; Jia, M.; Chen, C.; Xiong, J.; Zhang, Z.; Huang, J.; Hou, L.; Yang, H.; Cao, X.; Liang, Z.; Sun, S.; Lin, Z.; Wang, T. Potential autophagy enhancers attenuate rotenone-induced toxicity in SH-SY5Y. Neuroscience 2011, 199, 292-302 DOI:10.1016/j.neuroscience.2011.10.031.

Xu, D.; Yao, Y.; Lu, L.; Costa, M.; Dai, W. Plk3 Functions as an Essential Component of the Hypoxia Regulatory Pathway by Direct Phosphorylation of HIF-1α. The Journal of biological chemistry 2010, 285, 38944-38950 DOI:10.1074/jbc.M110.160325.

Xu, Q.; Guo, H.; Zhang, X.; Tang, B.; Cai, F.; Zhou, W.; Song, W. Hypoxia regulation of ATP13A2 (PARK9) gene transcription. Journal of neurochemistry 2012, 122, 251-259 DOI:10.1111/j.1471-4159.2012.07676.x.

Xu, Y.; Zhi, F.; Peng, Y.; Shao, N.; Khiati, D.; Balboni, G.; Yang, Y.; Xia, Y. δ-Opioid Receptor Activation Attenuates Hypoxia/MPP+-Induced Downregulation of PINK1: a Novel Mechanism of Neuroprotection Against Parkinsonian Injury. Mol Neurobiol 2019, 56, 252-266 DOI:10.1007/s12035-018-1043-7.

Yamakawa, M.; Liu, L. X.; Date, T.; Belanger, A. J.; Vincent, K. A.; Akita, G. Y.; Kuriyama, T.; Cheng, S. H.; Gregory, R. J.; Jiang, C. Hypoxia-Inducible Factor-1 Mediates Activation of Cultured Vascular Endothelial Cells by Inducing Multiple Angiogenic Factors. Circulation Research 2003, 93, 664-673 DOI:10.1161/01.RES.0000093984.48643.D7.

Yamazaki, K.; Fukushima, K.; Sugawara, M.; Tabata, Y.; Imaizumi, Y.; Ishihara, Y.; Ito, M.; Tsukahara, K.; Kohyama, J.; Okano, H. Functional Comparison of Neuronal Cells Differentiated from Human Induced Pluripotent Stem Cell–Derived Neural Stem Cells under Different Oxygen and Medium Conditions. SLAS Discovery 2016, 21, 1054.

Yan, S.; Lu, J.; Zou, Y. S.; Soh-Won, J.; Cohen, D. M.; Buttrick, P. M.; Cooper, D. R.; Steinberg, S. F.; Mackman, N.; Pinsky, D. J.; Stern, D. M. Hypoxia-associated Induction of Early Growth Response-1 Gene Expression. The Journal of biological chemistry 1999, 274, 15030-15040 DOI:10.1074/jbc.274.21.15030.

Yasuda, R.; Hayashi, Y.; Hell, J. W. CaMKII: a central molecular organizer of synaptic plasticity, learning and memory. Nature reviews. Neuroscience 2022, 23, 666-682 DOI:10.1038/s41583-022-00624-2.

Yeh, T.; Leissing, T. M.; Abboud, M. I.; Thinnes, C. C.; Atasoylu, O.; Holt-Martyn, J. P.; Zhang, D.; Tumber, A.; Lippl, K.; Lohans, C. T.; Leung, I. K. H.; Morcrette, H.; Clifton, I. J.; Claridge, T. D. W.; Kawamura, A.; Flashman, E.; Lu, X.; Ratcliffe, P. J.; Chowdhury, R.; Pugh, C. W.; Schofield, C. J. Molecular and cellular mechanisms of HIF prolyl hydroxylase inhibitors in clinical trials. Chem. Sci. 2017, 8, 7651.

Yfantis, A.; Mylonis, I.; Chachami, G.; Nikolaidis, M.; Amoutzias, G. D.; Paraskeva, E.; Simos, G. Transcriptional Response to Hypoxia: The Role of HIF-1-Associated Co-Regulators. Cells 2023, 12.

Yin, Y.; Shen, H. Common methods in mitochondrial research (Review). International journal of molecular medicine 2022, 50, 1 DOI:10.3892/ijmm.2022.5182.

Yu, X.; Li, X.; Jiang, G.; Wang, X.; Chang, H. C.; Hsu, W. H.; Li, Q. Isradipine prevents rotenone-induced intracellular calcium rise that accelerates senescence in human neuroblastoma SH-SY5Y cells. Neuroscience 2013, 246, 243-253 DOI:10.1016/j.neuroscience.2013.04.062.

Yue, J.; López, J. M. Understanding MAPK Signaling Pathways in Apoptosis. International Journal of Molecular Sciences 2020, 21, 2346 DOI:10.3390/ijms21072346.

Zabłocka, A.; Mitkiewicz, M.; Macała, J.; Janusz, M. Neurotrophic Activity of Cultured Cell Line U87 is Up-Regulated by Proline-Rich Polypeptide Complex and Its Constituent Nonapeptide. Cell Mol Neurobiol 2015, 35, 977-986 DOI:10.1007/s10571-015-0192-8.

Zalcman, G.; Federman, N.; Romano, A. CaMKII Isoforms in Learning and Memory: Localization and Function. Front. Mol. Neurosci. 2018, 11.

Zeng, X.; Geng, W.; Jia, J. Neurotoxin-Induced Animal Models of Parkinson Disease: Pathogenic Mechanism and Assessment. ASN NEURO 2018, 10, 1759091418777438.

Zhang, M.; Deng, Y.; Zhang, J.; Liu, J.; Li, Y.; Su, H.; Qu, Q. SIRT3 Protects Rotenone-induced Injury in SH-SY5Y Cells by Promoting Autophagy through the LKB1-AMPK-mTOR Pathway. Aging and Disease 2018, 9, 273-286 DOI:10.14336/AD.2017.0517.

Zhang, S.; Wang, Y.; Xu, J.; Kim, B.; Deng, W.; Guo, F. HIFα Regulates Developmental Myelination Independent of Autocrine Wnt Signaling. J. Neurosci. 2020, 41, 251.

Zhang, T.; Gygi, S. P.; Paulo, J. A. Temporal Proteomic Profiling of SH-SY5Y Differentiation with Retinoic Acid Using FAIMS and Real-Time Searching. Journal of proteome research 2021, 20, 704-714 DOI:10.1021/acs.jproteome.0c00614.

Zhang, W.; Han, B.; Zhang, H.; Fu, R.; Lu, Y.; Zhang, G. Integrated transcriptomic and metabolomic analysis of cortical neurons reveals dysregulated lipid metabolism, enhanced glycolysis and activated HIF-1 signaling pathways in acute hypoxia. Heliyon 2023, 9.

Zhang, X.; Le, W. Pathological role of hypoxia in Alzheimer's disease. Experimental neurology 2010, 223, 299-303 DOI:10.1016/j.expneurol.2009.07.033.

Zhang, X.; Yin, M.; Zhang, M. Cell-based assays for Parkinson's disease using differentiated human LUHMES cells. Acta pharmacologica Sinica 2014, 35, 945-956 DOI:10.1038/aps.2014.36.

Zhang, Z.; Yan, J.; Chang, Y.; Shidu Yan, S.; Shi, H. Hypoxia Inducible Factor-1 as a Target for Neurodegenerative Diseases. Current medicinal chemistry 2011, 18, 4335-4343 DOI:10.2174/092986711797200426.

Zhao, X.; Zhang, M.; Li, C.; Jiang, X.; Su, Y.; Zhang, Y. Benefits of Vitamins in the Treatment of Parkinson’s Disease. Oxidative Medicine and Cellular Longevity 2019, 2019, 9426867-14 DOI:10.1155/2019/9426867.

Zhdanov, A. V.; Dmitriev, R. I.; Golubeva, A. V.; Gavrilova, S. A.; Papkovsky, D. B. Chronic hypoxia leads to a glycolytic phenotype and suppressed HIF-2 signaling in PC12 cells. Biochimica et biophysica acta 2013, 1830, 3553-3569 DOI:10.1016/j.bbagen.2013.02.016.

Zhdanov, A. V.; Dmitriev, R. I.; Papkovsky, D. B. Bafilomycin A1 activates HIF-dependent signalling in human colon cancer cells via mitochondrial uncoupling. Bioscience Reports 2012, 32, 587-595 DOI:10.1042/BSR20120085.

Zheng, B.; Mao, J.; Qian, L.; Zhu, H.; Gu, D.; Pan, X.; Yi, F.; Ji, D. Pre-clinical evaluation of AZD-2014, a novel mTORC1/2 dual inhibitor, against renal cell carcinoma. Cancer letters 2015, 357, 468-475 DOI:10.1016/j.canlet.2014.11.012.

Zhou, J.; Brune, B. Cytokines and Hormones in the Regulation of Hypoxia Inducible Factor-1α (HIF-1α). Cardiovascular & hematological agents in medicinal chemistry 2006, 4, 189-197 DOI:10.2174/187152506777698344.